CORA Cork Open Research Archive
Cartlann Taighde Oscailte Chorcaí

| | |
|---|---|
| Title | Coherent wavelength division multiplexing: a novel transmission format for high spectral density optical communication networks |
| Authors | Healy, Tadhg Conor |
| Publication date | 2007 |
| Original Citation | Healy, T. C. 2007. Coherent wavelength division multiplexing: a novel transmission format for high spectral density optical communication networks. PhD Thesis, University College Cork. |
| Type of publication | Doctoral thesis |
| Link to publisher's version | http://library.ucc.ie/record=b1994841~S0 |
| Rights | © 2007, Tadhg C. Healy - http://creativecommons.org/licenses/by-nc-nd/3.0/ |
| Download date | 2026-11-14 16:05:46 |
| Item downloaded from | https://hdl.handle.net/10468/1523 |



UCC
University College Cork, Ireland
Coláiste na hOllscoile Corcaigh

DP2007 HEAL

# COHERENT WAVELENGTH DIVISION MULTIPLEXING: A NOVEL TRANSMISSION FORMAT FOR HIGH SPECTRAL DENSITY OPTICAL COMMUNICATION NETWORKS

by

Tadhg Conor Healy

A thesis submitted to the National University of Ireland, Cork
for the degree of Doctor of Philosophy

Tyndall National Institute
Department of Physics
National University of Ireland, Cork

September 2007

Research Supervisor: Dr. Andrew Ellis

Head of Department: Prof. John McInerney



ucc
Coláiste na hOllscoile Corcaigh, Éire
University College Cork, Ireland

University College Library Cork

# Contents

**Contents** ..... **1**

**List of Figures** ..... **6**

**List of Abbreviations** ..... **14**

**Acknowledgements** ..... **16**

**Abstract** ..... **17**

**Chapter 1** ..... **18**

**Introduction to High Capacity/Spectral Density Optical Communication Systems** ..... **18**

1.1 Historical Perspective ..... 18

1.2 WDM-based Optical Fibre Communication Systems ..... 22

1.3 WDM Transmission Impairments ..... 27

*1.3.1 Interchannel Crosstalk* ..... *27*

*1.3.2 Dispersion* ..... *29*

*1.3.3 Non-linear Effects* ..... *31*

1.4 Modulation Formats ..... 31

*1.4.1 NRZ-OOK and RZ-OOK* ..... *32*

*1.4.2 Phase Modulation Formats* ..... *33*

1.5 Forward Error Correction Codes ..... 34

*1.5.1 What is FEC* ..... *35*

*1.5.2 FEC in WDM Optical Transmission Systems* ..... *37*

1.6 State of the Art ..... 38

*1.6.1 Ultra High ISD Systems* ..... *38*

*1.6.2 Photonic Integrated Circuits* ..... *39*

*1.6.3 Summary* ..... *40*

1.7 Coherent WDM as a High ISD Transmission Technique ..... 40

1.8 Scope of the Thesis ..... 44

*1.8.1 Organisation of the Thesis* ..... *45*

*1.8.2 Contributions of the Thesis* ..... *46*

*1.8.3 Technical Acknowledgements* ..... *47*

**Chapter 2** ..... **48**
**Coherent Wavelength Division Multiplexing: Theory and Modelling** ..... **48**
2.1 Introduction ..... 48
2.2 Theory of Coherent WDM ..... 49
*2.2.1 Introduction* ..... *49*
*2.2.2 Standard WDM System Description* ..... *49*
*2.2.3 Conditions for CoWDM* ..... *54*
*2.2.4 Summary* ..... *55*
2.3 Coherent WDM modelling ..... 56
*2.3.1 Introduction* ..... *56*
*2.3.2 CoWDM Modelling – Influence of Optical Filtering* ..... *56*
*2.3.3 CoWDM Modelling – Interference* ..... *61*
2.4 Summary ..... 64

**Chapter 3** ..... **65**
**Coherent Wavelength Division Multiplexing Implementation** ..... **65**
3.1 Motivation ..... 65
3.2 Standard High Bit Rate WDM Transmitter ..... 66
*3.2.1 Optical Modulators at 40 Gbit/s* ..... *66*
*3.2.3 40 Gbit/s Pulsed Pattern Generator* ..... *71*
*3.2.2 D Flip-Flop and high speed RF Cables* ..... *73*
3.3 Standard High Bit Rate WDM Receiver ..... 75
*3.3.1 Experimental Setup* ..... *75*
*3.3.2 Clock Recovery and Error Detection* ..... *79*
3.4 Optical Comb Generation [82] ..... 81
*3.4.1 Comb Generation Theory* ..... *84*
*3.4.2 Experimental Configuration* ..... *89*
*3.4.3 Comb Stabilisation* ..... *90*
*3.4.4 Enhanced Comb Generator [94]* ..... *92*
3.5 CoWDM Transmitter Configuration ..... 94
*3.5.1 CoWDM Transmitter Overview* ..... *94*

*3.5.2 CoWDM Transmitter Alignment* ..... *96*
*3.5.3 Mach-Zehnder Interferometer Characterisation* ..... *102*
*3.5.4 Piezo Fibre Stretcher Characterisation* ..... *103*
*3.5.5 Dispersion Management of Optical Comb* ..... *106*
3.6 Phase Stabilisation [97] ..... 107
*3.6.1 Phase Stabilisation Circuit* ..... *107*
*3.6.2 Enhanced Phase Stabilisation Circuit* ..... *111*
*3.6.3 Performance Comparison* ..... *113*
3.7 Optical Filter Characterisation and Optimisation ..... 118
*3.7.1 Numerical Simulation* ..... *118*
*3.7.2 Optical Filter Characterisation* ..... *121*
*3.7.3 Experimental Filter Selection* ..... *122*
3.8 Experimental Verification of 2.2.3 ..... 124
*3.8.1 Introduction* ..... *124*
*3.8.2 Optical Phase Relationship in CoWDM Transmitter* ..... *124*
*3.8.3 Electrical Delay in CoWDM Transmitter* ..... *127*
*3.8.4 Sine Wave Term* ..... *130*
*3.8.5 Conclusion* ..... *133*
3.9 Conclusion ..... 135

**Chapter 4** ..... **137**
**CoWDM Performance Characteristics** ..... **137**
4.1 Introduction ..... 137
4.2 CoWDM at 1 bit/s/Hz ISD ..... 139
*4.2.1 Introduction* ..... *139*
*4.2.2 298 Gbit/s CoWDM with 1 bit/s/Hz ISD* ..... *139*
*4.2.3 Transmission of 298 Gbit/s CoWDM over 80 km [107]* ..... *148*
*4.2.4 Summary* ..... *151*
4.3 Performance Evaluation of CoWDM with FEC codes ..... 152
*4.3.1 Introduction* ..... *152*
*4.3.2 Overview of FEC codes* ..... *153*

*4.3.3 CoWDM and FEC [119]* ..... *157*
*4.3.4 Results* ..... *159*
*4.3.4 Summary* ..... *163*
4.4 Dispersion Tolerance of CoWDM [121] ..... 164
*4.4.1 Introduction* ..... *164*
*4.4.1 Dispersion in Optical Communication Systems* ..... *164*
*4.4.3 Investigation of Dispersion Effects on CoWDM* ..... *165*
*4.4.4 Summary* ..... *171*
4.5 Nonlinear Tolerance of CoWDM ..... 172
*4.5.1 Introduction to Nonlinear Effects in WDM Systems* ..... *172*
*4.5.2 Experimental Setup and Procedure [134]* ..... *176*
*4.5.3 Results* ..... *178*
*4.5.4 Summary* ..... *184*
4.6 Conclusion ..... 186

**Chapter 5** ..... **188**
**Extended CoWDM Experimental Investigations** ..... **188**
5.1 Introduction ..... 188
5.2 CoWDM and Polarisation Division Multiplexing [140] ..... 189
*5.2.1 Overview* ..... *189*
*5.2.2 Experimental Configuration* ..... *193*
*5.2.3 Polarisation Division Multiplexing Results* ..... *194*
*5.2.4 Summary* ..... *204*
5.3 Long Haul Transmission Experiment using CoWDM [152] ..... 205
*5.3.1 Overview* ..... *205*
*5.3.2 Long Haul Transmission Simulations* ..... *207*
*5.3.3 40 Gbit/s CoWDM* ..... *210*
*5.3.4 Experimental Setup* ..... *214*
*5.3.5 Experimental Results* ..... *220*
*5.3.6 Summary* ..... *226*
5.4 Multi-banded CoWDM [162] ..... 227

*5.4.1 Introduction* ..... *227*
*5.4.2 Multi-banded CoWDM* ..... *228*
*5.4.3 Experimental Setup* ..... *229*
*5.4.4 Multi-banded Results* ..... *233*
*5.4.5 Summary* ..... *240*
5.5 Conclusion ..... 241

**Chapter 6** ..... **243**
**Conclusions and Future Work** ..... **243**
6.1 Introduction ..... 243
6.2 Technical Findings/Achievements ..... 243
6.3 Conclusions ..... 246
6.4 Future Work ..... 247
*6.4.1 Information Spectral Density/Capacity Increase* ..... *247*
*6.4.2 Integration* ..... *249*

**Appendix A** ..... **250**
**Publications and Conference Papers** ..... **250**
**References** ..... **253**

# List of Figures

Figure 1.1. Schematic of a modern optical communications network ..... 21
Figure 1.2. Schematic of a WDM system ..... 23
Figure 1.3. Evolution of ISD of WDM systems ..... 26
Figure 1.4. 40 Gbit/s NRZ eyes for a WDM system with 100 GHz and 50 GHz channel spacing. ..... 28
Figure 1.5. Transmission distance as a function of bit rate for chromatic dispersion limited systems ..... 30
Figure 1.6. (a) NRZ-OOK modulation format (b) RZ-OOK modulation format ..... 33
Figure 1.7. RS code structure ..... 36
Figure 1.8 : (a) Simulated spectrum and received eye for 40 Gbit/s WDM signal with wide channel spacing. (b) Same for narrow channel spacing. Red line represents filter position ..... 41
Figure 1.9. Left : Schematic of filtered target channel (green)and high frequency components of adjacent channels (yellow and blue). Right: Simulated eye diagrams ..... 43
Figure 1.10 Simulated received CoWDM eye diagram ..... 44

Figure 2.1. Super Gaussian filters with various '*m*' values ..... 57
Figure 2.2. Super Gaussian filters with varying FWHM values ..... 58
Figure 2.3. Target signal and neighbour signal for various '*m*' values ..... 59
Figure 2.4. Target signal and neighbour signal for various FWHM values ..... 60
Figure 2.5. Contour plot showing the SNR between the centre channel and the interfering channel as a function of the filter FWHM and 'm' value ..... 61
Figure 2.6. 3D surface plot showing the interference as a function of both time (t) and channel number (k) ..... 62
Figure 2.7. Contour plot showing decreased levels of interference at integer values of 'k' (y-axis) ..... 63

Figure 3.1 Mach-Zehnder Interferometer with electrical contacts ..... 67
Figure 3.2. Transfer Function of a typical MZ modulator. ..... 68
Figure 3.3. Single drive x-cut Mach-Zehnder modulator ..... 69
Figure 3.4. Experimental setup to measure MZM performance ..... 70
Figure 3.5. Eye diagram (42.6 Gbit/s) at output of MZM ..... 70
Figure 3.6. Optical spectra at the transmitter output for 42.6 Gbit/s NRZ with PRBS pattern length of (a) $2^7$-1 and (b) $2^{31}$-1 ..... 71

Figure 3.7. Pulsed pattern generator sections ..... 72
Figure 3.8. (top) 40 Gbit/s data-bar, (bottom) 40 GHz clock signal ..... 73
Figure 3.9. 42.6 Gbit/s data and data-bar output electrical eye diagrams from DFF ..... 74
Figure 3.10. Pre-amplified optical receiver configuration ..... 76
Figure 3.11. Theoretical receiver sensitivity limit as a function of bit rate for receiver with EDFA NF = 3 dB (squares) and EDFA = 5.2 dB (circles) ..... 77
Figure 3.12. Received optical spectrum for a single NRZ 42.6 Gbit/s channel ..... 78
Figure 3.13. Receiver sensitivity curve and received eye diagram (inset) for a single back-to-back 42.6 Gbit/s channel without (squares) and with (circles) an AMZI ..... 79
Figure 3.14. Schematic diagram of comb generator experimental configuration ..... 84
Figure 3.15. Optimised comb flatness versus relative drive amplifier amplitude for 7 (squares), 9 (circles), 11 (triangles), 13 (diamonds) and 15 (star) comb lines ..... 87
Figure 3.16. Optimised comb flatness versus drive voltage applied to each modulator for (a) 7 (b) 9 (c) 11 and (d) 13 lines ..... 88
Figure 3.17. Experimental spectrum of a 7 channel optical comb ..... 89
Figure 3.18. (a) Simulated and (b) Experimental scope traces for a seven channel phase locked optical comb ..... 90
Figure 3.19. Experimental configuration of comb stabilisation circuit ..... 91
Figure 3.20. Algorithm for comb stabilisation of a seven channel comb. Inset: Four possible states for a 7 channel optical comb ..... 92
Figure 3.21. Experimental spectrum of an 11 channel optical comb ..... 93
Figure 3.22. (a) Ideal and (b) experimental CoWDM transmitter ..... 95
Figure 3.23. Output of CoWDM Transmitter (standard alignment strategy) ..... 97
Figure 3.24. Output after demultiplexing filter (AMZI) ..... 98
Figure 3.25. Transmitted eye diagram for enhanced alignment strategy ..... 101
Figure 3.26. Demultiplexed output using enhanced alignment strategy ..... 102
Figure 3.27. (a) Experimental set-up. (b) Optical power as a function of wavelength for AMZI (black solid line) and optical comb (red dashed line) ..... 103
Figure 3.28. (a) Experimental set-up. (b) $\pi$ phase shifts as a function of applied voltage for piezo fibre stretcher. Experimental points (black circles) and linear fit (red line) ..... 105

Figure 3.29. Phase stabilisation circuit ..... 108
Figure 3.30. Simulated (a) total output power and (b) BER as a function of relative phase ..... 109
Figure 3.31. Experimental results for (a) BER against relative phase, and (b) BER curves for best and worst phase settings ..... 110
Figure 3.32. Algorithm to select desired phase for standard phase stabilization circuit. 111
Figure 3.33. Enhanced phase stabilisation circuit set-up ..... 112
Figure 3.34. Enhanced phase stabilisation algorithm ..... 113
Figure 3.35. Experimental configuration for phase stabilisation circuit comparison ..... 114
Figure 3.36. Normalised error signals (left axis) for mixer based (dotted trace) and photodiode based (dashed trace) as a function of time. BER fluctuation (right axis) versus time also shown (bottom solid trace) ..... 115
Figure 3.37. Performance of (a) Photodiode based stabilisation circuit (b) Mixer based stabilisation circuit as a function of time ..... 116
Figure 3.38. CoWDM transmitter and receiver simulation setup ..... 119
Figure 3.39. Q factor as a function of filter bandwidth for a Gaussian filter with (open symbols) and without (closed symbols) an AMZ dis-interleaver ..... 120
Figure 3.40. Filter measurement setup ..... 121
Figure 3.41. Amplitude as a function of wavelength for three Gaussian filters (0.95 nm, 0.64 nm and 0.43 nm) as a function of wavelength ..... 122
Figure 3.42. (a) Rx Sensitivity for each channel for various filter configurations. Received 42.6 Gbit/s eye diagram for the worst tributary using (b) 0.64 nm & AMZI, (c) 0.43 nm & AMZI and (d) AWG & AMZI ..... 123
Figure 3.43. Receiver Sensitivity for each tributary for 42.6 Gbit/s CoWDM for best phase (squares), optimum phase (circles) and worst phase (triangles) ..... 125
Figure 3.44. Received eye diagrams for tributary -1 for best (top), optimised (middle) and worst (bottom) phase conditions ..... 127
Figure 3.45. (a) Rx Sensitivity for each channel for when the RF delay was correctly aligned (squares) and mis-aligned (circles) ..... 128
Figure 3.46. Received eye diagrams for tributary + 2 (42.6 Gbit/s) when RF delay was (a) aligned and (b) mis-aligned. (10 ps/division) ..... 129

Figure 3.47. Transmitted CoWDM eye diagrams when RF delay was (a) aligned and (b) mis-aligned. (10 ps/division) ..... 129
Figure 3.48. Experimental setup for unsynchronised CoWDM ..... 131
Figure 3.49. (a) BER evolution as a function of time for un-synchronized (circles) and synchronized CoWDM (squares), for best (closed symbols) and worst (open symbols) optical phase setting ..... 132
Figure 3.50. Received eye diagrams for (a) 42.0 GHz worst phase, (b) 42.0 GHz best phase, (c) 42.6 GHz worst phase and (d) 42.6 GHz best phase. (10 ps/division) ..... 133

Figure 4.1. Back-to-back CoWDM experimental setup ..... 140
Figure 4.2. Optical comb generator output ..... 140
Figure 4.3. Simulation setup for transmitted spectrum ..... 141
Figure 4.4. (a) Simulated transmitted optical spectrum (b) Experimental transmitted optical spectrum ..... 142
Figure 4.5. Spectra of 298 Gbit/s CoWDM signal (black trace) and 160 Gbit/s OTDM signal (red trace) ..... 143
Figure 4.6. Simulated spectra for (a) 42.6 Gbit/s NRZ, (b) 298 Gbit/s NRZ and (c) 298 Gbit/s CoWDM (OSA power vs optical frequency) ..... 144
Figure 4.7. Receiver sensitivity curves for back-to-back 42.6 Gbit/s CoWDM ..... 146
Figure 4.8. Received eye diagrams for back-to-back CoWDM (5 ps/div) ..... 147
Figure 4. 9. Simulated received 42.6 Gbit/s CoWDM eye diagram ..... 148
Figure 4.10. Transmission section ..... 149
Figure 4.11. Receiver sensitivity for all seven channels over 80.km of SMF ..... 150
Figure 4.12. Eye diagrams and spectra for three CoWDM tributaries after transmission over 80 km of SMF ..... 151
Figure 4. 13. Single stage RS code ..... 154
Figure 4.14. Output BER as a function of input BER for four different single stage RS codes ..... 155
Figure 4.15. Concatenated codes construction ..... 156
Figure 4.16. Encoding and decoding steps for a concatenated code ..... 158
Figure 4.17. BER vs total received power for selected RS codes ..... 159

Figure 4.18. $BER_{out}$ vs $BER_{in}$ for concatenated codes in the multi-channel (open symbols) and single channel (closed symbols) condition ..... 160
Figure 4.19. $BER_{out}$ vs $BER_{in}$ for single-stage codes in the multi-channel (open symbols) and single channel (closed symbols) condition ..... 161
Figure 4.20. -log(BER) as a function of the total received power for single code on single and multi channel ..... 162
Figure 4.21. Receiver sensitivity penalty as a function of fibre length (chromatic dispersion) for fixed phase condition ..... 166
Figure 4.22. Eye diagrams for tributary # 0 and tributary # -3 for each both back-to-back and 80 km transmission ..... 167
Figure 4.23. Receiver sensitivity penalty as a function of fibre length for both fixed optimised phase condition ..... 168
Figure 4.24. Receiver sensitivity penalty as a function of dispersion for phase-optimised CoWDM (2 and 7 modulator case) and for other reported high bit rate systems ..... 170
Figure 4.25. Ideal dispersion maps for various bit rate systems ..... 176
Figure 4.26. Experimental setup ..... 177
Figure 4.27. Receiver sensitivity per channel as a function of launch power per channel for single channel (squares) and for CoWDM (triangles). Circles represent sensitivity of each CoWDM tributary at a launch power of 6.2 dBm ..... 179
Figure 4.28. Received CoWDM eyes for -8 dBm+3 dBm and +7 dBm launch power after 112 km (5 ps per division) ..... 181
Figure 4.29. Nonlinear signal distortion for a single channel (left trace) and a CoWDM signal (right trace) over 112 km with a launch power of +8 dBm per channel ..... 182
Figure 4.30. Receiver sensitivity curves for back-to-back condition (closed symbols) and for transmission (open symbols) over 112 km of Corning® Vascade® fibre ..... 183
Figure 4.31. Receiver sensitivity as a function of OSNR for CoWDM after 112 km transmission ..... 184

Figure 5.1. Polarisation division multiplexing ..... 190

Figure 5.2. Schematic of polarisation multiplexing with CoWDM ..... 192
Figure 5.3. Experimental configuration for PDM CoWDM ..... 194
Figure 5.4. Single channel NRZ 42.6 Gbit/s received spectrum (left) and receiver sensitivity curve (right) ..... 195
Figure 5.5. –log(BER) vs total received power for 7 channel single polarisation CoWDM without (left) and with (right) polarisation demultiplexing stage ..... 198
Figure 5.6. 42.6 Gbit/s single polarisation CoWDM received eye diagrams for tributary #-3 without (a) and with (b) polarisation demultiplexing stage ..... 198
Figure 5.7. –log(BER) as a function of total received power for all 14 CoWDM tributaries incorporating polarisation multiplexing (left). Received spectrum (.01nm bw) for channel # 1, polarisation 1 (right) ..... 199
Figure 5.8. Receiver sensitivity curves for back-to-back single channel (closed squares), single polarisation CoWDM (closed circles) and polarisation multiplexed CoWDM (open and closed triangles) ..... 201
Figure 5.9. Transmission distance at 1 dB EOP vs Bit rate for single polarisation (black solid line) and polarisation division multiplexed signal (red dashed line) ..... 202
Figure 5.10. Receiver sensitivities for each tributary ..... 203
Figure 5.11. Eye diagrams for tributary -3 for both single polarisation CoWDM and for both polarisation states ..... 204
Figure 5.12. Recent transmission results for varying repeater spacing and amplification schemes ..... 206
Figure 5.13. Simulated loop configuration ..... 207
Figure 5.14. Q-factor as a function of the total signal launch power for 800 km (triangles), 1200 km (squares) and 1600km (circles) ..... 209
Figure 5.15. 40 Gbit/s CoWDM experimental setup ..... 210
Figure 5.16. (a) Receiver Sensitivity curves for all seven 40 Gbit/s CoWDM in back-to-back configuration. (b) Received eye diagram for channel -3 (worst channel) and (c) Received eye diagram for channel 0 (best channel) ..... 211
Figure 5.17. (a) Receiver Sensitivity curves for all seven 40 Gbit/s CoWDM tributaries over 40 km with an injected power of 7 dBm, (b) Received eye diagram

for tributary 3 (worst channel) and (c) Received eye diagram for tributary -1 (best channel) ..... 212
Figure 5.18. Receiver sensitivities of all 40 Gbit/s (black squares) and 42.6 Gbit/s (red circles) CoWDM tributaries in back-to-back configuration with average lines (dashed traces) ..... 213
Figure 5.19. Optical spectra for tributary 3 for both (a) 40 GHz and (b) 42.6 GHz channel spacing ..... 214
Figure 5.20. Experimental setup for long-haul transmission with CoWDM ..... 215
Figure 5.21. –log(BER) vs total received power for both data amplifiers at different pattern lengths ..... 216
Figure 5.22. 40 Gbit/s data and data-bar electrical eye diagrams from output of DFF .. 217
Figure 5.23. 40 GHz clock signal ..... 217
Figure 5.24. Transmitted CoWDM spectrum ..... 218
Figure 5.25. Pre-amplified receiver ..... 220
Figure 5.26. CoWDM back-to-back eye diagram ..... 220
Figure 5.27. Measured Q-factor for each tributary channel for 800 km and 1,200 km .. 221
.Figure 5.28 Received 40Gbit/s CoWDM eye diagrams for best and worst tributaries . 222
Figure 5.29. Measured Q-factor as a function of total launch power for 800 km and 1,200 km ..... 223
Figure 5.30. Measured and simulated Q-factor as a function of launch power for 800 km (triangles) and 1,200 km (squares) ..... 224
Figure 5.31. Measured Q-factor and OSNR as a function of launch power for 800 km and 1,200 km ..... 225
Figure 5.32. Schematic of a multi-banded CoWDM setup ..... 228
Figure 5.33. Simulated multi-banded (49 channels) optical comb ..... 229
Figure 5.34. Multi-banded CoWDM experimental setup ..... 230
Figure 5.35. 35 channel comb spectrum (5 independent DFB's) ..... 230
Figure 5.36. Optical spectrum before transmission ..... 232
Figure 5.37. Transmission link ..... 233
Figure 5.38. Optical spectrum after transmission over 80.4 km ..... 234

Figure 5.39. Receiver sensitivity values for all 35 channels in back-to-back configuration (open squares) and after 80.4 km transmission (closed triangles)..... 235
Figure 5.40: Receiver sensitivity as a function of peak channel power for all 35 tributaries..... 236
Figure 5.41. Receiver sensitivity curves for all 35 tributaries in the back to back configuration (top panel) and after transmission (bottom panel)..... 237
Figure 5.42. Receiver sensitivity curves and eye diagrams for channels 4, 16 and 30 (back to back)..... 239
Figure 5.43. Receiver sensitivity curves and eye diagrams for channels 4, 16 and 30 (80.4 km transmission)..... 240

Figure 6.1. ISD evolution showing potential for up to 4 bit/s/Hz ISD using CoWDM with PDM and multi-level modulation formats..... 248

# List of Abbreviations

| | |
|---|---|
| AMZI | Asymmetric Mach-Zehnder Interferometer |
| AWG | Arrayed Waveguide Grating |
| BCH | Bose-Chaudhuri-Hocquenghem |
| BER | Bit Error Ratio |
| CD | Chromatic Disperison |
| CoWDM | Coherent Wavelength Division Multiplexing |
| CPU | Central Processing Unit |
| CRU | Clock Recovery Unit |
| CW | Continuous Wave |
| DAQ | Digital Acquisition |
| DC | Direct Current |
| DCF | Dispersion Compensating Fibre |
| DCM | Dispersion Compensation Module |
| DFB | Distributed Feedback Laser |
| DFF | D-Flip-Flop |
| DGD | Differential Group Delay |
| DPSK | Differential Phase Shift Keying |
| DQPSK | Differential Quadrature Phase Shift Keying |
| ED | Error Detector |
| EDFA | Erbium Doped Fibre Amplifier |
| EOP | Eye Opening Penalty |
| FEC | Forward Error Correction |
| FM | Frequency Modulated |
| FSR | Free Spectral Range |
| FT | France Telecom |
| FTTC | Fibre to the Curb |
| FTTH | Fibre to the Home |
| FWHM | Full Width at Half Maximum |
| FWM | Four Wave Mixing |
| HDTV | High Definition Television |
| HNLF | Highly Nonlinear Fibre |
| ISD | Information Spectral Density |

| | |
|---|---|
| ITU-T | International Telecommunications Union-Telecommunication Standardization Sector |
| LDPC | Low Density Parity Check |
| LH | Long Haul |
| LO | Local Oscillator |
| MAN | Metropolitan Area Network |
| MZI | Mach-Zehnder Interferometer |
| MZM | Mach-Zehnder Modulator |
| NCG | Net Coding Gain |
| NF | Noise Figure |
| NRZ | Non Return to Zero |
| OADM | Optical Add Drop Multiplexer |
| OH | Overhead |
| OOK | On-Off Keying |
| OSA | Optical Spectrum Analyser |
| OSNR | Optical Signal to Noise Ratio |
| OTDM | Optical Time Division Multiplexing |
| OXC | Optical Cross Connects |
| PBS | Polsrisation Beam Splitter |
| PC | Polarisation Controller |
| PC | Personal Computer |
| PD | Photodiode |
| PDM | Polarisation Division Multiplexing |
| PIC | Photonic Integrated Circuit |
| PM | Polarisation Maintaining |
| PM | Power Meter |
| PMD | Polarisation Mode Dispersion |
| PPG | Pulse Pattern Generator |
| PRBS | Pseudo Random Bit Sequence |
| PSU | Power Supply Unit |
| RBW | Resolution Bandwidth |
| RF | Radio Frequency |
| RS | Reed-Solomon |

| | |
|---|---|
| Rx | Receiver |
| RZ | Return to Zero |
| SBS | Stimulated Brillouin Scattering |
| SC | Supercontinuum |
| SDH | Synchronous Digital Hierarchy |
| SMF | Single Mode Fibre |
| SMSR | Side Mode Suppression Ratio |
| SONET | Synchronous Optical Networks |
| SOP | State of Polarisation |
| SPM | Self Phase Modulation |
| SSMF | Standard Single Mode Fibre |
| TPS | Triple Play Service |
| TV | Television |
| Tx | Transmitter |
| UD | Ultra Dense |
| ULH | Ultra Long Haul |
| VI | Virtual Instrument |
| VOA | Variable Optical Attenuator |
| WDM | Wavelength Division Multiplexed |
| XPM | Cross Phase Modulation |

# Acknowledgements

There are a large number of people who influenced me in various ways during the last four years and I would like to take this opportunity to thank them for helping me along the way. I would firstly like to thank Andrew Ellis, my supervisor on this project who was always there to provide excellent advice throughout the course of my postgraduate studies and was the inspiration behind this project. His immense technical knowledge and willingness to dispense it was invaluable on many occasions. Secondly I would like to express my gratitude to Fatima Garcia Gunning together with whom much of the experimental work described in this thesis was carried out. I'm not sure I could have survived l'expérience française with anyone else!

In addition I would like to thank my all friends and colleagues in the Photonic Systems Group, especially Robin Giller (for the laughs), Mary McCarthy (for putting up with my messiness), Eimear MacHale (for the clipart), Iris Choi (for the baby Guinness entertainment), Giuseppe Talli (for the lifts), Benjamin Cuenot (pour le pain et le vin), Martina Connolly, Paul Townsend, Rod Webb, Bob Manning and David Cotter for their friendship and support over the last 4 years.

I would also like to thank all my personal friends, for being there for me and providing a much needed social outlet...especially the members of the Irish ultimate community (particularly the Cork ones) for all the craic both on and off the fields since I began playing four years ago and Ali, you kept me sane during les nuits française.

Finally I want to thank my family: my sister Fiona and my parents Tim and Tess for enabling me to get to where I am today. You gave me a great start and I hope I'm doing you proud.

This is for you.

This work was financially supported by Science Foundation Ireland under the EMBARK initiative and Intel.

# Abstract

In this thesis a novel transmission format, named Coherent Wavelength Division Multiplexing (CoWDM) for use in high information spectral density optical communication networks is proposed and studied. In chapter 1 a historical view of fibre optic communication systems as well as an overview of state of the art technology is presented to provide an introduction to the subject area. We see that, in general the aim of modern optical communication system designers is to provide high bandwidth services while reducing the overall cost per transmitted bit of information.

In the remainder of the thesis a range of investigations, both of a theoretical and experimental nature are carried out using the CoWDM transmission format. These investigations are designed to consider features of CoWDM such as its dispersion tolerance, compatibility with forward error correction and suitability for use in currently installed long haul networks amongst others. A high bit rate optical test bed constructed at the Tyndall National Institute facilitated most of the experimental work outlined in this thesis and a collaboration with France Telecom enabled long haul transmission experiments using the CoWDM format to be carried out. An amount of research was also carried out on ancillary topics such as optical comb generation, forward error correction and phase stabilisation techniques.

The aim of these investigations is to verify the suitability of CoWDM as a cost effective solution for use in both current and future high bit rate optical communication networks.

# Statement of Originality

Except where indicated in the acknowledgements section (1.8.3) or by reference, all the work presented in this thesis are solely attributed to the author. The author participated in the design and implementation of all experiments except where explicitly indicated. Precise details of collaborators may be ascertained from the lists of co-authors in Appendix A.

# Chapter 1

# Introduction to High Capacity/Spectral Density Optical Communication Systems

## *1.1 Historical Perspective*

Fibre-optic based communication systems have revolutionised the telecommunications field since their introduction in the mid-twentieth century. Prior to this data transmission was almost entirely carried out using basic digital (telegraph) and analog electrical (coaxial systems) techniques, both of which were severely limited in bandwidth, bit-rate and un-repeatered reach. The first of two vital breakthroughs in the transition to fibre-optic based communication systems came in 1960 when the ruby laser was invented and demonstrated at Hughes Research Laboratories by T.H. Maiman [1]. This provided an optical source, which could then be modulated with a data signal and transmitted via optical fibre between a transmitter and a receiver. The second breakthrough concerned the transmission medium, which until 1970 exhibited prohibitively large losses in excess of 1000 dB/km. Before this optical communication was carried out using high loss lens guided systems in free space [2]. In their seminal paper in 1966 Kao and Hockham proposed the use of optical fibre for use in communication systems [3]. This idea was made feasible in 1970 when Kapron and Keck of Corning Glass Works developed optical fibre which had a low loss value of 20 dB/km [4]. With these two technologies it now became feasible to attempt optical transmission experiments over appreciable distances (several hundreds of km) at much higher bit rates than was achievable using electrical or microwave communication systems.

The last thirty years have seen a range of other technological advancements which have brought us to the position where a number of groups have experimentally demonstrated multi-terabit/s transmission over trans-oceanic

distances using a number of different transmission techniques [5, 6, 7]. These technological advancements include but are not limited to:

- *Optical Amplifiers* such as erbium doped fibre amplifiers (EDFAs) and Raman amplification which were developed during the 1980's and provide a means of overcoming fibre induced loss by direct amplification of the optical signal.
- *Broadband Optical Components* such as optical filters, transmission fibre, operating with low loss over a large range of wavelengths.
- *Modulation Formats* with increased tolerance to specific fibre induced impairments (section 1.4).
- *Forward Error Correction (FEC) codes*, which are used in a communications system to improve the quality of transmission and thus optimise system margin. FEC codes used in optical communication systems are described in detail in section 1.5.

Arguably the most important of these technological advancements was the development of optical amplifier technology in the mid-1980's which enabled transmission over increasingly long fibre spans by providing low-noise high-gain response across a wide range of transmission wavelengths [8]. The wide bandwidth in the optical fibre which was now available for transmission encouraged the adoption of wavelength-division multiplexing (WDM) based transmission systems where data is transmitted on multiple optical channels spaced in wavelength. Optical time-division multiplexing (OTDM) is a transmission technique which is mainly used in lab based investigations where several optical signals are optically multiplexed together in the time domain to form a bit-stream at a particular carrier frequency.

Since the dawn of civilisation when smoke signals were used to communicate the news of victorious armies or impending danger data traffic has increased exponentially, growing from 3 billion to 24 billion gigabytes during the period from 2000-2003 alone [9]. The rapid growth of data traffic on global

communication networks was initiated by the explosion of internet traffic in the 1990's and superseded the amount of voice traffic on the network around the turn of the millennium. The expansion in the amount of data traffic on modern communication networks is being generated by the transition of many traditionally analogue services (e.g. TV) to the digital domain (e.g. HDTV) as well as the increasing demands of the scientific and large business users which require access to high bandwidth services. Residential users too are requiring increased data bandwidths to facilitate triple play service (TPS) where high speed internet, television and telephone services are available over a single broadband connection [10].

Optical networks can be divided into three categories as shown in the schematic below, (i) core networks primarily made up of long haul (LH) point-to-point transmission links but also including networking capability via optical cross connects (OXCs) and optical add drop multiplexers (OADMS), (ii) metro area networks (MANs) and (iii) access networks which provide the final connection to the end user via copper or fibre links (fibre to the home (FTTH) and fibre to the curb (FTTC)).

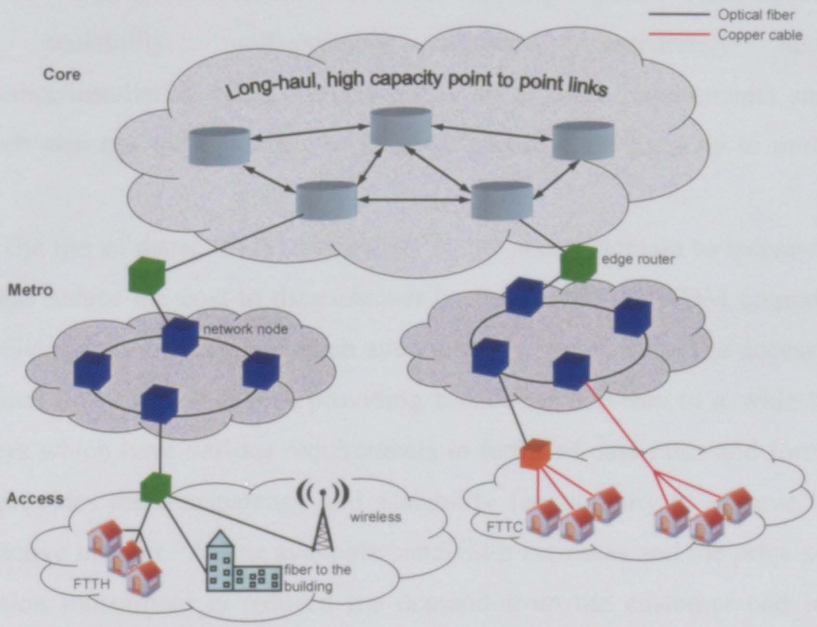



**Figure 1.1. Schematic of a modern optical communications network**

The LH or core network relies almost entirely on dense WDM transmission systems which are capable of providing high capacity over large distances and can be classified as terrestrial or submarine. The first transatlantic submarine optical communication system was the TAT-8 which was installed in 1988 and had a total capacity of 565 Mbit/s per fibre pair. Since then there has been an exponential increase in the capacity of undersea transmission systems with state-of-the-art systems such as the Tata Global Network Pacific capable of multi-terabit capacity over trans-oceanic distances [11]. Terrestrial LH systems have undergone similar increases in capacity and multi-terabit capacity has been demonstrated in field trials [12, 13, 14, 15, 16].

WDM technology has also become an attractive option for use in the other two network categories. MANs provide the link between the core network and the access network and tend to have a more diverse set of requirements than the core networks where capacity is of primary concern. This arises from the fact that they must be able to simultaneously connect to the high-speed core network and the bit-

rate/format-variable local access network. Amongst others these requirements include scalability, multi-protocol support, transparency and low maintenance/installation costs. WDM fulfils all of these requirements and as we have seen also has the capability to increase transmission capacity to multi-Tbit/s levels.

The use of dense WDM technology in the access domain to increase system reach, and reduce the cost to the customer by the sharing of WDM components is also receiving a lot of recent research attention [17, 18, 19, 20]. The access domain is the final link of the network providing broadband services to a wide range of customers which have various requirements in terms of data rates and formats and WDM provides the transparency and scalability functionality to achieve this in a cost effective manner. As the available bandwidth increases and the price per bit of information transmitted is reduced the demand from the customer end increases which results in a further increase in the available bandwidth. This circular trend of ever increasing demand requires the continuous development of new technologies to provide such service.

As the use of WDM proliferates throughout modern day optical communication networks, the ever increasing demands of data-centric networks require a continuous increase in system throughput (bits transmitted per second per km) while reducing the cost of the end-to-end transmitted bit to the customer. The next section looks in detail at the implementation of a typical point-to-point WDM system and considers some of the system design features required to meet this challenge.

## *1.2 WDM-based Optical Fibre Communication Systems*

The concept of WDM was first proposed by Delagne in 1970 in which he proposed to place a large number of channels of limited bandwidth adjacent to each other in the frequency spectrum to provide a wide-band composite signal [21]. Concerted research into WDM systems has been carried out since the early 1980's but it was

during the 90's that WDM systems were most actively developed resulting in a huge surge in reported system capacities [22, 23, 24, 25, 26]. This interest in WDM in the 90's was fuelled by the ever-increasing demand for a cost-effective method of delivering enough bandwidth to sustain the growth in internet traffic and bandwidth-hungry applications such as video conferencing and mass data transfer. WDM was recognised as a technique which allowed for large increases in the available bandwidth without the need to upgrade most of the existing infrastructure or the need to install more optical fibre. A typical WDM system transmits a number of optical channels simultaneously along an optical fibre at different wavelengths. This is achieved by independently data encoding each optical channel and then multiplexing them together in the wavelength domain to form one signal which is subsequently launched into the transmission medium (optical fibre in this case). At the receiver the signal is demultiplexed into its constituent wavelengths and the data is recovered from each optical channel. A simple schematic of a traditional WDM system is shown in figure 1.2 below.

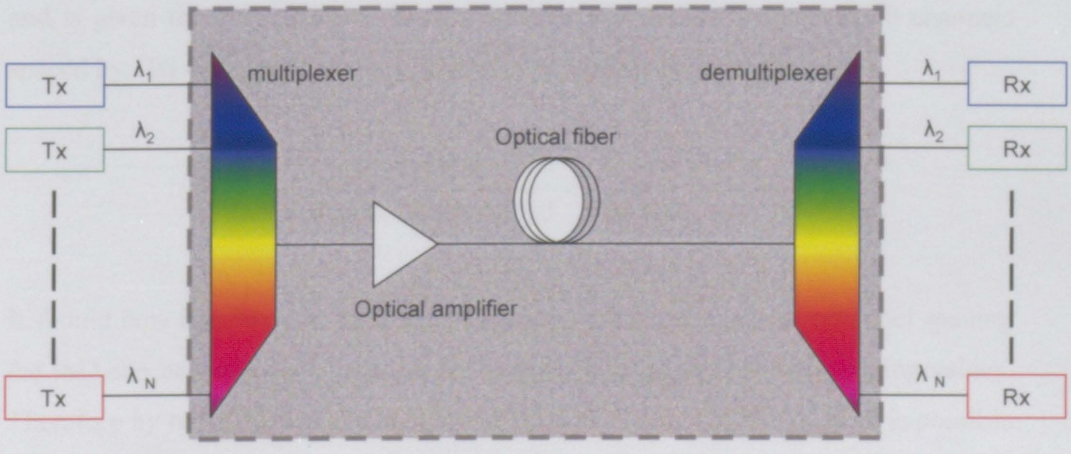



**Figure 1.2. Schematic of a WDM system**

As mentioned in the previous section the major focus of current WDM system development is to continue to increase system throughput while lowering cost. WDM systems have achieved this by sharing optical components such as fibre

amplifiers and optical fibre between all the WDM channels (all components inside the dashed box in figure 1.2 above). It becomes clear then that there are two main ways of increasing system capacity in a WDM system with a fixed optical bandwidth:

- Increasing the number of wavelengths on the fibre.
- Increasing the bit rate of data channels in the system.

The relationship between these two parameters can be quantified as the information spectral density (ISD) of a system which refers to the amount of information which can be transmitted over a given bandwidth in a communication system. The ISD is defined as

$$\text{ISD}=\frac{\text{Total Capacity}}{\text{Total Bandwidth Occupied}} \tag{1.1}$$

and is given the unit bit/s/Hz. So for example if a WDM system has 50 channels spaced by 100 GHz and operating at 40 Gbit/s the ISD of the system is

$$\text{ISD}=\frac{\text{Total Capacity}}{\text{Total Bandwidth Occupied}} \approx \frac{50\times 40}{50\times 100}=0.4 \text{ bit/s/Hz}$$

It should now be clear that for a WDM system which has fixed interchannel spacing the ISD can be calculated from the per channel bit rate and channel spacing values. Therefore by reducing the spacing between channels in a WDM system it is possible to increase the ISD of the system and consequently the overall capacity. When calculating the ISD of any system it is also important to adjust the value accordingly to consider the effect of FEC codes, which reduces the amount of information transmitted for a fixed bit rate. For example a WDM system similar to the one described above but requiring standard FEC (7% overhead) for error free operation

would have an adjusted ISD of 0.37 bit/s/Hz. All ISD values quoted in this thesis have been adjusted for the inclusion of FEC where appropriate.

The second way of increasing WDM system capacity is to increase the bit rate of each channel. Per channel bit rates in WDM systems have typically increased in multiples of 4 since the introduction of the synchronous digital hierarchy (SDH), the European standard in the telecommunications industry [27]. The first high capacity systems that underwent field trials in the early 90's operated at STM-16 with a per-channel bit rate of 2.5 Gbit/s [28] with long haul WDM systems operating at 10 Gbit/s being introduced in the late 1990's [29]. The transition from 2.5 Gbit/s to 10 Gbit/s was a difficult one as it required the introduction of inline dispersion compensation modules (DCMs) into fibre spans and the corresponding adjustment to the fibre amplifiers to account for the extra losses encountered. However it has been shown that by increasing the bit rate of the WDM systems by a factor of four the overall cost per transmitted information bit is reduced by a factor of almost two and it is at this point that operators are willing to accept the new line rate for use in their systems [30]. The next step along this roadmap is the transition from 10 Gbit/s to 40 Gbit/s. However 10 Gbit/s remains the operational bit rate for most long haul terrestrial and submarine systems today. This is because some of the impairments associated with transmission such as chromatic dispersion and nonlinear effects increase exponentially with bit rate and are relatively easier to manage at 10 Gbit/s than at 40 Gbit/s. Added to this is the fact that much of the fibre and infrastructure which was installed during the boom period which the fibre optic community enjoyed in the late 1990's was designed specifically for use with 10 Gbit/s systems. The deployment of 40 Gbit/s systems was also delayed by the crash which the industry experienced around the turn of the century. However the demand from the customer continues to drive a need for an increase in capacity and inevitably the next stage in the development of WDM systems, namely the transition from 10 Gbit/s to 40 Gbit/s is beginning to occur. Field trials of WDM systems with 40 Gbit/s line rates have been carried out since 2002 [31, 32], and transport subsystems allowing for 40 Gbits/s operation over deployed in-service networks using 10 Gbit/s signals are now commercially available [33].

Since the development of the first WDM transmission systems the achieved ISD values have been increasing linearly with time as a result of higher bit rates coupled with lower channel spacing. In addition to this the advent of advanced techniques such as FEC codes, polarisation division multiplexing (PDM) and multi-level modulation formats have resulted in recent reported ISD values as high as 3.2 bit/s/Hz [34]. Figure 1.3 below shows the evolution of the ISD in WDM systems reported in the literature over the last decade (the most significant results are referenced).

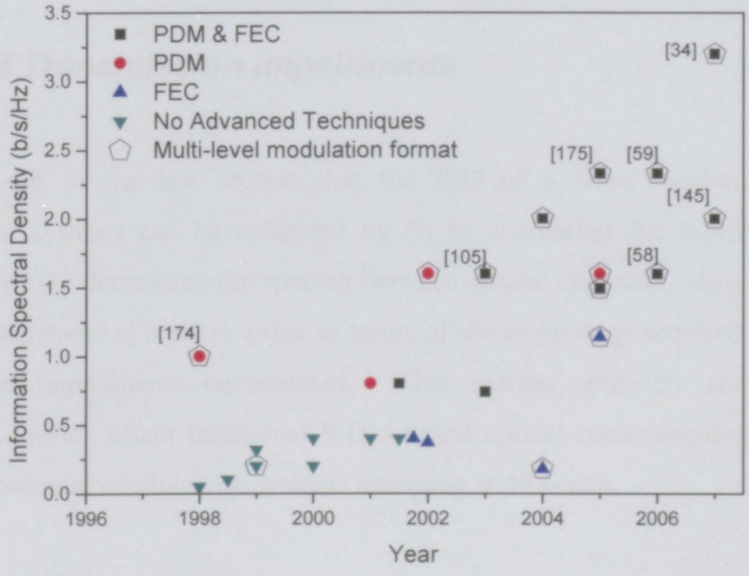



**Figure 1.3. Evolution of ISD of WDM systems**

The most recent reported results have all made use of multi-level formats, polarisation division multiplexing and FEC codes. This results in systems which are increasingly complex and expensive to implement (for example the 3.2 bit/s/Hz result was achieved using PDM, pre-filtered RZ-DQPSK and 7% overhead FEC) and one of the major challenges for system designers is to propose cost effective ways of increasing the ISD of future systems.

Furthermore as we continue along this trend-line to WDM systems with lower spaced channels operating at higher and higher bit rates the sensitivity of the systems to both linear and nonlinear impairments becomes significant, and can result in severe performance degradation. Higher bit rates mean narrower pulses (40 Gbit/s bit rate pulses are 25 ps wide) which are more susceptible to dispersion in the fibre and closer channel spacing increases the amount of interchannel crosstalk in the system. In the next section we will look in detail at some of these transmission impairments encountered by WDM systems operating at the limits of the system characteristics mentioned above.

## *1.3 WDM Transmission Impairments*

It was shown in the last section that the ISD of a fixed bandwidth WDM transmission systems can be enhanced by (i) by increasing the bit-rate of each channel or by (ii) decreasing the spacing between optical channels. However, these enhancements come at a price, either in terms of the technology required and/or the transmission impairments encountered. This section considers some of the impairments which affect traditional WDM-based optical communication systems, placing a particular emphasis on systems operating at 40 Gbit/s.

### 1.3.1 Interchannel Crosstalk

The most significant impairment encountered in traditional WDM systems is interchannel crosstalk which arises from power leakage between neighbouring optical channels and results in a degradation of system performance. The effects of interchannel crosstalk are relatively small when the optical channels are widely spaced but as the channel spacing is reduced in order to optimise system ISD adjacent channel spectra begin to overlap. In ultra dense WDM systems this overlapping of adjacent spectra causes neighbouring channels to interfere with each

other at the receiver. This crosstalk is inherently random in traditional WDM systems as each channel is typically generated by an individual wavelength source (laser) which has a random optical phase. Figure 1.4 below shows simulated received eye diagrams for a typical 40 Gbit/s NRZ WDM system for two different channel spacings. A Gaussian optical bandpass filter was used before the receiver to select the target channel. At 100 GHz spacing the eye is relatively clean and open but as the channels are placed closer together the quality of the eye degrades significantly and at 50 GHz spacing is closed entirely.

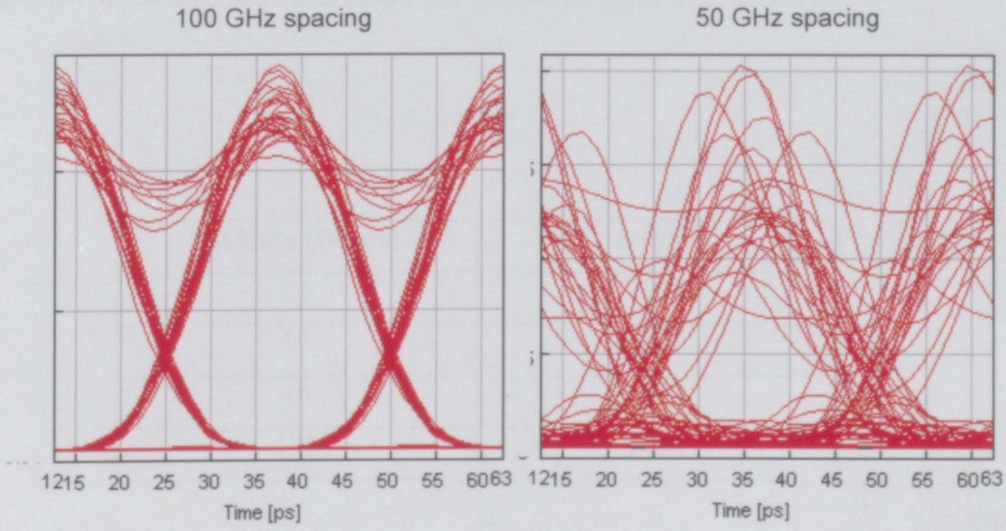



**Figure 1.4. 40 Gbit/s NRZ eyes for a WDM system with 100 GHz and 50 GHz channel spacing.**

Consequently, traditional installed 40 Gbit/s WDM systems are limited to a minimum channel spacing of 100 GHz resulting in an ISD of approximately 0.4 bit/s/Hz [35].

### 1.3.2 Dispersion

The chromatic dispersion of the transmission fibre can significantly impair the performance of a typical 40 Gbit/s WDM system. Chromatic dispersion occurs due to the fact that different wavelengths of light have different propagation speeds within a given transmission medium. If we consider that standard single mode fibre (SSMF), which has a dispersion value of approximately 17 ps/nm/km is the most common transmission medium for traditional WDM systems and calculate the maximum transmission distance (L) for a 1 dB eye opening penalty of a transform limited non-return-to-zero (NRZ) signal from the approximation in equation 1.2 [36] we obtain the results shown in table 1 for various bit-rates (B in Gbit/s).

$$L \propto \frac{1}{B^2} \tag{1.2}$$

| Bit Rate (Gbit/s) | L (km) |
|---|---|
| 2.5 | 1016 |
| 10 | 63.5 |
| 40 | 4 |
| 160 | 0.25 |

**Table 1.1. Distance limitation in SMF for various bit rates due to chromatic dispersion**

It is clear from looking at the values for L in table 1 that the impact of chromatic dispersion at 10 Gbit/s where the system is limited to ~60 km becomes even more pronounced at 40 Gbit/s and 160 Gbit/s where the transmission distance is limited to ~4 km and ~0.2 km respectively. The effects of chromatic dispersion at high bit rates require dispersion management strategies such as the insertion of dispersion compensation modules along the fibre link (DCM's) which compensate for this effect.

A second type of dispersion known as polarisation mode dispersion (PMD) also affects high bit-rate WDM transmission systems. PMD originates because of the different velocities with which the different states of polarisation propagate in the transmission fibre, and is generally caused by the non-uniform shape of the fibre core along its length. These random birefringences in the fibre can be caused by a range of factors including stress on the fibre, manufacturing flaws and fluctuating environmental conditions. Because of the nature of its origin PMD randomly varies with time, wavelength and is different for each individual fibre thus making it difficult to quantify theoretically and as a result compensate for in the field. As with chromatic dispersion PMD becomes increasingly problematic as the bit rate of the WDM system increases and is one of the major limiting factors affecting 40 Gbit/s WDM systems [37, 38]. This is because as the pulse widths become shorter at higher bit rates (bit slot is only 25 ps wide at 40 Gbit/s) the pulse spreading effect of PMD becomes more significant and results in a higher level of impairment.

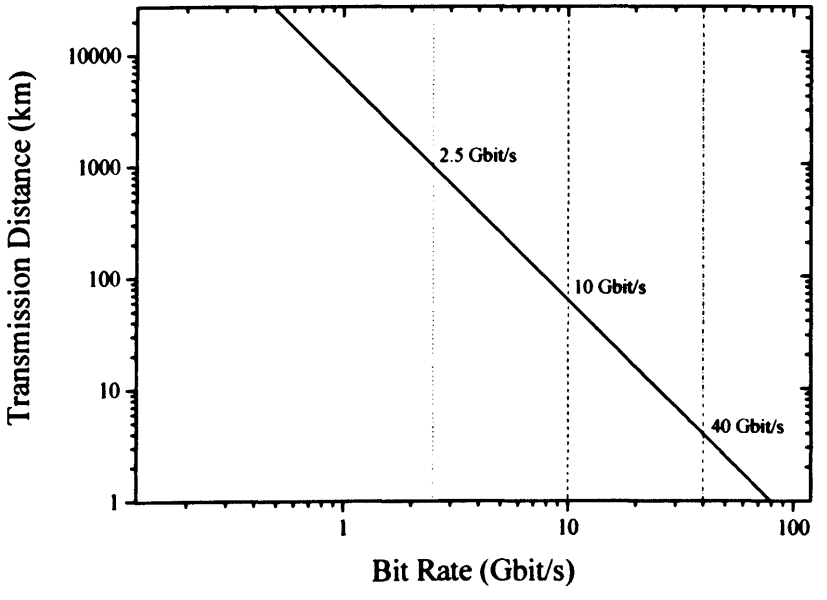



**Figure 1.5. Transmission distance as a function of bit rate for chromatic dispersion limited systems**

It is also important to note that both CD and PMD vary with wavelength and therefore careful planning is necessary to ensure correct compensation for these impairments in WDM systems which operate across wide wavelength ranges.

### 1.3.3 Non-linear Effects

The optical signal to noise ratio (OSNR) at the receiver determines the performance of an optical communication system. In order to maximise this OSNR value the launched signal must be launched from the transmitter at high power. However, it is well known that optical non-linear effects within transmission fibre impact on system performance, at these high signal launch powers. These non-linear effects arise from the fact that the refractive index of the fibre depends on intensity of the optical signal propagating therein, a phenomenon known as the Kerr effect [39]. Most WDM transmission systems make use of optical amplifier technology to overcome fibre losses by boosting signal power along fibre links. Optical nonlinearities such as self phase modulation (SPM), four wave mixing (FWM) and cross phase modulation (XPM), all arising from the Kerr effect can severely impact a WDM systems performance [40] at such high launch powers and, as with the previous impairments discussed become more evident with increasing bit rate.

## *1.4 Modulation Formats*

An optical modulation format is a way of applying an electrical data stream to an optical carrier signal. This section considers some of the modulation formats used in state-of-the-art WDM systems. There are a large range of modulation formats which can be applied to optical signals. The ideal modulation format for a WDM system would have some or all of the following characteristics:

- (1) A simple cost effective transmitter and receiver configuration.

- (2) A high tolerance to fibre induced impairments such as chromatic dispersion, polarisation mode dispersion and nonlinearities.
- (3) A high tolerance to the levels of interchannel crosstalk exhibited in high ISD WDM systems.
- (4) Spectrally efficient.
- (5) Resilience to the effects of multiple optical filters.

However a trade-off between these characteristics must be reached depending on the network which the modulation format is being applied in. For example the return-to-zero (RZ) modulation format is good for (2) but not for (4) whereas the system proposed in [34] is good for (4) but not for (1). Modulation formats can be grouped into two main categories, (i) intensity modulation formats and (ii) phase modulation formats depending on the physical aspect of the optical signal which is modulated to encode the data. Polarisation can also be used to encode data on an optical signal [41] but is not considered as a modulation format here. Polarisation is more often used to enhance the ISD of a WDM system by transmitting signals in orthogonal polarisations (polarisation division multiplexing) to reduce impairments such as inter channel crosstalk.

The two most common intensity modulation formats, non-return-to-zero on-off-keying (NRZ-OOK) and return-to-zero OOK (RZ-OOK) are described in some detail before a brief discussion on phase modulation formats which are gaining attention for use in modern WDM systems.

### 1.4.1 NRZ-OOK and RZ-OOK

OOK encodes data on an optical carrier simply by turning on and off the light. Direct detection using a photodiode is performed at the receiver to recover the encoded data. The two most common intensity modulation formats are NRZ-OOK and RZ-OOK. Both are shown in figure 1.6 below.

NRZ-OOK maintains an optical pulse in the 'on' state for the entire duration of the bit period and its amplitude remains high for two or more consecutive '1' bits. In contrast with this the optical pulse for the RZ modulation format is shorter than the duration of the bit period and its amplitude always returns to the zero level before the end of the bit slot. The bandwidth of the NRZ-OOK format (50% duty cycle) is typically half that of the RZ-OOK format because on-off transitions occur less frequently. This results in the better tolerance of NRZ-OOK to the effects of dispersion and makes it more suitable to closely spaced WDM systems. RZ-OOK however does have the advantage of having an improved tolerance to single channel non-linear effects than NRZ-OOK. A range of studies both in experiment and simulation have been carried out to compare the performances of NRZ-OOK and RZ-OOK in WDM systems [42, 43].

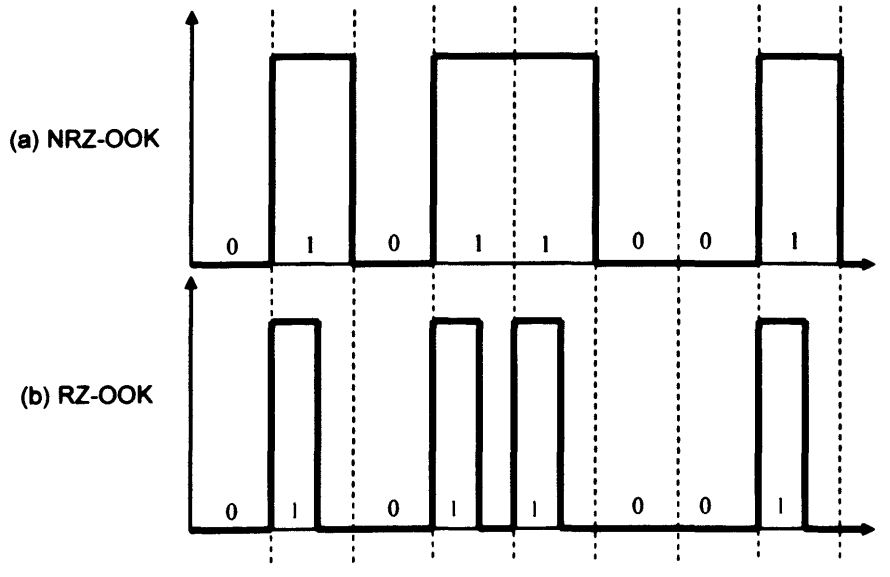



**Figure 1.6. (a) NRZ-OOK modulation format (b) RZ-OOK modulation format**

### 1.4.2 Phase Modulation Formats

Phase modulation formats encode data in the phase of the optical signal and this information is detected at the receiver by performing phase-to-amplitude conversion

before the photodiode. Differential phase shift keying (DPSK) is becoming considered as a potential modulation format for WDM systems as it gives a theoretical 3 dB receiver sensitivity improvement over OOK due to the increased symbol spacing compared to OOK for a fixed optical power [44, 45]. The DPSK modulation format represents a '1' bit with a $\pi$ phase change between successive bits whereas a '0' bit is represented by a zero phase change. At the receiver a balanced detector consisting of two photodiodes preceded by a delay interferometer is required to perform phase to amplitude conversion and recover the data.

Differential quadrature phase shift keying (DQPSK) is an enhancement of DPSK which encodes 2 information bits per optical symbol, and has been used to achieve very high ISD values due to its narrow spectrum [46, 47]. Data is modulated onto the phase of the optical carrier using one of four phases [$0, \pi/2, \pi, 3\pi/2$]. At the receiver two of the balanced receivers similar to that described above are required to detect the DQPSK signal which increases the cost and complexity of the receiver significantly. In addition two MZMs are required as phase modulators in a DQPSK transmitter.

As mentioned above the choice of modulation format is highly dependant on the type of optical network which is under consideration. For high capacity, high ISD WDM systems it is important to have a spectrally compact format, with good tolerance to CD and PMD, and a simple cost-effective configuration to reduce systems complexity and cost.

## *1.5 Forward Error Correction Codes*

Error correction codes are used in communication systems to improve the quality of transmission and are commonly used in optical communication systems to correct errors encountered during transmission. In the previous section we have seen how transmission impairments such as dispersion and interchannel crosstalk can introduce errors in a WDM system. For any particular application there is usually an error rate threshold above which the received data becomes unusable. For most

commercial systems this is currently set at a BER of $10^{-9}$, although many deployed systems have thresholds of much lower than this to allow a margin for deterioration of equipment and other impairments which increase with time. State-of-the-art WDM systems operate in a high bit rate ($\geq$ 40 Gbit/s), narrow channel spacing ($<$ 100 GHz) regime over large transmission distances ($>$ 1000 km) and may have a fundamental BER of the link above these thresholds. FEC codes are often used on a specific link to bring the received BER to below allocated threshold levels. This section introduces the basic concepts of FEC codes and describes the operation of the most commonly used FEC code in optical communications.

### 1.5.1 What is FEC

FEC is the incorporation of a suitable code into a data stream for the detection and correction of data errors about which there is no a priori information [48]. At the transmitter side FEC adds parity information to the data stream. At the receiver end this parity information can be used to determine if errors have occurred during transmission and can also be used to correct these errors. The FEC most commonly used in DWDM systems is termed out-of-band (OOB) as it is added as an overhead to the data, which effectively causes and increase in the bit rate of the system. In contrast the SDH/SONET standards for telecommunication allows for in band FEC within the existing overhead. Research into error correcting codes began in the late 40's when a number of significant developments occurred. In 1948 Claude Shannon proved that for a noisy channel communication with arbitrarily low error probabilities is possible if the data transmission rate $R$ is equal or less than the channel capacity $C$ [49]. Shannon proved that a code that enables error free transmission across a noisy channel exists provided certain constraints are adhered to. However Shannon's paper does not give any indication of how to construct such a code. Around the same time Richard Hamming developed the first error correcting code [50]. The next few decades saw the rapid advancement of this field of study with the development of many error-correcting codes. The standard FEC code used

in optical communications (ITU-T G.975) is an algebraic block code known as a Reed-Solomon (RS) code [51].

Reed Solomon codes were first proposed in 1960 by Irving Reed and Gus Solomon [52] and since then have been used for error correction in a huge variety of applications including compact disc players and satellite communication. RS codes are based on Galois or finite fields, which have the property that the results of arithmetic operations on field elements are also field elements. A RS code is specified as RS($n$,$k$) with $m$-bit symbols, where $n$ is the total number of code symbols in the encoded block, $k$ is the number of data symbols and $m$ is any positive integer greater than 2. For the RS codes which are used in this work

$$0 < k < n \tag{1.3}$$

and

$$(n, k) = (2^m - 1, 2^m - 1 - 2t) \tag{1.4}$$

apply. The difference, i.e. '$n$-$k$' is called the overhead or the parity of the code and is equal to '$2t$' where $t$ is the maximum number of errored symbols which the code can correct. A typical RS codeword is shown in figure 1.7 below.

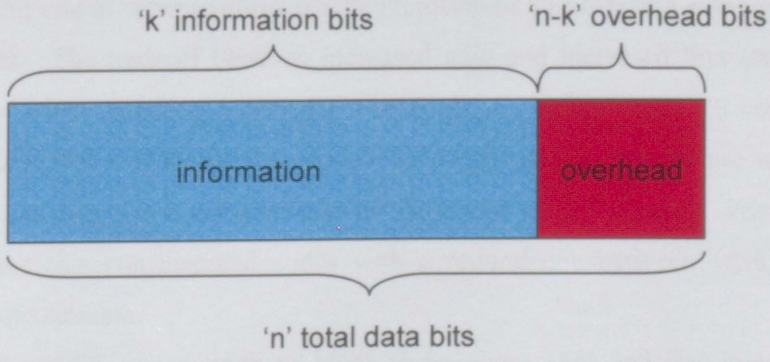



**Figure 1.7. RS code structure**

The higher the number of bits assigned to the overhead ('*n-k*') the more errors the code can correct but the lower the amount of information ('*k*') which can be transmitted per codeword. This is taken into consideration by the net coding gain (NCG) value of any particular FEC code which is given by the gross coding gain in dB - the bit rate increment in dB due to additional overhead.

The next section looks at the most commonly used RS codes and their application in WDM systems. Further details on the implementation of FEC codes are contained in chapter 4.

### 1.5.2 FEC in WDM Optical Transmission Systems

FEC technology plays an important role in modern day WDM optical transmission systems. Almost all recently deployed fibre systems rely on some kind of FEC in order to enhance system performance, increasing the system margin available to improve other system parameters such as reducing launch power or increasing transmission distance. The ITU-T G.975 standard recommends an interleaved 7% overhead RS(255, 239) code which gives approximately 6.2 dB of coding gain (i.e. 6.2 dB of OSNR margin over an un-coded system for a give BER). For a 40 Gbit/s WDM system a 7% overhead FEC code increases the operating bit rate per channel to 42.6 Gbit/s. Many of the experimental results presented in this thesis are at this modified bit rate in order to allow for the inclusion of a FEC frame along with the 40 Gbit/s data. The tradeoff between increased gain and increased line rate must be considered when choosing a code for a transmission system. For RS codes it was concluded in [53] that single RS codes with a redundancy of 6.7% are suitable for systems operating over sub-transatlantic distances (< 6500 km). For distances greater than this concatenated codes with a redundancy between 10% and 14% proved more suitable.

Other FEC codes, such as block turbo codes [54] and low density parity check (LDPC) codes [55] which give higher coding gain values are attracting

attention from research groups for use in optical transmission systems but have yet to become adopted by the carrier companies for use in the field because of their increased implementation complexity. The next section looks at the state of the art technologies that are currently being used to implement high capacity WDM systems.

## *1.6 State of the Art*

As already mentioned the recent rapid growth in demand for high bandwidth services has necessitated the development of high capacity, flexible, low-cost optical communication networks. This section presents some of the most recent 'state of the art' research results and looks at the technology on which these solutions are based.

### 1.6.1 Ultra High ISD Systems

As we have seen in section 1.2 current state-of-the-art deployed 40 Gbit/s systems are limited to channel spacings of approximately 100 GHz in order to avoid the deleterious effects of interchannel crosstalk, limiting the ISD to 0.4 bit/s/Hz with NRZ modulation. In order to enhance the ISD techniques such as advanced modulation formats [56], transmitter pre-filtering [57] and PDM have been employed [58] amongst others. Each of these techniques requires complicated transmitter and/or receiver configurations, further increasing the cost and complexity of the system. For example the highest reported ISD of 2.33 bit/s/Hz in a 40 Gbit/s WDM system was achieved using quadrature phase shift keying QPSK combined with PDM and FEC [59]. This required a local oscillator at the receiver to perform coherent detection and a complex transmitter in order to achieve QPSK modulation, all of which increase system cost. Indeed almost all reported systems achieving ISD values approaching 1 bit/s/Hz rely on combinations of these advanced techniques. The highest reported ISD value in an optical WDM system at the time of writing this

thesis was 3.2 bit/s/Hz which was achieved by Gnauck et al. and reported in [34]. In that work polarisation division multiplexed RZ-DQPSK signals at 85.4 Gbit/s were placed on a 50 GHz grid and error free performance over 240 km was achieved with the aid of FEC. A total capacity of 25.6 Tbit/s was achieved by using 80 DFB lasers in both the C and L band. Optical equalisation (OEQ) was also used after polarisation demultiplexing to reduce the influence of distortions caused by the narrow receiver side filtering of the optical signal. It is evident from this work and other reported high ISD results that a combination of PDM, advanced modulation formats and other advanced techniques such as transmitter pre-filtering or OEQ is necessary to achieve these high ISD values in WDM systems. Consequently these systems can be complex and expensive to implement and are not necessarily the most suitable candidates for modern optical communication networks where lowering cost is a major objective of system designers.

### 1.6.2 Photonic Integrated Circuits

In contrast with the complex high ISD systems mentioned in the previous section InP-based photonic integrated circuit (PIC) based solutions have emerged in recent years as a potential low cost solution for use in WDM networks. A PIC integrates multiple discrete optical components into a single device. Early research focussed on integrating single passive optical components such as arrayed waveguide gratings (AWG) in the late 1980's [60] and the development of other devices such as OADMs and OXCs followed in the 1990's [61, 62]. For a fully integrated transmitter or receiver however active components such as optical modulators and amplifiers must be combined with the already mentioned passive optical components. This level of integration has led to the development of complete optical transmitter and receiver modules based on PIC technology [63, 64]. Transmission experiments in a lab research environment using such modules were carried out in the 1990's [65, 66]. In a typical modern optical communication network a DWDM PIC transmitter and receiver combination could be used to

achieve high capacity throughput with a low cost and complexity footprint. Infinera have recently developed a single chip PIC capable of transmitting 1.6 Tbit/s [67]. The PIC consists of 40 x 40 Gbit/s channels on a 50 GHz grid (ISD = 0.8 bit/s/Hz) which are modulated with NRZ data using an integrated electroabsorption modulator (EAM). Transmission of one wavelength at a time over 100 km of Corning LEAF™ fibre was reported in [68] using a 10 x 40 Gbit/s channel transmitter (200 GHz channel spacing) and receiver PIC pair. This recent success of large scale PIC based technology augurs well for the future of optical device integration which should greatly facilitate the development of novel solutions for increasing system capacity in a cost effective manner.

### 1.6.3 Summary

In this section we have looked at two different types of state of the art technology. The first are systems based on combinations of advanced techniques which have high levels of implementation cost and complexity but have achieved record high spectral density values. Secondly we considered PIC based solutions which can provide a low cost solution for WDM systems by integrating many devices onto a single chip but with a lower ISD. A middle ground between these two approaches which combines the advantages of both is desirable.

## *1.7 Coherent WDM as a High ISD Transmission Technique [69]*

The major challenge facing WDM transmission systems of today is to maintain the rate of increase of system capacity while reducing the cost per transmitted information bit. The continuously increasing demand for low cost, high bandwidth services is driving the evolution of WDM systems to higher bit rates and lower inter-channel spacing and we have seen in earlier sections how certain technologies (advanced modulation formats and FEC) are being exploited to achieve this. In many current high ISD WDM systems the system setup is as shown in figure 1.2.

Because of the fact that the WDM signal is generated using a set of independent lasers, each with a random phase, a sinusoidal beat signal which is inherently random is generated between adjacent channels. At 100 GHz channel spacings (shown in figure 1.8 (a)) this does not affect the system and an open eye is observed at the receiver. However as we increase the ISD of the signal by packing more channels into the same bandwidth, i.e. the channel spacing is reduced (figure 1.8(b)) the received eye is degraded significantly.

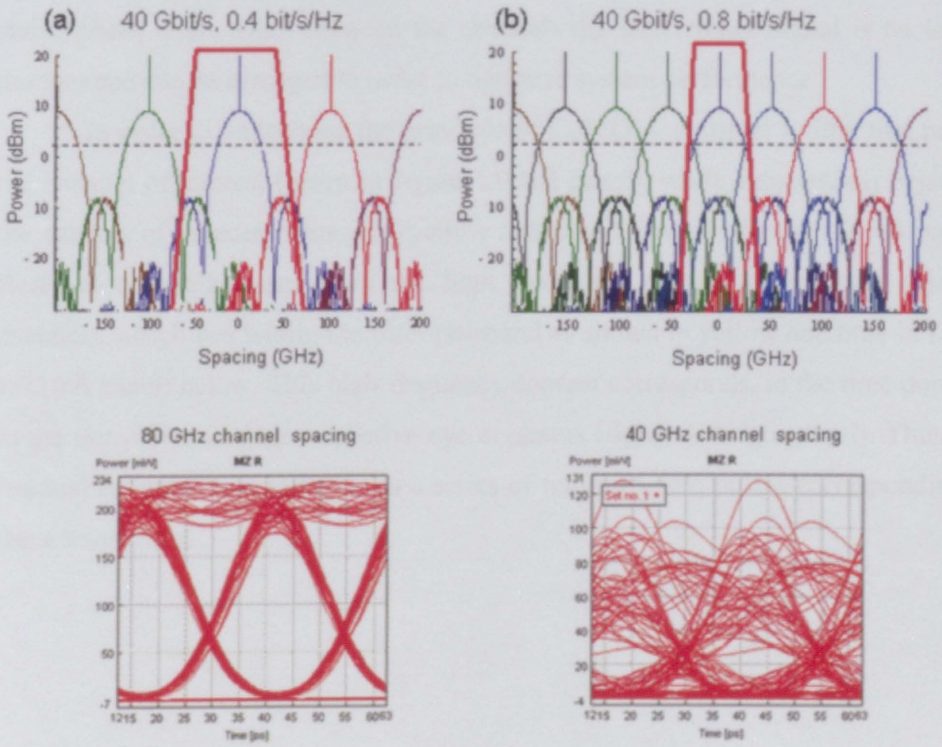



**Figure 1.8 : (a) Simulated spectrum and received eye for 40 Gbit/s WDM signal with wide channel spacing. (b) Same for narrow channel spacing. Red line represents filter position**

In this thesis we will introduce a novel solution known as coherent wavelength division multiplexing (CoWDM) which we will show enables high ISD values, up to 1 bit/s/Hz at 40 Gbit/s in a single polarisation using simple NRZ modulation with no pre-filtering at the transmitter and a standard pre-amplified receiver configuration and without relying on FEC. This combination of a low cost simple experimental configuration and high ISD values at 40 Gbit/s makes CoWDM an attractive solution for low cost high capacity/ISD modern WDM networks. In contrast with the setup for high ISD systems described above CoWDM uses a comb generator to generate an optical comb of 'n' phase locked channels. Because of this stable phase relationship between the channels the interference signal is no longer random and can be arranged in order to optimise system performance.

In order to understand the principle of CoWDM, consider a filter that passes the channel of interest (green in figure 1.9 left panel), while substantially rejecting the carriers of adjacent channels (yellow and blue arrows in figure 1.9 left panel). Residual crosstalk arises from the high frequency content of the two adjacent channels, which lies within the filter passband as shown in yellow and blue in figure 1.9 (left panel) below. This high frequency content corresponds, in the time domain, to the transitions in their respective eye diagrams (figure 1.9 right panel). Thus, the residual crosstalk is manifested as a series of return-to-zero pulses corresponding to these transitions.

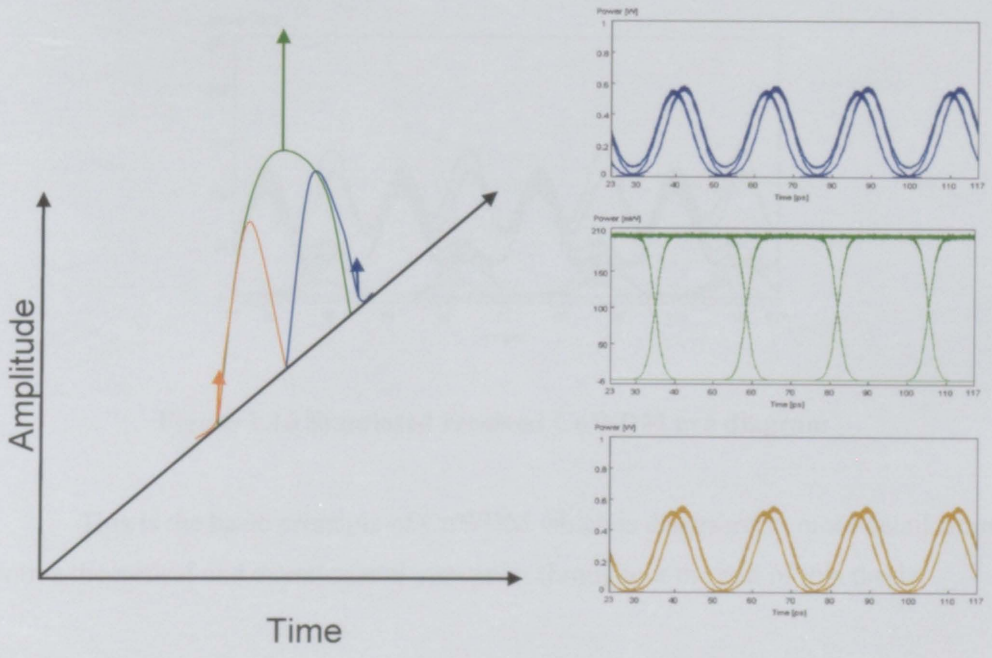



**Figure 1.9. Left : Schematic of filtered target channel (green)and high frequency components of adjacent channels (yellow and blue). Right: Simulated eye diagrams**

In order to open the center of the eye diagram of the channel of interest, it is necessary adjust the delay of the data patterns in the time domain to align these transitions to the eye crossing. It is also necessary to optimise the relative optical phase of the channels to minimize the impact of the pulse tails at eye center. This condition is only satisfied if the channel spacing is precisely equal to the bit rate, such that the interference varies periodically through the eye. If these conditions are met and the interference terms are adjusted accordingly a received CoWDM eye diagram (at 42.6 Gbit/s) as shown in figure 1.10 below can be obtained at the receiver.

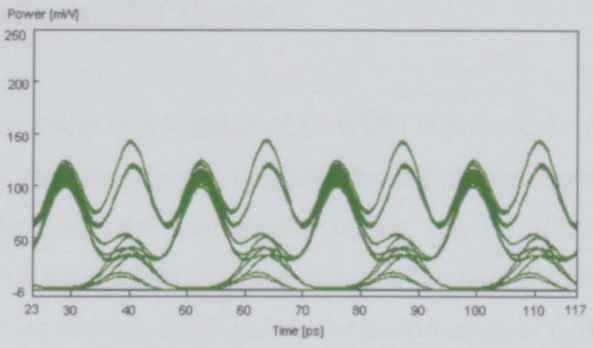



**Figure 1.10 Simulated received CoWDM eye diagram**

This is the basic principle of CoWDM which is discussed in more detail from both a theoretical and experimental viewpoint throughout the rest of this thesis.

## *1.8 Scope of the Thesis*

In this work we present a novel transmission format, Coherent Wavelength Division Multiplexing (CoWDM) for use in high ISD WDM transmission systems. The aim of the thesis is to provide a thorough theoretical and experimental investigation of the CoWDM transmission format, with a view to evaluating its suitability as a transmission format for low cost, high capacity, high ISD WDM systems. To achieve this, a range of both numerical and experimental investigations were carried out. Experimentally a 40 Gbit/s optical testbed with a CoWDM transmitter was developed which enabled the subsequent investigations of certain transmission characteristics of CoWDM (e.g. its tolerance to nonlinear effects in fibre). In addition to the initial investigations to characterise the performance of CoWDM in the presence of transmission impairments, experiments to verify the compatibility of CoWDM with existing WDM fibre infrastructure and FEC techniques were also performed amongst others.

### 1.8.1 Organisation of the Thesis

In Chapter 2 a theoretical investigation of CoWDM is presented. A standard WDM system is initially considered and it is shown that by placing certain constraints on such a system the CoWDM transmission format can be achieved. Numerical simulations are presented which show the impact of certain system parameters such as the optical filtering strategy employed on the performance of CoWDM.
The description of the implementation of the CoWDM based 40 Gbit/s optical testbed including the transmitter and receiver configurations forms a major part of Chapter 3. Details on auxiliary experimental work performed to support the implementation of CoWDM such as the development of a phase locked optical comb generator are also included in this chapter.

In Chapter 4 results from the investigations on the performance of various FEC codes with CoWDM are presented, along with a detailed study on the tolerance of CoWDM to dispersion and nonlinear effects in transmission fibre. The work presented in this chapter verifies CoWDM's compatibility with FEC codes and its high tolerance to transmission impairments common in WDM systems. These are important benchmarks in the overall consideration of CoWDM as a candidate transmission format for use in WDM systems.

Chapter 5 presents the high capacity and long-haul transmission experiments which were performed using CoWDM. The basic CoWDM format described in chapter 4 is extended by using advanced techniques such as polarisation multiplexing and multiple wavelength sources to demonstrate methods of further enhancing the achievable capacity of a CoWDM transmission system, without compromising the high ISD. The performance of CoWDM over a long haul link is evaluated both by simulations (performed by Benjamin Cuenot) and experimental work which was carried out in France Telecom laboratories (in collaboration with Erwin Pincemin).

Finally in Chapter 6 the main findings of the thesis are summarised and suggestions for further work are discussed.

### 1.8.2 Contributions of the Thesis

The main contributions of this thesis are listed below:

(i) The development and characterisation of a novel optical transmission format called CoWDM for use in high capacity high ISD WDM systems.

(ii) A theoretical explanation of CoWDM.

(iii) The experimental verification of the principle of CoWDM using a 40 Gbit/s optical testbed developed at the Photonic Systems Group laboratory.

(iv) The development of an optical comb generator capable of generating up to 11 phase locked optical channels for use as a wavelength source for CoWDM.

(v) Results from the experimental investigation of the nonlinear tolerance of CoWDM which outlines the primary non linear effects which impact upon CoWDM at high signal launch powers.

(vi) Results from an experimental investigation of the dispersion tolerance of CoWDM showing that CoWDM behaves in a similar fashion to conventional widely spaced WDM systems.

(vii) An investigation of the compatibility of CoWDM with standard forward error correction codes used in optical transmission systems.

(viii) Experimental results from long-haul transmission experiments which show that CoWDM is a promising technique for low cost, high capacity, high ISD WDM systems and is compatible with existing installed infrastructure.

(ix) A demonstration of multi-banded CoWDM resulting in ultra-high capacities.

### 1.8.3 Technical Acknowledgements

The topic of this thesis required a major part of the groups research activity. Consequently the work presented in this thesis is the result of collaboration between me and Dr. Fatima Garcia Gunning under the supervision of Dr. Andrew D. Ellis. Precise details on all collaborators can be obtained from the list of co-authors in appendix A. More specifically the following people were involved with contributing directly to certain sections.

Andrew D. Ellis: 2.2.2 Standard WDM System Description, 3.4.1 Optical Comb Generation Theory.
Benjamin Cuenot: 5.3.2 Long Haul Transmission Simulations
Erwan Pincemin: 5.3.4 Experimental Setup

# Chapter 2

# Coherent Wavelength Division Multiplexing: Theory and Modelling

## *2.1 Introduction*

In chapter 1 we proposed CoWDM as a potential solution for use in modern optical communication networks where high information spectral density is required to provide services requiring high bandwidths at a low cost. In this chapter we consider the theoretical basis for CoWDM, by identifying the terms which control the amount and location of the inter-channel crosstalk in a standard WDM system and explaining their origin. We then extend this basis to consider the special case which must be considered for CoWDM and show that CoWDM is based on controlling the optical phase relationship between adjacent channels in a WDM system in order to minimise the amount of interference experienced by the target channel at the receiver. Certain constraints are placed on a standard WDM system in order to achieve CoWDM operation and these are discussed in the following section. In section 2.3 some of the factors affecting the crosstalk terms in a CoWDM system are modelled using Mathematica 5.1.

## 2.2 Theory of Coherent WDM

### 2.2.1 Introduction

In order to fully understand the performance characteristics of CoWDM presented in the experimental chapters later in this work a complete understanding of the fundamental concept of CoWDM is advantageous. This section provides a detailed theoretical explanation of the CoWDM transmission format beginning with the electric field equation for an optical channel and finally expressing a term for the received signal taking into account the receiver side optical filters together with the data patterns of both the target and neighbouring channels for a standard WDM system. Following from this the conditions which lead to CoWDM are presented and the various constituent terms that make up the final equation are discussed in terms of the system parameters which they represent. The experimental investigation which considers the effects of these terms on the performance of CoWDM can be found later in the thesis in section 3.8.

### 2.2.2 Standard WDM System Description

In order to begin the derivation of the equation for the received signal we can consider the ideal electric field, $E_k^0(t)$ of the $k^{th}$ optical channel as

$$E_k^0(t) = d_{k,n}(t)E_0 e^{j(\omega_k t+\phi_k)} + c.c. \qquad (2.1)$$

where $d_{k,n}(t)$ represents the amplitude and phase of the $n^{th}$ data bit in an ideal square pulsed data sequence, $E_0$ the electric field amplitude, $\omega_k$ the optical frequency of the $k^{th}$ channel, $c.c$ the complex conjugate term, and $\phi_k$ the optical phase of the $k^{th}$ channel. We account for the finite rise and fall time of a practical signal arising

from the limited optical and electrical bandwidth by convolving the ideal optical signal with an impulse response $H_1(t)$ and allow for a variable time delay $t-\tau_k$ by evaluating

$$E_k(t) = E_k^0(t-\tau_k) \otimes H_1(t-\tau_k) \qquad (2.2)$$

If we now consider the signal in the frequency domain by taking the Fourier transform of this electric field over a period $NT$ of the $N$-bit periodic sequence $d_{k,n}$

$$\varepsilon_k(\omega) = \int_0^{NT} E_k(t) e^{-i\omega t} dt \qquad (2.3)$$

Substituting ( 2.2 ) into the integral in ( 2.3 ) we obtain the following expression

$$\varepsilon_k(\omega) = \int_0^{NT} \left[ E_k^0(t-\tau_k) \otimes H_1(t-\tau_k) \right] e^{-i\omega t} dt \qquad (2.4)$$

$$= e^{-i\omega\tau_k} \int_0^{NT} \left[ E_k^0(t) \otimes H_1(t) \right] e^{-i\omega t} dt \qquad (2.5)$$

By using the convolution theorem for Fourier transforms on ( 2.5 ) we get the following expression for $\varepsilon_k(\omega)$

$$\varepsilon_k(\omega) = e^{-i\omega\tau_k} h_1(\omega-\omega_k) \int_0^{NT} E_0 e^{-i\omega t} e^{i(\omega_k t+\phi_k)} d_{k,n}(t) dt \qquad (2.6)$$

During any given bit period, that is the interval $t \in \{(n-1)T \rightarrow nT\}$ both the electric field $E_0$ and the data sequence $d_{k,n}(t)$ can be assumed to be constant so we can represent $\varepsilon_k(\omega)$ as the sum of the integrals over 1 bit period for the entire bit stream as shown in equation ( 2.7 ) below.

$$\varepsilon_k(\omega) = E_0 e^{-i\omega\tau_k} h_1(\omega-\omega_k)\sum_{n=0}^{N-1} d_{k,n}\int_{nT}^{(n+1)T} e^{-i\omega t} e^{i(\omega_k t+\phi_k)} dt \qquad (2.7)$$

If we now calculate this integral we obtain the final expression for a practical optical signal with a variable time delay which has been convolved with an impulse response

$$\varepsilon_k(\omega) = E_0 e^{-i\omega\tau_k} h_1(\omega-\omega_k)\sum_{n=0}^{N-1} d_{k,n} e^{-i((\omega-\omega_k)t-\phi_k)} \frac{e^{-i(\omega-\omega_k)T}-1}{-i(\omega-\omega_k)} \qquad (2.8)$$

For a WDM signal we have $J$ such optical channels which are multiplexed together at the transmitter before transmission in the optical media. This is equivalent to forming the sum of ( 2.8 ) over all channels. At the receiver the target channel ($j$) is demultiplexed using a filter with a frequency response of $h_{2_j}(\omega)$ resulting in a target optical channel spectrum of

$$\varepsilon_{j'}(\omega) = h_{2_j}(\omega)\sum_{k}^{all\ J} \varepsilon_k(\omega) \qquad (2.9)$$

By substituting ( 2.8 ) into ( 2.9 ) and calculating the inverse Fourier transform we obtain the temporal function of the electric field

$$E'_j(t) = E_0 \sum_{k}^{all\ J}\sum_{n=0}^{N-1} e_{k,n} I_k(t-nT-\tau_k) \qquad (2.10)$$

where

$$e_{k,n} = d_{k,n} e^{i(\omega_k(t-\tau_k)+\phi_k)} \qquad (2.11)$$

takes the data sequence, optical and electrical delays into account and

$$I_k(t) = \int_{-\infty}^{\infty} h_1(\omega - \omega_k) h_{2_j}(\omega) \frac{e^{-i(\omega-\omega_k)T} - 1}{-i(\omega - \omega_k)} e^{i(\omega-\omega_k)t}\, d\omega \qquad (2.12)$$

considers the optical filters and channel frequencies. Direct detection of the optical signal occurs at the receiver-side photodiode where an electrical signal proportional to the intensity of the incident optical signal is generated. This intensity value can be expressed as

$$V_j(t) = \left[ \sum_{K=J_{min}}^{J_{max}} \sum_{n=0}^{N-1} e'_{K,n} \right] [c.c] \qquad (2.13)$$

If we assume that the receiver side filtering function is sufficient to eliminate contributions from all but the nearest neighbours to the target channel we can consider ( 2.13 ) to be reduced to the following expression

$$V_j(t) = \left[ \sum_{n=0}^{N-1} e'_{(j-1),n} + e'_{(j),n} + e'_{(j+1),n} \right] [c.c] \qquad (2.14)$$

where

$$e'_{K,n} = e_{K,n} I_{K,n} \qquad (2.15)$$

From ( 2.14 ) and ( 2.15 ) it becomes evident that the response of a WDM system at the receiver is governed by inter-channel crosstalk terms of the form

$$S_{\alpha\beta\gamma\delta} = e_{\alpha\beta} I_{\alpha\beta} e^*_{\gamma\delta} I^*_{\gamma\delta} \qquad (2.16)$$

If we combine this term with equations ( 2.11 ) and ( 2.12 ) and perform the following algebraic reduction steps we obtain equation ( 2.17 ) below

$$S_{\alpha\beta\gamma\delta} = d_{\alpha\beta} e^{j(\omega_\alpha (t-\tau_\alpha)+\phi_\alpha)} I_{\alpha\beta} d^*_{\gamma\delta} e^{j(\omega_\gamma (t-\tau_\gamma)+\phi_\gamma)} I^*_{\gamma\delta}$$

$$= d_{\alpha\beta} d^*_{\gamma\delta} I_{\alpha\beta} I^*_{\gamma\delta} e^{j(\omega_\alpha t - \omega_\alpha \tau_\alpha + \phi_\alpha - \omega_\gamma t + \omega_\gamma \tau_\gamma - \phi_\gamma)}$$

$$= d_{\alpha\beta} d^*_{\gamma\delta} I_{\alpha\beta} I^*_{\gamma\delta} e^{j((\omega_\alpha - \omega_\gamma)t - \omega_\alpha \tau_\alpha + \omega_\gamma \tau_\gamma + \phi_\alpha - \phi_\gamma)}$$

$$= d_{\alpha\beta} d^*_{\gamma\delta} I_{\alpha\beta} I^*_{\gamma\delta} e^{j(\Delta\omega_{\alpha\gamma} t - \omega_\alpha \tau_\alpha + \omega_\gamma \tau_\alpha - \omega_\gamma \tau_\alpha + \omega_\gamma \tau_\gamma + \Delta\phi_{\alpha\gamma})}$$

$$S_{\alpha\beta\gamma\delta} = d_{\alpha\beta} d^*_{\gamma\delta} I_{\alpha\beta} I^*_{\gamma\delta} e^{j(\Delta\omega_{\alpha\gamma} t - \Delta\omega_{\alpha\gamma} \tau_\alpha - \Delta\tau_{\alpha\gamma} \omega_\gamma + \Delta\phi_{\alpha\gamma})} \quad (2.17)$$

Because of the receiver side filter function $\alpha, \gamma \in (j-1, j, j+1)$ and if the channels have low inter symbol interference (ISI) then $\beta, \delta \in (n-1, n, n+1)$. Equation ( 2.17 ) can be broken down into six constituent parts which represent the various sources of impairments in a typical WDM system. By adjusting any or a combination of these terms accordingly the overall effect of the crosstalk in a WDM system can be reduced. These terms are as follows:

1. The $d_{\alpha\beta} d^*_{\gamma\delta}$ term represents the data patterns of the adjacent channels. Yamazaki et al showed in [70] that by suitably encoding each data channel with its own data and data from its adjacent channel that the effects of interchannel crosstalk can be suppressed in densely spaced WDM systems.

2. The $I_{\alpha\beta} I^*_{\gamma\delta}$ term represents the transmitter and receiver side filter profiles which can be adjusted to determine the amount of inter-channel crosstalk at the receiver.

3. The $e^{j(\Delta\omega_{\alpha\gamma} t)}$ term represents the sine wave beat signal located at the channel spacing

4. The $e^{-j(\Delta\omega_{\alpha\gamma}\tau_\alpha)}$ term represents the electrical delay of the target channel with respect to the adjacent channels.

5. The term $e^{-j(\omega_\gamma\Delta\tau_{\alpha\gamma})}$ term represents the relative optical delay of the target channel with respect to the adjacent channels.

6. The final term, $e^{-j(\Delta\phi_{\alpha\gamma})}$ is related to the phase of the target channel.

In the next section we will show that by placing certain constraints on a standard WDM system we can reduce the impact of a number of these terms, leading to suppressed levels of interchannel crosstalk.

### 2.2.3 Conditions for CoWDM

In the previous section the six terms governing the amount of crosstalk in a standard WDM system were isolated. If we now consider a WDM system where we constrain the spacing between the optical channels to be equal to the bit rate of the data encoding such that

$$\Delta\omega_{\alpha\gamma} = \frac{2\pi}{T}(\alpha-\gamma) \tag{2.18}$$

we find that the crosstalk term from equation (2.18) can be rewritten as follows

$$S_{\alpha\beta\gamma\delta} = d_{\alpha\beta}d^*_{\gamma\delta}I_{\alpha\beta}I^*_{\gamma\delta}e^{j(\frac{2\pi}{T}(\alpha-\gamma)t-\frac{2\pi}{T}(\alpha-\gamma)\tau_\alpha-\Delta\tau_{\alpha\gamma}(\omega_\gamma)+\Delta\phi_{\alpha\gamma})} \tag{2.19}$$

This '*channel spacing = bit rate*' constraint on a standard WDM system is what defines a CoWDM system. For $t-\tau_k$ approaching zero which is reasonable to assume as we are condsidering a square pulse shape and if $\tau_\alpha = 0$ for all $\alpha$ the

crosstalk in the system is now dominated by the data patterns, the filter profiles and the optical phase term, which can be actively tuned to achieve optimum performance. The tuning of the optical phase relationship between adjacent channels is dealt with in detail in chapter 3 where an experimental technique for selecting and controlling the phase is proposed and implemented.

### 2.2.4 Summary

This section has provided a detailed mathematical description of a standard WDM system beginning with the electrical field equation for an optical channel. The resultant equation provides an insight into the factors which determine the level of crosstalk experienced by a target channel due to its neighbours and the receiver side filter. By constraining a standard WDM system to have a channel spacing equal to the bit rate we have seen that many of the terms in the final equation can be suppressed leaving the 'optical phase relationship' term available to optimise the system. The next section looks in detail at results of numerical modelling of equation (2.18) which shows how CoWDM, by setting the bit rate equal to the channel spacing and by optimising the optical phase relationship between adjacent channels can reduce the impact of deterministic inter-channel crosstalk which occurs in high ISD optical communication systems.

## 2.3 Coherent WDM Modelling

### 2.3.1 Introduction

In the last section it was shown that the deterministic crosstalk in a typical WDM system can be attributed to six terms. Moreover by constraining the channel spacing to be equal to the bit rate (as is the case for CoWDM) we showed analytically that many of these terms become suppressed and the remaining term (optical phase relationship) could be used to optimise the level of residual crosstalk. In addition to this we saw that both the transmit and receiver side optical filters play a large role in determining the amount of crosstalk affecting the target channel. In this section we present the result of numerical simulations which consider these effects. These simulations were carried out using Mathematica Version 5.1.

### 2.3.2 CoWDM Modelling – Influence of Optical Filtering

The optical filters used in a CoWDM system have a significant impact on the level of crosstalk in the system. If we consider equation (2.12) we can determine the amount of crosstalk arising from a particular channel within the filter bandwidth of a particular target channel. This equation was modelled in Mathematica in order to determine the impact of various types of filters on the crosstalk. The filters modelled were super Gaussian type filters described by equation (2.21) below [39]

$$U(0,T) = \exp\left[-\frac{1+iC}{2}\left(\frac{T}{T_0}\right)^{2m}\right] \qquad (2.20)$$

where the parameter $m$ controls the degree of sharpness of the edge of the filter (higher $m$ values give a more square shaped filter). $C$ is the chirp parameter and is left equal to zero for this investigation. For a Gaussian filter

$$T_{FWHM} = 2\sqrt{(\ln 2)}T_0 = 1.665T_0 \qquad (2.21)$$

and the full width half maximum ($T_{FWHM}$) of the filter is determined by equation 2.22. Figure 2.1 below shows filter shapes for '*m*' values of 1, 2, 3, 4 and 5 each with a FWHM value of π.

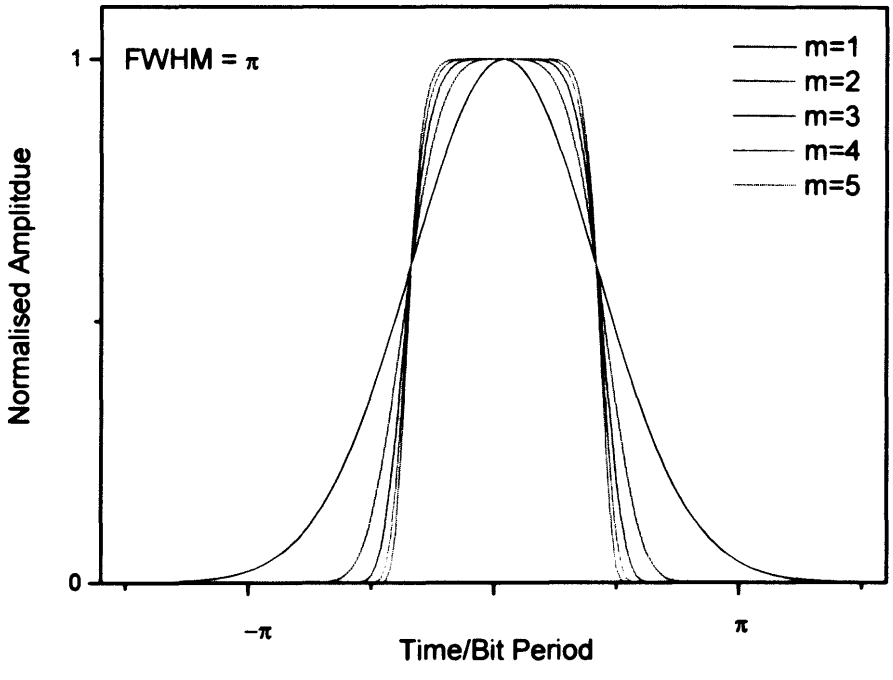



**Figure 2.1. Super Gaussian filters with various '*m*' values**

The FWHM of the filter can also be varied and figure 2.2 shows the shape of the filter for a number of different values of FWHM with a fixed $m = 1$.

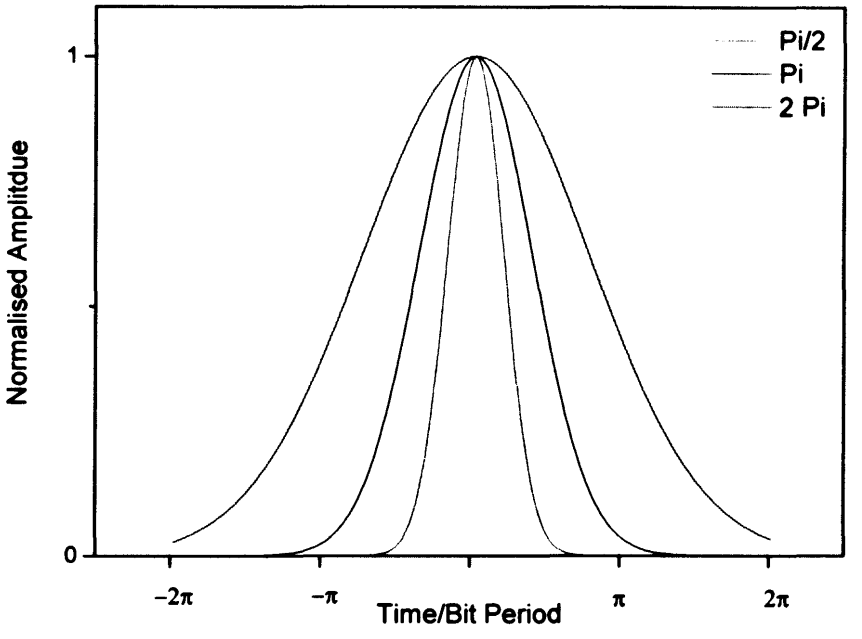



**Figure 2.2. Super Gaussian filters with varying FWHM values**

The interchannel spacing for the simulations was $2\pi$. Figure 2.3 shows a plot of the amount of signal passing through the filter for the target channel (solid trace) and for the nearest neighbour channel (dashed trace) for a number of different '*m*' values for a set FWHM value. In this case the FWHM value of the filter is close to the experimental value chosen.

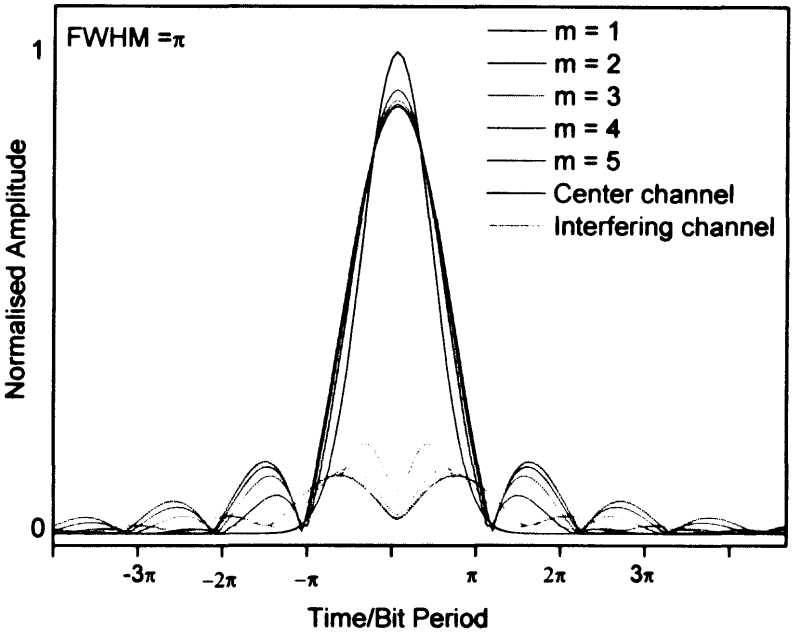



**Figure 2.3. Target signal and neighbour signal for various '*m*' values**

It is clear that as the filter becomes more square shaped the SNR improves, but the rate of improvement is very small beyond an '*m*' value of 3. Figure 2.4 below shows the amount of signal passing through the filter (m = 2) for the target and neighbour channels for varying FWHM values.

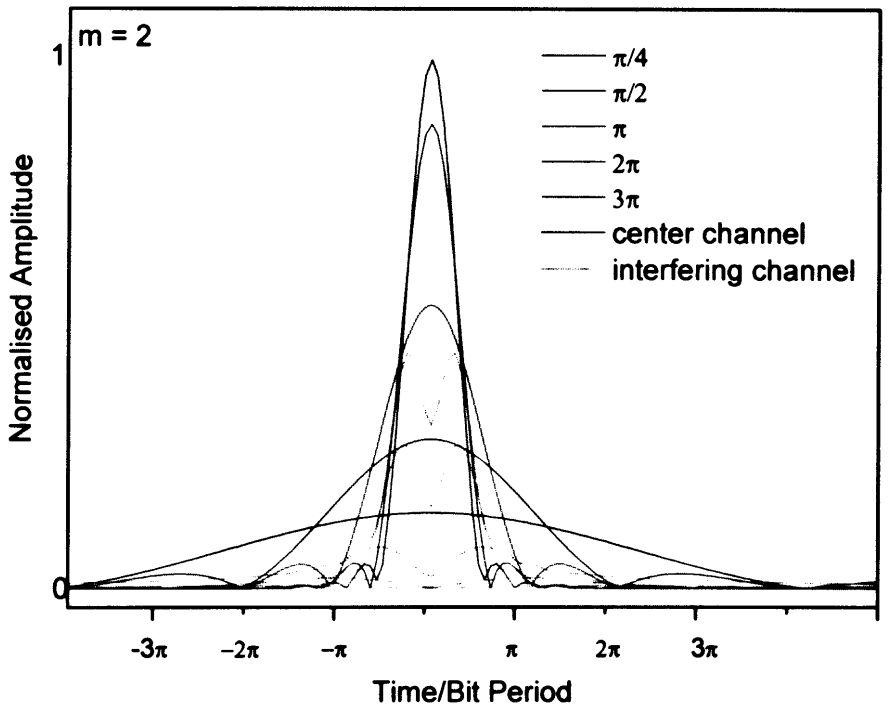



**Figure 2.4. Target signal and neighbour signal for various FWHM values**

As the filter becomes increasingly narrow the output spectra of the target channel and the crosstalk from the interfering channel broaden. The contour plot in figure 2.5 below combines these results of the simulations described above and it is evident that the FWHM of the filter (y-axis) is a more significant parameter than the 'm' value (x-axis) of the filter when selecting a filter for use in a CoWDM receiver.

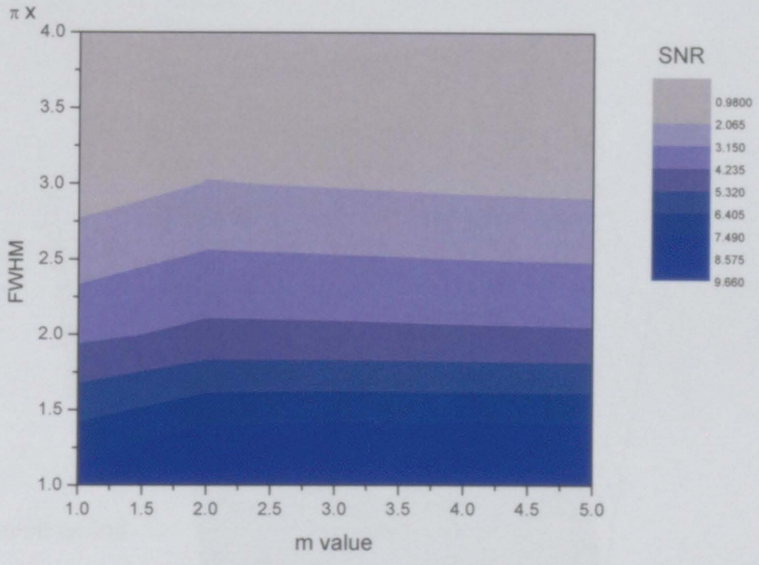



**Figure 2.5. Contour plot showing the SNR between the centre channel and the interfering channel as a function of the filter FWHM and 'm' value**

If an 'm' value of the filter is greater than ~2 the SNR depends solely on the FWHM of the filter.

### 2.3.3 CoWDM Modelling – Interference

If we again consider equation (2.12) it is evident that the interference, in addition to being dependent on the optical filter is also affected by the channel frequencies. Figure 2.6 below is a 3D surface plot of the interference described by equation (2.12) in terms of 'time/bit period' and 'relative frequency/bit rate'. It is clear from the plot that the interference is minimised when the normalised channel position is an integer value (i.e. $\pm 1, \pm 2, \pm 3, \pm 4, \pm 5 \ldots$), that is, at the position of the neighbouring channels. The level of the interference is symmetrical for channels to the left and right of the centre channels. This model used a filter with an m value of 1 and a FWHM of $\pi$.

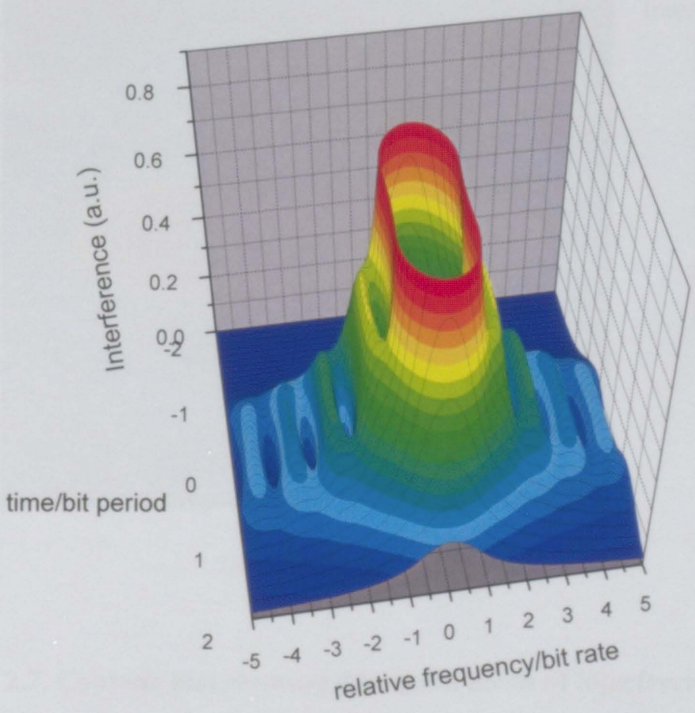



**Figure 2.6. 3D surface plot showing the interference as a function of both time/bit period and relative channel frequency/bit rate**

This feature of minimised interference levels at the channel positions is a fundamental characteristic of the CoWDM transmission format and leads to improved performance at tight channel spacing when compared to a standard WDM system as will be demonstrated in later chapters. Figure 2.7 below plots the data in a different way, using a contour plot to highlight the reduced levels of interference at the integer channel positions (y-axis). The areas of dark blue represent the lowest level of interference and these can clearly be seen at the positions where 'k' is an integer value.

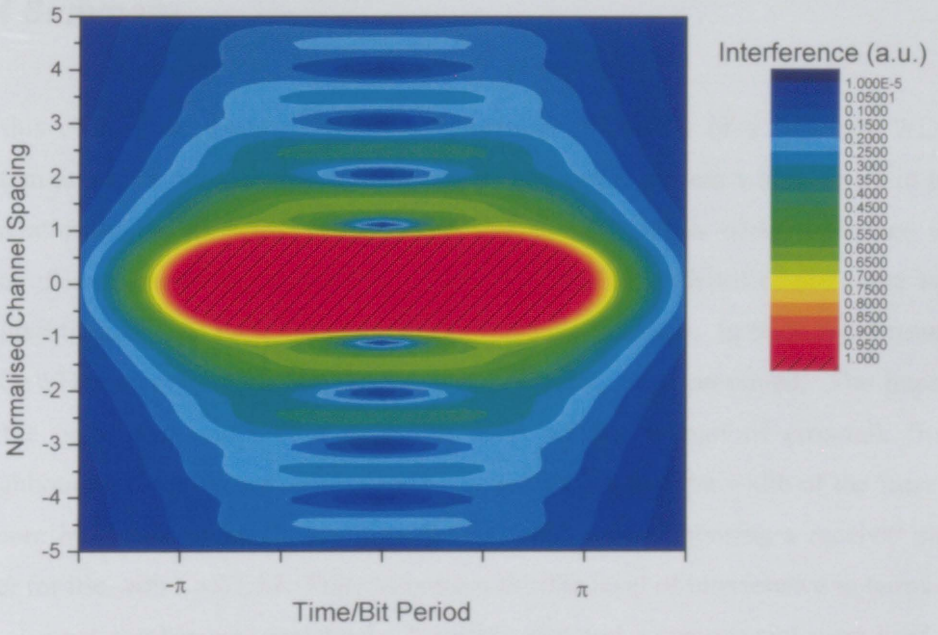



**Figure 2.7. Contour plot showing decreased levels of interference at integer values of 'the normalised channel frequency (y-axis)**

## 2.4 Summary

In this chapter we have presented a theoretical derivation of a standard WDM system and then proposed certain constraints on such a system which result in the generation of the CoWDM transmission format. The terms which influence the level of interference experienced by a target channel were identified and these will be investigated in an experimental context in the next chapter. In section 2.3 results of CoWDM modelling carried out using Mathematica were presented. The impact of the order and width of a Gaussian filter on the amount of crosstalk from neighbouring channels was investigated. It was shown that the width of the filter is a more important consideration than the 'm' value when choosing a receiver side filter for use with CoWDM. Following from this the level of interference in terms of the channel number was presented. A surface plot and a contour plot were used to show that the level of crosstalk was minimised at the exact channel locations due to the CoWDM constraint, implying that improved performance with respect to a standard WDM system should be achievable. In the next chapter we look at the actual implementation of a high speed optical test bed and a CoWDM transmitter. These are used to experimentally verify the impact of certain terms outlined in section 2.2 on system performance.

# Chapter 3

# Coherent Wavelength Division Multiplexing Implementation

## *3.1 Motivation*

As we have seen in the earlier chapters the current trend in optical communications is towards operating at higher and higher transmission bit rates, in order to maximise the throughput of fibre links. The majority of installed long-haul fibre links are designed for transmission systems operating at line rates of $\leq$ 10 Gbit/s. However in a research environment where next generation systems are being investigated as candidates for use in future optical communication networks it becomes necessary to consider higher bit rates such as 40 Gbit/s. In this chapter we describe the implementation of a 40 Gbit/s optical testbed incorporating a CoWDM transmitter that was established at the Photonic Systems Group laboratories, Tyndall National Institute, Cork.

We begin by discussing standard high bit rate WDM transmitter and receiver configurations with particular emphasis on the devices and components which are necessary for the implementation of systems operating at bit rates in excess of 40 Gbit/s. Following from this, details on the modifications to a standard transmitter which were necessary for the implementation of the CoWDM transmitter, including optical comb generation and optical phase stabilisation are presented. In the final section we will describe the implementation of the pre-amplified optical receiver which was used with CoWDM and look at the receiver side filter characterisation that was carried out. The CoWDM transmitter and optical testbed described in this chapter are the central experimental devices which were used throughout this work and were constructed over a number of years with the aid of colleagues in the Photonic Systems Group.

## *3.2 Standard High Bit Rate WDM Transmitter*

Optical communication systems operating at bit rates of ~40 Gbit/s require optical, opto-electronic and electronic components capable of operating at high speeds. In general the performance of many passive optical components such as optical filters tend to be independent of the data-rate of the system. One obvious exception is optical fibre which has much higher losses at high bit-rates due to the effect of impairments such as dispersion on the increasingly narrow pulses at high bit rates. In addition to this the design and implementation of opto-electronic and electronic components becomes increasingly complex at higher frequencies. In this section we look at the implementation of standard high bit rate WDM optical transmitters with particular emphasis on the operation of a number of such components. These include amongst others the data modulator, the pattern generator and the D-flip-flop (DFF), which are central to the operation of a typical 40 Gbit/s optical transmitter.

### 3.2.1 Optical Modulators at 40 Gbit/s

The role of the optical modulator in a standard optical transmitter is to encode or modulate the optical carrier signal with an RF data sequence. This can either be performed directly by modulating the light directly at its source or externally by using an optical modulator. Direct modulation techniques suffer from excessive amounts of chirp and are limited to bit rates of 10 Gbit/s and lower for practical implementations [71, 72, 73] although transmission of 40 Gbit/s signals has also been achieved in lab experiments [74, 75, 76]. At high bit rates such as 40 Gbit/s external modulation of the optical carrier signal does not suffer from the high chirp induced impairments associated with the other techniques and as a result external optical modulators capable of operating in this range are essential for high bit rate systems experiments. The two most common types of optical modulator designed for use in optical communication systems are the electro-absorption modulator (EAM) and the Mach-Zehnder Interferometer (MZI) modulator. The large chirp and

lower output power values associated with the EAM solution make them less suitable for high bit rate data modulation whilst a MZI based optical transmitter is capable of providing low chirp and high output power with relatively low drive voltages. For this reason we consider only Mach-Zehnder based solutions in the remainder of this work.

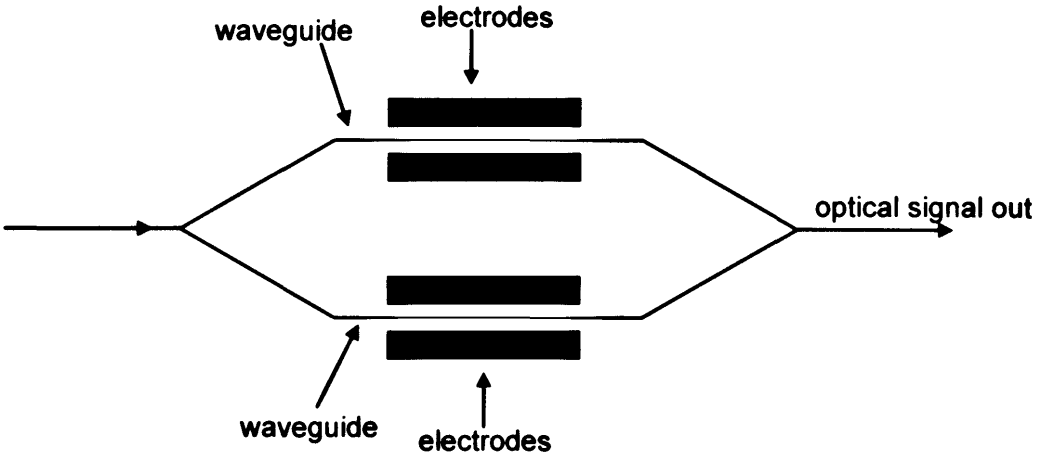



**Figure 3.1 Mach-Zehnder Interferometer with electrical contacts**

A MZI can be constructed as shown in figure 3.1 above where the input is split into two arms of equal length which are coupled at the output of the device. The waveguide is fabricated from a material such as $LiNbO_3$, the refractive index of which can be changed by applying a voltage to the electrical contacts. The change in refractive index in the waveguide causes a phase shift in the optical signal propagating through that particular path. When this phase shift is equal to $\pi$, no light is transmitted at the output due to the destructive interference between the signals. Conversely when there is no applied voltage the phase shift is zero and the signals interfere constructively resulting in a maximum amplitude signal at the output of the device. If we consider an electrical bit pattern applied to a MZI and monitor the output optical signal it is evident how a MZI can be used as an optical modulator. Figure 3.2 shows the operation of a typical MZI modulator for the given input bit

stream '1101'. The optical output of the MZ modulator (MZM) is shown as a function of bias voltage. We can see that when a bias voltage corresponding to a '1' bit (orange signal) is applied to the modulator the transfer function of the MZM is at a maximum and a corresponding optical signal is observed at the output of the device (blue signal). When the electrical input is '0' destructive interference causes no light to be transmitted. The $V_\pi$ of the modulator is the bias voltage required to go from minimum to maximum output on the MZ transfer function curve i.e. that voltage required to obtain a $\pi$ phase shift.

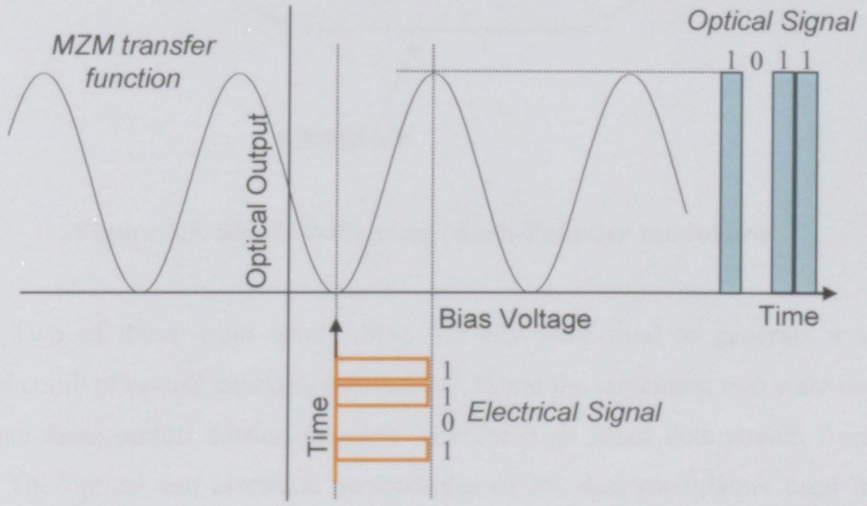



**Figure 3.2. Transfer Function of a typical MZ modulator.**

There are two main types of MZM, x-cut and z-cut, determined by the orientation of the crystal axis in the waveguide [77]. The CoWDM transmitter consisted of four single drive x-cut Avanex 40Gbit/s $LiNbO_3$-based, electro-optically controlled, MZI optical modulators. X-cut MZMs exhibit zero chirp, has better efficiency (lower $V_\pi$) and are easy to drive than z-cut modulators. The modulation is polarisation sensitive due to the polarisation dependence of the electrooptic effect and polarisation controllers were used to control the state of polarisation (SOP) at the input to the devices. Figure 3.3 below shows a schematic of an x-cut modulator, where the 'hot' electrode is placed between the waveguides and therefore induces and equal but

opposite phase shift in each branch thus producing zero chirp. In contrast a z-cut MZM (not shown) has its 'hot' electrode directly by one waveguide and induces a phase difference in that branch only, giving rise to chirp.

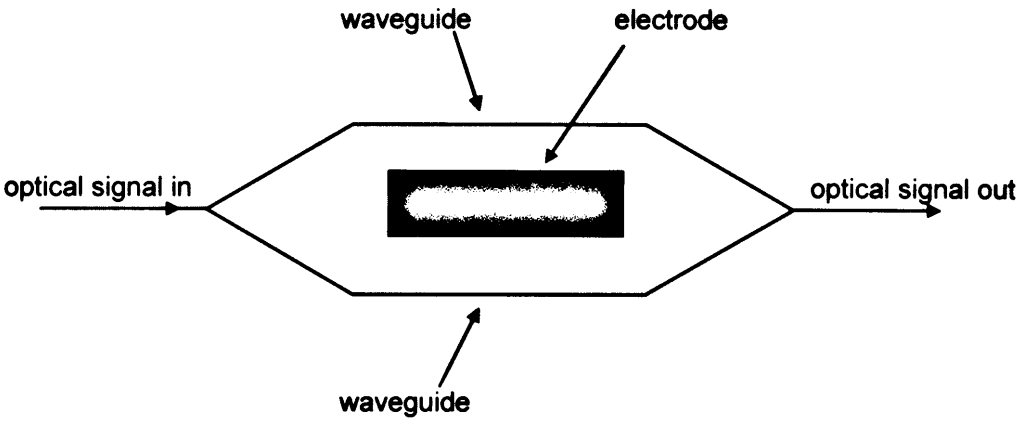



**Figure 3.3. Single drive x-cut Mach-Zehnder modulator**

Two of these x-cut single drive MZM's were used to generate a seven channel comb of optical channels (section 3.2.3) and the remaining two were used to modulate these optical carrier channels with the high speed data stream from the PPG. The optical and electrical performance of the data modulators used in the CoWDM experiments described later in the thesis was measured using the setup shown in figure 3.4. The MZM was driven by a 42.6 Gbit/s PRBS generated from the PPG via a DFF and RF amplifier. The unused output of the DFF was terminated using a 50 Ω terminator in order to avoid reflections which would affect the output data signal. This data signal was modulated onto a single carrier wavelength generated and amplified by a single distributed feedback (DFB) laser and an EDFA respectively. Polarisation controllers at the input to and output from the modulator ensured optimum performance. The modulated optical signal was converted to an electrical eye diagram using a high speed photodiode (PD) and was detected using a high speed oscilloscope.

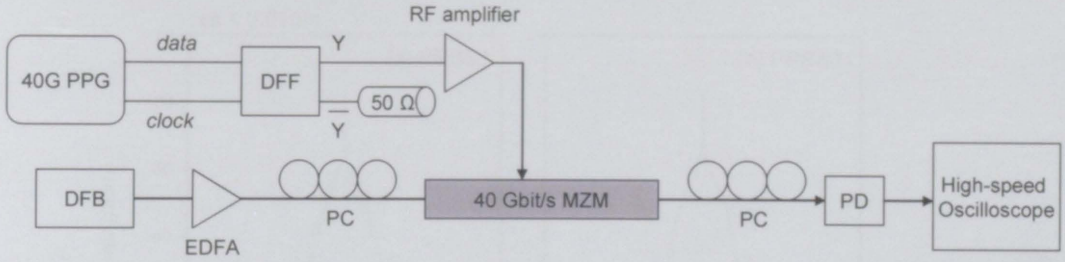
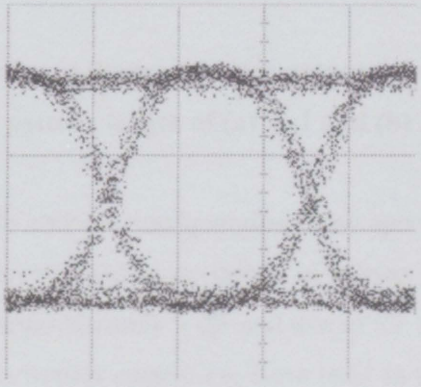



**Figure 3.4. Experimental setup to measure MZM performance**

The DC bias on the modulator and the polarisation was optimised to maximise eye opening. The measured eye at the output of the modulator is shown below in figure 3.5.



10 ps/division

**Figure 3.5. Eye diagram (42.6 Gbit/s) at output of MZM**

The optical spectrum at the output of the transmitter for a single NRZ channel modulated at 42.6 Gbit/s is shown in figure 3.6 below. The data pattern for spectrum (a) is a $2^7$-1 long PRBS, and in (b) the pattern length was increased to $2^{31}$-1. The effect of the shorter pattern data modulation on the spectrum is clearly visible on spectrum (a).

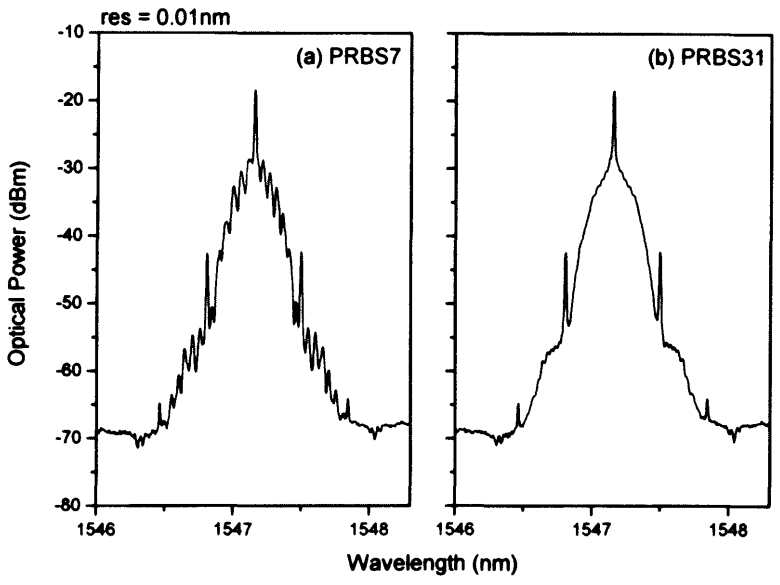



**Figure 3.6. Optical spectra at the transmitter output for 42.6 Gbit/s NRZ with PRBS pattern length of (a) $2^7$-1 and (b) $2^{31}$-1**

In the back-to-back single channel configuration these spectra are the input to the pre-amplified optical receiver which is described in section 3.3. The insertion loss of these modulators was approximately 5 dB and due to the fact that the devices are polarisation sensitive polarisation controllers were used to ensure optimum output power (described in the experimental setup in section 3.3.2). A pair of Versawave 40 Gbit/s GaAs electro-optic polarization modulators was also tested successfully in the comb generator, the details of which are discussed in section 3.3.4.

### 3.2.3 40 Gbit/s Pulsed Pattern Generator

The function of a pulsed pattern generator (PPG) in an optical transmitter is to generate a known electrical bit stream at a specific bit-rate, which can then be modulated onto the optical carrier. Many research optical testbeds rely on the external electrical multiplexing of a number of lower bit-rate tributaries (e.g. 4 x 10

Gbit/s) to generate a 40 Gbit/s data stream [78, 79, 80, 81]. In the majority of the work described in this thesis (section 5.3 being the exception) however a commercially available ANDO 40 Gbit/s PPG was used to generate a true 40 Gbit/s data signal of a pre-selected pattern length [82]. The ANDO PPG is composed of four primary sections as shown in the diagram below. These are connected to a central processing unit (CPU) and a power supply unit (PSU).

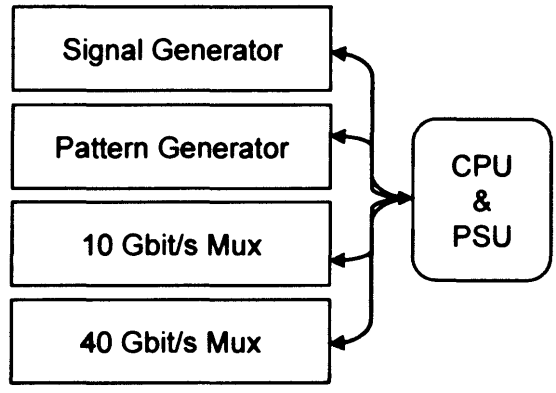



**Figure 3.7. Pulsed pattern generator sections**

The signal generator produces a clock signal in the frequency range 19.5 GHz to 22.5 GHz. The pattern generator section is capable of producing a range of data patterns of which the PRBS pattern was the most commonly used during this work. The 10 Gbit/s multiplexer generates 4 x 10 Gbit/s data streams for the output and 4 x 10 Gbit/s streams which are passed to the 40 Gbit/s multiplexer where they are time division multiplexed to produce a 40 Gbit/s data stream. Figure 3.8 shows (top) the 40 Gbit/s data-bar output and (bottom) the 40 GHz clock output from the PPG.

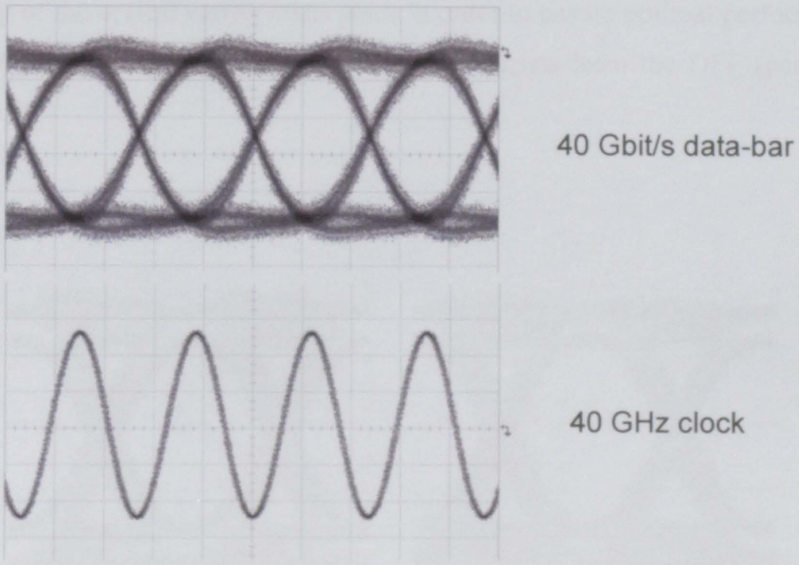



**Figure 3.8. (top) 40 Gbit/s data-bar, (bottom) 40 GHz clock signal**

The availability of this 40 Gbit/s data stream allowed us to perform evaluation of FEC codes (section 4.2) on the CoWDM system for the first time at the true 40 Gbit/s line rate. The PPG also provided a 40 GHz clock signal which was subsequently divided and distributed throughout the system to synchronise components such as the comb generator to the bit-rate.

### 3.2.2 D Flip-Flop and high speed RF Cables

A D flip-flop (DFF) is a relatively simple electrical device which has a data input and a clock signal input. The DFF has two outputs, one representing the data and one representing the inverted data. High speed DFFs are used in standard optical transmitters in order to retime and reduce waveform distortions of high speed RF data. This is necessary because high speed RF data (> 40Gbit/s) is susceptible to errors from a range of sources e.g. small bends in RF cables and high loss RF connections. In our experimental setup a 50 Gbit/s SHF DFF is used to retime the data signal from the PPG (shown in figure 3.8 in the previous section) before

modulating of the optical carrier takes place in order to ensure optimal performance. Figure 3.9 below shows both data and data-bar outputs from the DFF (pattern is PRBS $2^{31}$-1).

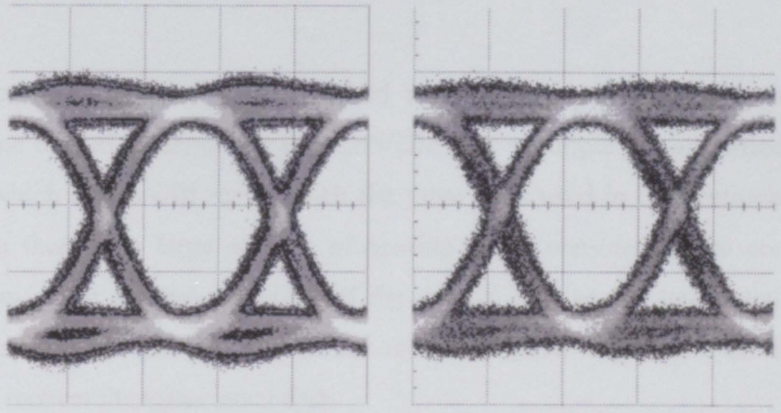



**Figure 3.9. 42.6 Gbit/s data and data-bar output electrical eye diagrams from DFF**

The peak-to-peak voltage for the data and data-bar DFF outputs was 685 mV and 663 mV and the peak-to-peak jitter was 6.2 ps and 5.1 ps respectively. These were both measured using a 70 GHz electrical head on a high speed oscilloscope. Both eyes are clearly open and these data signals were used to drive the data modulators described in the previous section. These signals were subsequently amplified by two commercially available RF drive amplifiers (SHF 824H, 26dB gain) in order to achieve an adequate signal for data modulation.

Another important consideration when designing high bit rate optical transmitters which rely on high speed RF data is the choice of RF cabling and connectors. We have seen that at high frequencies RF signals are subject to very high transmission impairments in copper cabling. Therefore in a research lab environment it becomes essential to optimise the distance and media through which high speed RF signals travel. In order to achieve this short cables with a very good frequency response at high frequencies were used to transmit the high speed RF

signals in the system, for example from the PPG to the external DFF and to the drive amplifiers in the data encoding section.

## *3.3 Standard High Bit Rate WDM Receiver*

This section looks in detail at the standard WDM receiver configuration for use in high bit rate optical systems. In fact CoWDM uses a simple pre-amplified optical receiver, which as we will see is much the same as is used in conventional WDM systems so there is a large amount of overlap when considering the constituent components. The primary function of the optical receiver in traditional optical communication systems is to convert the received optical signal into an electrical one and to recover the transmitted data.

### 3.3.1 Experimental Setup

A schematic of the pre-amplified receiver is presented in figure 3.10. A typical optical receiver in a WDM system will use at least one optical filter in order to select the target channel from the received spectrum. These WDM systems, especially at high bit rates have approximately 100 GHz spacing between the channels and therefore a simple bandpass filter can be used to select the target channel. As will be outlined in section 3.7 the optimum filter configuration for use with 42.6 Gbit/s CoWDM consisted of a tuneable 0.64 nm bandpass filter to select the target channel and an 85.2 GHz FSR AMZI to cancel the crosstalk from adjacent channels. In figure 3.10 the AMZI is surrounded by a dashed box indicating it is only required in the receiver when CoWDM is the transmission format in use. This is the only additional level of complexity required in the receiver when moving from standard WDM to CoWDM.

Two low noise-figure (< 6 dB) EDFAs, with output powers of 1 mW (gain = 34 dB) and 23 dBm (gain = 38 dB) respectively, were used in the receiver to amplify

the received signal. A pair of variable optical attenuators (VOA) enabled full control of the optical power incident on the amplifiers and on the high speed photodiode used to convert the optical signal to its electrical equivalent. The power meter (PM) positioned after the first VOA was used to monitor the optical power on the receiver.

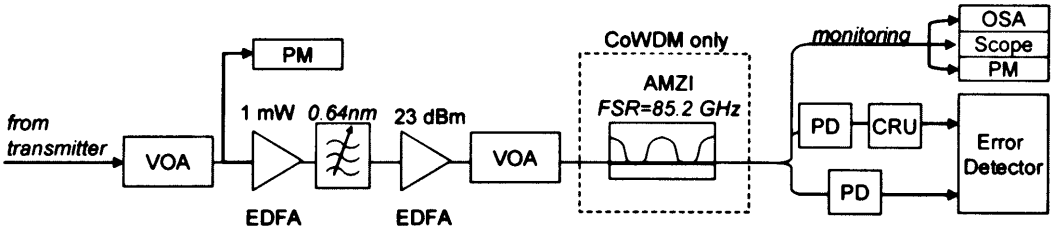



**Figure 3.10. Pre-amplified optical receiver configuration**

A series of optical taps were placed after the VOA to allow for real-time monitoring of the received optical spectrum, received optical eye and optical power incident on the photodiode.

The performance of an optical receiver can be determined by measuring the BER as a function of the average optical power incident on the receiver. The 'receiver sensitivity' is then defined as the minimum average optical power at a BER of $10^{-9}$.and is typically measured in dBm. Throughout the course of this work receiver sensitivity was used to determine the performance of the system. If we consider a pre-amplified optical receiver which is dominated by amplifier noise the receiver sensitivity ($P_{rec}$) can be defined in empirical terms by equation 3.1 which considers the noise figure of the amplifier ($NF$) in dBs, and the bit rate ($B$) in b/s [83]

$$P_{rec} = NF + 10\log_{10}(B) - 143 \tag{3.1}$$

where $NF = 3$ dB for a quantum limited amplifier. Figure 3.11 below shows a plot of receiver sensitivity as a function of bit rate for an optical receiver using (i) a very

good EDFA with a low NF of 3 dB (squares) and (ii) the EDFA which was used in our receiver which had a NF = 5.2 dB (circles).

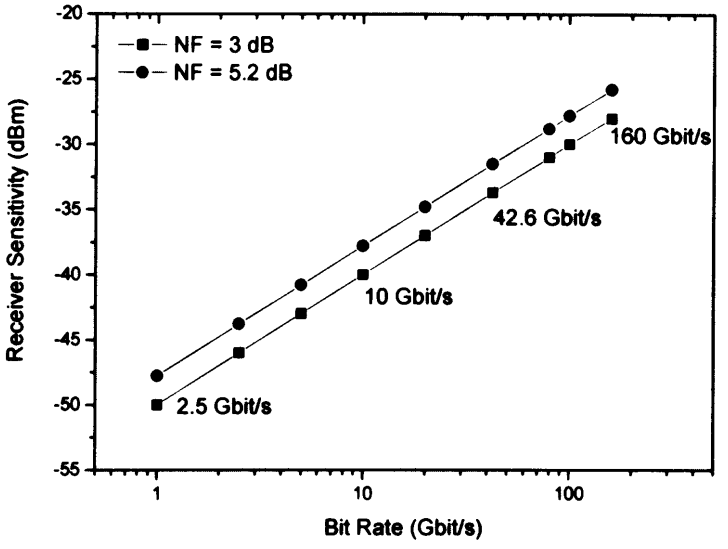



**Figure 3.11. Theoretical receiver sensitivity limit as a function of bit rate for receiver with EDFA NF = 3 dB (squares) and EDFA = 5.2 dB (circles)**

For a single 42.6 Gbit/s NRZ (PRBS $2^7$-1) channel the receiver sensitivity of the experimental receiver described above was approximately -30.6 dBm. This is approximately 3.1 dB away from the limit when using a very low NF EDFA and approximately 0.9 dB away from the limit when considering the actual EDFA used in our receiver. The single channel received spectrum for both pattern lengths ($2^7$-1 and $2^{31}$-1) was measured by an OSA with 0.01 nm resolution and is shown in figure 3.12 below. The centre wavelength is at 1546.9 nm and the effect of the $2^7$-1 PRBS pattern on the spectrum is clearly visible. The suppressed sidebands arise from the presence of ASE from the amplifiers in the spectrum which is passes through the AMZI. The slight unevenness in the sidebands is a result of the shape of the ASE profile of the system.

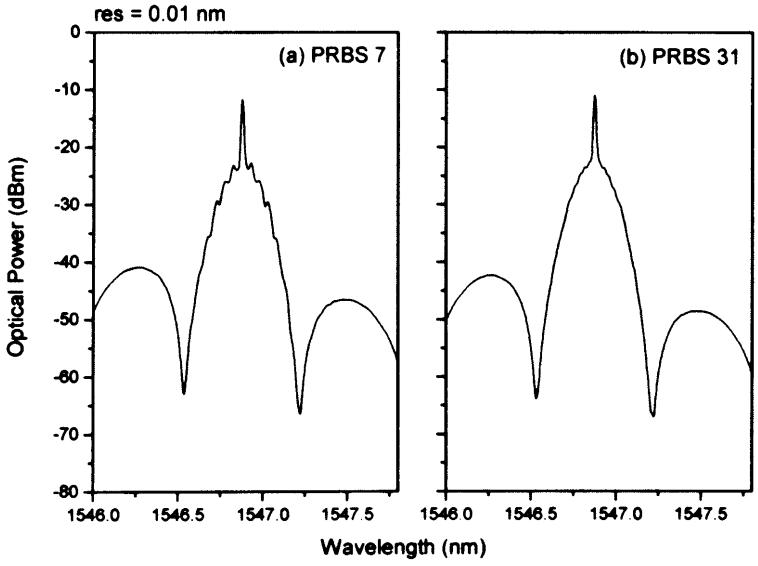



**Figure 3.12. Received optical spectrum for a single NRZ 42.6 Gbit/s channel**

The receiver sensitivity curve for single channel operation both with and without the AMZI and the corresponding eye diagram with the AMZI at the receiver is shown in figure 3.13 below. The eye diagram is shown on a 10 ps/division grid and the width of the eye is approximately 23 ps. As expected for single channel operation there is no sign of an error floor in either of the receiver sensitivity curves.

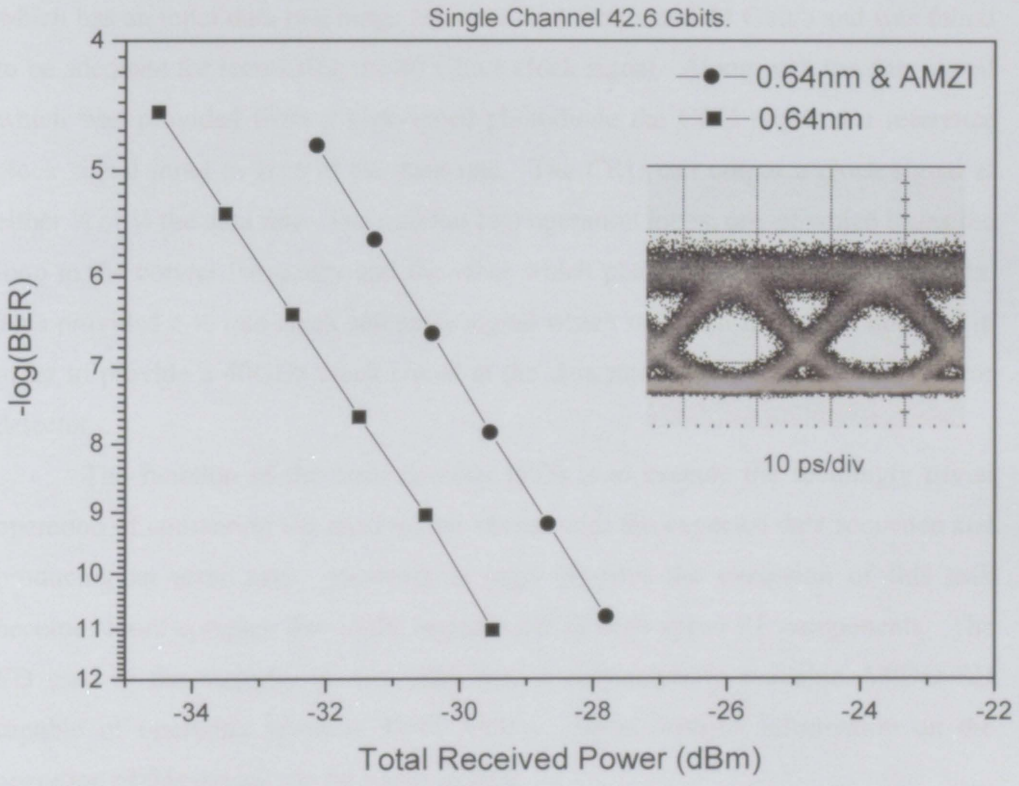



**Figure 3.13. Receiver sensitivity curve and received eye diagram (inset) for a single back-to-back 42.6 Gbit/s channel without (squares) and with (circles) an AMZI. Pattern length = $2^{31}$-1**

The receiver sensitivity value for without and with the AMZI in the receiver are -30.6 and -28.6 respectively. The 2 dB penalty is due to the additional filtering effect which the AMZI has on the signal.

### 3.3.2 Clock Recovery and Error Detection

The purpose of the clock recovery unit (CRU) in an optical receiver is to provide a spectral component at a frequency equal to the bit-rate of the received signal in order to help synchronize the decision process [82]. The CRU employed in



University College Library Cork

the CoWDM receiver was a commercially available Centellax 40 Gbit/s SiGe CRU which has an input data rate range between 39.8 Gbit/s and 44 Gbit/s and was found to be adequate for recovering the 40 Gbit/s clock signal. Along with the data signal which was provided from a high-speed photodiode the CRU required a reference clock signal input at 1/16 of the data rate. The CRU can output a clock signal at either ½ or ¼ the data rate. The unit has two operation loops, one of which trains the loop to the correct frequency and the other which phase locks the loop to the data. This provided a ½ rate clock reference signal which was then frequency doubled in order to provide a 40GHz clock signal at the data rate to the Ando 40 Gbit/s error detector.

The function of the error detector (ED) is to execute the seemingly trivial operation of comparing the received bit stream with the expected data sequence and producing an error rate. However at high bit-rates the execution of this task becomes more complex due to the requirement of high speed RF components. The ED used in the majority of this work was a commercially available ANDO ED capable of operating between 40-43 Gbit/s. More detailed information on the operation of this device can be found in [80].

Error rate information from the ED can be presented in a number of ways. One of the most common of these as described earlier is to use 'receiver sensitivity' curves which gives a performance measure of an optical receiver and is defined as the minimum received power incident on the receiver for a measured BER of $10^{-9}$. In the following chapters the performance of various implementations of the CoWDM transmission system will often be presented by showing BER as a function of received power.

## 3.4 Optical Comb Generation [84]

In the traditional WDM system outlined in Chapter 2 we have seen that the optical channels which carry the data are generated by individual DFB lasers that are typically spaced by of the order of 100 GHz. These individual lasers have random phases which lead to random interference signals at low channel spacing. However as we have seen for CoWDM it is necessary to have a set of optical channels which are spaced by a specific frequency (equal to the bit rate) and that have a stable inter-channel phase relationship. It is also desirable (especially in a research lab environment) to reduce the inventory required to generate the optical channels. As a result multi-wavelength generation (also called multi-frequency or comb generation) was employed as the wavelength source for CoWDM. This section gives brief overview of the applications of optical combs, considers some of the well known comb generation techniques and describes in detail the method which we used to generate a phase locked optical comb for use with CoWDM.

There are a large range of applications (in addition to CoWDM) in photonics technology for optical combs and much of the published work on comb generation techniques has been carried out with these applications in mind. For example, in optical communications ultra-dense wavelength division multiplexing (UD-WDM) uses tightly spaced optical channels (<50 GHz spacing) generated from spectrally sliced optical combs to transmit data in both access and long-haul networks requiring large channel counts. Zeller et al suggested that optical combs generated from mode-locked lasers are suitable sources for test and measurement of DWDM systems [85]. Optical combs are also finding application in the microwave regime where they have been used to implement photonic microwave filters [86], and the frequency up-shifting of arbitrary microwave waveforms [87], where tunability is a key parameter.

A wide variety of techniques have been described in order to generate these optical combs, each resulting in a comb with different properties. Six of these reported techniques are summarised in table 3.1 below. Some of the key

characteristics of an optical comb such as the spacing between channels, the number of channels produced and the spectral width of the comb signal are also listed.

| | | | | |
|---|---|---|---|---|
| (1) Mode locked laser | 50 GHz | >100 | 43 nm | 84 |
| (2) Fibre ring laser | 10.6 GHz | 8 | 1.8 nm | 87 |
| (3) Mode locked semiconductor laser | 100 GHz | 7 | 6 nm | 88 |
| (4) Self-oscillating phase modulator | 9.95 GHz | 13 | 0.91 nm | 89 |
| (5) Amplitude modulator and HNLF | 12.5 GHz | >1000 | 100 nm | 90 |
| (6) Cascaded MZM and phase modulator | 12.5GHz | 9 | 0.75 nm | 92 |
| (7) Cascaded amplitude modulators | 42.6GHz | 11 | 3.3 nm | 83 |

**Table 3.1. Comb generation techniques**

(1, 2 and 3) The use of amplitude or frequency modulated (FM) mode-locked lasers (such as ERGO (Er:Yb:glass laser oscillator) lasers [84], fibre ring lasers [88], or mode-locked semiconductor lasers [89]), give good OSNR values, and the range of channel spacing achievable is suitable for WDM applications (10 – 100 GHz). However these techniques rely on precise control of the laser cavity length and an amount of optical fibre to which adds to the complexity of the experimental setup. For example in [84] a piece of dispersion compensating fibre (DCF) and 50 m of highly nonlinear photonic crystal fibre (HNLF) is needed to generate a 43 nm wide set of 50 GHz spaced channels whilst in [86] a combination of SMF and erbium doped fibre (EDF) is required to generated an 8 channel optical comb. Additional complexity is also a feature of these techniques due to the difficulty in starting and maintaining suitable mode-locking, a problem arising from the inherent multi-mode optical cavities and therefore multiple stabilities, of mode-locked lasers.

(4) This technique employs a wideband $LiNbO_3$ phase modulator in self-oscillating mode [90] i.e. the modulator is driven with a feedback signal from its output, which makes oscillation easier to start and maintain than mode-locked lasers because it is essentially a single-mode oscillator at a microwave frequency and results in a 13 channel optical comb with 9.95 GHz channel spacing. The drawbacks of this method are that it requires large RF power amplifiers (~30 dBm input RF power required) with precise control of the output voltage for the feedback loop, in addition

to an extra photodiode and RF filters the optical feedback signal and select the appropriate RF content respectively.

(5) A section of specialised fibre (in this case polarisation-maintaining dispersion flattened dispersion-decreasing supercontinuum (SC)) is again used in [91] together with an amplitude modulator in order to generate a SC source based on optical pulse compression of more than 1000 frequency spaced optical channels with 12.5 GHz spacing. These channels span most of the C-band and such a source would be suitable for UD-WDM systems as has been demonstrated in [92]. However, the scalability of such combs to higher bit rates may not be easy due to spectral broadening of the optical channels which would lead to increased interchannel interference. In addition to this limitations to this scheme include the requirement of high optical launch powers, long specialised fibre lengths and stimulated Brillouin scattering (SBS) suppression. For most applications such a large number of channels is undesired and appropriate filtering is necessary which affects the overall power efficiency of the generator.

(6) Finally in [93] an assembly consisting of a concatenated Mach-Zehnder (MZ) and phase modulator was used to generate a uniform (< 3dB flatness) optical comb of 9 channels separated by 12.5 GHz. This technique is similar to the one eventually employed as a comb generator in our experimental setup but requires the use of large drive voltage amplifiers and precise control of the applied voltage. In addition its poor side mode suppression ratio (SMSR) of approximately 3 dB could lead to unwanted interchannel crosstalk affecting the channels furthest from the centre wavelength.

The comb generation technique which was employed for use with CoWDM in this work was based on a pair of cascaded amplitude modulators. In the following subsections we present an analysis of the production a phase locked optical comb using this technique. We also demonstrate a practical implementation of the scheme, where a 7 channel, 298 GHz bandwidth comb is generated using two Avanex 40 Gbit/s intensity modulators. It is shown that the additional tuning freedom offered by replacing the phase modulator described in [92] by a second amplitude modulator allows excellent flatness (<1 dB) and high SMSR values (>12

dB) without the need to precisely tune RF amplitudes. This method of optical comb generation is used throughout the experimental sections as the optical channel source for CoWDM. An enhancement to this technique is described in the final section where we replace the Avanex modulators with two Versawave electro-optic polarization modulators which enable an 11 channel comb resulting in an increased overall bandwidth of 468.6 (11 x 42.6 GHz) GHz with a flatness of less than 2 dB and SMSR values above 12 dB. This increased channel count is due to the combination of a wideband frequency response and low $V_\pi$ of the electro-optic polarisation modulators.

### 3.4.1 Comb Generation Theory

The proposed comb generation module is shown in figure 3.14, and comprises a single DFB laser source at 1546.8nm, and two sine wave driven balanced 40 Gbit/s amplitude modulators.

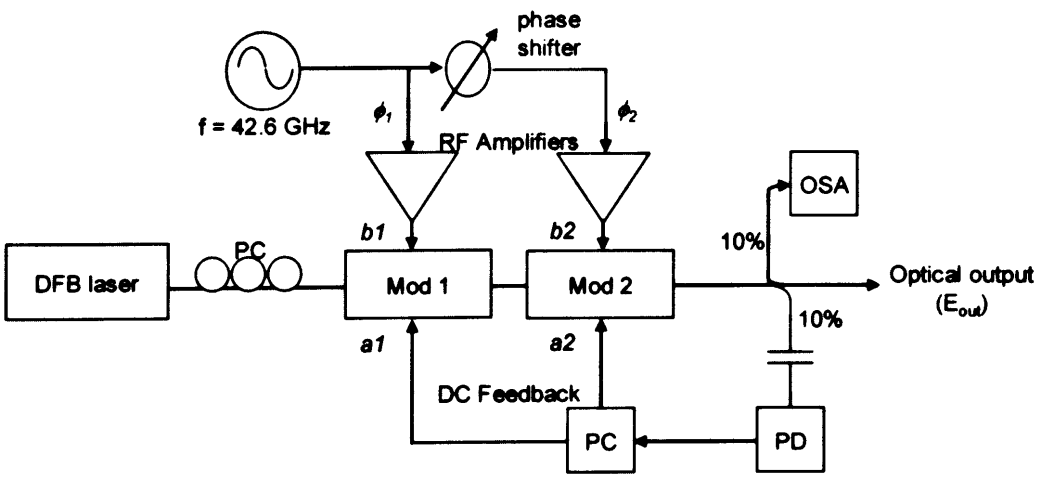



**Figure 3.14. Schematic diagram of comb generator experimental configuration**

It is well known that for a continuous wave input with frequency $f_0$, amplitude $E_0$ and phase $\phi_{in}$, the output optical field $E_k$ of the $k^{th}$ modulator can be represented as a series of harmonic frequency components $f_0+pf$ where $f_0$ is the optical carrier frequency, $f$ is the frequency of the sine wave drive, and $p$ represents the harmonic number, $p \in \{0, \pm 1, \pm 2, ...\}$ [94]. The total field $E_k$ is given by

$$E_k = |E_0| \sum_p \varepsilon_p \tag{3.2}$$

where

$$\varepsilon_p = A_{p,k} cos\left[2\pi(f_0 + pf)t + \theta_{p,k}\right] \tag{3.3}$$

and the amplitudes $A_{p,k}$ and phases $\theta_{p,k}$ of the components are given by

$$A_{p,k} = \frac{1}{2} cos[(a_k + p)\frac{\pi}{2}] J_p(\frac{b_k \pi}{4}) \tag{3.4}$$

$$\theta_{p,k} = [1 + p + (-1)^p]\frac{\pi}{2} + p\phi_k + \phi_{in} \tag{3.5}$$

In both equations, $a_k$, $b_k$ and $\phi_k$ represent the DC offset, peak-to-peak amplitude, and phase of the drive signal of the $k^{th}$ modulator respectively, and $J_p$ is the Bessel function of the first kind of order $p$.

By considering each component generated from the first modulator as a CW input to the second, and summing all of the terms which result in an output from the second modulator at a given harmonic frequency component $f_0+qf$ we obtain the total output field ($E_{out}$) from the second modulator. Assuming, without loss of generality, that this results in a total output field ($E_{out}$) of

$$E_{out} = |E_0| \sum_q \varepsilon_q' \tag{3.6}$$

It can be shown that

$$\varepsilon_q' = \frac{1}{2} \sum_p A_{p,1} \left\{ \left[ (-1)^{2p-q} A_{p-q,2} + (-1)^q A_{q-p,2} \right] \cos\left[ 2\pi (f_0 + qf)t + q\frac{\pi}{2} + (q-p)\phi_2 \right] \right\} \tag{3.7}$$

We can see from equations 3.4 and 3.5 respectively that the RF amplitudes ($b_{1,2}$), DC bias ($a_{1,2}$) and relative phase difference ($\phi_2$-$\phi_1$) between the RF drive signals may be used to control the relative amplitudes of each comb line, giving excellent control of the profile of the generated comb signal. In particular, we may use these five variables to solve a set of five simultaneous equations matching the amplitudes of the first five harmonics to the central carrier component ($\varepsilon_0 = \varepsilon_q$, $q=0, 1, 2, 3, 4, 5$). Given the inherent symmetry of the system $\varepsilon_q = \varepsilon_{-q}$ this implies that ideally an 11 channels comb could be generated with 0 dB power variation. Note that, if one of the amplitude modulators is replaced by a phase modulator [95], the cosine term, along with the term $(-1)^p$ is omitted from equation 3.4 and 3.5 respectively, thus reducing by one the number of control parameters available which results in a reduction of the number of flat comb lines to 9.

Figure 3.15 illustrates, for various numbers of comb lines, the calculated power variation (flatness) of the side-bands when the same RF power ($b_k$) is applied to both modulators simultaneously and the RF phase and DC biases are optimised for each point. Under these restrictive conditions negligible power variation is obtained for up to 11 comb lines, whilst a flatness of less than 2 dB is obtained for up to 13 comb lines. It is interesting to note that total bandwidths of close to or above 0.5 THz can be obtained with this method whilst maintaining a good flatness and that by tuning the RF amplitude to between 4.37 and 4.45 $V_\pi$ an optimum flatness value may be achieved.

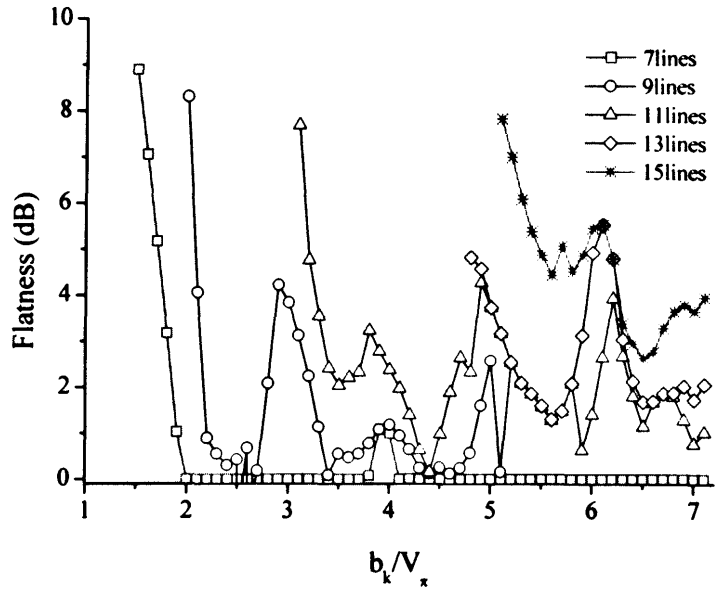



**Figure 3.15. Optimised comb flatness versus relative drive amplifier amplitude for 7 (squares), 9 (circles), 11 (triangles), 13 (diamonds) and 15 (star) comb lines**

A more detailed analysis of the impact of the RF amplitudes on flatness for a comb of 7, 9, 11 and 13 lines is shown in figure 3.16(a), (b), (c) and (d) respectively. In this case, $b_k$ was set independently for each modulator, while the DC biases and relative optical phases were optimised. In the 7 line case shown in figure 3.16(a) we can see there are a wide range of voltages which result in a flatness below 1 dB. As we move to higher numbers of comb lines this range of voltages decreases significantly and for 13 lines very high drive voltages are required to obtain flatness approaching 1 dB. For 11 lines, it is clear that whilst voltages above 3.5 $V_\pi$ are necessary in order to achieve good flatness, values of less than 1 dB are possible for a wide range of drive voltages, eliminating the need for controlled drive amplitudes, suggesting that the comb can be controlled by $a_1$, $a_2$ and $\phi_2$ alone. For target drive voltage values of around 4.5 $V_\pi$, an almost ideal flatness of 0 dB may be obtained, again with a reasonable tolerance to the drive signal amplitudes.

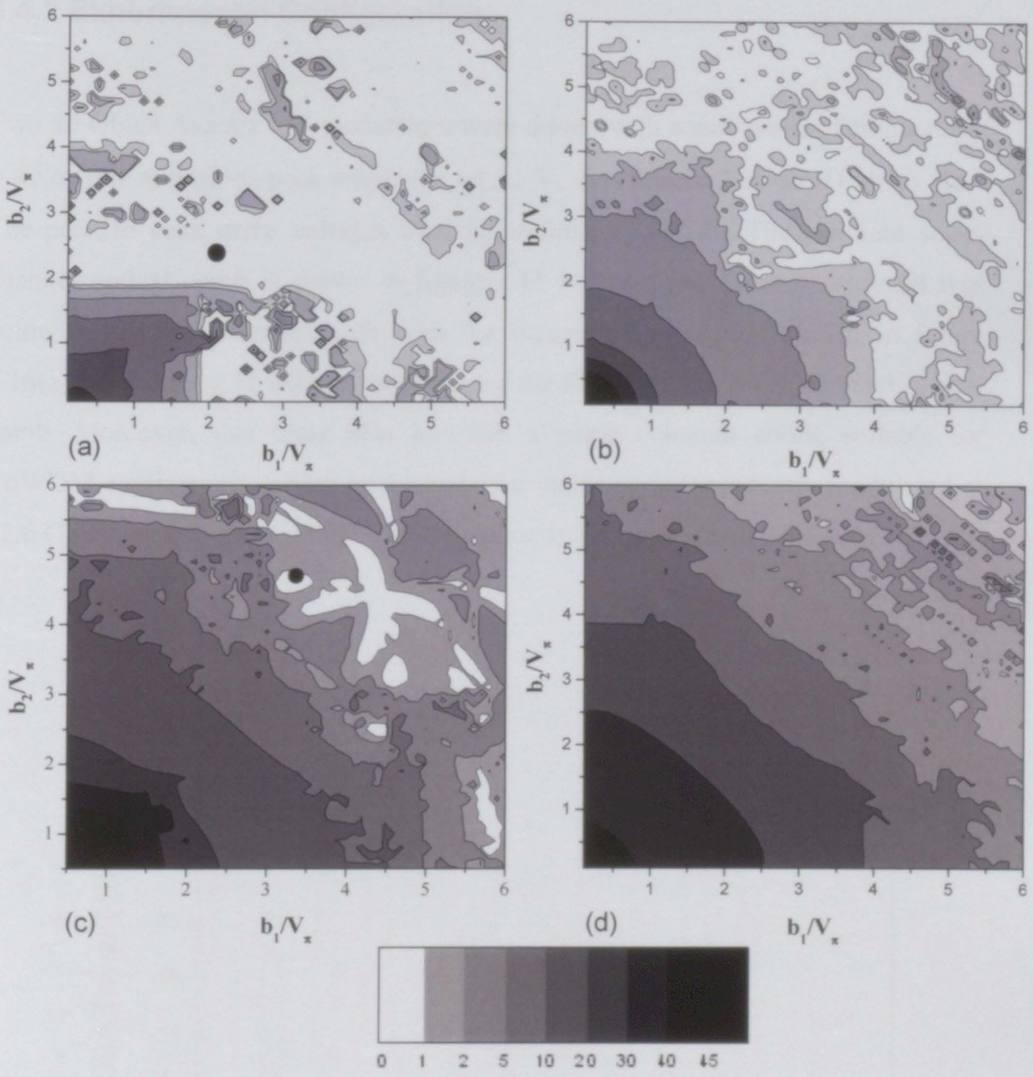



**Figure 3.16. Optimised comb flatness versus drive voltage applied to each modulator for (a) 7 (b) 9 (c) 11 and (d) 13 lines**

The point marked with a circle on figure 3.16(c) represents the experimental operating position for figure 3.21, with a flatness of less than 2 dB. For the 7 channel comb shown in figure 3.17 the experimental operating position is marked by the circle in figure 3.16(a)

### 3.4.2 Experimental Configuration

Two 40 Gbit/s Avanex MZ modulators were driven with a sine wave of frequency $f$ = 42.6 GHz at peak-to-peak amplitude of 2.1 $V_\pi$ synchronised by an RF delay line. The peak to peak drive voltages were approximately 30 V. The resultant seven channel optical comb is shown in figure 3.17 below. The flatness achieved was below 1 dB which agrees well with the theoretical prediction shown in figure 3.16(a). A value of 11 dB was obtained for the SMSR of the seven channel optical comb. Moreover, this setup also provides a phase coherent comb, suitable for CoWDM applications, where each comb line could be independently modulated at 42.6 Gbit/s, enabling almost 0.3 Tbit/s of capacity using only one DFB laser.

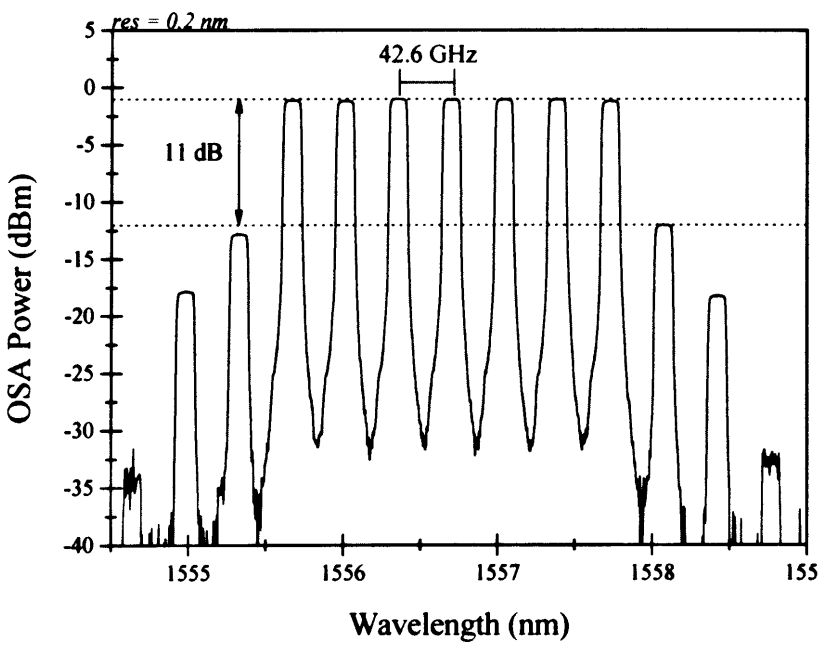



**Figure 3.17. Experimental spectrum of a 7 channel optical comb**

Figure 3.18 below shows the simulated and experimental patterns when the comb signal is detected on a high speed oscilloscope using a 50 GHz bandwidth

photodiode. The experimental trace exhibits a certain amount of noise compared to the simulated result but the shape of the traces is similar.

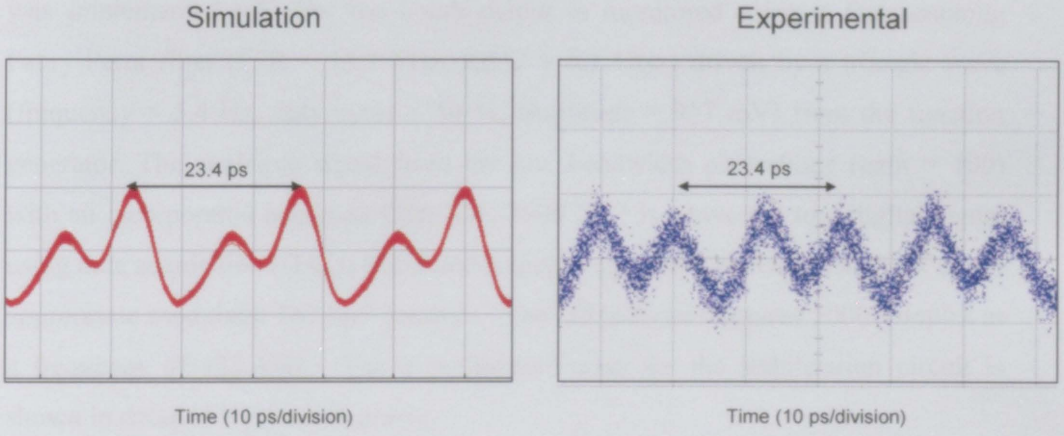



**Figure 3.18. (a) Simulated and (b) Experimental scope traces for a seven channel phase locked optical comb**

Because of the narrow bandwidth of the photodiode only the neighbour channels are detected on the scope and the high frequency components of these parts of the signal result in the RZ-type pulses which appear on the scope. The period of the signal on the scope is approximately 23 ps which is in agreement with the 42.6 GHz sine wave used to generate the comb signal. The apparent time reversal between the simulated trace and the experimental version is due to the particular phase of the comb signal.

### 3.4.3 Comb Stabilisation

As with all applications of amplitude modulators, a degree of feedback control is necessary in order to compensate for thermally induced bias point and RF power level drifts. Observing from equation. 3.2 and 3.3 that, $a_k$ and $b_k$, only appear in $A_{p,k}$, and that they are independent, so small changes in one are likely to be able to be compensated for by small changes in the other, in certain circumstances. Regions where these circumstances exist are correspond to regions in figure 3.16 ($a_1$, $a_2$

optimized) where the variation of flatness with $b_1$, $b_2$ is low. Consequently the amplitudes of the comb lines generated by the modulators may be effectively controlled by the DC bias values of the modulators and a simple stabilisation circuit was implemented whereby the comb output is monitored using a fast scanning Fabry-Perot filter (FSR = 13.7 THz, RBW = 6.1 GHz) driven by a triangle wave (frequency = 5.4 Hz, duty cycle = 50 %, amplitude = 957 mV) from the function generator. The analogue signal from the low bandwidth photodiode (gain = 100) with an incorporated bandpass filter (DC-3000 Hz ) is converted to a digital signal using data acquisition (DAQ) board and a simple algorithm provides feedback to the appropriate modulator DC bias controls. The DAQ board acquires 5000 samples at a frequency of 125 kHz. The experimental setup for the stabilization circuit is shown in detail in figure 3.19 below.

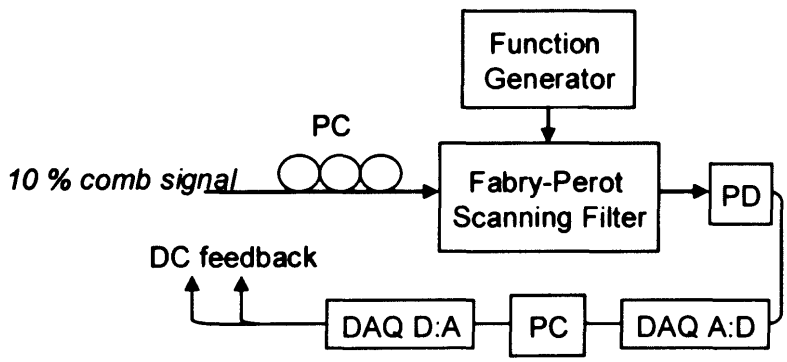



**Figure 3.19. Experimental configuration of comb stabilisation circuit**

With the stabilisation circuit turned on a constant comb flatness of less than 1 dB was achievable over a period of several hours as is demonstrated in the FEC section in chapter 4. The algorithm used to control the DC bias values of the modulators is shown in figure 3.20 below. The algorithm is designed for use with a 7 channel optical comb. If the phase term is correct the optical comb will be in one of the four positions depicted by the insets in figure 3.20. By adjusting the DC bias of the appropriate modulator the comb can be effectively flattened. In each iteration the DC bias of one of the comb modulators is adjusted. The comb modulator which is

adjusted is determined by whether the difference between average amplitudes of comb lines (-3, -1, +1, +3) and comb lines (-2, 0, +2) is greater than or less than the difference between the average amplitudes of comb lines (-2, 0, +2) and comb line (0). The DC bias is then adjusted by an amount proportional to a gain control factor.

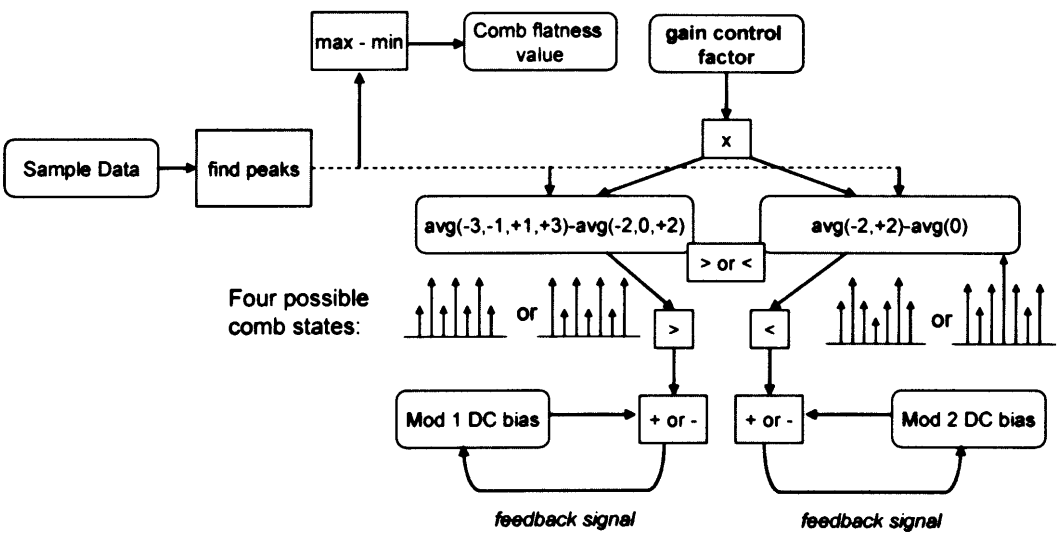



**Figure 3.20. Algorithm for comb stabilisation of a seven channel comb. Inset: Four possible states for a 7 channel optical comb**

### 3.4.4 Enhanced Comb Generator [96]

We have shown in figure 3.16(c) in section 3.3.2 that in theory for the case of 11 comb lines there is a range of voltages above 3.5 $V_\pi$ which result in a flatness of less than 1 dB. By using two 40 Gbit/s Versawave electro-optic polarisation modulators which were driven with the same sine wave at a frequency of 42.6 GHz, but with amplitudes $b_1$ = 3.36 $V_\pi$ and $b_2$ = 4.70 $V_\pi$, synchronised by an RF delay line. The Versawave modulators were based on GaAs polarisation mode converters, with low $V_\pi$ (3.3 V and 3.7 V at 20 GHz), low insertion loss (4.3 dB and 6.0 dB), and 3 dB bandwidths of 31 GHz and 49 GHz respectively. The combination of a wideband frequency response and low $V_\pi$ enables a significant increase in the number of

generated comb lines without an increase in RF power levels in comparison to typical $LiNbO_3$ based MZ modulators. The low drive voltage of the GaAs mode converter results from the tight mode confinement that is possible with etched semiconductor waveguides, while the high bandwidth results from low-loss, velocity matched slow-wave electrodes [97]. A further advantage of GaAs over $LiNbO_3$ for high-power applications is that GaAs has much higher thermal conductivity (55 vs. 5.6 $Wm^{-1}K^{-1}$), potentially increasing the reliability during high power operation. This configuration yields a compact and square-shaped-like 11 channel optical comb, as shown in figure 3.21.

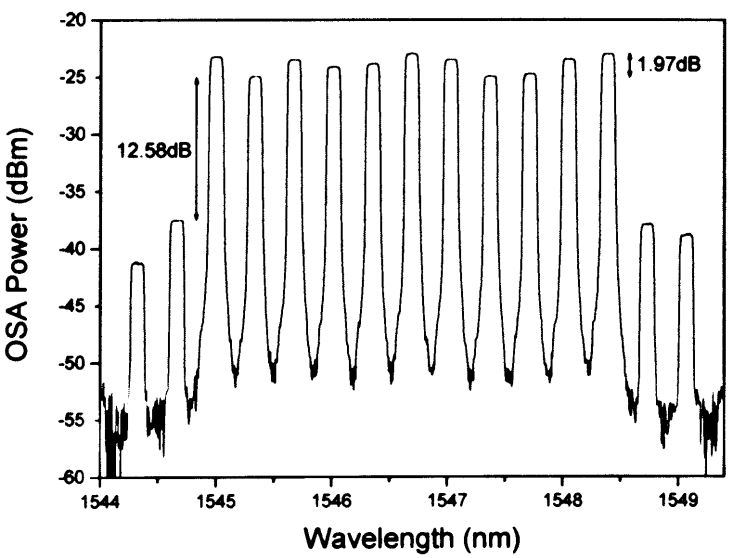



**Figure 3.21. Experimental spectrum of an 11 channel optical comb**

The flatness achieved was 1.97 dB which is higher than the theoretical prediction from figure 3.16(c) of less than 1dB. We believe this is due to features of the experimental setup such as the large amount of fibre between the two modulators which causes the optical phase to drift slightly more than in the seven channel case where we had a short piece of fibre between the two Avanex modulators. A value of 12.6 dB was obtained for the SMSR of the optical comb; representing a 1.6 dB improvement over the seven channel $LiNbO_3$ based MZ solution. This setup also

provides a phase coherent comb, suitable for CoWDM applications, where each comb line could be independently modulated at 42.6 Gbit/s, and would therefore enable almost 0.5 Tbit/s of capacity using only one DFB laser, which would represent a 0.2 Tbit/s enhancement per laser over the 7 channel comb generator.

## *3.5 CoWDM Transmitter Configuration*

In the context of a fibre based optical communication system the role of the optical transmitter is to convert an electrical data signal to an optical signal and to launch it into the transmission fibre. Earlier in the chapter the operation of a standard high bit rate optical WDM transmitter was described with particular emphasis on the major constituent components such as the MZM's, the PPG and the DFF. In this section the concept of an optical transmitter is expanded to consider and describe the implementation of a CoWDM transmitter. Essentially the CoWDM transmitter is a fibre based interferometer with a MZ data modulator on each arm, and pairs of delay lines to enable full control of the relative optical phase relationship between the arms.

### 3.5.1 CoWDM Transmitter Overview

This section is concerned with the experimental implementation of the CoWDM transmitter. As discussed in chapter 2 CoWDM is based on controlling the optical phase difference between adjacent optical channels in order to create a deterministic interference signal which can then be controlled. The input signal for the CoWDM transmitter was the 7 channel phase coherent optical comb derived from the optical comb generator described in section 3.3 via a 27 dBm output power EDFA. In an ideal transmitter implementation each of the optical channels would be separated by an arrayed waveguide grating (AWG) and independently encoded in a phase preserving modulator array before being wavelength multiplexed at the output of the transmitter as depicted in figure 3.22 (a). The experimental setup shown in figure

3.22 below shows how the transmitter was implemented in the lab. Instead of an AWG a double stage thin film filter (DS TFF) with a FSR of 85.2 GHz which gave good extinction ratio (~45 dB) and had a square shaped transfer function was employed to separate the odd and even optical channels, which were then encoded with NRZ data and data-bar patterns at the bit rate of the PPG (42.6 Gbit/s in this case) in a two modulator array.

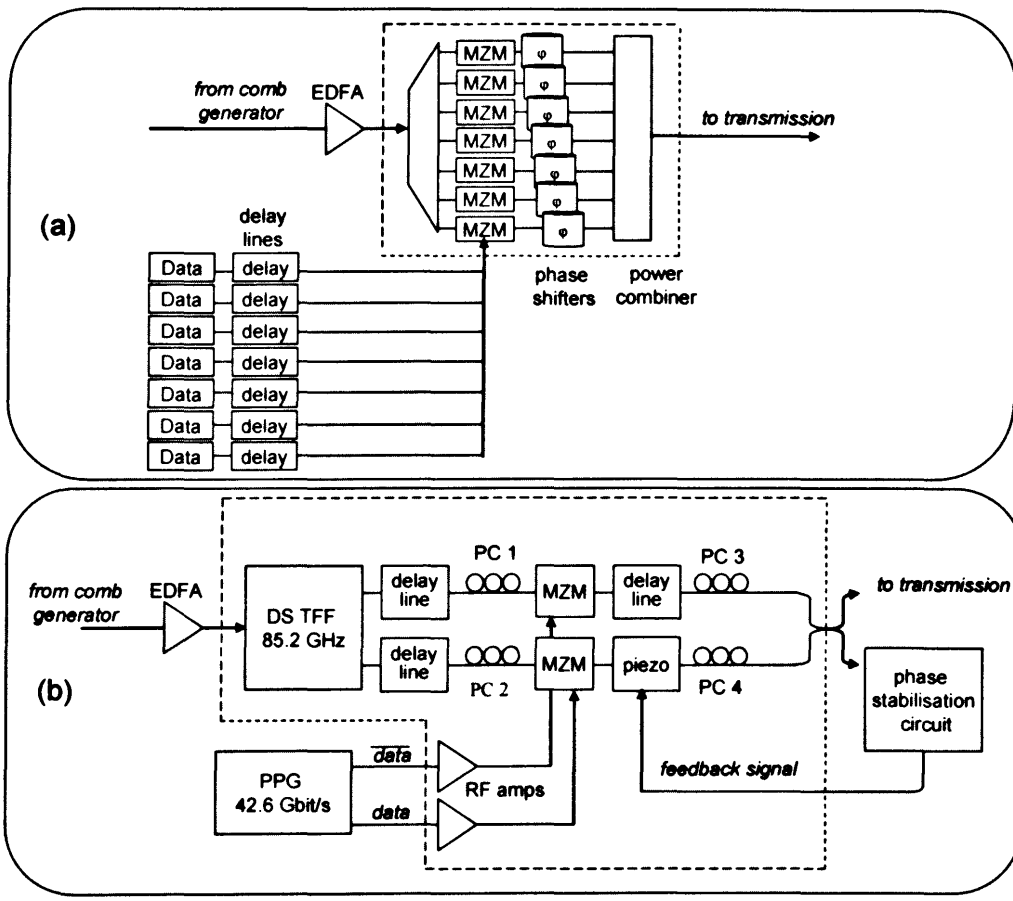



**Figure 3.22. (a) Ideal and (b) experimental CoWDM transmitter**

This method of data encoding represents a 'worst case' scenario as it permits the inclusion of the dominant crosstalk from adjacent channels, since any target channels 'nearest neighbours' after the demultiplexing filter in the receiver have been encoded with the same data sequence. Three optical delay lines and a piezo

fibre stretcher enabled the optimization of the data time delays and optical phases, the detail of which is contained in the next section. A pair of input polarisation controllers (PC) were used to control the state of polarisation of the signals before the polarisation sensitive data modulators. The odd and even channels were passively multiplexed at the output of the transmitter using a fibre coupler.

The output of the transmitter was split, with 90 % going to the transmission fibre and the remainder used as an input to the phase stabilisation circuit, the operation of which is described in detail in section 3.6. The CoWDM transmitter in the form shown in figure 3.22 was essentially a fibre interferometer. The optical fibre within the transmitter was highly sensitive to mechanical vibrations and temperature fluctuations. In order to negate the effects of this the CoWDM transmitter (inside the dashed lines in figure 3.22) was assembled and housed in a purpose built aluminium case and placed on an air-table during most of the experimental work.

### 3.5.2 CoWDM Transmitter Alignment

In the CoWDM transmitter we have seen that when the bit rate of the system and the frequency driving the comb generator are equal a stable interference signal is generated. The CoWDM simulations presented in chapter 2 showed that by time aligning the contributions from the interfering neighbour channels such that the optimum interference which reduces the impact of the crosstalk occurs at the eye centre (where wemake a decision) and the orthogonal interference condition which increases the impact of the crosstalk occurs at the eye crossing (where we don't care) we can effectively control the position of the residual crosstalk thus improving performance. Intuitively it would be thought that optimal performance would be achieved by increasing the eye opening at the transmitter using the following procedure (the alignment procedures described here deal with the 'two modulator' case):

1. Arrange for the data signal delays on the even numbered channels to align with, for example, the 80 GHz beat frequency (or twice the data rate) between the even numbered comb lines, such that the eye crossing of each data signal is aligned to the maximum of one of the 80 GHz cycles, similarly (but harder to measure) the eye opening.
2. Align the data delay for odd numbered channels to the odd numbered comb in the same way.
3. Align the relative delay between even and odd numbered channels such that all of the eye crossings are aligned.
4. Stabilise the optical phase and signal polarisations such that the interference signal is maximised. Ideally, the intensity at the eye crossing should vary quadratically with the level number.

If the CoWDM transmitter is aligned in the manner described above the output of the transmitter is as shown below in figure 3.23.

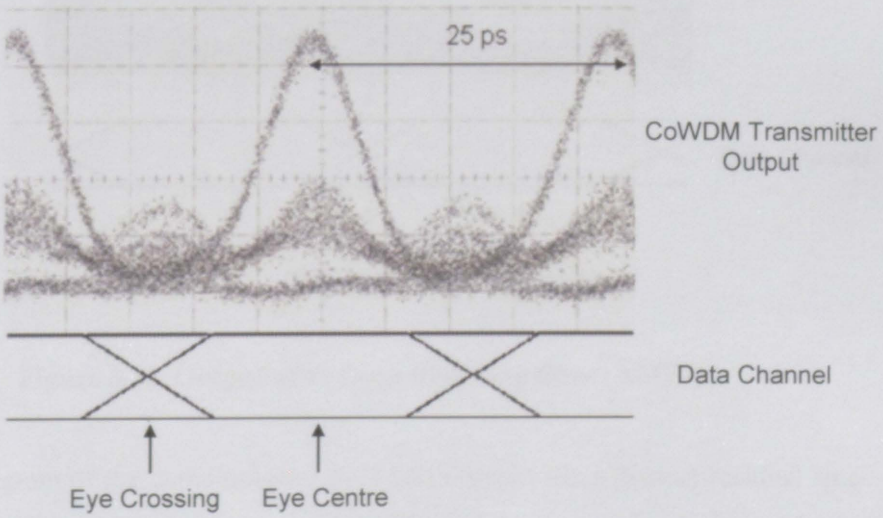



**Figure 3.23. Output of CoWDM Transmitter (standard alignment strategy)**

The eye at the output of the transmitter has a strongly RZ shaped multi-levelled signal at the eye centre, where the amplitude of the signal varies quadratically with the number of channels transmitting a 'one'. A complementary area between adjacent eye centres, where transitions between 'ones' and 'zeros' for all of the channels occur, appears as a shaped burst of noise. However, when the system was aligned according to the strategy described above, that is to give the clearest eye opening at the transmitter, and was then demultiplexed at the receiver using an AMZI, or another filter with a similar transfer function, the received eye diagram shown in figure 3.24 showed a significant amount of distortion. There was therefore a need for an enhanced alignment technique to achieve optimal performance, in the case where an AMZI (or other similar filter) is used in the receiver.

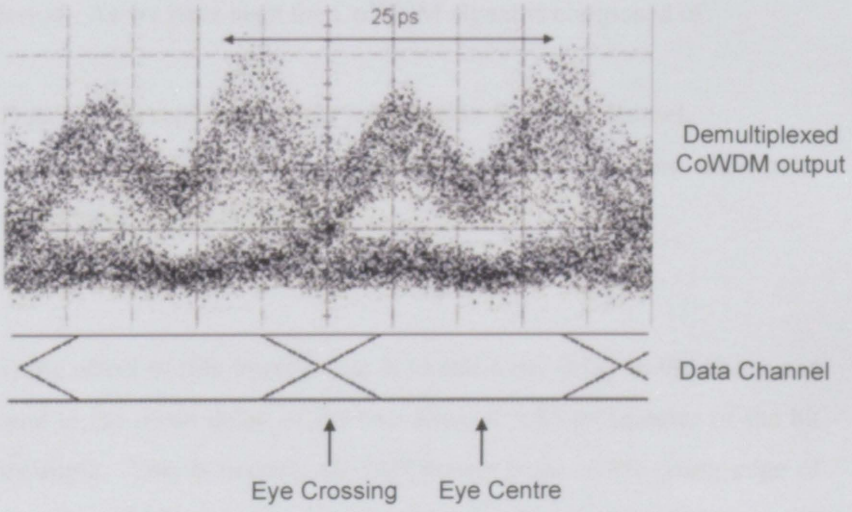



**Figure 3.24. Output after demultiplexing filter (AMZI)**

The eye diagram of the demultiplexed CoWDM channel has a distinct residual sine wave signal at the twice the channel frequency (80 GHz in the above eye) which is superimposed on the data of the target channel. With this alignment strategy the minimum of this sine wave coincides with the eye centre (the decision point) thereby reducing system performance (BER or Q-factor). This is in contrast to the figure at

the output of the transmitter where the interference signal appears to be well controlled and the data and sine wave oscillations are aligned. It was realised that the enhanced alignment strategy needed to take into account the characteristics of the transmission link and even more importantly the characteristics of the optical receiver used to detect the signal.

It was shown in in sections 3.3 and 3.7 that the receiver configuration implemented for the detection of a 42.6 Gbit/s CoWDM signal consists of an AMZI with a FSR of 85.2 GHz equal to twice the channel spacing and a tunable bandpass filter with a 3 dB bandwidth of 0.64 nm. The misalignment after detection described above is a direct consequence of the delay properties of the AMZI which has a delay of half of the signal bit period (~11.7 ps for a 42.6 Gbit/s signal). The output signal from the AMZI consists of the interference between an un-delayed copy of the CoWDM signal entering the AMZI, and a copy of the CoWDM signal delayed by half of the bit period. As we have seen the CoWDM signal is composed of:

(i) Data signals representing the information for each channel.

(ii) Sine wave signals which represent the beating between the carrier components of each signals.

(iii) Residual crosstalk.

In the case of (i) the effect of this interference is to add a net delay to the rising and falling edges equal to the mean delay of the two arms or 5.85 ps (quarter of the bit period) in this example. This is because the half power point of the rising edge of the pulses exiting the AMZI should correspond to the interference between the 'zero' level of the undelayed copy and the 'one' level of the delayed copy of pulses entering the AMZI. For (ii) the 11.7 ps delay corresponds to exactly one oscillation period for an 85.2 GHz sine wave. As a result the output is the simple in-phase addition of two infinite sine waves which results in no phase shift. Therefore the interference induced by the presence of the AMZI affects the relative delays of the of the CoWDM signal in a non-uniform fashion leading to a reduction in system performance.

This modified alignment strategy takes into account the delay induced on certain components of the signal by the AMZI

1. At the transmitter add a quarter bit period relative delay between the data signals and the beat frequency signal for both odd and even channel groups. This was achieved by aligning the transmitter such that the eye crossing corresponds to a minimum of the 85.2 GHz beat signal. In order to obtain a stable phase relationship between adjacent channels the 85.2 GHz tone was set to a particular value. Any harmonics or sub-harmonics of this tone should also vary accordingly with phase and in section 3.6 a technique for using these harmonics as an error signal for the phase stabilisation circuit is described.
2. In order to control the exact location of the static residual interference after the AMZI the relative optical phases within the transmitter were adjusted from their initial values to pre-compensate for the expected delay characteristics of the transmission link and the optical receiver.

The transmitted eye diagram if this alignment strategy is followed is shown in figure 3.25.

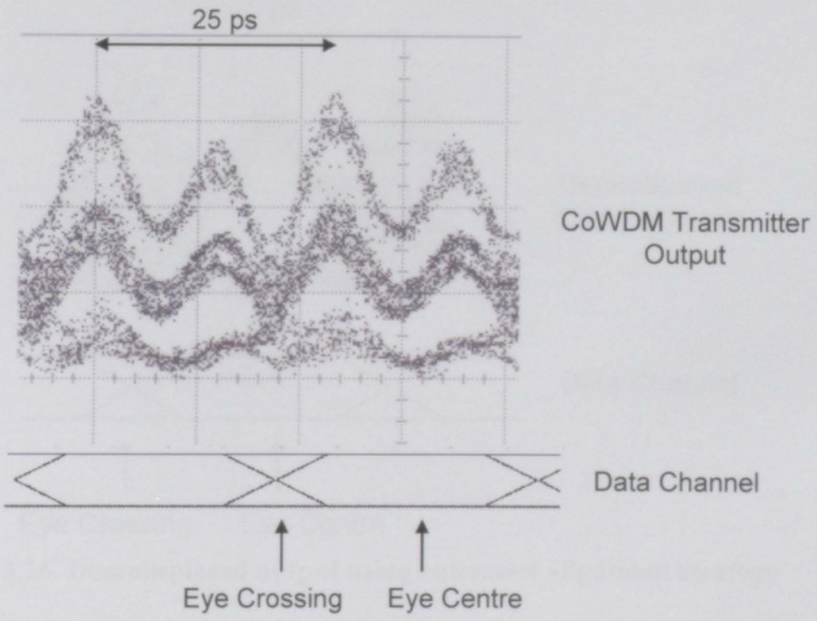



**Figure 3.25. Transmitted eye diagram for enhanced alignment strategy**

There is an apparent degradation in the eye relative to figure 3.25 but after demultiplexing with the AMZI the eye pattern is significantly improved and this is the characteristic received CoWDM eye shape which is shown throughout this thesis.

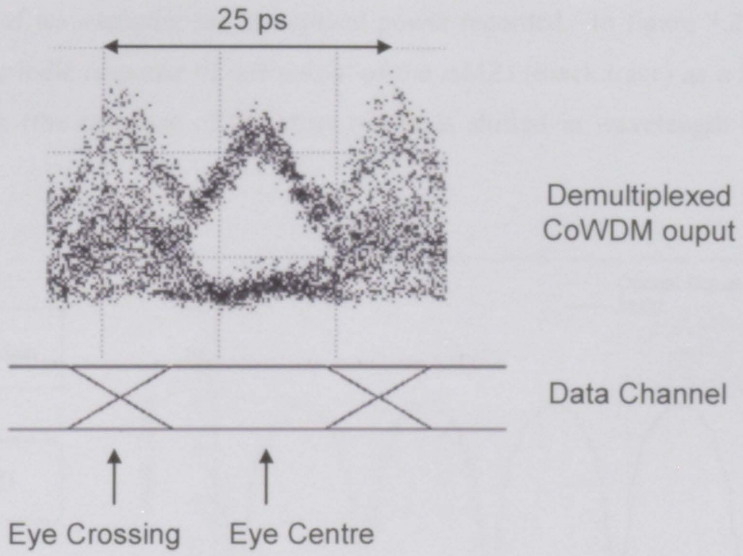



**Figure 3.26. Demultiplexed output using enhanced alignment strategy**

It should now be clear that correct alignment of the CoWDM transmitter is dependant on the transmission link and the demultiplexing filters employed in the system. An enhanced alignment strategy was outlined for use with CoWDM when an AMZI is used in the receiver to demultiplex the channels as was the case for all of the work presented in this thesis. This was achieved in the experimental CoWDM demonstrator by using three optical delay lines to align the data signals and the sine wave signals and a piezo-electric fibre stretcher to control the relative phase between the channels.

### 3.5.3 Mach-Zehnder Interferometer Characterisation

An asymmetric MZ interferometer (AMZI) with a FSR of 85.2 GHz was used in the CoWDM transmitter to separate the odd and even channels of the optical comb before data encoding. The FSR of the AMZI was matched to the channel spacing of the optical comb to ensure optimum performance. Figure 3.27(a) shows the simple experimental configuration used to characterize the AMZI. The CW laser was swept

over a range of wavelengths and the optical power recorded. In figure 3.27(b) we can see the periodic response of one output of the AMZI (black trace) as a function of wavelength (the response of the other output is shifted in wavelength by ~0.6 nm).

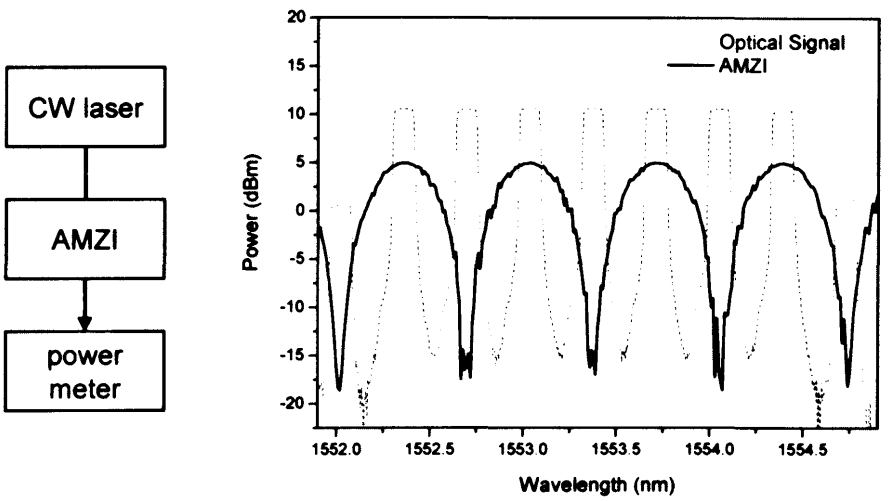



**Figure 3.27. (a) Experimental set-up. (b) Optical power as a function of wavelength for AMZI (black solid line, res = 0.01nm) and optical comb (red dashed line, res 0.2nm)**

The optical comb signal (red dashed trace) produced by the comb generator is overlaid on the AMZI trace to show that the AMZI separates odd and even channels effectively. The AMZI provides an extinction ratio of approximately 25 dB which is sufficient to suppress most of the contributions from the nearest neighbour channels. A temperature controller is used to align the AMZI to the centre wavelength of the optical comb.

### 3.5.4 Piezo Fibre Stretcher Characterisation

As we have seen in section 3.4.1 a piezo fibre stretcher is used to control the optical phase relationship between adjacent channels within the CoWDM transmitter. Piezoelectricity is the ability of certain materials, ceramic in this case, to generate a

voltage in response to mechanical stress [98]. This property is reversible and for our experiment we make use of the response of a piezo-ceramic cylinder when a voltage is applied across it. By wrapping the cylinder with the optical fibre through which one set of the CoWDM channels is passing and applying a voltage to the cylinder, therby causing it to change in diameter, the effective path-length of the fibre can be changed. This enables full control of the optical phase relationship between the two sets of CoWDM channels as they propagate through the CoWDM transmitter.

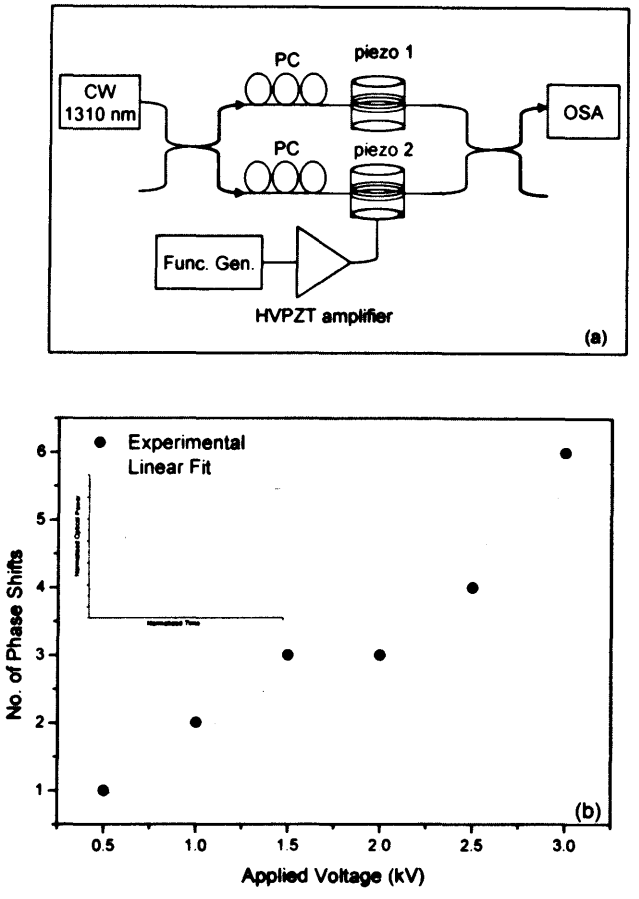



**Figure 3.28. (a) Experimental set-up. (b) $\pi$ phase shifts as a function of applied peak-to-peak voltage for piezo fibre stretcher. Experimental points (black circles) and linear fit (red line)**

The sensitivity of the phase change experienced by the optical signal depends on a number of parameters, namely the piezo-ceramic material, the amount of fibre wound around the cylinder and the tension on the fibre surrounding the cylinder due to the winding process. Figure 3.28(a) above shows the experimental set-up used to characterize the piezo fibre stretcher used in the CoWDM transmitter. A CW signal at 1310 nm was coupled into a fibre interferometer with a polarization controller and a piezo-ceramic cylinder in each arm. One of the cylinders was subject to an oscillating voltage (10 Hz) generated by a function generator and a high-voltage plumbum zirconate titanate (HVPZT) amplifier. The output of the interferometer

was analysed using an OSA and the number of $\pi$ phase shifts as a function of the applied voltage is shown in figure 3.28(b). The inset (optical power as a function of time on the OSA) in figure (b) shows a schematic of when 5 $\pi$ phase shifts were measured. In the final experimental CoWDM transmitter phase control was achieved using a piezo fibre stretcher, with a dynamic range of ~110 $\pi$ radians, more than sufficiently allowing for the large phase drifts expected for a CoWDM transmitter constructed from fibre-pigtailed devices. A substantially smaller dynamic range of a few $\pi$ radians would be required for a hybrid or monolithically integrated modulator array due to the significantly reduced optical phase drifts associated with such an implementation. The piezo was controlled during the experiment by a feedback signal from the phase stabilization circuit which is discussed in detail in the next section.

### 3.5.5 Dispersion Management of Optical Comb

As we can see from figure 3.22 which shows the experimental setup of the CoWDM transmitter there is a certain amount of single mode fibre between the comb generator and the data encoding section. This fibre caused a delay of the comb signal relative to the data signal at the data encoding section, which resulted in a deterioration of the measured spread of receiver sensitivities of the CoWDM tributaries as described in the next chapter. This issue, while present during single banded CoWDM operation, arose as a major problem during the initial experimental work on the multi-banded CoWDM setup (section 5.4) where we found an unacceptably large spread in the receiver sensitivity values between the channels at the extremeties of the comb spectra. The total fibre length between the comb and the data encoder, taking into account the EDFA (20m), polarisation controller (6m), splitters (4m) and other patch cords (~10m) was estimated to be approximately 40m. If we consider a multi-banded CoWDM signal which may have a total bandwidth of up to ~20 nm the total delay in 40 m of SMF would be ~15 ps. This figure represents approximately 64 % of the bit period of a 42.6 Gbit/s CoWDM tributary,

a figure that would significantly delay the comb signal with respect to the data signal and cause a large spread in the measured receiver sensitivity values. In order to cancel the effect of this delay on the comb signal before the CoWDM transmitter a ~6 m long piece of DCF (-127.29 ps/nm/km) was inserted between the optical comb generator and the 27 dBm EDFA. This resulted in a reduction in the spread of the receiver sensitivity values, as shown in figure 4.30 where the receiver sensitivity spread of the tributaries was reduced to just over 3 dB in a 112 km transmission experiment.

## *3.6 Phase Stabilisation [99]*

The Coherent WDM transmitter operates on the principle of controlling and optimising the optical phase relationship between adjacent optical channels, such that the interference between adjacent channels is coherent and is aligned to increase the eye opening at the receiver as shown in the previous section. Such fundamental phase control necessitates continuous monitoring and stabilisation of the relative phase delays throughout the operational lifetime of the transmitter. In the previous section we showed the CoWDM transmitter configuration in detail and noted the role of the piezo-ceramic cylinder in controlling the phase relationship between adjacent channels. The high voltage feedback signal controlling the expansion and contraction of the piezo cylinder was generated by a phase stabilisation circuit which is described in sections 3.6.1 and 3.6.2. Finally two different implementations of the circuit based on different technologies are discussed and compared.

### 3.6.1 Phase Stabilisation Circuit

In this phase stabilisation technique an error signal was acquired by monitoring the power levels of the interfering channels at the output of the transmitter and a feedback signal based on this error signal was used to control the piezo fibre stretcher.

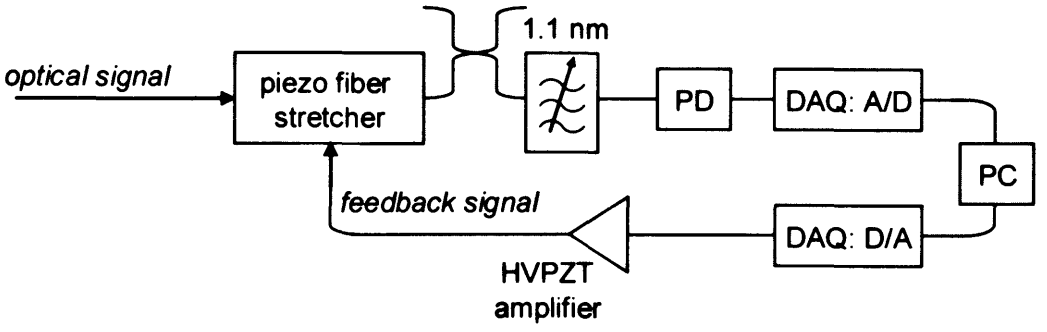



**Figure 3.29. Phase stabilisation circuit**

Numerical simulations, using VPI Transmission Maker 6.5, showed that the total output power of the CoWDM transmitter is highly correlated with its bit error rate (BER) performance at the receiver, as per figures 3.30(a) and 3.30(b). This encouraging result led to an experimental phase stabilisation circuitry, as shown in figure 3.29, where an error signal was extracted from the CoWDM transmitter output using an optical filter. Despite the fact that a CoWDM signal generated from a seven channel optical comb has a narrow bandwidth of ~0.3 nm a broad (1.1 nm) filter was used in order to make the stabilisation circuit compatible with multi-banded operation (section 5.4). A simple low frequency photoreceiver was used to convert the optical signal to the electrical domain which was then passed to a data acquisition board (DAQ). The board was set to a sampling rate of 1 kHz, with 20 averages, in order to enable real time monitoring of the output power (or the error signal), and hence the relative optical phase.

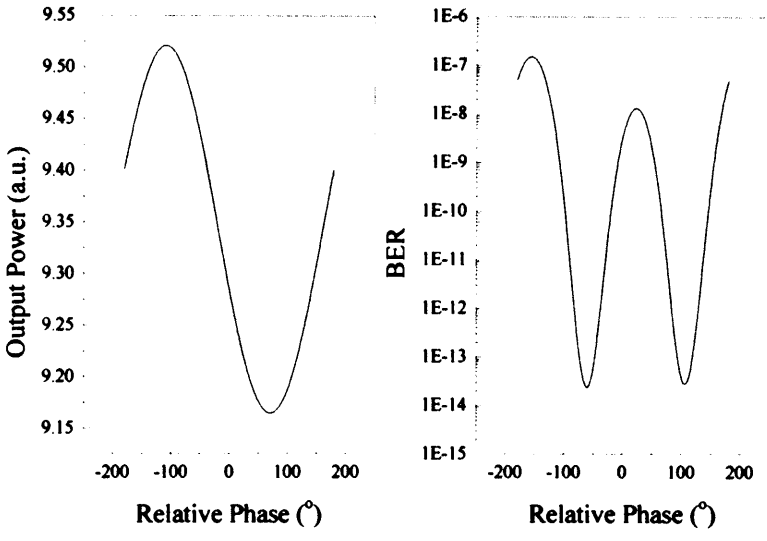



**Figure 3.30. Simulated (a) total output power and (b) BER as a function of relative phase**

Typical BER measurements correlated to this monitor are shown in figure 3.31. This correlation is maintained even when the output was not spectrally filtered, suggesting that only immediately adjacent channels are required to generate the error signal. This gives us confidence to predict that this control strategy may be applied to arrays of multiple modulators, with independent error signals for each arm generated either via tap couplers within the modulator array or by spectrally resolving the overall transmitter output.

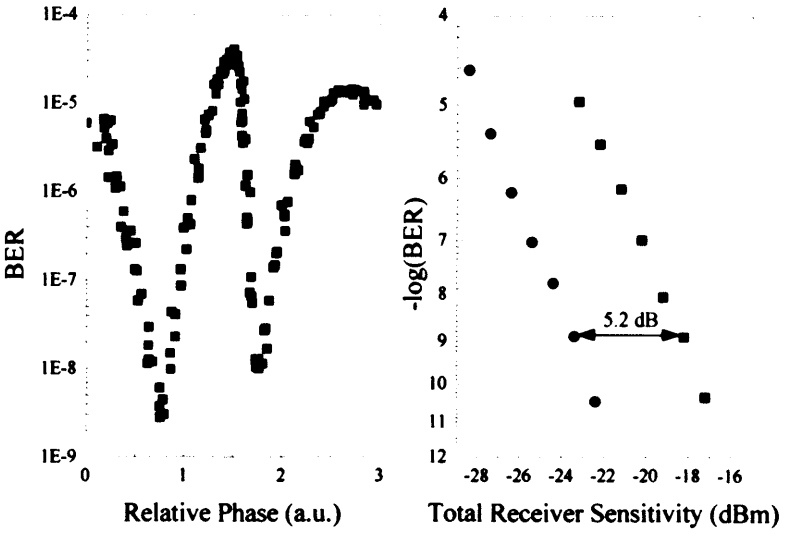



**Figure 3.31. Experimental results for (a) BER against relative phase, and (b) BER curves for best and worst phase settings**

The control loop was closed using a stabilisation algorithm on the PC based on a simple low amplitude dither (resulting in less than ± 5 degrees peak-to peak phase modulation). The LabVIEW and DAQ settings were selected to optimise the loop bandwidth, by taking into account the observed frequency of the error rate fluctuations (~ 0.14 Hz) and the signal-to-noise ratio of the error signal. The algorithm used to select the desired phase which is based on adding or subtracting a fixed preset step value to the current feedback signal based on the value of the phase obtained by the DAQ card with respect to the target value is shown in figure 3.32 below.

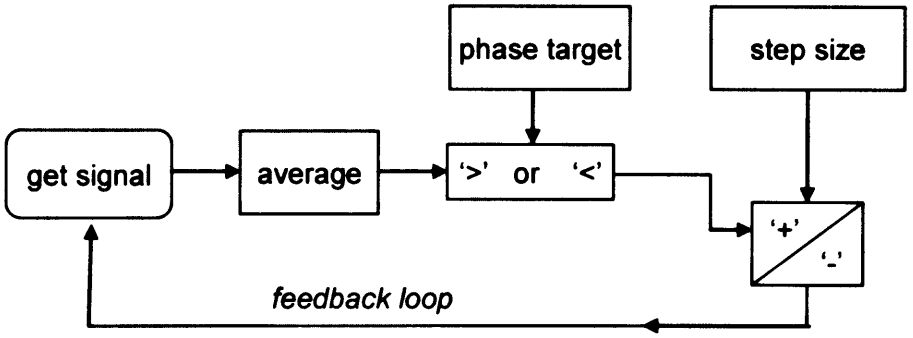



**Figure 3.32. Algorithm to select desired phase for standard phase stabilization circuit**

### 3.6.2 Enhanced Phase Stabilisation Circuit

Whilst the phase stabilisation circuit described in section 3.5.1 is a simple cost-effective monitor, the contrast ratio of the error signal is low (as shown in 3.6.3), necessitating the use of an artificial dither signal, which would be expected to reduce the speed of the phase stabilisation circuitry. To enhance the contrast ratio of the error signal, the power of the residual 42.6 GHz beat signal between adjacent channels was monitored. In section 3.5.2 it was hypothesized that any harmonics or sub-harmonics of the 85.2 GHz sine wave should vary accordingly with changing phase. This hypothesis was verified by using a 50 GHz photodetector and a double balanced mixer to generate an error signal based on the amplitude of the residual component of the 42.6 GHz optical signal after the transmitter.

The configuration of the enhanced circuit is shown below in figure 3.33.

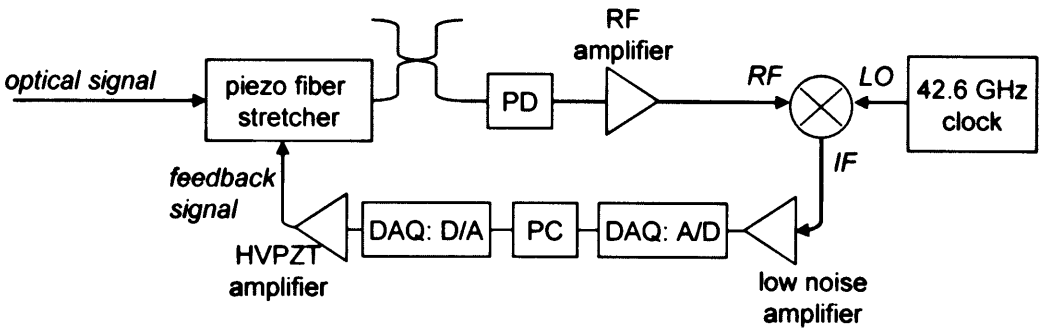



**Figure 3.33. Enhanced phase stabilisation circuit set-up**

The double balanced mixer was used to obtain the difference between the 42.6 GHz clock signal generated by the PPG (local oscillator (LO) input) and the 42.6 GHz RF component of the signal (RF input) from the output of the transmitter as shown in figure 3.25. The resultant low frequency RF signal was amplified using a low-noise preamplifier with an incorporated 6 dB/oct roll-off low-pass filter with a cutoff frequency of 3 Hz and a gain figure of 20, and was then converted to a digital signal using a DAQ A/D board. Similar to the circuit described in 3.5.1 the control loop was closed using an enhanced stabilisation algorithm on the PC. This VI, implemented in LabVIEW 7.0, enabled full monitoring and control of the optical phase relationship between adjacent channels and was based on a PI algorithm (as shown in figure 3.34 below) which eliminated the effect of the amplitude dither on the stabilisation performance of the original circuit. In the algorithm the samples obtained from the DAQ are averaged and the absolute difference between this average and the desired phase value is obtained. This is multiplied by a 'gain control' term and added or subtracted to the previous error signal value to generate the new error signal. This error signal is fed back to the DAQ and subsequently amplified before being used to drive the piezo fibre stretcher which controls the phase condition in the transmitter.

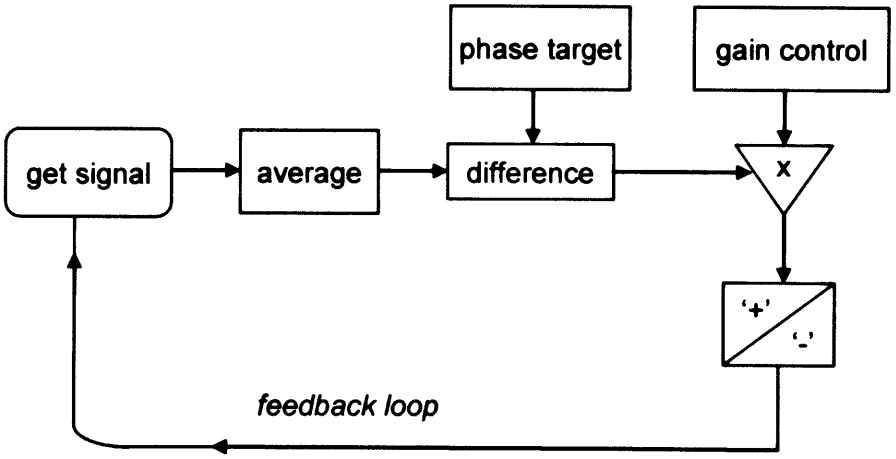



**Figure 3.34. Enhanced phase stabilisation algorithm**

Section 3.6.3 provides a detailed comparison between the performances of the two phase stabilisation circuits.

### 3.6.3 Performance Comparison

In order to compare the error signals generated by the two phase stabilisation circuits the HVPZT amplifier connected to the piezo-ceramic fibre stretcher in the CoWDM transmitter was driven with a linear ramp and the error signals from both phase circuits were monitored simultaneously using the set-up shown in figure 3.35 below.

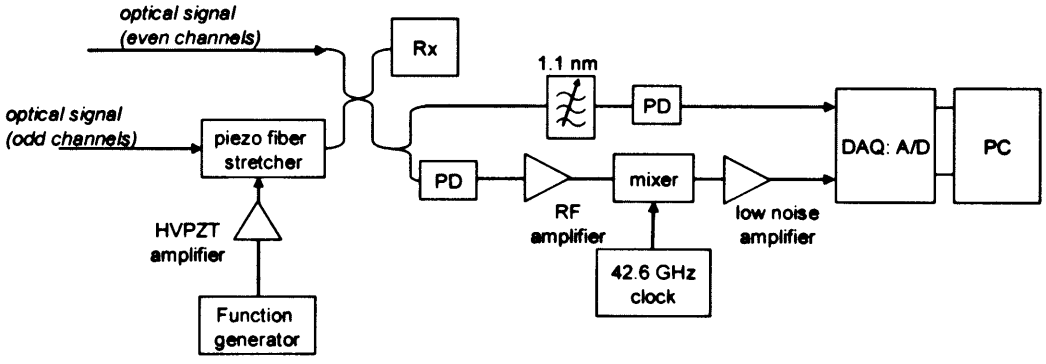



**Figure 3.35. Experimental configuration for phase stabilisation circuit comparison**

The linear ramp was applied to the piezo-ceramic fibre stretcher over a duration of approximately 2 minutes and resulted in oscillations of the BER at the receiver (from $10^{-4}$ to $10^{-10}$). During this time the error signals generated by each phase stabilisation circuit were monitored and the results are presented in figure 3.36 below. The fluctuation of the BER over the duration of the experiment is also shown in figure 3.36 (bottom solid trace).

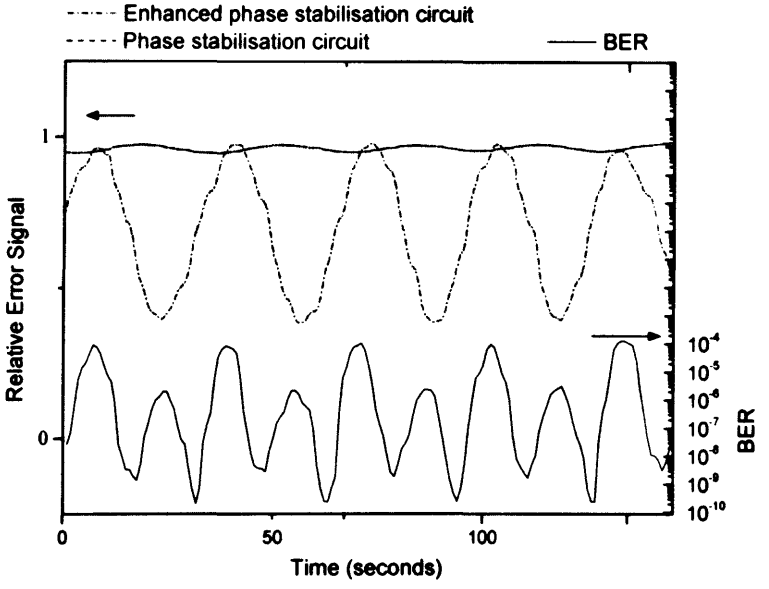



**Figure 3.36. Normalised error signals (left axis) for mixer based (red dot-dash trace) and photodiode based (blue dashed trace) as a function of time. BER fluctuation (right axis) versus time also shown (bottom solid trace)**

It is clear from figure 3.36 where the normalised outputs of both phase detectors are plotted as a function of time that the contrast ratio of the error signal generated by the enhanced phase stabilisation circuit (dotted trace) is significantly enhanced with respect to the original one (dashed trace). The resultant SNR increase enabled a more precise selection of any particular relative optical phase between adjacent channels in the CoWDM transmitter, and in turn this lead to a more stable BER at the receiver.

The stability of both phase stabilisation circuits as function of time is shown in figure 3.37, where the BER of the CoWDM system was monitored over a period of approximately two hours. In both cases the power to the levels input to the preamplified receiver were reduced somewhat, in order to enable full visibility of the error rate variation. In this experiment, the relative phase was locked to its optimum value, and the BER at the receiver was monitored. The first 10 minutes shows the expected BER fluctuations when the stabilisation control was switched off, as the

phase was left to drift over time. On the other hand, when the stabilisation circuit was switched on, and locked to a particular phase value, the BER was maintained constant throughout the remainder of the experiment, within experimental errors. For the photodiode based phase stabilisation circuit (a) the BER can be seen to fluctuate between $10^{-7}$ and below $10^{-10}$ during the period of time when the phase stabilisation circuit was switched on. The corresponding level of fluctuation for the mixer based phase stabilisation circuit was between $10^{-8}$ and below $10^{-10}$. While the average BER during the phase locked period is approximately the same ((a) $BER_{avg}$ = 4 x $10^{-9}$ and (b) $BER_{avg}$ = 3 x $10^{-9}$) for both phase stabilisation circuits the difference in the standard deviation value ((a) $BER_{stdev}$ = 1 x $10^{-8}$ and (b) $BER_{stdev}$ = 1 x $10^{-9}$) verifies that the enhanced stabilisation circuit is able to maintain a more stable phase position than the photodiode based circuit. Locking the system over a much longer period of time (> 48 hours) using the photodiode based stabilisation circuit has shown little degradation, when analysing FEC performance with CoWDM, as shown in chapter 4.

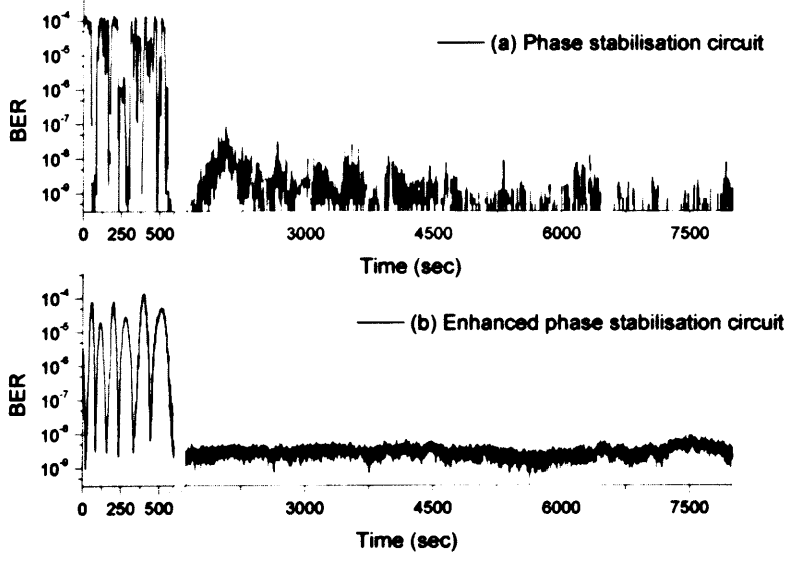



**Figure 3.37. Performance of (a) Photodiode based stabilisation circuit (b) Mixer based stabilisation circuit as a function of time**

In addition to this, the original stabilisation circuitry described above was also used with a multi-band CoWDM system, across a bandwidth of over 1.5 nm which is described in detail in chapter 5. The 1.1 nm tuneable bandpass filter was still used, and the same randomly selected channel locked the relative phase of the whole system throughout the experiment. This is promising as it shows than a transmitter implementation consisting of an 'n x modulator' array could be easily phase locked, and would be independent of the channel being analysed. This is significant for high capacity multi-banded CoWDM where a number of CoWDM bands would be independently modulated and transmitted over the same fibre link.

## *3.7 Optical Filter Characterisation and Optimisation*

The purpose of an optical filter in a typical WDM-based optical communication system is to select the channel of interest at the receiver. In order to be successful in this the optical filter must have a sufficient bandwidth to transmit the target channel but narrow enough to cancel the effect of neighbouring WDM channels. In a traditional WDM system where channel spacing is of the order of 100 GHz optical filter design and selection is a relatively straightforward issue [100, 101]. However for a 42.6 Gbit/s CoWDM system where the channels are tightly spaced (channel spacing equal to the bit rate) correct optical filter selection at the receiver is not trivial and has a large impact on system performance. This section deals with the optical filter characterisation and optimisation process for CoWDM by both simulation (3.7.1) and experimental methods (3.7.3).

### 3.7.1 Numerical Simulation

In this section we present numerical simulations performed using VPI Transmission Maker V7.0 which evaluate the performance of a number of different receiver-side optical filtering strategies. Figure 3.38 shows the configuration of the CoWDM transmitter and receiver used for the simulations presented in this section. Where possible, parameters such as insertion loss, gain and noise figure were taken from the experimental components described in previous sections. The schematic differs from the experimental setup shown in previous sections by having an array of 7 independent chirp free MZ modulators for the data encoding of the optical channels and is an extension of the schematic described in [102] where 5 channels are simulated.

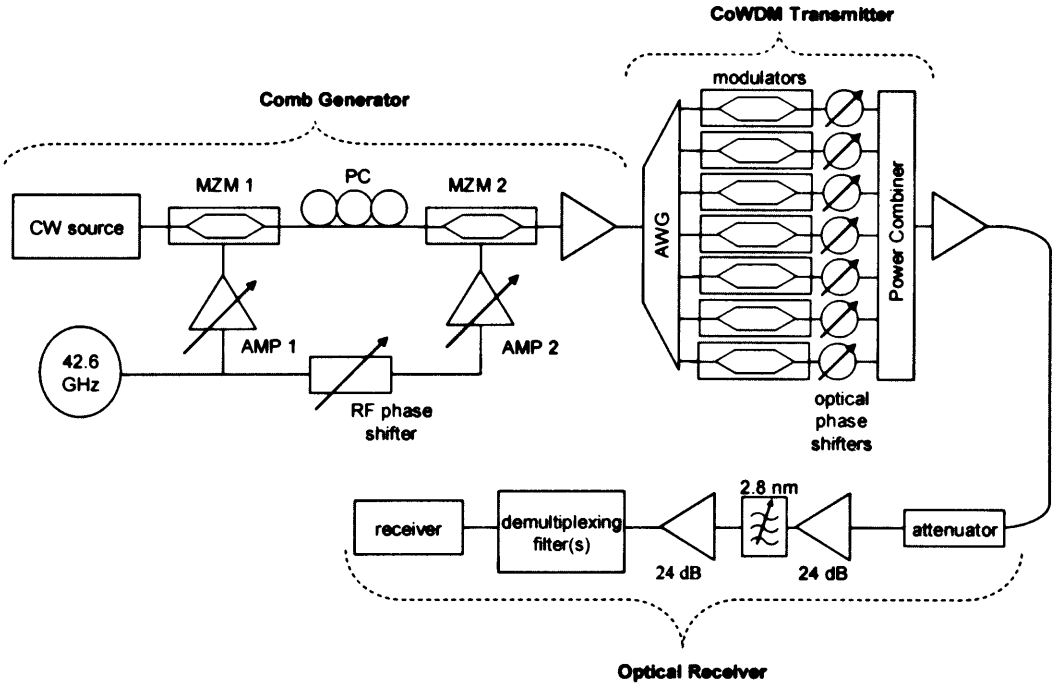



**Figure 3.38. CoWDM transmitter and receiver simulation setup**

The simulated optical receiver employed two optical amplifiers (noise figure = 5 dB), a broad bandpass filter (2.8 nm) for band selection and a demultiplexing filter to select the target channel. As the impact of the demultiplexing filter on the performance of the system was the subject of this investigation the other elements of the CoWDM transmitter and receiver block were optimised for each filter configuration. The results of these simulations for are presented in figure 3.39 below.

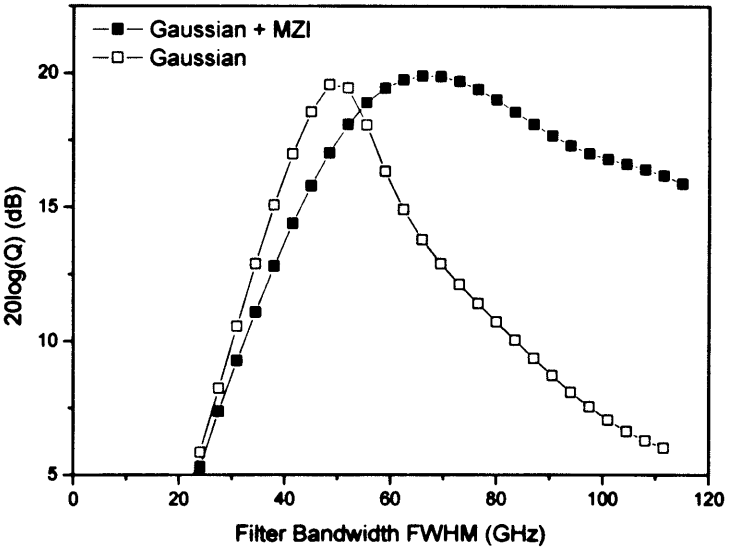



**Figure 3.39. Q factor as a function of filter bandwidth for a Gaussian filter with (open symbols) and without (closed symbols) an AMZI**

Figure 3.39 shows the Q factor of the system as a function of the optical bandwidth of the Gaussian bandpass filter. An AMZI with a fixed free spectral range (FSR) equal to twice the channel spacing (85.2 GHz) was then concatenated with the Gaussian filter and the Q factor measured for a range of bandwidths. For the lower filter bandwidths (20-40 GHz) the system is limited by inter-symbol interference (ISI). As the filter bandwidth is increased the ISI is reduced but degradations due to inter channel crosstalk become more significant. This increased crosstalk strongly affects the system without the AMZI, limiting the optimum Q-factor to ~20 dB when a 50 GHz FWHM Gaussian filter is used. The effect of the AMZI is to suppress the carrier contributions from the two nearest neighbour channels, thus reducing the impact of the interchannel crosstalk. This resulted in optimal performance for a wider range of filter bandwidths (approximately 25 GHz for a 1 dB penalty). An optimum Q-factor of ~20 dB was measured for a ~70 GHz FWHM Gaussian filter concatenated with the AMZI.

It is apparent from the numerical investigation presented above that an optimum filtering strategy is central to the operation of CoWDM. In the next section we will present a discussion on the experimental characterisation of a number of optical filters and finally present the results of a comparison study to determine the optimum filter configuration.

### 3.7.2 Optical Filter Characterisation

The numerical investigation presented above suggests that a Gaussian optical filter concatenated with an AMZI is the optimum filtering strategy for 42.6 GHz spaced CoWDM. The experimental set-up shown in figure 3.40 was used to characterise the response of three Gaussian optical filters with 3 dB bandwidths of 0.43 nm, 0.64 nm and 0.95 nm (broad filter) respectively.




**Figure 3.40. Filter measurement setup**

Figure 3.41 shows the measured amplitude response of the three filters as a function of wavelength. The filters were tuneable across a wide range so an arbitrary centre wavelength of approximately 1553.4 nm was chosen for the investigation.

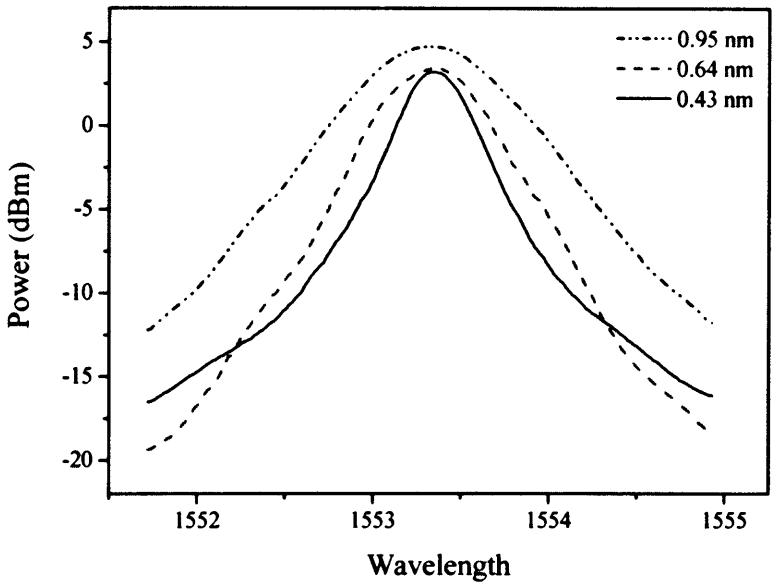



**Figure 3.41. Amplitude as a function of wavelength for three Gaussian filters (0.95 nm, 0.64 nm and 0.43 nm) as a function of wavelength**

An AMZI with a FSR of 85.2 GHz, identical to the one characterised in section 3.4.2 was used in concatenation with both the 0.64 nm and 0.43 nm bandpass filter in the experimental demonstration described in the next section.

### 3.7.3 Experimental Filter Selection

In order to select the optimum receiver-side filter strategy for the CoWDM testbed a number of different filter combinations were tested. Receiver sensitivities for all seven 42.6 Gbit/s CoWDM channels were measured for two of the filter configurations shown in figure 3.41. For the 0.43 nm and AMZI, whilst the signal experienced low levels of ISI, the modest roll-off and phase response of the filter de-localised the crosstalk somewhat, resulting in a degradation of the zero level of the CoWDM signal. Moving from a 0.43 nm to a 0.64 nm bandwidth filter resulted in a more satisfactory location of the crosstalk and an improvement of ~5 dB in the

average receiver sensitivity across the channels. The system did not run error free when the 0.43 nm bandpass filter was used without the AMZI. The performance of a 100 GHz spaced flat-top arrayed waveguide grating (AWG) with a 3 dB bandwidth of 75 GHz together with the AMZI was also investigated but was again found to induce additional dispersion, redistributing the crosstalk in this case for the '1' pulses.

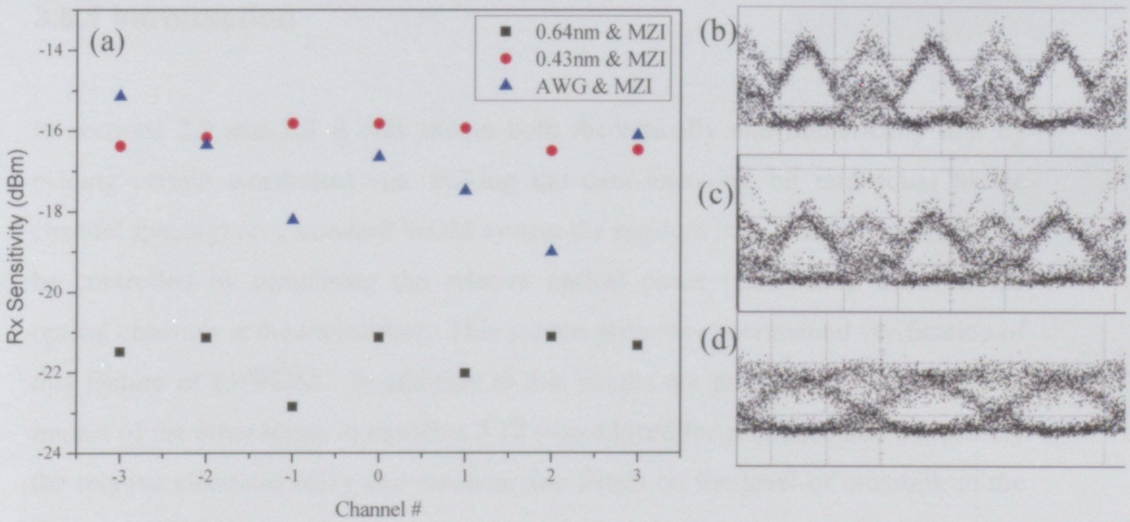



**Figure 3.42. (a) Rx Sensitivity for each channel for various filter configurations. Received 42.6 Gbit/s eye diagram for the worst tributary using (b) 0.64 nm & AMZI, (c) 0.43 nm & AMZI and (d) AWG & AMZI**

These results compare favourably with the results of the simulations presented above as optimum performance given the constraints of the system, is obtained using a combination of a Gaussian bandpass filter and an AMZI. The 0.64 nm filter (approximately 80 GHz) combined with the AMZI results in the best system performance.

In conclusion we have shown both numerically and experimentally that the optimal experimental implementation of a filter for a CoWDM receiver is the combination of a narrowband Gaussian filter for channel selection and an AMZI

with a FSR of twice the channel spacing to reject the carrier contribution from the nearest neighbour channels. Experimentally this was implemented by using a 0.64 nm Gaussian filter and an 85.2 GHz FSR AMZI.

## *3.8 Experimental Verification of 2.2.3*

### 3.8.1 Introduction

In sections 2.2 and 2.3 it was shown both theoretically and numerically that by placing certain constraints (i.e. making the data encoding bit rate equal to the channel spacing) on a standard WDM system the residual inter channel crosstalk can be controlled by optimising the relative optical phase relationship between the optical channels at the transmitter. This section presents experimental verification of this feature of CoWDM. In addition to this results are presented which show the impact of the other terms in equation 2.18 (reproduced for reference below), namely the relative electrical delay and receiver side filters on the level of crosstalk in the system.

$$S_{\alpha\beta\gamma\delta} = d_{\alpha\beta} d^*_{\gamma\delta} I_{\alpha\beta} I^*_{\gamma\delta} e^{j(\Delta\omega_{\alpha\gamma} t - \Delta\omega_{\alpha\gamma}\tau_a - \Delta\tau_{\alpha\gamma}(\omega_\gamma) + \Delta\phi_{\alpha\gamma})} \tag{2.18}$$

Finally the impact of misalignments between the channel spacing and the bit rate are discussed.

### 3.8.2 Optical Phase Relationship in CoWDM Transmitter

In chapter 2 it was proposed that optical phase relationship between the channels in the transmitter has a significant impact on the overall performance of the CoWDM transmitter, i.e the crosstalk depends on the optical phase: $S_{\alpha\beta\gamma\delta} \propto e^{j(\Delta\phi_{\alpha\gamma})}$. In the

CoWDM condition where the channel spacing is constrained to be equal to the bit rate the optical phase term remains and can be used to suppress the residual inter channel crosstalk arising in the system. Experimentally the optical phase relationship between the channels is controlled in the transmitter by using an electrically driven piezo fibre stretcher on one path of the interferometer as described in section 3.6. This simple feedback circuit can be used to select and maintain a particular phase relationship in the transmitter. Figure 3.43 below shows the receiver sensitivity values at a BER of $10^{-9}$ for all seven CoWDM tributaries at three different phase settings.

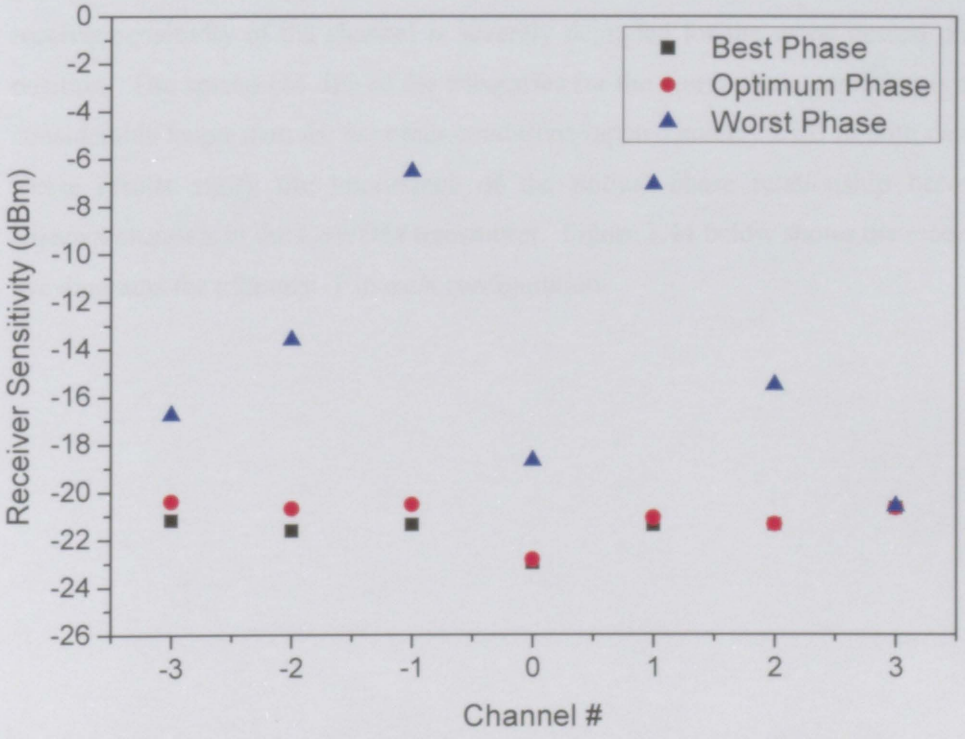



**Figure 3.43. Receiver Sensitivity for each tributary for 42.6 Gbit/s CoWDM for best phase (squares), optimum phase (circles) and worst phase (triangles)**

The squares represent the condition where the optical phase term was adjusted to obtain the best receiver sensitivity for each tributary and has an average receiver

sensitivity of -21.5 dBm. However, this would not be practical for a real system as all channels would be received simultaneously and therefore twaeaking of the phase of the individual channels would not be possible. It is much more feasible to have a system where a single optimum fixed optical phase value is selected to give acceptable performance across all channels at the same time. The circles represent this condition where the initial optical phase was maintained at the same optimum value throughout the receiver sensitivity measurements for all tributaries resulting in an average receiver sensitivity value of -21.1 dBm. Finally the worst phase for each tributary was selected and the receiver sensitivity measured. This condition is represented by triangles in the figure above. A large average receiver sensitivity penalty of approximately 7 dB was measured. It is clear that in every case the receiver sensitivity of the channel is severely degraded for the worst optical phase position. The spread (14 dB) of the tributaries for the worst phase condition is also considerable larger than for the other conditions (approximately 2 dB in both cases). These results verify the importance of the optical phase relationship between adjacent channels in the CoWDM transmitter. Figure 3.44 below shows the received eye diagrams for tributary -1 in each configuration.

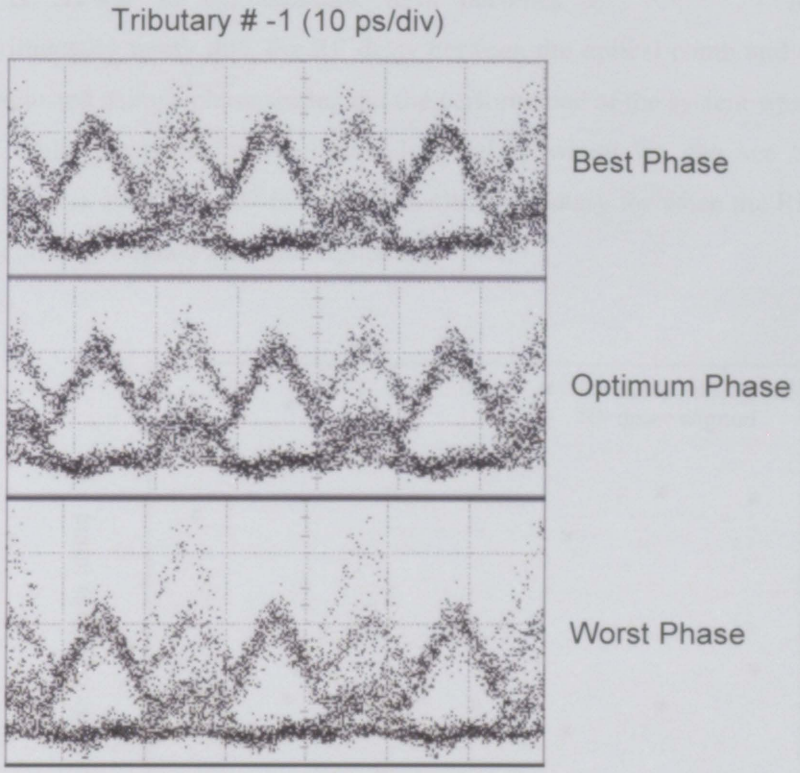



**Figure 3.44. Received eye diagrams for tributary -1 for best (top), optimised (middle) and worst (bottom) phase conditions**

The eye diagrams for the best and optimum phase configuration are similar and show an open centre with the crosstalk at the crossing. However the effect of the optical phase on system performance is more evident if we consider figure 3.44 (bottom) where we can see a degraded eye centre and higher crosstalk contributions at the crossings.

### 3.8.3 Electrical Delay in CoWDM Transmitter

In addition to the optical phase relationship equation 2.18 also predicts that the RF delay of the target channel with respect to the adjacent channels will have an impact on the overall level of the crosstalk experienced by the target channel at the receiver,

that is $\Delta\tau \neq 0$ so the crosstalk term becomes $e^{-i(\Delta\tau_{\alpha\gamma}\omega_\gamma + \Delta\phi_{\alpha\gamma})}$. In order to experimentally verify this, the RF delay between the optical comb and data signals was adjusted using a phase shifter and the performance of the system was monitored. The results are presented in figure 3.45 below where we can see the receiver sensitivity at a BER of $10^{-9}$ for each 42.6 Gbit/s tributary for when the RF delay was both correctly aligned and mis-aligned.

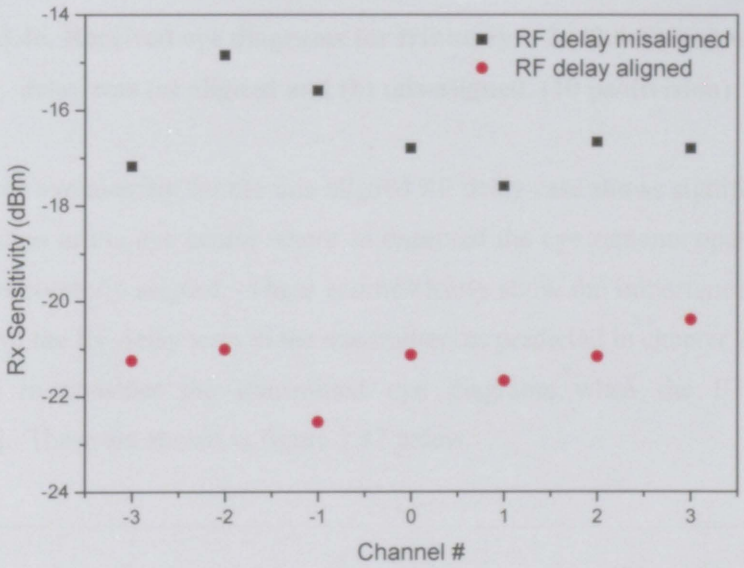



**Figure 3.45. (a) Rx Sensitivity for each channel for when the RF delay was correctly aligned (squares) and mis-aligned (circles)**

The average receiver sensitivity for the system with aligned RF delay was -21.31 dBm and a penalty of 4.8 dB was observed when the RF delay was mis-aligned. The received eye diagrams for tributary 2 for both cases are shown in figure 3.46 below.

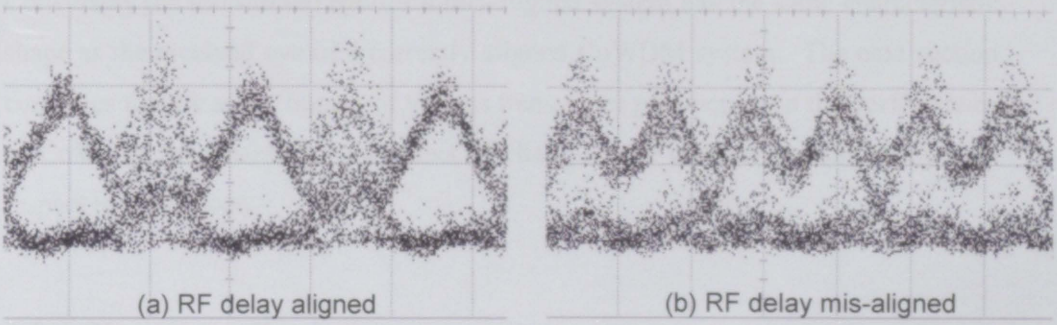



**Figure 3.46. Received eye diagrams for tributary + 2 (42.6 Gbit/s) when RF delay was (a) aligned and (b) mis-aligned. (10 ps/division)**

The received eye diagram for the mis-aligned RF delay case shows significant levels of degradation at the eye centre where as expected the eye remains open when the RF delay is correctly aligned. These results clearly show the importance of correct alignment of the RF delay term in the transmitter, as predicted in chapter 2. It is also interesting to consider the transmitted eye diagrams when the RF delay is misaligned. These are shown in figure 3.47 below

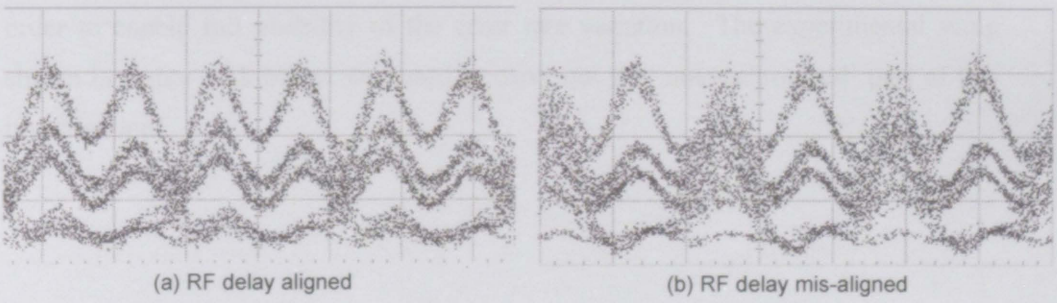



**Figure 3.47. Transmitted CoWDM eye diagrams when RF delay was (a) aligned and (b) mis-aligned. (10 ps/division)**

It is clear that the shape of the transmitted eyes are closely related to the received eyes. When the RF delay is correctly aligned the lower two levels of the eye at the transmitter is similar to the received eye diagram for a mis-aligned system.

Conversely the transmitted eye for a mis-aligned system has the same characteristic shape as the received eye of a correctly aligned CoWDM system. The next section continues to look at the impact of various transmitter parameters on the performance of CoWDM by considering the effect of changing the channel spacing value with respect to the bit rate.

### 3.8.4 Sine Wave Term

In the conventional CoWDM system which has been introduced in this chapter precise coincidence of the data rate and comb spacing is necessary and is achieved by using a common clock source from the PPG. However in equation 2.18 we observed we observe that deviation from this ideal condition may be accommodated via appropriate adjustment of alternative parameters, such as the optical phase in the transmitter. In this section we highlight the effect which this sine wave, located at the channel spacing has on the performance of the CoWDM transmitter ($e^{i(\Delta\omega_{\sigma 7}t+\Delta\phi_{\sigma 7})}$). For the following BER evolution graphs it is important to note that the power levels input to the pre-amplified receiver were intentionally reduced in order to enable full visibility of the error rate variation. The experimental setup shown in figure 3.48 below was used to carry out the 'unsynchronised' part of this investigation.

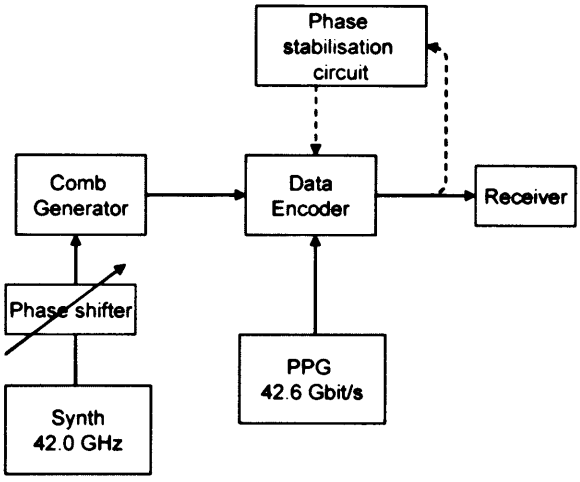



**Figure 3.48. Experimental setup for unsynchronised CoWDM**

In figure 3.49 below the phase stabilised BER is plotted for two comb frequencies, a synchronous drive signal at 42.6 GHz (squares) and an asynchronous drive signal at 42.0 GHz (circles) with the phase stabilisation circuit set for best (closed symbols) and worst (open symbols) BER performance. The original phase stabilisation circuit described in section 3.6.1 was used for this investigation.

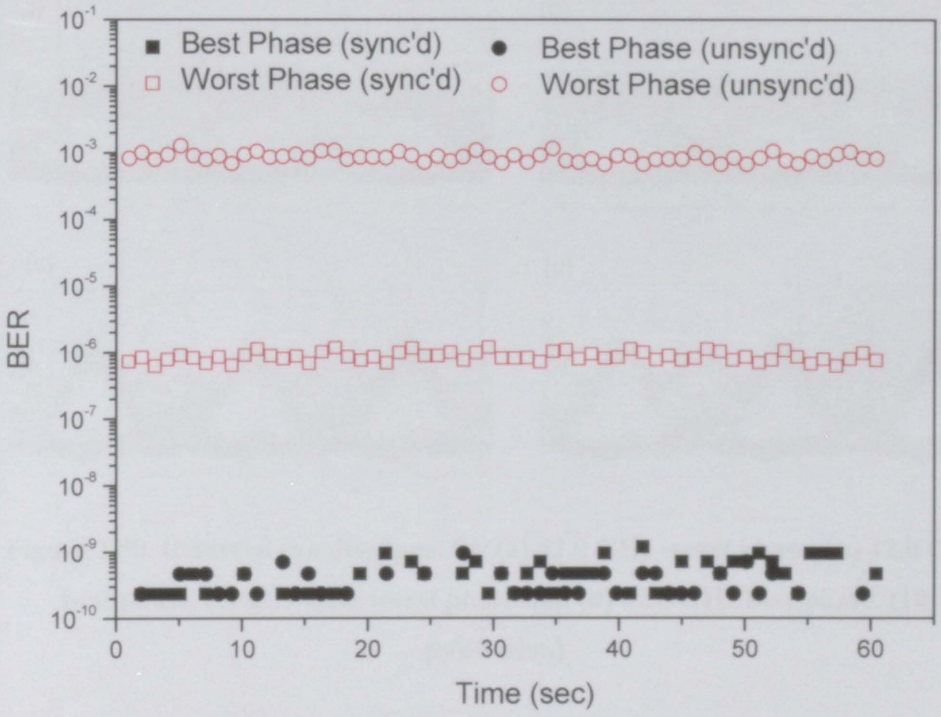



**Figure 3.49. (a) BER evolution as a function of time for un-synchronized (circles) and synchronized CoWDM (squares), for best (closed symbols) and worst (open symbols) optical phase setting**

Whilst a significant difference in performance is observed at the worst optical phase, reflecting both the slightly narrower channel spacing and the increased number of bits contributing to crosstalk, it was possible to select an optimum optical phase where both systems demonstrated identical performance. This is confirmed by the eye diagrams shown below where the most significant differences at the optimum phase occur at the eye crossing, whilst for the worst phase positions the distribution of the crosstalk is significantly degraded.

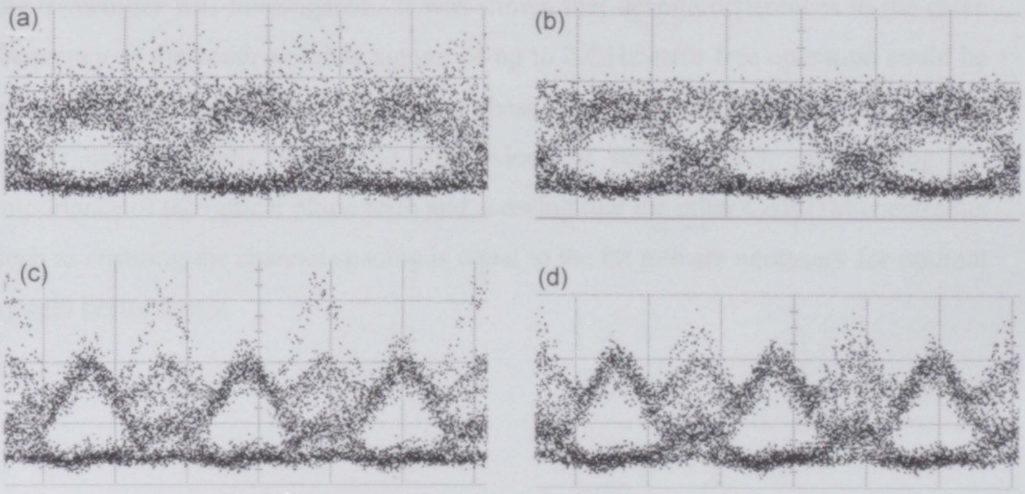



**Figure 3.50. Received eye diagrams for (a) 42.0 GHz worst phase, (b) 42.0 GHz best phase, (c) 42.6 GHz worst phase and (d) 42.6 GHz best phase. (10 ps/division)**

This investigation has shown that it is possible to compensate for slight variations in the relative difference between the channel spacing and the bit rate by correct alignment of the optical phase relationship between the channels.

### 3.8.5 Conclusion

In this section we have considered the effect of various parameters arising from equation 2.18 on the performance of CoWDM. We have presented experimental results showing that the optical phase relationship between adjacent channels in the CoWDM transmitter can be adjusted to minimise the level of interchannel crosstalk at the receiver and thus improve system performance. We have also investigated the impact of the relative RF delay between the comb and the data signals and shown that an improvement in receiver sensitivity of almost 5 dB can be achieved by correct alignment of this parameter. Finally the relationship between system performance and the level of synchronisation of the frequency of the drive signals in

the transmitter was investigated. It was shown that despite differences in the drive frequency of the comb and data signals of up to 2 GHz error free operation could be achieved by correct tuning of the optical phase relationship in the transmitter. These results experimentally verify the conclusions of section 3.6.3, highlighting the importance of the optical phase term and showing that the other CoWDM constraints such as ensuring the channel spacing is equal to the bit rate are necessary for optimal system performance.

## 3.9 Conclusion

In this chapter we have presented details on the design and implementation of a CoWDM optical testbed capable of operating in the 40-43 Gbit/s range, with which the majority of the experimental work described in subsequent chapters was carried out.

In sections 3.2 and 3.3 a method of optical comb generation using a pair of amplitude modulators and its suitability as a wavelength source for WDM systems was discussed. It was shown that up to 11 comb lines can be generated with flatness of less than 2 dB and a SMSR of ~12 dB by using an enhanced comb generator based on a cascaded pair of Versawave electro-optic 40 Gbit/s polarisation modulators. This comb generation technique exhibits many advantages over alternative techniques and has potential for application across a range of WDM technologies (e.g. a wavelength source for 100 Gbit/s Ethernet). Following this the CoWDM transmitter was described in detail and the role of a phase stabilisation circuit in the transmitter was outlined. The CoWDM transmitter is based on a phase preserving data modulator array with an electrically driven piezo fibre stretcher to maintain the optical phase relationship between the adjacent channels. The operation of the fibre stretcher and the associated phase stabilisation circuit was the subject of section 3.5 where we showed two different implementations of the circuit and illustrated the enhanced stabilisation performance of the mixer based signal by monitoring both error signals as a function of time with a fluctuating BER. The impact of the receiver side optical filters on the performance of CoWDM was investigated by experiment and simulation in section 3.7. A number of different filters were experimentally characterised and used to filter the target CoWDM channel at the receiver. It was shown that in the case of 42.6 GHz spaced CoWDM a 0.64 nm bandpass filter used to select the target channel and a 85.2 GHz FSR asymmetric MZD for rejection of the crosstalk from adjacent channels represent the optimum filter configuration. In this section we also presented a description of the pre-amplified optical receiver configuration used in the CoWDM experimental work. Finally the characteristics of CoWDM which were introduced in chapter 2

were investigated experimentally in section 3.8. It was demonstrated that the optical phase relationship between adjacent channels in the transmitter can be used to control the level of crosstalk occurring between channels at the receiver. The results of investigations to assess the impact of other CoWDM transmitter parameters such as the RF delay between the comb and the data were also presented. In addition, some of the key devices such as high speed optical modulators, PPG and ED, which enabled the development of the CoWDM system, were discussed.

In the next chapter we will look at a range of performance characteristics of CoWDM as a transmission format, including its tolerance to various fibre induced transmission impairments.

# Chapter 4

# CoWDM Performance Characteristics

## *4.1 Introduction*

Recent demonstrations of high ISD in optical communication systems have required the use of combinations of complex techniques such as advanced modulation formats, polarisation multiplexing and transmitter prefiltering [103, 104, 105]. In chapters 2 and 3 we have presented a novel transmission format called CoWDM which we believe to be a simple cost-effective technique for achieving similarly high ISD without the need for much of the complexity. We have described in detail the experimental implementation of a CoWDM transmitter as well as the alignment strategy required to achieve CoWDM. In addition to this the implementation of a simple preamplified optical receiver for use with the CoWDM transmitter was discussed.

In this chapter we set out to investigate a wide range of performance features of CoWDM using the transmitter and receiver configurations described previously. In section 4.2 we consider the basic back-to-back performance of CoWDM in order to verify that an ISD of 1 bit/s/Hz can be achieved using NRZ modulated CoWDM at 42.6 Gbit/s. We then consider the transmission of such a signal over a moderate length of standard SMF in order to determine if there are any transmission induced penalties which need to be considered for the CoWDM format. In section 4.3 the performance of CoWDM when combined with FEC codes is considered. FEC codes are widely used in modern optical communication systems to correct for errors at the receiver thus allowing for increased system margins in terms of transmission distance, repeater spacing, launch power etc. Given the channel correlation of CoWDM and the potential dominance of crosstalk penalties the Gaussian noise statistics of the system may be altered. Therefore if CoWDM is to be considered as a candidate transmission format for use in such systems it is necessary to verify its

compatibility with standard FEC techniques. Furthermore many high ISD systems reported in the literature [106, 107] require FEC in order to correct for back-to-back errors. Section 4.3 in this chapter will verify that CoWDM allows a system designer to use the additional margin afforded by FEC for genuine transmission impairments.

The final sections in this chapter deal with the impairments which can affect optical signals during transmission in fibre, namely dispersion and nonlinear effects. While the issue of PMD is not explicitly covered in this chapter the performance of CoWDM in transmission links with PMD is considered in chapter 5. As we have shown earlier in this work CoWDM requires a fixed phase relationship between adjacent optical channels in the transmitter. The investigation presented in these sections assesses the impact of dispersion and nonlinearities on this phase relationship by monitoring the performance of CoWDM.

## *4.2 CoWDM at 1 bit/s/Hz ISD*

### 4.2.1 Introduction

This section is concerned with the performance of a standard 42.6 Gbit/s NRZ CoWDM transmitter as outlined in Chapter 3. We will first look at the back-to-back performance of the transmitter when combined with a simple preamplified receiver (section 3.3) and present results showing an ISD of 1 bit/s/Hz for the CoWDM transmission format with a total throughput of 298 Gbit/s for a single polarisation NRZ signal. Following this we consider transmission of a CoWDM signal over approximately 80 km of standard SMF using a standard EDFA amplification scheme.

### 4.2.2 298 Gbit/s CoWDM with 1 bit/s/Hz ISD

The experimental configuration that was used to achieve 298 Gbit/s capacity with an ISD figure of 1 bit/s/Hz consisted of the CoWDM transmitter as described in section 3.5 and the preamplified receiver as outlined in section 3.3. An overview schematic of the back-to-back setup is shown in figure 4.1 below.

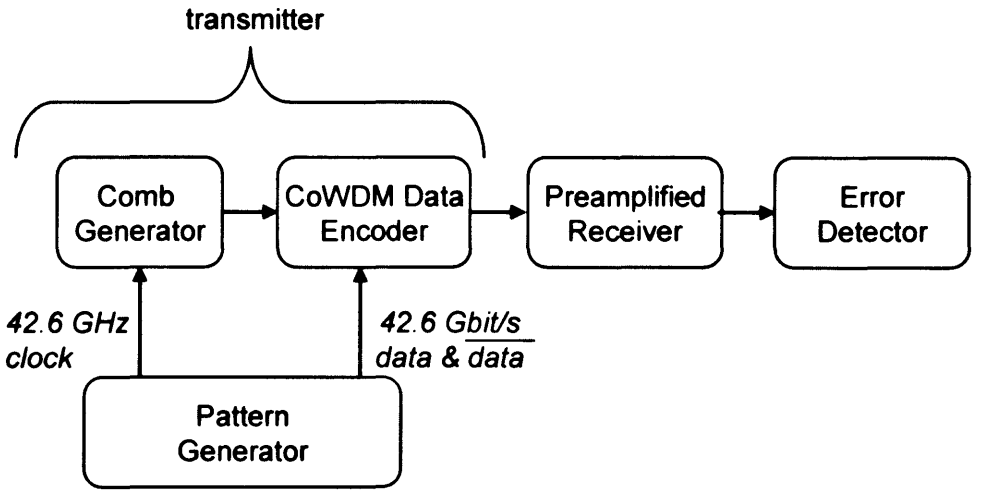



**Figure 4.1. Back-to-back CoWDM experimental setup**

The output of the comb generator was a seven channel optical comb with 42.6 GHz spacing between adjacent channels and a flatness of <0.2 dB, resulting in a total bandwidth of approximately 0.3 nm as shown in figure 4.2.

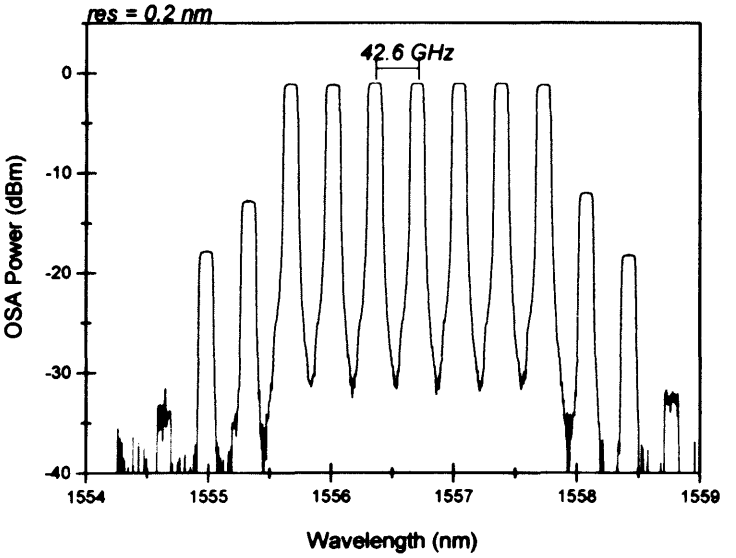



**Figure 4.2. Optical comb generator output**

The comb flatness was maintained by a simple feedback loop (section 3.4.3). The SMSR was kept above 12 dB and the SNR from the peak was approximately 45 dB. An optical pre-amplifier with 27 dB gain and 5 dB noise figure placed before the transmitter was used to in order to overcome the losses within the fibre-based interferometric transmitter. The transmitter was aligned for optimal performance according to section 3.5.2 and polarisation controllers within the transmitter were adjusted to ensure co-polarised output. The odd and even channels were separated using a disinterleaver at the input of the data encoding section and were NRZ data encoded with NRZ $2^7$-1 PRBS data and delayed data-bar patterns respectively at a bit rate of 42.6 Gbit/s. Within the modulator array, optical delay lines and a feedback controlled piezo fibre stretcher were used to maintain the optical phase relationship between the channels. The simulated and experimental optical spectra at the output of the transmitter are shown in figure 4.4 (a) and (b) respectively. The simulations were carried out using VPI Transmission Maker 7.0 and a block diagram of the simulation setup is shown below.

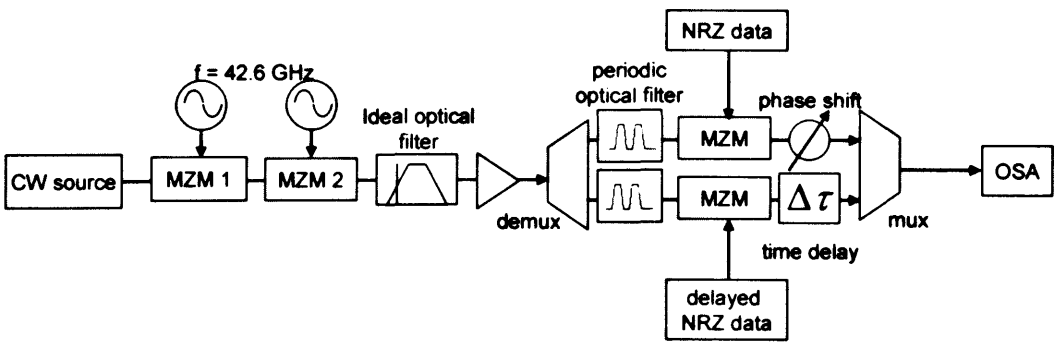



**Figure 4.3. Simulation setup for transmitted spectrum**

Seven 42.6 Gbit/s tributaries spaced by 42.6GHz resulted in a total capacity of 298 Gbit/s and an ISD of 1 bit/s/Hz.

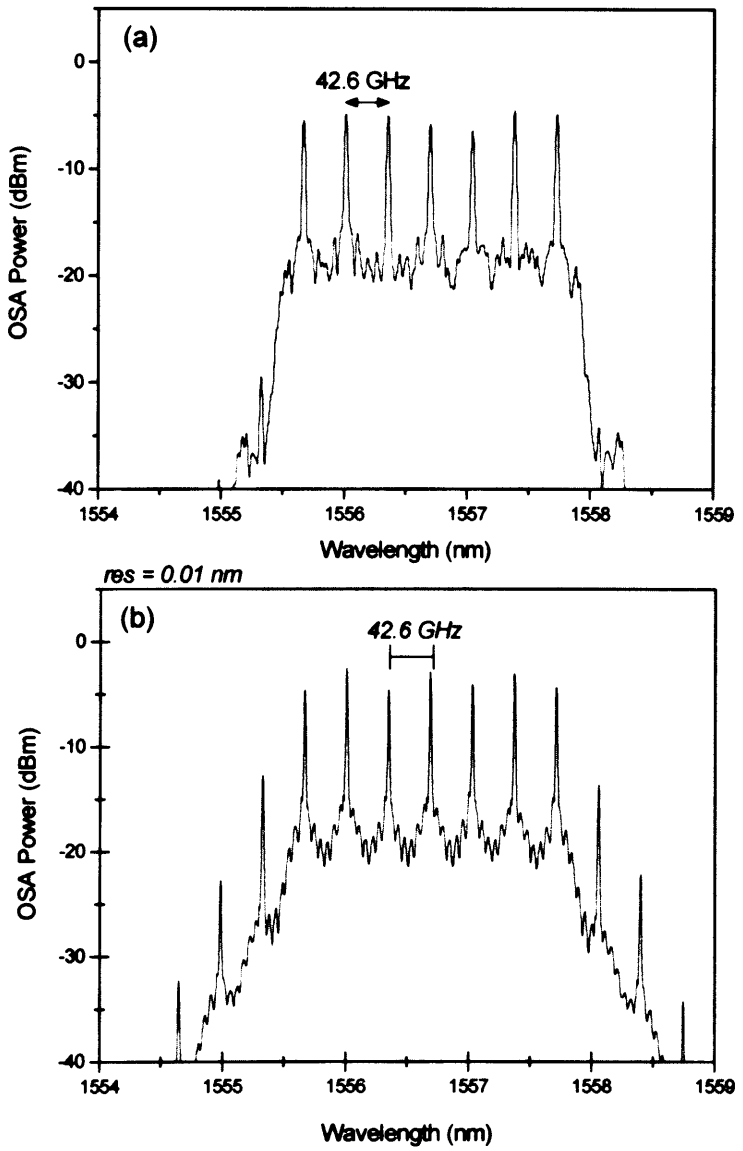



**Figure 4.4. (a) Simulated transmitted optical spectrum (b) Experimental transmitted optical spectrum**

The main difference between the two spectra is the presence of a number of unwanted side modes in the experimental spectrum. These are generated by the side modes of the optical comb generator as described in the previous chapter, and have the effect of slightly reducing the achievable ISD in the more advanced multi-

banded implementation of CoWDM which is described in chapter 5. An ideal implementation of CoWDM would not suffer from the presence of these sidebands. Despite this the CoWDM signal shows very good spectral density when compared to alternative high capacity solutions. In figure 4.5 below for example the CoWDM spectrum (black trace) is overlaid on a wavelength converted 160 Gbit/s OTDM signal (red trace).

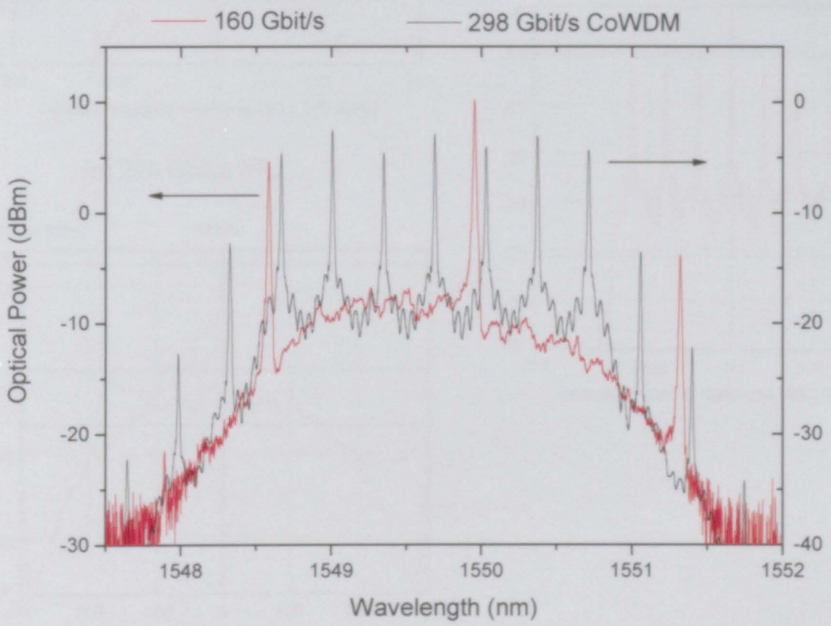



**Figure 4.5. Spectra of 298 Gbit/s CoWDM signal (black trace) and 160 Gbit/s OTDM signal (red trace)**

It is evident that the CoWDM signal is appreciably narrower than the OTDM signal despite being almost twice the bit rate. The OTDM signal was obtained by multiplexing 10 Gbit/s RZ signals to 40 Gbit/s and subsequently to 160 Gbit/s [108]. In order to fully appreciate the advantage in terms of ISD which CoWDM holds over similar bit rate system simulated spectra for 42.6 Gbit/s NRZ, 298 Gbit/s NRZ and 298 Gbit/s CoWDM are shown in figure 4.6 below.

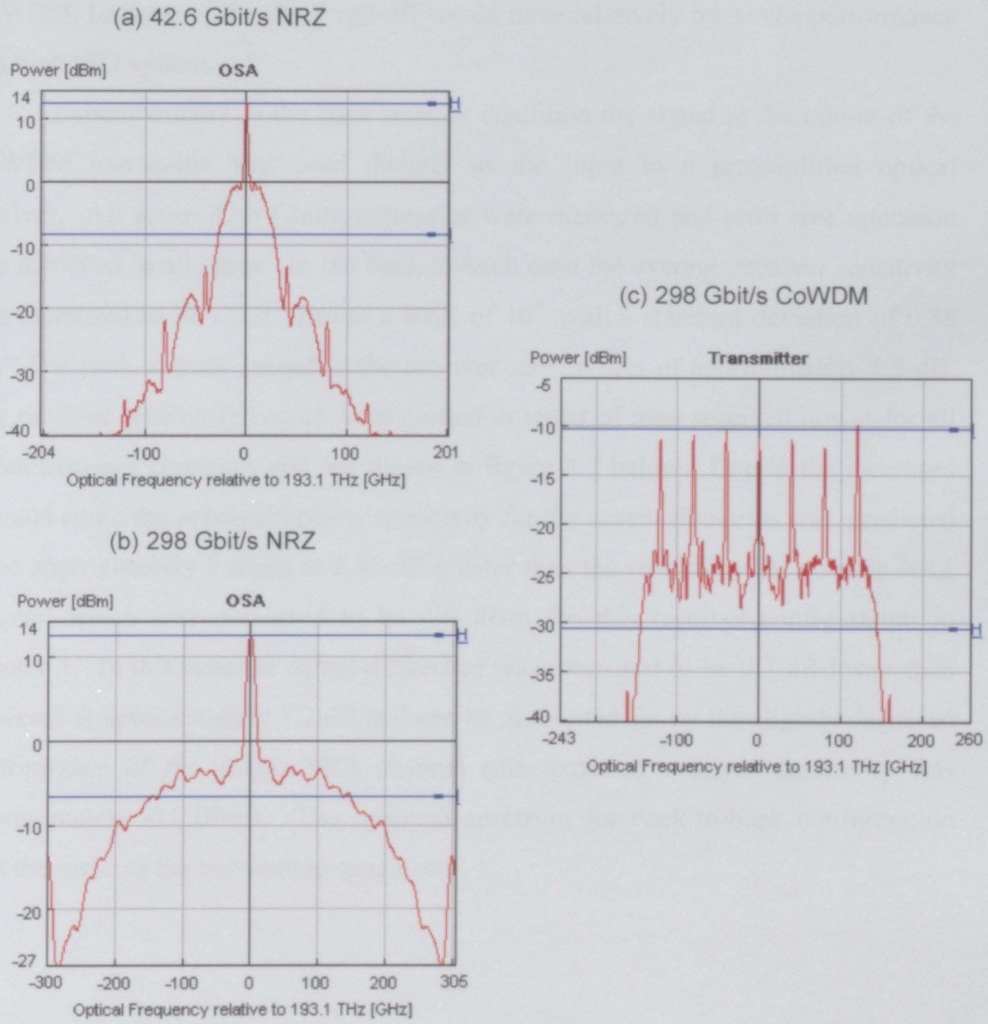



**Figure 4.6. Simulated spectra for (a) 42.6 Gbit/s NRZ, (b) 298 Gbit/s NRZ and (c) 298 Gbit/s CoWDM (OSA power vs optical frequency)**

It is well understood that the spectral width at the 20 dB point (denoted by the blue lines) of the signals varies according to the bit rate. What is important to note however is the steepness of the signal roll-off after this 20 dB level. If we consider the bandwidth at say 30 dB from the peak it is evident that the CoWDM signal exhibits the same sharp roll-off as the 40 Gbit/s NRZ signal whereas the 298 Gbit/s NRZ signal remains spectrally broadened at low power levels. This would lead to increased levels of crosstalk between adjacent channels in high ISD systems.

CoWDM, because of the sharp roll-off would have relatively improved performance in a high ISD system.

Experimentally in the back to back condition the signal at the output of the CoWDM transmitter was used directly as the input to a preamplified optical receiver. All seven 42.6 Gbit/s tributaries were measured and error free operation was achieved in all cases. In the back-to-back case the average receiver sensitivity was measured to be -22.3 dBm at a BER of $10^{-9}$ with a standard deviation of 0.58 dB. The peak-to-peak spread in the receiver sensitivities of approximately 1.5 dB. The receiver sensitivity curves were plotted in terms of total received power for all seven tributary channels, and are shown in figure 4.7 below. Due to the increased channel count the average receiver sensitivity for the seven tributaries was predicted to be approximately 7 times or 8.45 dB greater than the sensitivity for a single NRZ channel which was measured to be -30 dBm for this receiver configuration in chapter 3. In this case the actual difference was measured to be 0.7 dB lower than expected at approximately 7.7 dB and can be accounted for by the slightly degraded performance of the single NRZ channel (the expected receiver sensitivity was approximately -31 dBm). The received spectrum for back-to-back configuration was the same as the transmitted spectrum.

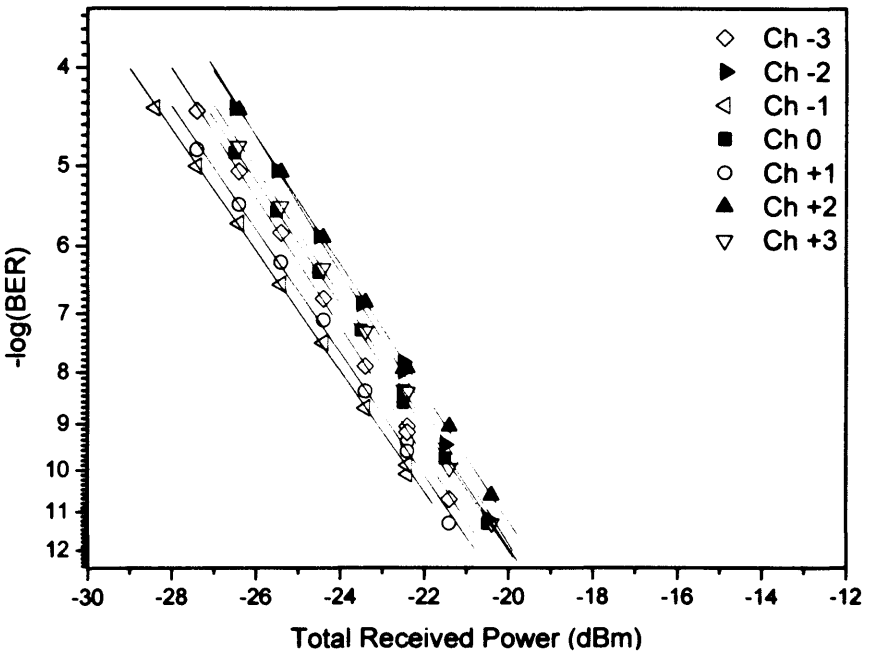



**Figure 4.7. Receiver sensitivity curves for back-to-back 42.6 Gbit/s CoWDM**

The received eye diagrams for each of the 42.6 Gbit/s tributaries are also shown. Each of the eyes shows the characteristic CoWDM shape and is open at the centre and has the residual crosstalk pushed to the eye crossing. The distance between the peaks of adjacent eyes is approximately 23.4 ps.

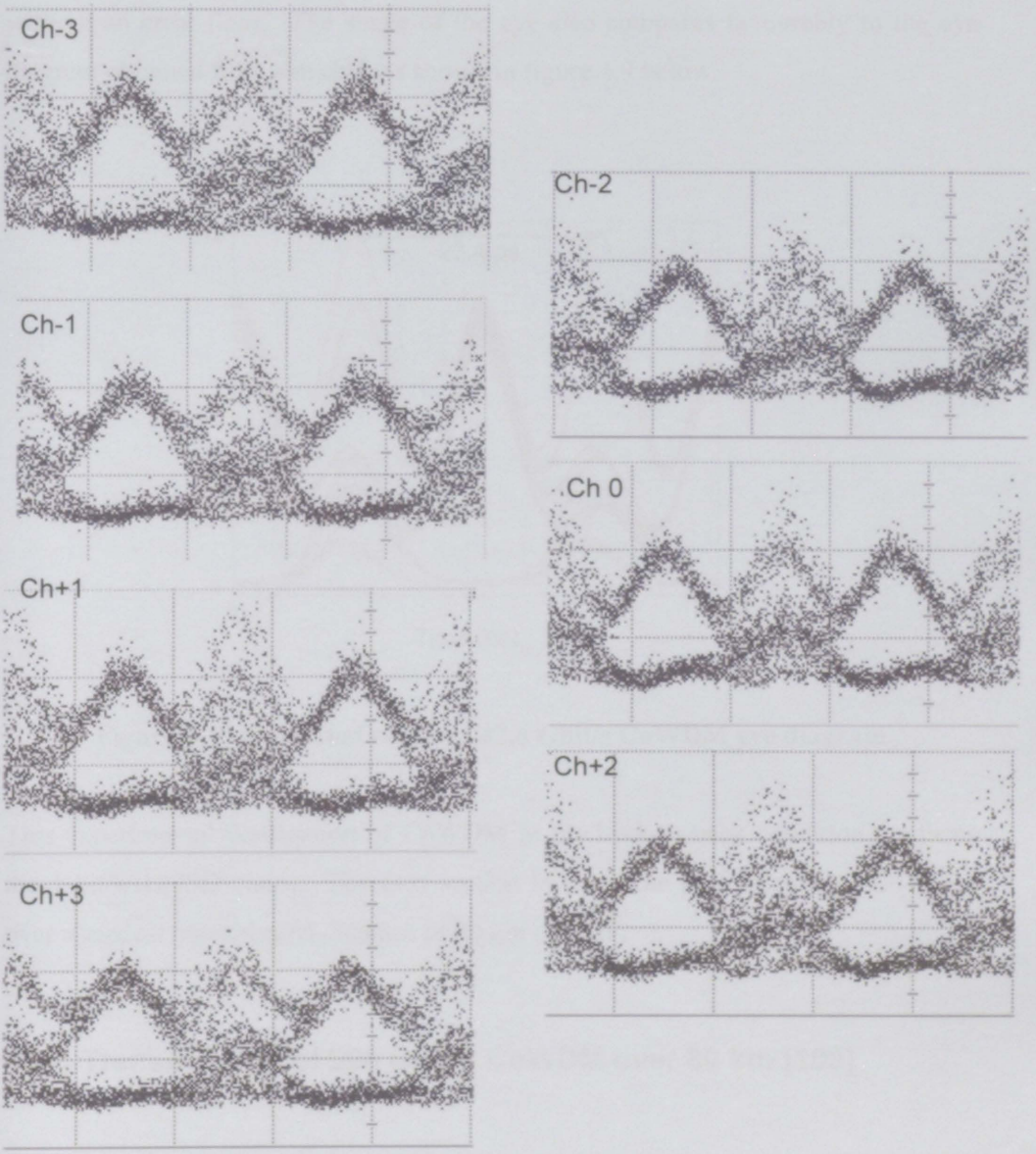



**Figure 4.8. Received eye diagrams for back-to-back CoWDM (5 ps/div)**

There are very slight variations in the shape of the crosstalk at the eye crossing for the different tributaries, with tributaries 0 and +1 showing slightly higher levels of noise at the eye crossing. This was possibly due to slight variations in the phase position at the transmitter but did not prevent each of the channels from operating

without an error floor. The shape of the eye also compares favourably to the eye diagram obtained from simulations shown in figure 4.9 below.

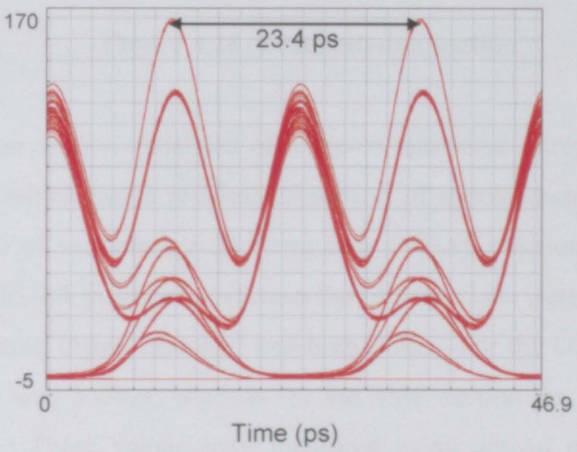



**Figure 4. 9. Simulated received 42.6 Gbit/s CoWDM eye diagram**

This experimental verification of CoWDM in the back-to-back condition confirms the 1 bit/s/Hz ISD claim. The next section looks at the performance of CoWDM over a modest transmission distance of 80 km of SMF.

### 4.2.3 Transmission of 298 Gbit/s CoWDM over 80 km [109]

In the last section we saw how a 298 Gbit/s CoWDM signal was generated to give an overall ISD of 1 bit/s/Hz in the back-to-back condition. However modern optical communication systems rarely, if ever operate in a back-to-back configuration so an evaluation of the performance of CoWDM over a fibre section was necessary. In order to achieve this we introduced a transmission section after the CoWDM transmitter as shown in figure 4.10.

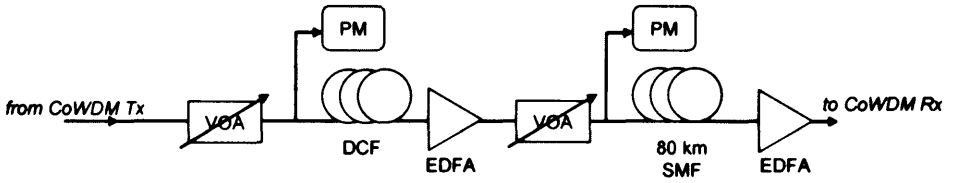



**Figure 4.10. Transmission section**

This transmission section consisted of a pre-compensated unrepeatered link of 80 km of SMF-28 which had a residual dispersion of approximately -7 ps/nm at the receiver. A pair of variable optical attenuators (VOA), positioned before the fibre sections and an EDFA positioned between the fibre sections were used to control the power of the optical signal launched into both fibres. For the DCF section the total launched power was 3 dBm, whereas for the SMF section the total launch power was 11.6 dBm. These values were measured using optical power meters (PM) placed before the fibre sections and were chosen such that nonlinear effects in the fibre were not generated. The EDFA positioned between the fibre sections to boost the signal had a gain of 20 dB and a noise figure of 5.5 dB. Another EDFA with the same characteristics was used after the transmission section to compensate for the fibre losses before the receiver.

In the same manner as for the back-to-back condition all seven CoWDM tributaries were measured at the receiver. All of the tributaries demonstrated error free performance and the receiver sensitivity curves are shown in figure 4.11 below.

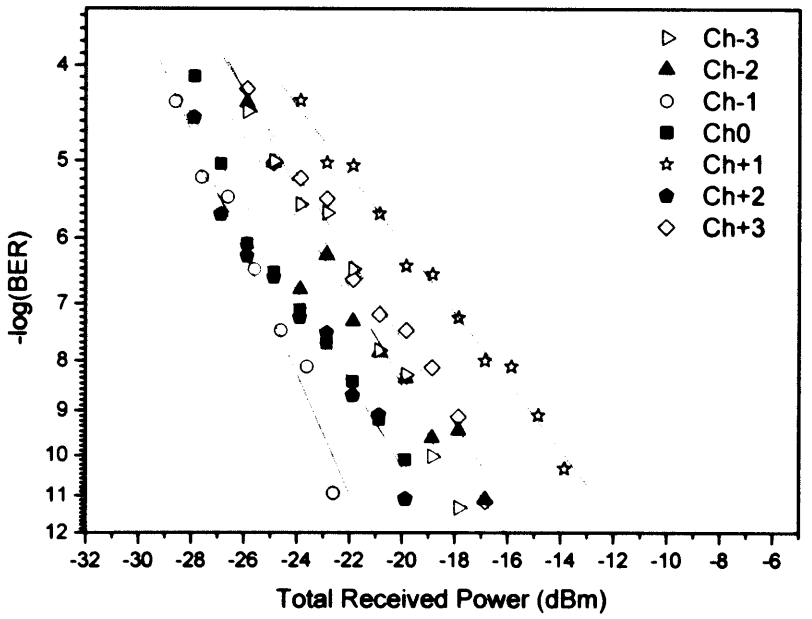



**Figure 4.11. Receiver sensitivity for all seven channels over 80.km of SMF**

The average receiver sensitivity of -19.4 dBm, with a standard deviation of 3 dB after transmission is slightly degraded with respect to the back-to-back case. The residual dispersion of -7 ps/nm was responsible for the larger spread of the receiver sensitivity values than in the back-to-back case. This is because the residual dispersion causes a walkoff in the phase relationship between adjacent channels which results in an increased variation in the receiver sensitivity values. Section 4.4.3 shows the impact of dispersion on the CoWDM format and we can see from figure 4.23 that a residual dispersion figure of -7 ps/nm is predicted to result in a receiver sensitivity penalty of approximately 3 dB. In addition to this much of the spread can be attributed to the dispersion of the optical comb signal with respect to the data in the transmitter which was in place when this investigation was conducted. This feature of the transmitter was discussed in the section 3.5.5 in the previous chapter where a solution to the problem was proposed and the implementation details discussed. As will be shown later in the thesis improved results (reduced spread in receiver sensitivity values) were obtained with optimised implementation. The received 42.6 Gbit/s spectra and eyes for three tributaries are shown below in

figure 4.12. Again similar to the back-to-back eyes all show a clean open centre with the crosstalk located at the eye crossing. As expected due to the addition of the 80 km section of fibre the shape of the eye is slightly dispersed when compared to the back-to-back eye. Slight misalignment of the transmitter is evident for tributary +2 where the position of the 80 GHz component can be seen to be slightly skewed to the right with respect to the centre of the eye.

Despite this error free transmission over 80.4 km was achieved for the 298 Gbit/s CoWDM, NRZ encoded, 1 bit/s/Hz signal confirming CoWDM as a candidate transmission format for high ISD modern optical communication networks.

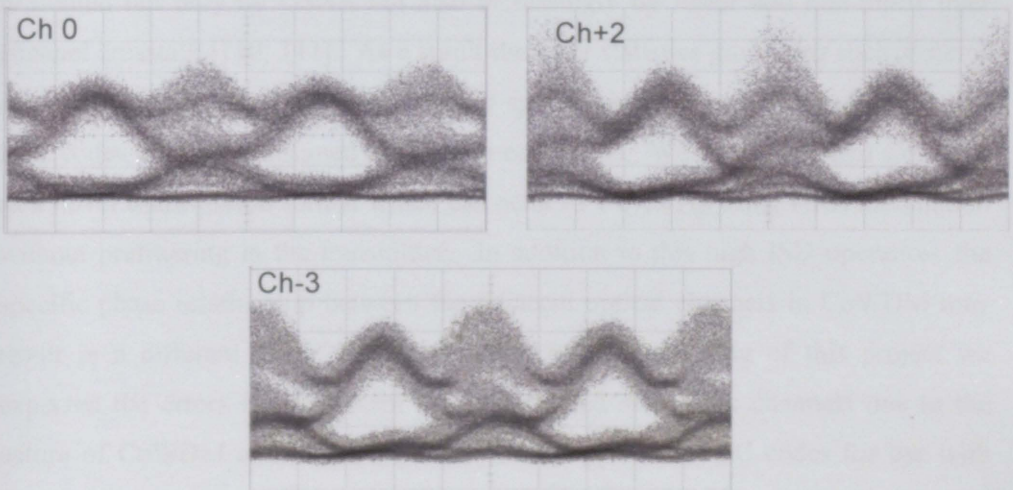



**Figure 4.12. Eye diagrams and spectra for three CoWDM tributaries after transmission over 80 km of SMF**

### 4.2.4 Summary

In this section the performance of both back-to-back and 80.4 km transmission of a 298 Gbit/s CoWDM signal has been presented. Seven co-polarised NRZ encoded 42.6 Gbit/s channels separated by 42.6 GHz were successfully transmitted error free over 80 km of SMF without the use of FEC codes resulting in an ISD of 1 bit/s/Hz. Despite a residual dispersion value of -7 ps/nm all tributaries were shown to be error

free after transmission. This is a significant result as it confirms that the CoWDM transmission format is not adversely affected by transmission impairments in standard fibre.

## *4.3 Performance Evaluation of CoWDM with FEC codes*

### 4.3.1 Introduction

As modern high bit rate optical communication systems achieve higher and higher ISD values by using a wide range of techniques the BER of the transmitted channels is limited not only by OSNR but also increasingly by linear and non-linear inter channel crosstalk [110, 111]. As a result the error statistics governing such systems may no longer be the same as for widely spaced channels and the performance of FEC codes cannot be assumed under such conditions. We have presented CoWDM as a novel transmission format which can achieve 1 bit/s/Hz using NRZ modulation without prefiltering in the transmitter. In addition to this high ISD operation, the specific phase relationship between the adjacent optical channels in CoWDM may result in a different set of error statistics. At the beginning of this project we expected the errors in the system to be correlated across the channels due to the nature of CoWDM and it was intended to develop novel FEC codes for use with CoWDM. On examination of the error statistics however it became apparent that this would be unnecessary as the error distribution of a CoWDM system was the same as for a standard widely spaced WDM system. Therefore in this section we demonstrate CoWDM in combination with a range of FEC codes in order to fully investigate the performance of FEC codes with the novel transmission format CoWDM. In order to provide a reference to a standard system these results are compared with the performance of the same FEC codes on a single 42.6 Gbit/s NRZ channel. The investigations described in this chapter were also the first reported full line rate FEC measurements at 42.6 Gbit/s as all previous work reported in the literature was carried out at the demultiplexed line rate of ~10 Gbit/s or lower.

### 4.3.2 Overview of FEC codes

As was mentioned in chapter 1 FEC codes play an important role in modern optical communication systems. Most installed optical systems make use of standard Reed-Solomon (RS) FEC codes in order to correct for errors at the receiver [82]. As a result, where before the introduction of FEC a BER of $<10^{-15}$ was necessary for acceptable performance in an optical communication system at the beginning of life, FEC codes allow for a degradation of the received BER before decoding to as high as $\sim 10^{-3}$. This gives system designers additional margin which they can use to improve other areas of the system, for example to increase transmission distance, repeater spacing or reduce launch power. The main trade-off required when using FEC codes is a slight increase in the overall bit rate of the system which is dependant on the characteristics of the FEC code employed [112].

The most commonly used FEC codes in modern optical communication systems are standard (1) single stage and (2) concatenated RS codes [113]. RS codes are a member of the non-binary Bose-Chaudhuri-Hocquenghem (BCH) code family and have a wide range of applications e.g. (data storage, data transmission). A full description of the operation of block FEC codes and more specifically the encoding and decoding of RS codes is beyond the scope of this work but can be found in [114, 115, 114].

(1) Single stage RS codes

Single stage RS codes are implemented as shown in figure 4.13 below. An information sequence divided into fixed length blocks is encoded using an FEC encoder and the resultant FEC frame (of total length '$n$') is transmitted. There are '$n$-$k$' information bits and '$k$' overhead bits in any given FEC frame. Errors introduced in the transmit section (represented by dashed vertical lines on the FEC frame) are corrected using a FEC decoder and ideally the original information sequence is recovered. Single stage codes are relatively simple to

encode and decode and perform optimally when there is a Gaussian distribution of the errors. One drawback, however is that they cannot correct burst errors of length greater than $k/2$, i.e. half the length of the overhead.

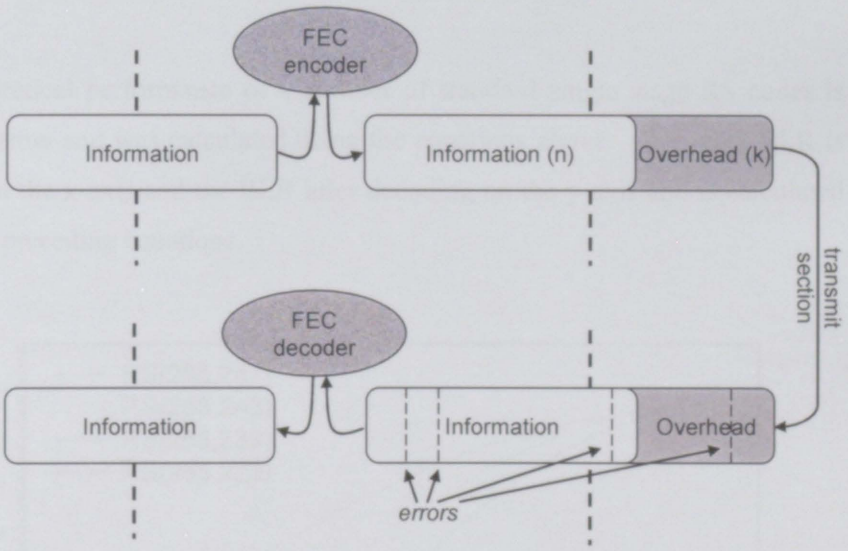



**Figure 4. 13. Single stage RS code**

The theoretical relationship between the BER after FEC correction and the BER before FEC correction is used as a criterion for evaluating the effectiveness of any particular FEC code. Equations 4.1, 4.2 and 4.3 define this relationship for RS codes and assume independent errors and perfect decoder operation (i.e. the probability of incorrect decoding is zero) [51]

$$P_E \approx \frac{1}{2^m - 1} \sum_{j=t+1}^{2^m-1} j \binom{2^m - 1}{j} P_{SE}{}^j (1 - P_{SE})^{2^m - 1 - j} \tag{4.1}$$

$P_E$ is the probability of an uncorrected error, m is the number of bits per symbol, t is the number of correctable symbols and $P_{SE}$ is the probability of a symbol

error. The input and output BERs are related to the symbol error rates by the following two equations.

$$BER_{in} = 1-(1-P_{SE})^{1/m} \tag{4.2}$$

$$BER_{out} = 1-(1-P_{E})^{1/m} \tag{4.3}$$

The theoretical performance of a number of standard single stage RS codes is shown below and was calculated using the equations above. The input BER is shown on the x-axis and the BER after decoding on the y-axis and is calculated from the preceding equations.

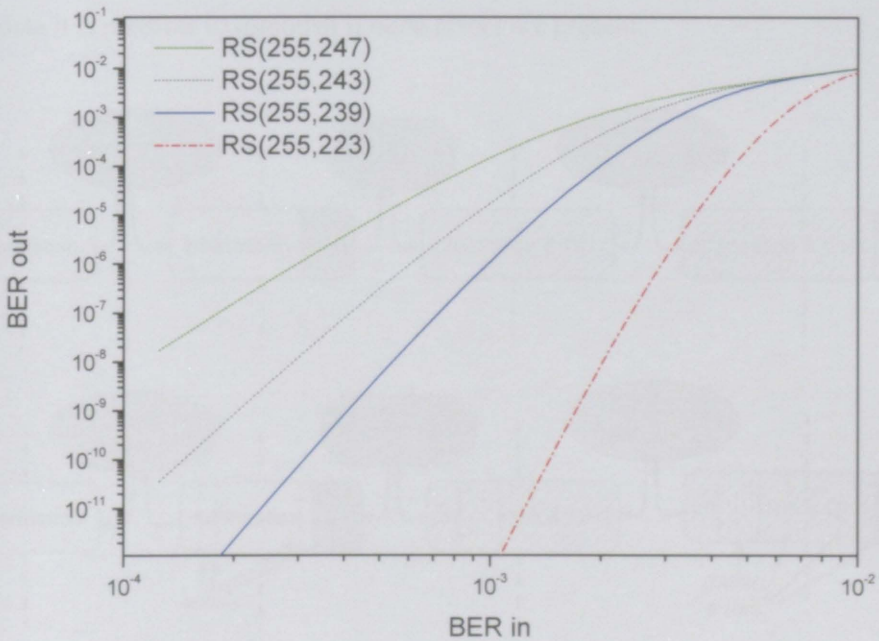



**Figure 4.14. Output BER as a function of input BER for four different single stage RS codes**

It is clear from this plot that the higher the overhead the better the performance of the FEC code.

(2) Concatenated RS codes

Concatenated RS codes make use of an interleaver/disinterleaver combination which is placed between two data encoding/decoding stages as shown in the figure below. By interleaving the bits between the encoding steps before transmission and disinterleaving them between the two independent decoding steps (thus spreading any errors which may have occurred during transmission across the entire frame) concatenated codes have a much higher tolerance to burst errors than single stage codes [116, 117, 118]. Because of this if we compare the performance of single stage and concatenated codes with the same data it is possible to establish if burst errors are present.

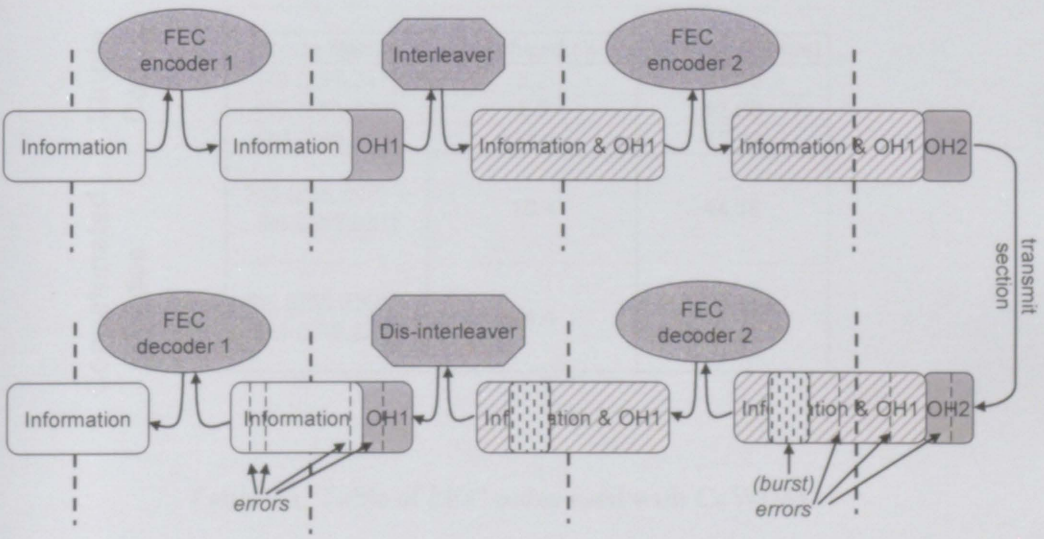



**Figure 4.15. Concatenated codes construction**

In this section we look at the performance of the CoWDM transmission format when used in combination with both single stage and concatenated RS codes.

The interleaver used to scramble the bits in the FEC frame for this work was a block interleaver. These types of interleaver takes in a set of symbols and rearranges them according to a mapping function without repeating or deleting any

of the elements in the set. In this work a random block interleaver and a corresponding disinterleaver, both implemented in MATLAB were used [119, 120].

### 4.3.3 CoWDM and FEC [121]

In order to evaluate the performance of FEC codes with CoWDM, PRBS data was generated and encoded in software to form the code words for each of the RS codes considered. A list of the RS codes investigated in this section along with the overhead associated with each code is shown in table 4.1. The standard code used in optical communications is a concatenated version of the RS (255,239) code.

| | Code Name | Overhead (%) | Bit Rate (Gbit/s) |
|---|---|---|---|
| Single Codes | RS (255,247) | 3.2 | 41.28 |
| | RS (255,239) | 6.7 | 42.68 |
| | RS (255,223) | 14.4 | 45.76 |
| Concatenated Codes | RS (255,243) + RS (243,231) | 10.4 | 44.16 |
| | RS (255,239) + RS (239,223) | 14.4 | 45.76 |

**Table 4.1. Table of FEC codes used with CoWDM**

The encoding and decoding functions [122] were adapted for the concatenated codes by incorporating a block interleaver section which scrambled the bitstream according to a randomly generated seed, and a zero padding function which ensured that there were no 'leftover' bits as a result of the double stage encoding. This was necessary for the correct uploading of the test words to the pattern generator which only accepted data patterns of specific fixed lengths. This also determined the number of PRBS blocks which were encoded. The FEC overhead and data frames

were converted from binary format to hexadecimal format and loaded onto the PPG where they were subsequently used to encode the optical signals in the CoWDM transmitter. The bit rate of the transmitter was maintained at 42.6 Gbit/s for each of the codes which were used. This meant that the amount of information which was transmitted during any particular investigation depended on the overhead of the code which was used. Figure 4.16 below shows the flow of the encoding and decoding processes for a concatenated code.

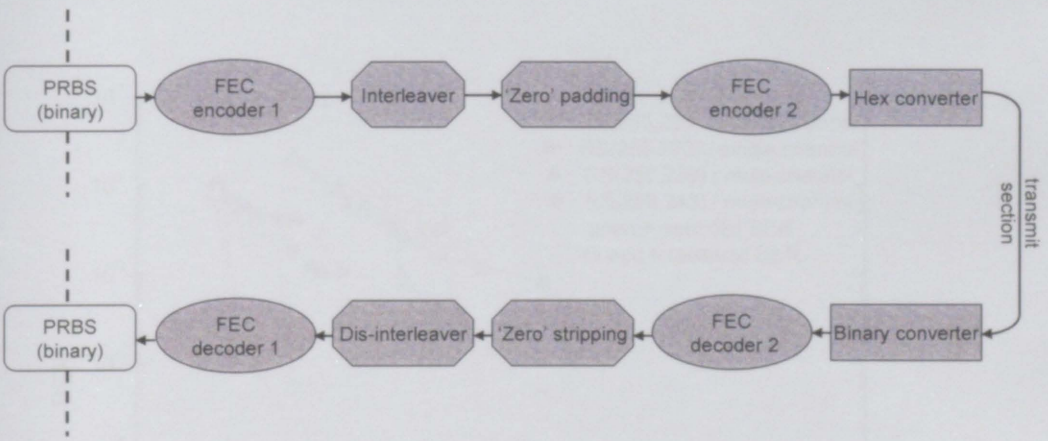



**Figure 4.16. Encoding and decoding steps for a concatenated code**

Following detection at the receiver, the waveform was converted into a digital bit stream, and a portion of the data consisting of at least one full code word was stored using a field programmable gate array built into the error detector. The stored data was then transferred to a PC where it was decoded in software using the Berlekamp iterative algorithm [113] to give a decoded data stream. This data sequence was then compared with the original PRBS sequence and a BER was evaluated. This process was repeated until an accurate estimate of the residual error probabilities was obtained. This method, due to the limited transfer capacity between the error detector and the PC restricted the decoded error rate to approximately $10^{-6}$. Acquisition time for such an error rate typically took several hours.

### 4.3.4 Results

Figure 4.17 shows typical performance of a selection of FEC codes when applied to both a single NRZ channel (squares and circles) and a multi channel CoWDM system (triangles and diamonds). It is clear from the plot that the higher the coding overhead the better the coding gain achieved (for example the separation between the decoded and received BER for RS (255,239) is much larger than that for RS (255,243)).

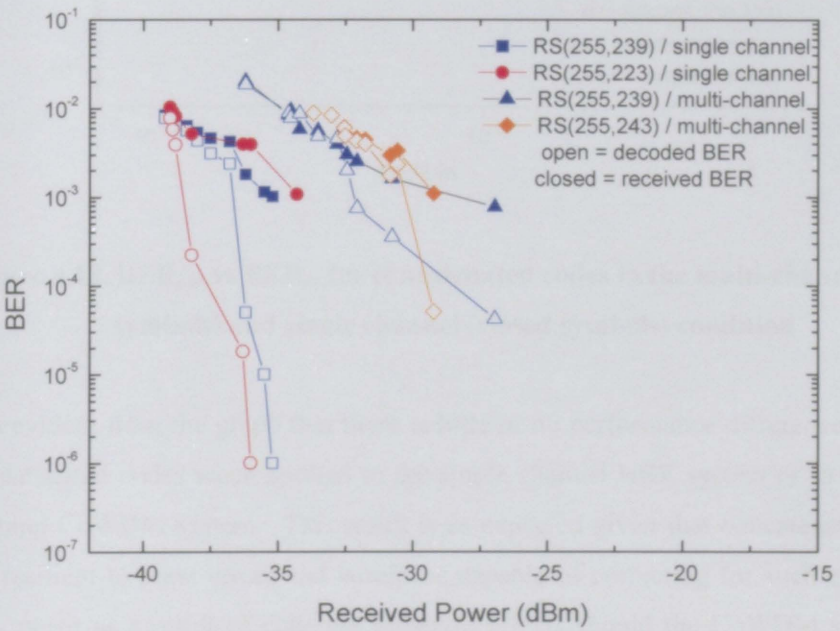



**Figure 4.17. BER vs total received power for selected RS codes**

From such data the plot of the $BER_{out}$ as a function of $BER_{in}$ may be plotted (figure 4.18). This shows the typical performance of the concatenated codes when applied to a single 42.6 Gbit/s NRZ channel (closed symbols) and a multi channel CoWDM system (open symbols).

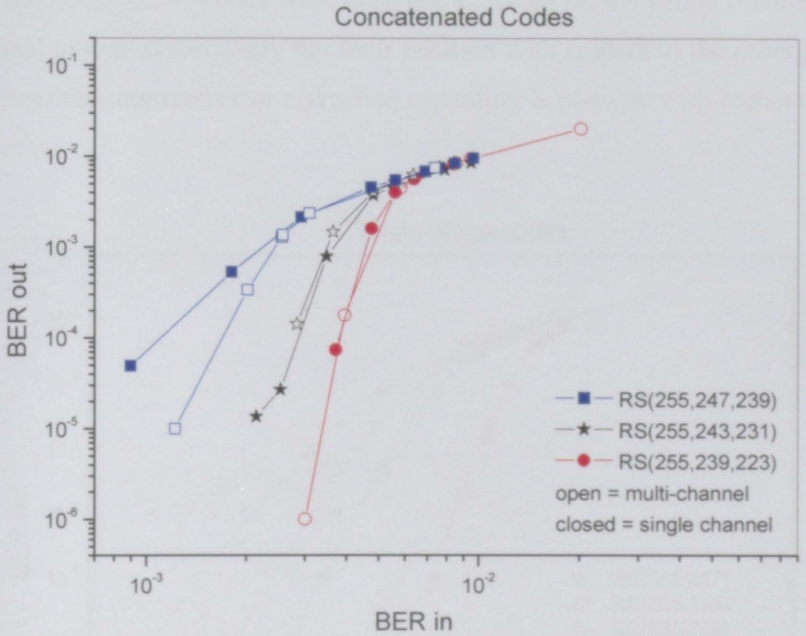



**Figure 4.18. $BER_{out}$ vs $BER_{in}$ for concatenated codes in the multi-channel (open symbols) and single channel (closed symbols) condition**

It is evident from the graph that there is little or no performance difference between concatenated codes when applied to the single channel NRZ system or to the multi channel CoWDM system. This result is as expected given that concatenated codes are resilient to burst errors and would be capable of correcting for such errors that may occur as a result of coherent crosstalk effects should the CoWDM system be governed by a different set of error statistics than a single NRZ channel. In contrast to this single stage codes are more susceptible to burst errors and consequently would be less effective if CoWDM were to produce a different distribution of errors. Figure 4.19 shows the typical performance of a range of single stage RS codes when applied to a single 42.6 Gbit/s NRZ channel (closed symbols) and a multi channel CoWDM system (open symbols). The theoretical plots for the various single stage codes are also included in this figure and there is very good agreement between these and the experimental results. This result also verifies the case that CoWDM is not degrading the performance of FEC codes in any way. The RS (255,223) code

and the RS (255,243) code were only implemented on the single channel and multi-channel system respectively but their position with respect to the other points again verifies that improved error correction capability is possible with higher overhead.

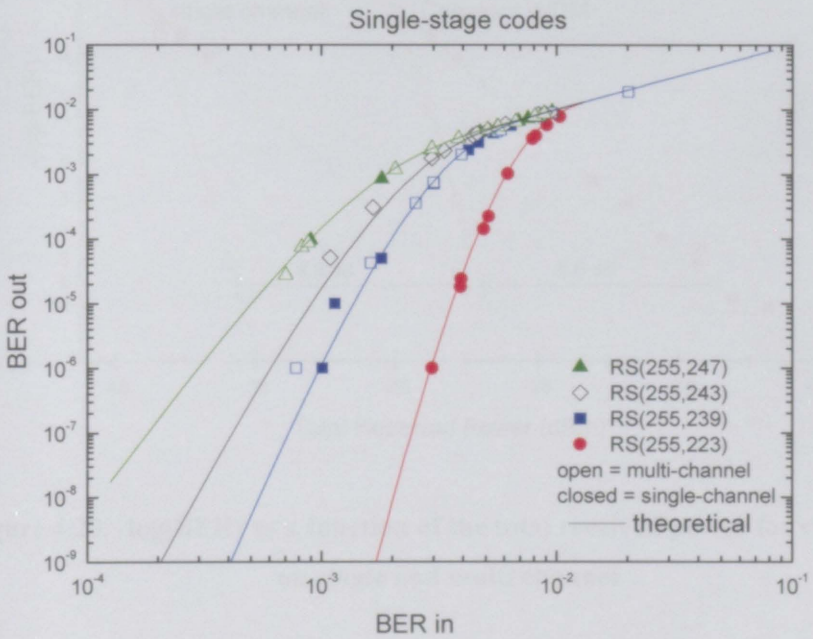



**Figure 4.19. $BER_{out}$ vs $BER_{in}$ for single-stage codes in the multi-channel (open symbols) and single channel (closed symbols) condition**

It is clear from the figure that approximately the same net coding gain (NCG) was achieved by the single stage codes in both cases, implying that the error statistics arising in a multi channel CoWDM system despite its high ISD are the same as those generated by a single NRZ channel. For ease of comparison the log of the BER is plotted as function of the total received power for a single stage code for both the single NRZ channel case and the multi channel CoWDM case, together with extrapolations to lower bit rates is plotted in figure 4.20. The difference between the received BER and the decoded BER at the $10^{-9}$ extrapolation is 6.5 dB and 6.6 dB for the single-channel and multi-channel condition respectively.

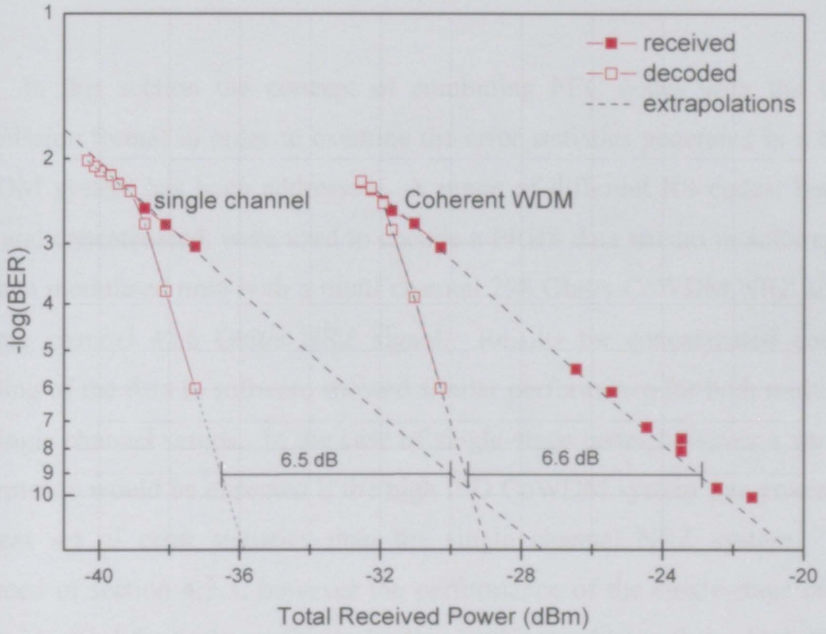



**Figure 4.20. -log(BER) as a function of the total received power for single code on single and multi channel**

From these figures it is evident that approximately the same NCG was achieved in both cases. This significant result demonstrates that RS FEC codes designed for use with single channel or widely spaced WDM systems continue to function correctly for high ISD WDM systems and more specifically for high ISD systems based on the CoWDM transmission format. It also confirms that the error statistics which govern a CoWDM system are exactly the same as those which influence a single channel NRZ signal. In addition in a real system the FEC margin could be applied directly to improve the OSNR of the system as CoWDM is capable of running error free without FEC.

### 4.3.4 Summary

In this section the concept of combining FEC codes with the CoWDM transmission format in order to examine the error statistics generated in a high ISD CoWDM system has been addressed. A range of different RS codes, both single stage and concatenated, were used to encode a PRBS data stream in software which was then modulated onto both a multi channel 298 Gbit/s CoWDM NRZ signal and a single channel 42.6 Gbit/s NRZ signal. Results for concatenated codes after decoding of the data in software showed similar performance for both multi channel and single channel setups. In the case of single-stage codes however a variation in performance would be expected if the high ISD CoWDM system was governed by a different set of error statistics than the single channel NRZ system. As was presented in section 4.3.3, however the performance of the single-stage codes was almost identical for both conditions leading to the conclusion that a high ISD multi channel CoWDM system is governed by the same error statistics at those affecting a tributary channel, i.e. a single 42.6 Gbit/s NRZ channel.

In conclusion we have confirmed the compatibility of CoWDM with the standard RS FEC codes used in modern optical communication systems and we have demonstrated that there are no changes to the error distribution affecting a high ISD CoWDM signal when compared to single channel operation.

## *4.4 Dispersion Tolerance of CoWDM [123]*

### 4.4.1 Introduction

We have already seen that the principle of the CoWDM transmitter is based on control of the relative optical phase relationship between adjacent channels in order to allow optimal alignment of the relative optical phases thus increasing the eye opening at the receiver. Optical signals in modern communication systems are typically transmitted over several hundreds of kilometres and as a result fibre induced impairments such as chromatic dispersion and fibre nonlinearities must be considered when choosing a transmission format. In this section we consider the impact of dispersion on a CoWDM signal and present the results of an investigation to determine if the signal walk off which one might expect to occur in the presence of dispersion has an effect on the performance of CoWDM.

### 4.4.1 Dispersion in Optical Communication Systems

Fibre induced dispersion effects can severely degrade the performance of a typical 40 Gbit/s high ISD WDM system. There are different types of dispersion but this section is primarily concerned with chromatic dispersion, where pulses at different wavelengths propagate through the fibre at different speeds leading to pulse broadening. For high bit rate, high ISD systems this leads to an increased amount of temporal broadening which can cause intersymbol interference within the channel and may increase the width of the crossing region between adjacent channels and reduces the performance of the system. Figure 1.5 in chapter 1 showed the transmission distance as a function of bit rate for a single NRZ channel in standard SMF which has a CD value of approximately 17 ps/nm/km. It is evident from this figure that high bit rate systems without dispersion compensation strategies are limited to very low transmission distances (<5 km for 40 Gbit/s) because of the effects of dispersion. In addition to this pulse broadening effect it might be expected

that a high ISD system using the CoWDM transmission format would suffer an additional penalty due to the importance of the phase relationship between adjacent channels in the transmitter. The impact of dispersion on this phase relationship as the signal propagates in the fibre is crucial in the evaluation of CoWDM as a candidate transmission format for use in medium to long haul optical links, where the effects of dispersion are unavoidable.

### 4.4.3 Investigation of Dispersion Effects on CoWDM

The experimental setup used for the investigation of dispersion on CoWDM was the same as that shown in section 4.2.3 except that varying lengths of SMF without optical amplifiers were used in place of the transmission link. Total SMF lengths of 0, 200, 400 and 600 m were used to increase the amount of dispersion in the link. The dispersion tolerance for a 298 Gbit/s CoWDM system was investigated by measuring the receiver sensitivity penalty at a BER of $10^{-9}$ between the back-to-back condition (zero dispersion) and the various conditions where fibre was introduced between the transmitter and receiver. The results of these measurements which were initially performed with the optical phase value maintained throughout at a fixed value (optimised value for the back-to-back condition) are shown in figure 4.21. The open squares represent the experimental data and the dashed line shows the performance as predicted by simulations performed in VPITransmission MakerV6.5. The initial simulations were performed using the setup shown in figure 4.3 where two data modulators were used to encode the 7 tributary channels.

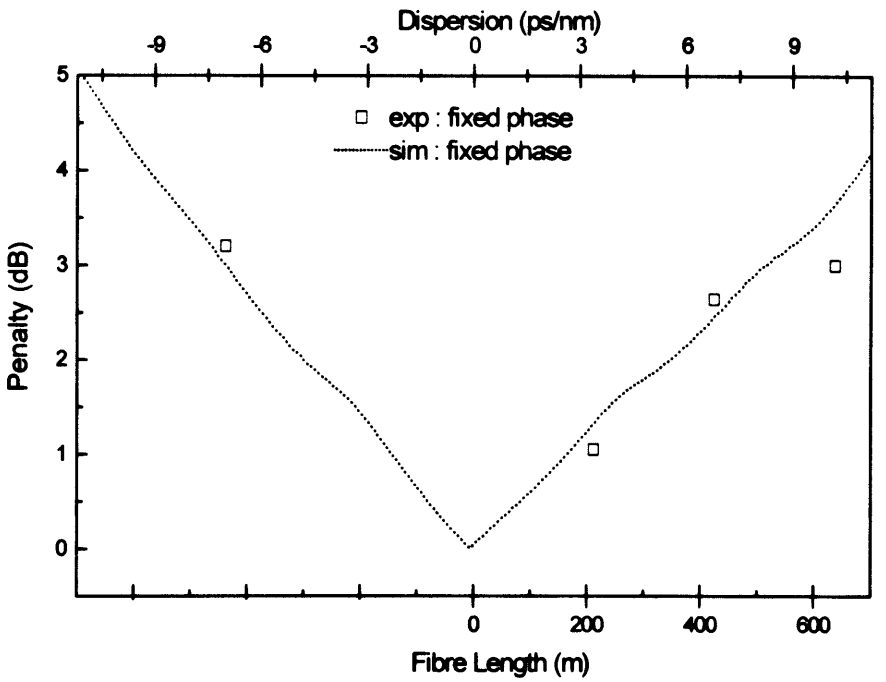



**Figure 4.21. Receiver sensitivity penalty as a function of fibre length (chromatic dispersion) for fixed phase condition**

The experimental results obtained are in clear agreement with the predictions and a 1 dB receiver sensitivity penalty is observed at approximately 3 ps/nm. This value is comparable to the 1 dB penalty for an 80 Gbit/s OTDM signal [124]. A sensitivity penalty of 2 dB or less is predicted across a 9.8 ps/nm range between -4.8 and +5.6 ps/nm. Figure 4.22 below shows received eye diagrams for a randomly selected tributary before and after transmission over 80 km of fibre (as described in section 4.2.3). It is interesting to note that while the eye diagrams after transmission do not shown distortion at the centre of the eye, the shape of the eye crossings have changed somewhat with respect to the back-to-back received eye diagrams. As expected the interference is in the form of RZ-shaped pulses from transitions in adjacent tributaries which are aligned at the eye crossing.

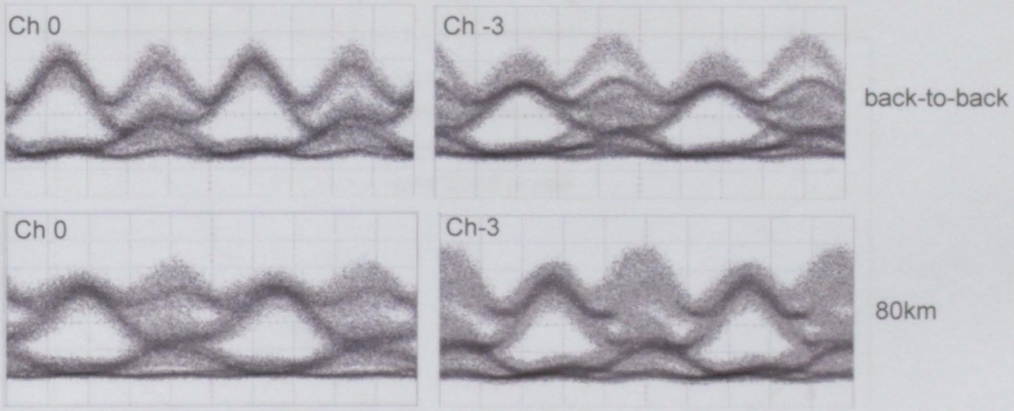



**Figure 4.22. Eye diagrams for tributary # 0 and tributary # -3 for each both back-to-back and 80 km transmission**

It was suspected that this change in the shape of the eye at the crossing was due to the phase relationship between adjacent tributaries which was selected at the transmitter. This hypothesis is in line with the idea presented in chapter 3 that the optimal alignment of the transmitter is closely linked to the transmission link and the filters in the optical receiver. Therefore it should be possible to improve the performance of the system by 'pre-compensating' the optical phase at the transmitter to better suit the different amounts of dispersion. In order to investigate this effect the same simulation as before was carried out but with optimised optical phase values for each amount of residual dispersion, ranging from -11 to + 11 ps/nm. In the experimental setup the target phase value of the phase stabilisation circuit was selected to give optimum performance after transmission in each case. These results are presented (solid line, closed symbol) in figure 4.23 below where we can see a marked improvement in performance with respect to the fixed phase case (dashed line, open symbol).

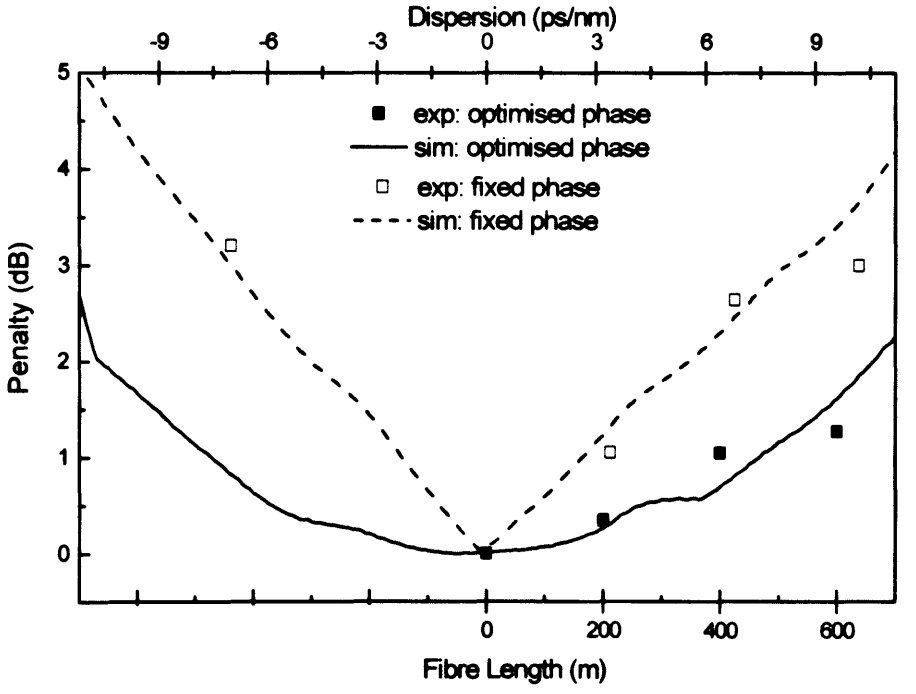



**Figure 4.23. Receiver sensitivity penalty as a function of fibre length for both fixed optimised phase condition**

For this phase optimised condition the 1 dB receiver sensitivity penalty is observed at ±7 ps/nm, which is comparable to a 40 Gbit/s signal when the same optical filters are used in the receiver. The performance improvement can be further quantified in terms of a receiver sensitivity penalty reduction from 2.64 to 1.05 dB for the experimental point at 6.4 ps/nm. Moreover the predicted dispersion range for a 2 dB receiver sensitivity penalty has increased from ± 9.1 ps/nm to ± 10.7 ps/nm, thereby confirming the benefits of a phase precompensation strategy to combat the effects of dispersion in a CoWDM system.

In both the simulations and experimental work described above two data modulators were used in the CoWDM transmitter to independently encode the odd and even channels with data and delayed data bar NRZ data at 42.6 Gbit/s. However a 'real-world' implementation of a CoWDM system would use '$n$' data modulators to modulate the '$n$' optical channels. In order to verify that the unavoidable

correlation between interfering channels which occurs in the experimental 2 data modulator case does not benefit the system in any way we performed the simulations incorporating seven independent modulators driven by independent data sequences. These results are presented in figure 4.24 (dashed trace) and it is evident that even further enhancement of the phase precompensation is possible under these conditions.

This result is understandable as we now have full control over the optical phase of each individual channel. When this result is compared with the results presented earlier in figure 4.23 we can confirm that the experimental demonstration using two independent modulators represents a 'worst case' scenario in terms of receiver sensitivity penalty. Figure 4.24 also shows the experimental (closed symbols) and predicted results (solid trace) for a phase optimised system together with the estimated 1 dB penalty dispersion tolerances of a number of high bit rate systems [36, 125].

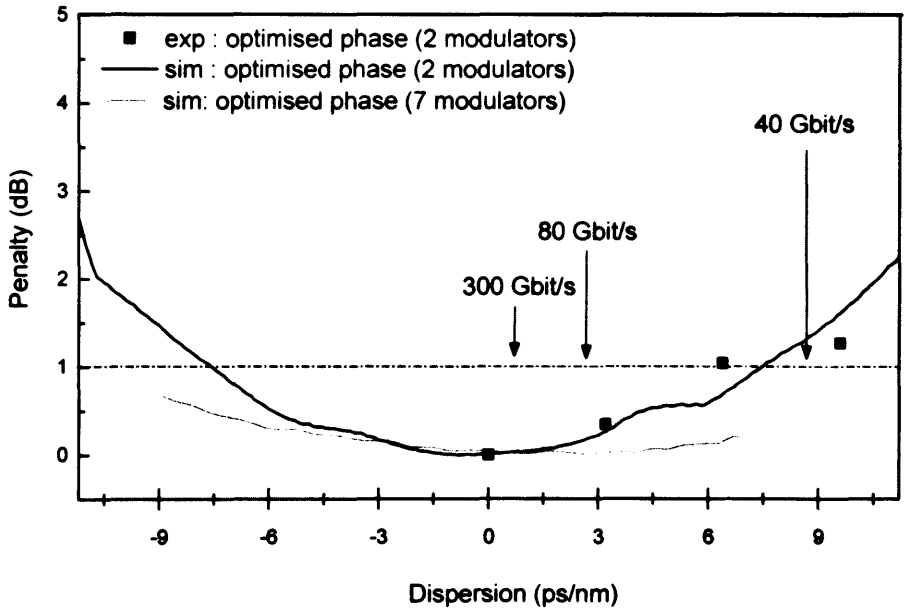



**Figure 4.24. Receiver sensitivity penalty as a function of dispersion for phase-optimised CoWDM (2 and 7 modulator case) and for other reported high bit rate systems**

It is clear from this figure that the 298 Gbit/s CoWDM signal has a similar dispersion tolerance to a single 40 Gbit/s NRZ channel when the filter configuration optimised for CoWDM is used. In contrast with this the 300 Gbit/s reported result is severely impaired by the effects of dispersion with a tolerance of less than 1 ps/nm at the 1 dB receiver sensitivity penalty. These results indicate that CoWDM has a distinctly improved dispersion tolerance with respect to other transmission techniques with a similar throughput, further strengthening its position as a potential candidate for use in medium and long haul transmission networks where dispersion due to propagation in SMF can be a limiting factor

The results presented in this section also indicate that the phase relationship between adjacent optical channels in the transmitter is not destroyed by the effects of dispersion as the signal propagates through the fibre. This can be understood by considering what happens at the optical receiver where the CoWDM tributaries are detected. The target channel is detected in a bandwidth of < 80 GHz which means that only the phase relationship to the nearest neighbour channels need be

considered. Because of the low channel spacing (42.6 GHz) of CoWDM the phase relationship between adjacent channels does not deviate sufficiently from that at the output of the transmitter to destroy the alignment of the channels.

### 4.4.4 Summary

This section has presented a detailed investigation of the dispersion tolerance of the CoWDM transmission format. It was concluded that a 298 Gbit/s CoWDM behaves similarly in terms of dispersion tolerance to a single channel 42.6 Gbit/s NRZ channel. This follows the emerging trend which shows the performance of CoWDM scaling with its tributary line rate (42.6 Gbit/s in this case) as opposed to its overall bit rate (298 Gbit/s in this case). This trend augurs well for CoWDM as a potential candidate for transmission systems which are pushing for higher and higher ISDs by reducing the interchannel spacing and increasing the bit rate. In section 4.4.3 it was shown that it is possible to mitigate the impact of dispersion to a certain extent by using phase precompensation in the transmitter. This benefit of this phase precompensation technique was predicted in Chapter 3 where it was noted that optimal alignment of the transmitter was dependent on the transmission link and the demultiplexing filters used in any given system. Moreover the results of this section imply that the dispersion values investigated do not affect phase relationship between adjacent channels by enough to destroy the CoWDM condition. The next section considers the impact of another set of fibre induced impairments, namely nonlinear effects on CoWDM.

## 4.5 Nonlinear Tolerance of CoWDM

In chapter 1 the advent of the EDFA was listed as one of the primary technological breakthroughs which allowed for the widespread development and deployment of medium and long haul WDM systems. The EDFA provided a way of overcoming fibre-induced losses across wide range of wavelengths. In the same way the development of various dispersion compensation techniques including electronic dispersion compensation (EDC) and pre-chirping have allowed system designers to combat the effects of group-velocity dispersion (GVD) on the optical signal propagating in the fibre. This leaves the impact of nonlinear effects on the transmitted signal as one of the remaining most important impairments to consider when considering fibre-based communication systems based on EDFA amplification schemes. In such modern optical communication networks optical signals are typically transmitted over increasingly long spans of fibre (~100 km) [126, 127] and consequently the launch power required at the transmitter and at the input to each fibre span has to be increased. Due to the fact that the response of any dielectric to light becomes nonlinear for intense electromagnetic fields [39] the effects of fibre nonlinearities must be taken into account when designing medium and long haul links. As mentioned already many of these systems use some kind of dispersion management strategy to reduce the impact of GVD and nonlinear effects and it is desirable that any new transmission formats such as CoWDM are backwards compatible with existing dispersion maps. This section describes the experimental investigation which was carried out to assess the impact of fibre nonlinearities on CoWDM.

### 4.5.1 Introduction to Nonlinear Effects in WDM Systems

The intensity of optical signals propagating in optical fibre based communication systems result in the generation of a wide range of nonlinear effects. These nonlinear effects which dominate optical communication systems are determined to

a large extent by certain features of the system itself. Some of these features are listed in table 4.2 below.

| Factors affecting nonlinearities in WDM systems |
|---|
| Operational Wavelength |
| Amplifier Spacing |
| Total Link Length |
| Fibre Type |
| Launch Power |
| Dispersion |
| Channel Spacing |
| Bit Rate |

**Table 4.2. Factors affecting nonlinearities in WDM systems**

In general system designers are limited in their ability to change many of the characteristics listed above, for example most installed WDM systems use standard SMF and the distribution of channels is fixed to that specified by the ITU-T grid (100 GHz channel spacing). As this work is concerned with transmission formats used in systems which attempt to achieve higher and higher ISD values by increasing the bit rate and reducing the channel spacing we will consider the impact of various nonlinear effects on the design of dispersion management techniques for use in such systems.

Four-wave mixing (FWM) has been identified as one of the primary nonlinear effects influencing tightly spaced WDM systems [128, 129, 130]. In a multi-channel system FWM results in the generation of a new wave at a frequency related to the frequencies at which the other waves are propagating within the fibre. This relationship is described in equation 4.4 below, where $\omega_{ijk}$ represents the frequency of the new wave and $\omega_i$, $\omega_j$ and $\omega_k$ represent the frequencies of the waves already propagating in the fibre.

$$\omega_{ijk} = \omega_i \pm \omega_j \pm \omega_k \tag{4.4}$$

In a multi-channel system $i,j$ and $k$ can vary depending on the number of channels and consequently a large range of FWM components can be generated. These FWM components are not a significant problem when they fall outside the bandwidth of interest but in some cases they can occur where there already exists a channel frequency leading to in-band crosstalk. The efficiency of FWM in optical fibre depends on the chromatic dispersion of the fibre and is at a maximum near the zero-dispersion wavelength resulting in severe system degradation [131, 132].

Self phase modulation (SPM) is a nonlinear phenomenon which occurs as a result of the power dependence of the refractive index of optical fibre. It results in the modulation of the phase of a signal as a result of its own intensity and leads to spectral broadening of the propagating pulse. In a multi-channel system the effects of cross phase modulation (XPM) where the nonlinear phase shift of a target channel can also be affected by the intensity of neighbouring channels. This phase modulation is also affected by the dispersion properties of the transmission fibre and it should now be clear that the dispersion in a fibre link must be considered together with the non-linear properties of the fibre during the system design stage. The dispersion strategy used must attempt to achieve an overall cumulated dispersion figure close to zero while making sure that the local dispersion is sufficiently high to suppress inter channel nonlinear effects. This local dispersion value must also be carefully chosen as a small local dispersion value with respect to the pulse width results in an SPM dominated system and a high local dispersion value with respect to the pulse width results in dominant intra channel effects.

There is an optimum local dispersion for all bit rates which minimises both of these effects. To manage inter-channel FWM effectively the local dispersion must remain relatively high and in order to minimise intra channel FWM the accumulated dispersion must be kept low. Therefore the correct selection of a dispersion map is vital. For systems operating at bit rates of 10 Gbit/s and lower it is sufficient to simply use N (where $N \geq 1$ but small, e.g. ~3) sections of standard SMF followed by an appropriate length of DCF [133, 134]. At 40 Gbit/s the optimum solution is a fibre map based on alternating pieces of '+' and '-' dispersion fibre, for example using spans consisting of SMF/inverse dispersion fibre (IDF). As we move

to higher bit rates (≥ 160 Gbit/s) the period of the optimum dispersion map becomes much shorter as it becomes necessary to suppress fibre dispersion and fibre nonlinearities to an even greater extent due to the reduced pulse width of the higher bit rate systems. In [135] it was demonstrated that a short period dispersion map allow for the doubling of the transmission distance for a 160 Gbit/s signal when compared to a standard dispersion map designed for lower bit rates. Figure 4.25 below shows the typical configurations of the dispersion maps discussed above. The dispersion map in figure 4.25 (a) is typical of that used in lower bit rate systems where a span of SMF is compensated for by a piece of DCF. This is the map that was used in section 3.2.1 to enable transmission of CoWDM over a total link length of 80 km. Figure 4.25 (c) is a short period or dense dispersion map designed for use with high bit rate systems. However due to the small lengths of alternating dispersion fibre which must be concatenated in a low loss manner to form a fibre span this dispersion map is complex and expensive to implement and is therefore not seen as a practical dispersion management solution for optical communication systems. Finally figure 4.25 (b) represents a dispersion map optimised for 40 Gbit/s operation where the fibre spans are longer than in a dense dispersion map and can therefore be implemented in a more cost effective manner.

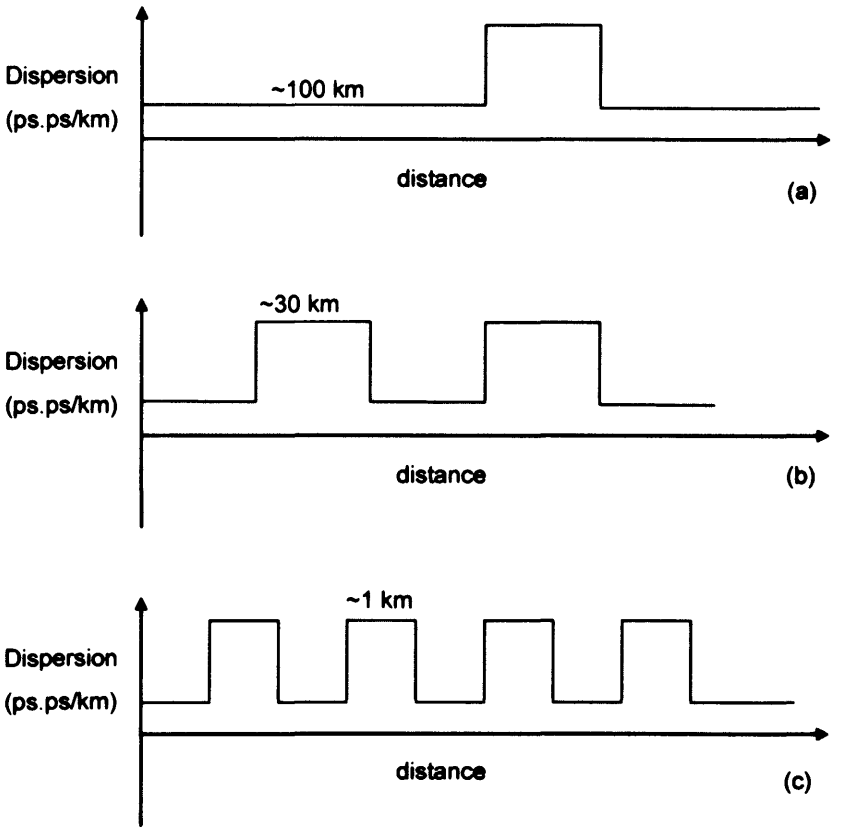



**Figure 4.25. Ideal dispersion maps for various bit rate systems**

In this investigation we consider the performance of a single banded ~300 Gbit/s CoWDM signal as it propagates through a fibre link which has a dispersion map similar to that shown in figure 4.25 (b) above that has been optimised for 40 Gbit/s NRZ signals. We look at the nonlinear effects arising from such a configuration and present results from a single 42.6Gbit/s NRZ channel for comparison.

### 4.5.2 Experimental Setup and Procedure [136]

The experimental setup used for this study was the same as that described in section 4.2.1 except for the transmission link which was replaced with two 50 km spans of

dispersion managed fibre and a 12 km span of standard SMF, as shown in figure 4.26 below.

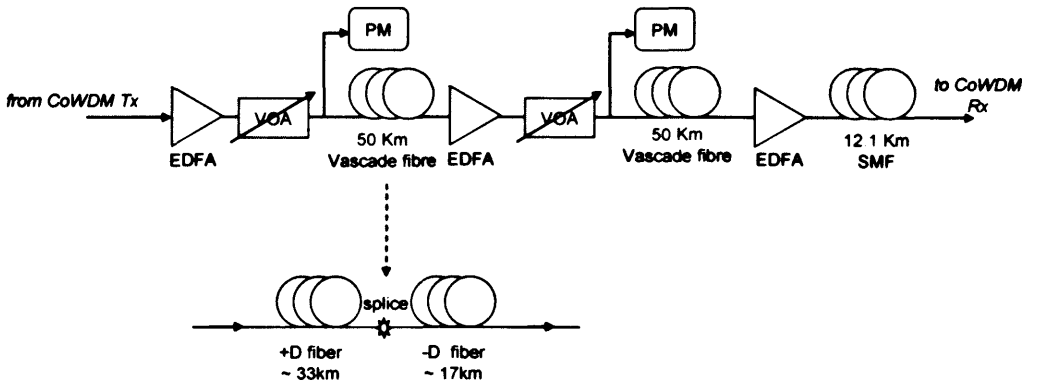



**Figure 4.26. Experimental setup**

The fully compensated transmission link consisted of two spans of 50 km Corning® Vascade® R1000 fibre and an additional 12.1 km of Corning® SMF-28e® optical fibre to enable adequate compensation for the residual chromatic dispersion. The 50 km Vascade® fibre consisted of two sections, a 33 km long '+D' section spliced to a 17 km long '–D' section. A pair of variable optical attenuators and EDFAs was used to control the launch power of the signal into each span of Vascade® fibre. The optical amplifiers were kept at a constant launch power of 19 dBm throughout the experiment and the optical attenuators were used to control the launch power of the optical signals. Power monitors before each fibre span allowed for the measurement of the optical power being launched. The preamplified receiver was as described in chapter 3. For comparison a 42.6 Gbit/s NRZ single channel operation was also investigated by disabling the comb generator, but with the same receiver.

The Corning® Vascade® R1000 dispersion-managed fibre solution consists of large effective area, low attenuation positive dispersion Vascade® L1000 optical fibre (+D) followed by negative dispersion Vascade® S1000 optical fibre (-D). Two spans (50 km each) were engineered to have an overall dispersion of $D_{map}$ = -1.98

ps/nm/km and an overall dispersion slope of 0.0034 ps/nm$^2$/km by adjusting the relative lengths of the $+D_{local}$ and $-D_{local}$ fibres to 33 km and 17 km respectively. The average of the equivalent effective areas of the spans was 75μm$^2$. The Corning® Vascade® R1000 fibre was designed for use in ultra long haul systems and high bit rate applications [137]. Because of the large effective area of the Vascade® fibre an increased nonlinear threshold level compared to standard SMF was expected.

In order to investigate the impact of nonlinear effects on the CoWDM transmission format the receiver sensitivity of the system was measured as a function of the increasing signal launch power into the fibre. In addition this procedure was carried out for the single channel condition in order to provide a reference measurement. The pulse patterns of received single channel and CoWDM signal were also captured and analysed to determine the nature of the nonlinear effects which were present in the system.

### 4.5.3 Results

Firstly in order to provide a reference measurement single channel 42.6 Gbit/s NRZ transmission over the 112 km of dispersion managed fibre was carried out. Figure 4.27 shows receiver sensitivity as a function of launch power for both a single NRZ 42.6 Gbit/s channel (squares) and a 298 Gbit/s multi channel CoWDM signal (triangles). The circles represent all 7 CoWDM tributaries at launch power of 6.2 dBm.

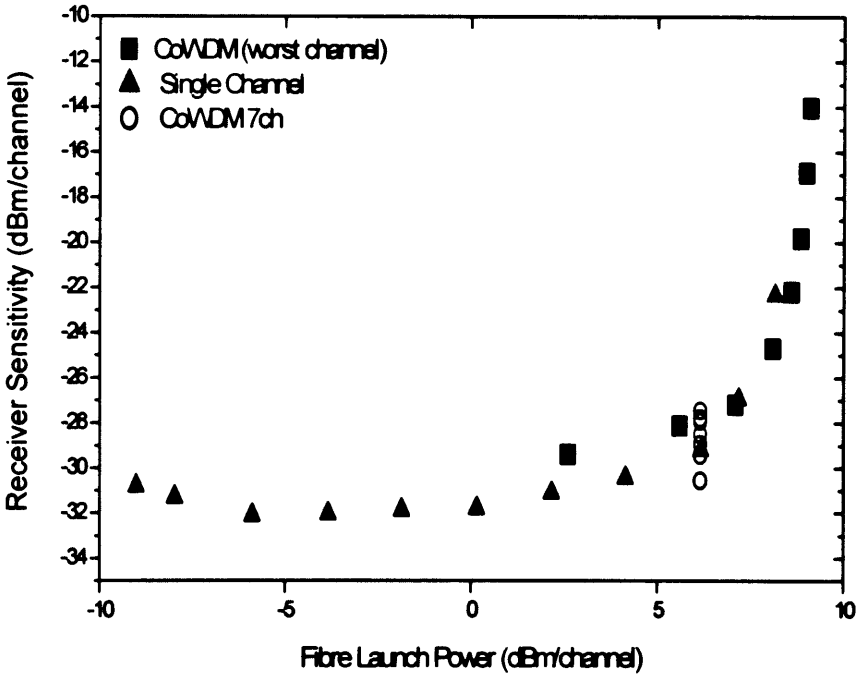



**Figure 4.27. Receiver sensitivity per channel as a function of launch power per channel for single channel (squares) and for CoWDM (triangles). Circles represent sensitivity of each CoWDM tributary at a launch power of 6.2 dBm**

There are two distinct regions to the single channel plot, firstly below ~5 dBm launch power where the system behaves in a linear fashion with a receiver sensitivity approaching -30 dBm. At the low power end of this region the system is noise limited and there are no nonlinear effects in evidence. However, above 5 dBm launch power the receiver sensitivity begins to degrade sharply as a result of the introduction of nonlinear effects. At even higher launch powers the system quickly becomes limited by these nonlinear effects and an error floor is introduced.

This shape of the CoWDM plot shows similar features to the single channel results, it has a flat region between -5 dBm and +5 dBm where the average receiver sensitivity value per tributary is -31.5 dBm and is limited by noise at the lower launch powers and a region above +5 dBm where the receiver sensitivity degrades rapidly due to the introduction of nonlinear effects at high launch powers. In the

CoWDM case the launch power values were adjusted to consider the launched power per tributary (power value reduced by 8.4 dB). The receiver sensitivity value for each CoWDM tributary at a launch power of 6.2 dBm is also shown (open circles). Due to the fixed output power configuration of the amplifiers, both curves were limited at low powers by the maximum amplifier gain (20 dB). Both curves also become limited by non-linearity at per channel launch powers above +5 dBm. Significantly the receiver sensitivity penalties arising from these nonlinear effects are shown to be almost identical for both configurations.

The effect of the nonlinear impairments can also be seen in the degradation of the CoWDM received eye diagram as the launch power is increased. Figure 4.28 below shows the received eye diagrams for three different launch power values. The received eye diagram for -8 dBm launch power is clean and open (no nonlinear effects). The middle received eye (3 dBm launch power) is still quite open at the centre but there is an increase in the noise on the 'ones' (nonlinear effects beginning to cause errors). However at the higher launch power values such as +7 dBm there is a significant amount of noise on both the 'one' and 'zero' rails and a marked reduction in the size of the eye opening (nonlinear effects severely impacting on performance).

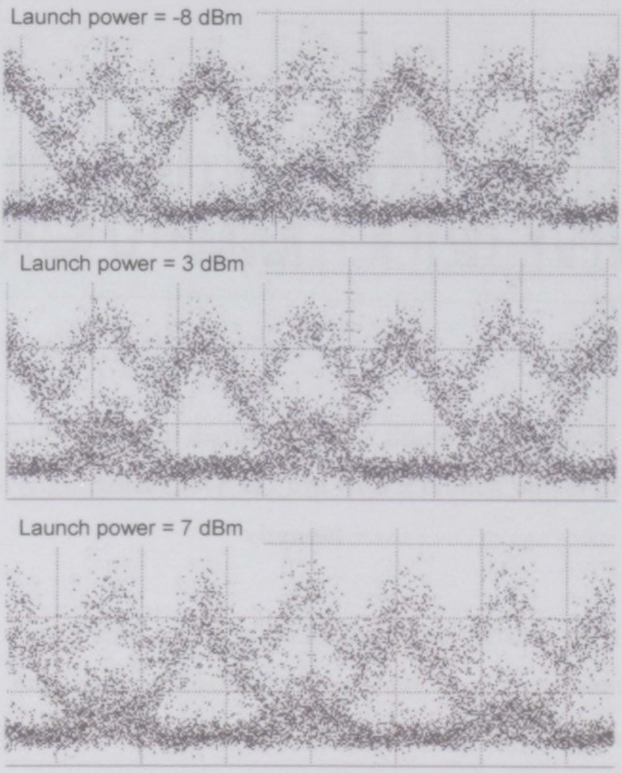



**Figure 4.28. Received CoWDM eyes for -8 dBm+3 dBm and +7 dBm launch power after 112 km (5 ps per division)**

In order to further analyse the type of nonlinear impairment affecting the system the received pulse patterns for a launch power of 8 dBm per channel were analysed. These pulse patterns which were obtained after demultiplexing at the receiver showed remarkable similarity for both single channel and CoWDM signals, with the main differences arising from residual linear crosstalk (sinusoidal variation of data 'ones'). The CoWDM pulse pattern also shows an absence of ghost pulses and timing jitter, features which would normally be associated with nonlinear impairments affecting high (>160 Gbit/s) bit rate systems on this dispersion map.

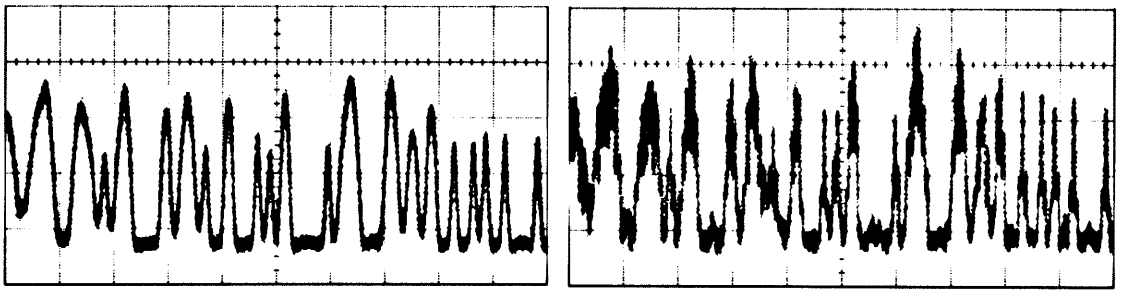



**Figure 4.29. Nonlinear signal distortion for a single channel (left trace) and a CoWDM signal (right trace) over 112 km with a launch power of +8 dBm per channel**

In both cases, as shown above in figure 4.29 the pulse patterns are dominated by a reduction in the amplitude of isolated 'ones' and in a significant distortion of consecutive 'ones', both features which are consistent with self phase modulation limited performance. SPM results in these features because it induces pulse broadening which is a consequence of the time varying dependence of the nonlinear phase shift in the fibre. New frequency components are generated as the pulse travels in fibre which results in pulse broadening. This is significant as it provides further evidence that CoWDM is being affected by the same nonlinear impairment (SPM) that is known to affect lower bit rate single channel and WDM systems with a similar dispersion map as the one used here. The effects of both inter and intra channel are reduced because the phase matching condition which is required for FWM is not met due to the high $D_{local}$ values of the fibre. Intra channel FWM manifests itself as amplitude fluctuations and the appearance of ghost pulses in 'zero' bit slots, which are not seen in the pulse patterns shown above. Here again we see the CoWDM transmission format, behaving in a similar fashion with respect to transmission impairments as a lower bit rate single channel or widely spaced WDM signal on this particular dispersion map which has been designed for 40 Gbit/s signals.

The receiver sensitivity curves for all 7 tributaries before and after transmission are shown in figure 4.30 below, and despite the penalty arising from the nonlinearities all channels remained error free. The receiver sensitivity curves below were obtained at a launch power per channel of 6.2 dBm.

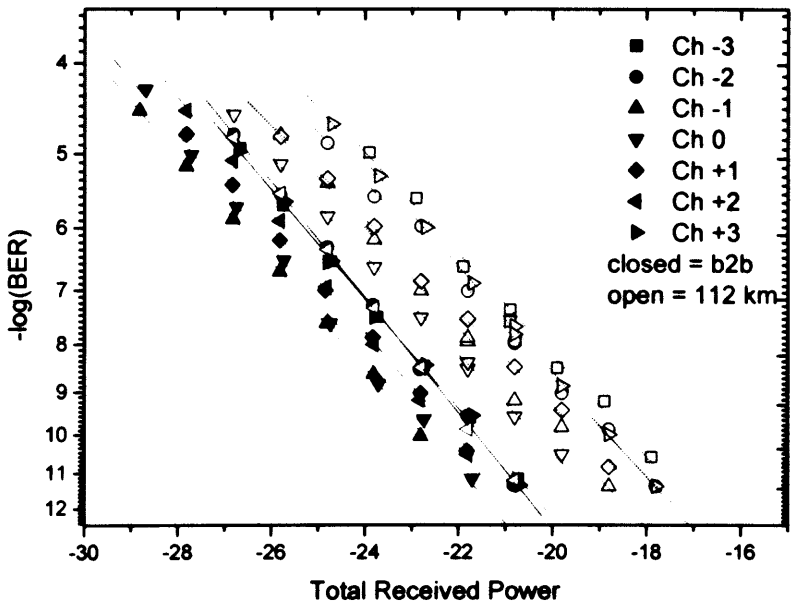



**Figure 4.30. Receiver sensitivity curves for back-to-back condition (closed symbols) and for transmission (open symbols) over 112 km of Corning® Vascade® fibre**

The average receiver sensitivity for the back-to-back condition was -22.8 dBm with a spread of approximately 1.3 dB between the values. For the transmitted case which represented an ISD of 1 bit/s/Hz over 112 km of dispersion managed fibre the average receiver sensitivity at a BER of $10^{-9}$ was -20.2 dBm (2.6 dB penalty with respect to the back-to-back) and the spread was 3.1 dB.

At lower launch powers the transmitted CoWDM signal was characterised in terms of the output OSNR, revealing a 1 dB receiver sensitivity penalty for an OSNR (total power of 298 Gbit/s signal divided by noise power in 0.1 nm

bandwidth) value of ~38 dB. This is shown in figure 4.31 below. A curve fit of the data is also shown which extrapolates the OSNR to show how the the receiver sensitivity increases gives an asymptotic OSNR value of ~33 dB which is consistent with theoretical expectations [110].

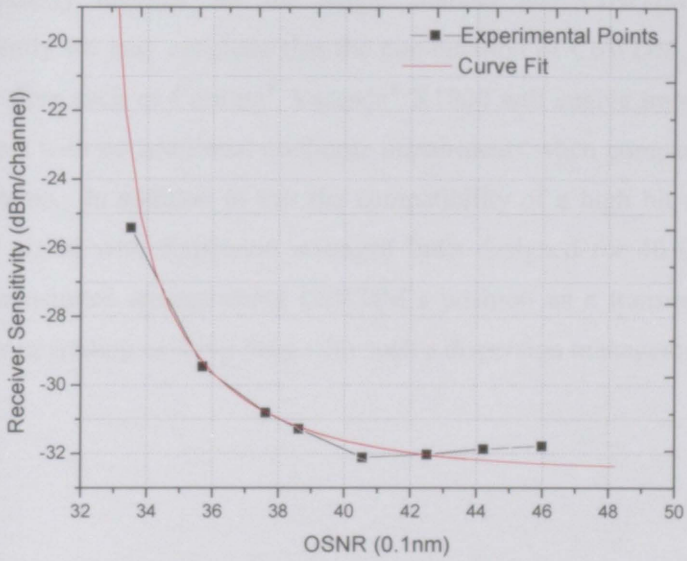



**Figure 4.31. Receiver sensitivity as a function of OSNR for CoWDM after 112 km transmission**

### 4.5.4 Summary

In this section we have demonstrated 298 Gbit/s transmission of CoWDM over 112 km of dispersion managed Corning® Vascade® R1000 fibre with an ISD of 1 bit/s/Hz.

The nonlinear effects limiting the launched fibre power to below 5 dBm per channel were analysed by examining pulse patterns and receiver sensitivity penalties at high launch powers. This analysis of the nonlinear effects strongly suggests that the

CoWDM system was limited by the same nonlinear processes that degrade the performance of a single channel, namely self phase modulation. No evidence of ghost pulse formation or timing jitter, impairment features characteristic of higher bit rate systems affected by nonlinearities were observed on the pulse patterns, highlighting the fact that CoWDM is behaving according to its tributary line rate of 42.6 Gbit/s. In was also shown that the receiver sensitivity values per channel scaled almost exactly together for the single channel and CoWDM configurations. Consequently we may conclude that the combination of CoWDM and a dispersion managed fibre such as Corning® Vascade® R1000 will enable transmission of high ISD signals with no additional nonlinear impairments when compared to lower ISD NRZ systems. In addition to this the compatibility of a high bit rate (298 Gbit/s) CoWDM signal with dispersion managed links designed for 40 Gbit/s signal has been demonstrated strengthening CoWDM's position as a transmission format of choice for upgrading existing links with such a dispersion management strategy.

## 4.6 Conclusion

Modern optical communication systems require optical transmission formats that are simple and cost effective to implement, robust in the face of fibre impairments and capable of operating at high bit rates while maintaining good spectral density. This chapter has provided details on a range of investigations which were carried out in order to verify CoWDM as a transmission format with such characteristics.

In section 5.2 the receiver sensitivity of a 1 bit/s/Hz ISD 298 Gbit/s CoWDM signal was evaluated in the back-to-back condition and the signal was subsequently transmitted over 80 km of standard SMF. Error free performance was observed for all seven CoWDM tributaries, despite a residual dispersion at the receiver of -7 ps/nm. This result was obtained using the CoWDM transmitter and simple preamplified receiver outlined in chapter 3. Comparisons with single channel results using the same optical receiver show there to be no additional penalties arising from the use of the CoWDM format in a standard EDFA amplified 80 km SMF link.

Another feature of modern optical communications systems is that they typically use RS FEC codes in order to improve system margin. The investigation of the performance various types of FEC code in combination with CoWDM was described in section 4.3. It was shown that the coding gain of a single stage RS (255,239) code (~6 dB) when used with a 298 Gbit/s CoWDM signal was approximately the same as that for a single 42.6 Gbit/s NRZ channel confirming the compatibility of CoWDM with standard FEC codes. This similarity in the performance of FEC was experimentally demonstrated for a range of both single-stage and concatenated RS FEC codes implying that the error statistics governing the high bit rate, high ISD CoWDM signal are the same as those for a single channel 42.6 Gbit/s NRZ system. This significant result is the first from a series of investigations which show the characteristics of CoWDM in relation to impairments to be consistent with those of a single NRZ channel at the tributary line rate (42.6 Gbit/s in this case).

Fibre induced dispersion which results in pulse spreading can severely limit the transmission distance of optical signals, particularly at high ISD values where

the interchannel spacing is reduced and at high bit rates where the optical pulses are increasingly narrow. Section 4.4 contained a detailed investigation of the effects of fibre dispersion on CoWDM. It was shown that the experimental receiver sensitivity penalty due to dispersion for a 298 Gbit/s CoWDM signal scales with that of a single 42.6 Gbit/s NRZ channel and is significantly lower than other reported systems with similar overall bit rate. In addition to this the impact of phase precompensation at the transmitter was evaluated and it was shown how such a scheme could be used to improve the dispersion tolerance of the CoWDM signal as predicted earlier in chapter 3.

Finally in section 4.5 the impact of fibre nonlinearities at high launch powers was investigated in detail. A CoWDM signal was transmitted over a total of 112 km (100 km Corning Vascade R1000 and 12 km of SMF) for a range of launch powers. Error free transmission for all tributaries at a launch power of 6.2 dBm confirmed CoWDM's compatibility with dispersion managed fibre solutions designed for use with standard widely spaced 40 Gbit/s WDM systems. The nonlinear impairments at high launch powers for both 298 Gbit/s CoWDM and 42.6 Gbit/s single channel operation were also investigated. The measured receiver sensitivity penalty for both configurations was shown to scale together at high launch powers and this result combined with examinations of the received pulse patterns suggested that CoWDM and the single NRZ channel were being affected by the same nonlinear effects, namely self phase modulation. No evidence of ghost pulses or timing jitter (typical impairment effects for high (>160 Gbit/s) systems) were seen in the received CoWDM pulse patterns.

The set of conclusions derived from the results presented in this chapter confirms CoWDM's compatibility with existing infrastructure and shows behaviour with respect to impairments consistent with that of a lower bit rate single channel. This is promising in the consideration of CoWDM as a transmission format for high ISD modern optical communication systems given the required set of characteristics listed at the start of this section. In the next chapter we will look at some advanced investigations including the enhanced transmission performance of CoWDM where the signal is simultaneously subjected to all the major transmission impairments.

# Chapter 5

# Extended CoWDM Experimental Investigations

## *5.1 Introduction*

We have already shown in chapter 4 that the CoWDM transmission format is an attractive solution for low complexity (NRZ and no transmitter prefiltering), high spectral density (up to 1 bit/s/Hz) optical communication systems. However in order to continue to satisfy the ever increasing demands of the bandwidth hungry applications mentioned in chapter 1 future optical networks will have to deliver even higher overall capacities over transmission distances approaching several thousands of kilometres . In this chapter we look at how the basic CoWDM transmission format can be extended in terms of capacity, ISD and transmission distance in order to demonstrate it as a suitable candidate for such future networks.

In section 5.2 the standard 1 bit/s/Hz, single polarisation, NRZ CoWDM signal is combined with polarisation multiplexing resulting in a 2 bit/s/Hz signal with an overall capacity of 596.4 Gbit/s from a single laser. Modern long-haul optical communication systems are capable of transmitting data over several thousands of km of optical fibre [138, 139, 140, 141]. In order to demonstrate CoWDM's compatibility with the infrastructure typical of many installed long haul terrestrial systems we present the results of a recirculating loop transmission experiment where a 280 Gbit/s CoWDM signal was transmitted over 1,200 km with the Q-factor of all the measured tributaries above the FEC threshold level. Increasing the overall throughput of the system can also be achieved by using additional available bandwidth. Thusfar CoWDM from a single wavelength source has occupied a relatively narrow slice (approximately 2.3 nm) of the C-band. In section 5.4 we demonstrate the scalability of CoWDM by expanding the single wavelength source CoWDM configuration with a bank of 5 distributed feedback

(DFB) lasers which were used to generate a multi-banded CoWDM signal to achieve 1.5 Tbit/s overall capacity.

## *5.2 CoWDM and Polarisation Division Multiplexing [142]*

### 5.2.1 Overview

Terabit capacity architectures have been studied for future optical networks in recent years, in order to meet increasing bandwidth demands from end-customers. As we have already discussed in chapter 1 such capacities can be achieved, whilst maintaining manageable network architectures, with techniques such as optical time domain multiplexing (OTDM) and wavelength division multiplexing (WDM). By using multi-level modulation formats such as RZ-DQPSK it has been shown that capacities as high as 4.3 Tbit/s in a single polarisation with an ISD of 1.14 bit/s/Hz can be achieved in a WDM configuration [56].

Further increasing the ISD's of such systems is necessary for cost-effective increase in system capacity. In a fixed bandwidth system simply reducing the channel spacing becomes limited by high levels of crosstalk. Another solution to this problem is known as polarisation division multiplexing (PDM), a technique which allows for two optical channels to be transmitted at the same wavelength in a fibre by orthogonally polarising the signals at the input to the fibre, thus achieving even higher ISD's and increasing the overall system capacity of modern optical communication systems. Despite the fact that random polarisation changes occur within the transmission fibre the signals are still orthogonal to each other at the output and can be polarisation demultiplexed using standard techniques [82]. In a WDM system this has the effect of doubling system capacity within a fixed spectral bandwidth. A schematic of polarisation division multiplexed channels is shown in figure 5.1. Because of the fact that the there is a doubling in the number of channels

there is an inherent 3 dB reduction of the receiver sensitivity when considering a PDM system.

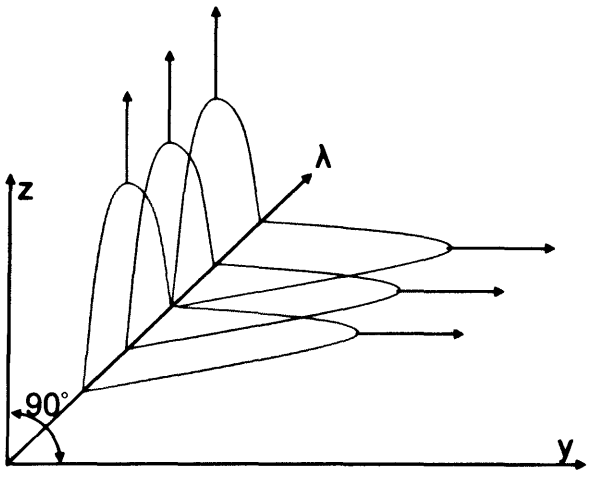



**Figure 5.1. Polarisation division multiplexing**

PDM was first proposed as a means of doubling the system capacity of optical communication systems in the late 1980's with a number of groups carrying out investigations on the topic [143, 144]. Despite field implementation difficulties due to the effects of PMD [145] and nonlinear depolarisation in installed fibre links, PDM is now used in ultra high capacity laboratory transmission experiments [34, 146, 147]. Tracking of the state of polarisation which is necessary for longer transmission distances because of the presence of PMD has to date made implementation of PDM in the field prohibitively complex and expensive to implement [148, 149]. Indeed even in a lab environment impairments in polarisation division multiplexed systems can arise due to misalignments of the polarisers of polarisation beam splitters which results in coherent crosstalk from one polarisation to the other. The impact of these misalignments can be quantified in if we consider that the maximum tolerable limit for the eye closure due to coherent crosstalk is approximately 1 dB which corresponds to a 20 % reduction in the upper rail of an

eye pattern. If we have two PDM channels, $A$ and $B$ which are ideally orthogonal to each other we can write the intensities ($Wm^{-2}$) of the two channels as

$$I_A = AA^* \text{ and } I_B = BB^* \tag{5.1}$$

Misalignment of the PBS which is used in the receiver to spilt the polarisations or polarisers will cause a small coupling coefficient '$k$' which is related to the angle of misalignment $\theta$ by

$$k = \sin(\theta) \tag{5.2}$$

It was shown in [150] that the coherent crosstalk from an orthogonally multiplexed channel can be written as

$$2k\sqrt{I_A I_B} \tag{5.3}$$

which for a 1 dB eye opening penalty (EOP) (or 20% of the original $I_A$ so $k = 0.1$) equates to a misalignment of approximately 6°.

Polarisation multiplexing can be combined with the CoWDM transmission format using either of the configurations shown in the schematic below.

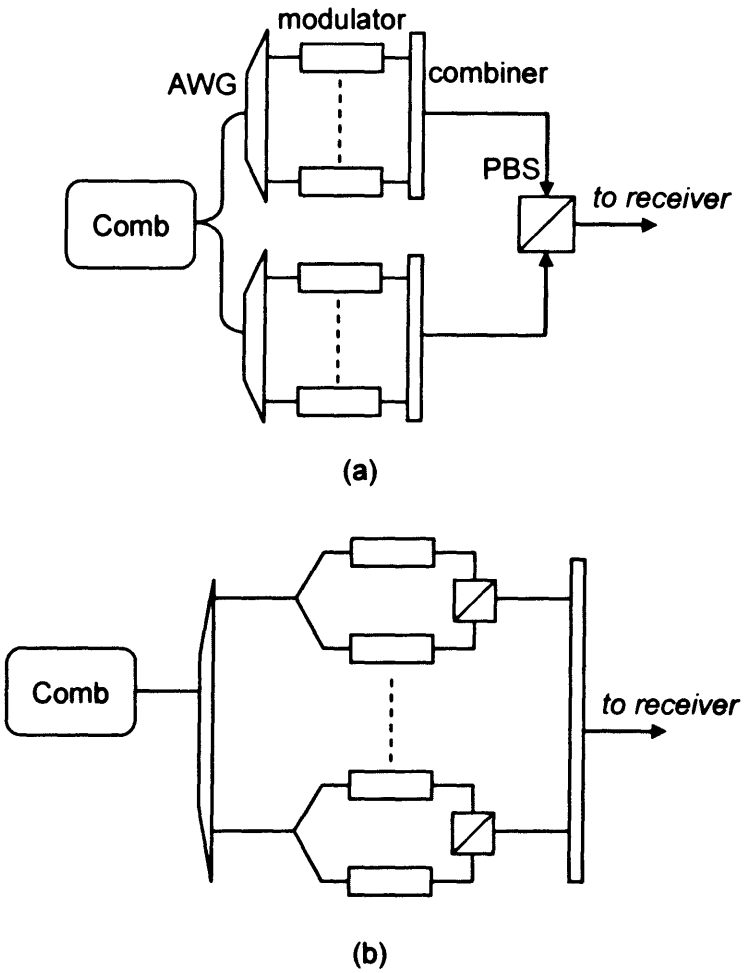



**Figure 5.2. Schematic of polarisation multiplexing with CoWDM**

The schematic shown in figure 5.2 (a) was emulated with the experimental setup described below. It generates an identical pair of 'n' data modulated channels which are then polarisation multiplexed. In contrast with this the schematic shown in figure 5.2 (b) carries out the polarisation multiplexing stage on a 'per-channel' basis. This is more difficult to implement in a lab environment due to increased inventory requirement in terms of polarisation multiplexing stages, but may be more suited to monolithic integration.

In this section we show how the capacity of a single-source CoWDM system from 298.2 Gbit/s to 596.5 Gbit/s by introducing PDM at the transmitter. This was achieved by generating a band of seven non-return-to-zero (NRZ) encoded channels at 42.6 Gsymbol/s. A total ISD of 2 bit/s/Hz was consequently obtained without the use of multi-level formats within the band. This offers the potential of overall ISDs in the region of 1.8 bit/s/Hz for a multi-banded (multi-Terabit/s) system which is discussed in detail in Chapter 5.4.

### 5.2.2 Experimental Configuration

The experimental configuration described in this section is presented in figure 5.3. The CoWDM transmitter was as described in chapter 3 and consisted of a comb generator module, a phase preserving data encoding section, and the enhanced phase stabilisation circuit was used to maintain the optimum relationship in the transmitter throughout the experiment. In order to implement polarisation multiplexing a polarisation multiplexer and a polarisation demultiplexer were incorporated in the system at the transmitter and receiver stages respectively. The polarisation division multiplexer is shown in figure 5.3 (a), which resulted in a doubling of the ISD from 1 bit/s/Hz to 2 bit/s/Hz within the fixed spectral width available. The multiplexer consisted of a sequence of polarisation controllers (PC) and a polariser, followed by a 45°-launch of the signal with respect to the principal axis of the polarisation maintaining (PM) fibre, in order to equally excite the fast and slow axes of the fibre. The polariser was used to ensure that the energy was confined to the same state of polarisation before being launched to the PM fibre. This was necessary as the rest of the transmitter was not polarisation maintaining and PMD in the transmitter would have resulted in fluctuations in the SOP of the signal before the multiplexing stage. In this experiment, a 100m-long PM fibre section was used, with an arbitrary net differential delay of 137 ps, which therefore decorrelated the patterns by approximately 5.8 bits. No additional phase control was performed at this stage.

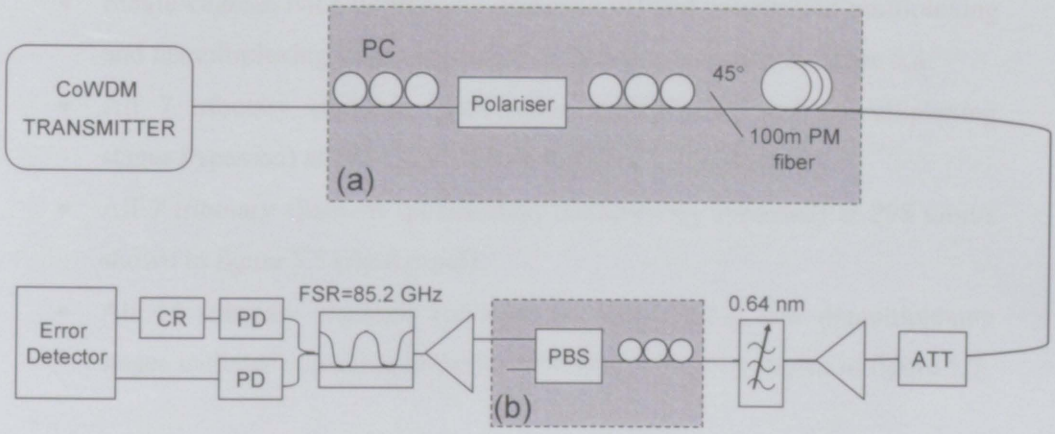



**Figure 5.3. Experimental configuration for PDM CoWDM**

The output of the comb generator after amplification was similar to that presented in chapter 3. The output of the 596.4 Gbit/s transmitter was then launched to the standard pre-amplified receiver, which enabled each individual tributary channel to be selected using a 0.64 nm tunable band-pass filter. This was followed by a polarisation demultiplexing stage to separate the different polarisations consisting of a single PC and a polarisation beam splitter (PBS) as shown in figure 5.3 (b). Each set of seven channels (one in each of the orthogonal polarisations) was measured from a different port of the PBS, with only very slight tweaking of the polarisation controller between measurements. The impact of residual co-polarised crosstalk from adjacent tributaries was minimised by the asymmetric Mach-Zehnder dis-interleaver (85.2 GHz-FSR).

### 5.2.3 Polarisation Division Multiplexing Results

Bit-error rate (BER) measurements were performed for a number of different configurations (listed below) and the BER was plotted as a function of the total received power at the input to the receiver:

- Single-channel NRZ (with comb-generator off and polarisation multiplexing and demultiplexing stages bypassed) at 42.6 Gbit/s shown in figure 5.4.
- All 7 tributary channels (polarisation multiplexing and demultiplexing stages bypassed) at 298 Gbit/s shown in figure 5.5 (left panel).
- All 7 tributary channels (polarisation multiplexing bypassed) at 298 Gbit/s shown in figure 5.5 (right panel).
- All 14 tributary channels (polarisation multiplexing and demultiplexing stages included) resulting in the full 596 Gbit/s capacity shown in figure 5.7.

For single channel (closed squares in figure 5.4 ), a receiver sensitivity, at a BER of $10^{-9}$, of -28.4 dBm was obtained, as expected given the noise figures of the amplifiers used for this experiment. The optical spectrum of the single NRZ channel is shown on the left side of figure 5.4. The data modulation of the $2^7$-1 data pattern is observable on the spectrum.

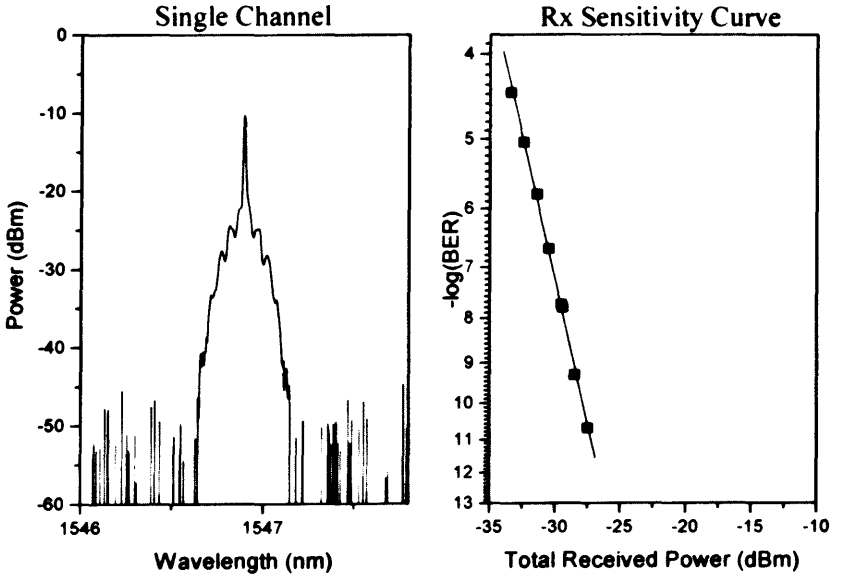



**Figure 5.4. Single channel NRZ 42.6 Gbit/s received spectrum (left) and receiver sensitivity curve (right)**

In figure 5.5 the receiver sensitivity curves are shown for single polarisation 7 channel CoWDM when the polarisation demultiplexing stage is bypassed (left of figure) and included (right of figure). An average receiver sensitivity improvement of ~0.7 dB from -20.66 dBm to -21.38 dBm at a BER of $10^{-9}$ was observed when the polarisation demultiplexing stage was incorporated in the receiver. This was due to a reduction in spontaneous-spontaneous beat noise in the orthogonal polarisation. This is as expected if we consider the Q factor of a system as

$$Q = \frac{\bar{\upsilon}_1 - \bar{\upsilon}_0}{\sigma_1 - \sigma_0} \tag{5.4}$$

where $\bar{\upsilon}_0$ and $\bar{\upsilon}_1$ are the mean levels for '0' and '1' bits respectively and $\sigma_0$ and $\sigma_1$ represent the noise powers of the '0' and '1' bits respectively. If we just look at the signal-spontaneous and spontaneous-spontaneous noise terms and assume that both shot and thermal noise terms are negligible we get

$$\text{spon-spon} = n'^2/2\Delta f \text{ (on both ones and zeros)} \tag{5.5}$$

$$\text{sig-spon} = 2sn'/\Delta f \text{ (only on data ones)} \tag{5.6}$$

where $\Delta f$ is the bandwidth of a signal with power '$s$' and with noise power '$n$'. The electrical variances are given by

$$\sigma_0^2 = 2B\left[n'^2/2\Delta f\right] \tag{5.7}$$

$$\text{and } \sigma_1^2 = 2B\left[2sn'/\Delta f + n'^2/2\Delta f\right] \tag{5.8}$$

where B is the receiver bandwidth. The contribution from signal-spontaneous noise is in one polarisation only and remains the same for both system configurations.

Spontaneous-spontaneous noise however exists in two polarisations so its effect is more noticeable when the polarisation demultiplexing stage is not included before the receiver. With the polarisation demultiplexing stage the spontaneous-spontaneous noise contribution is reduced by a factor of 2. If we now consider the Q factor for both setups

$$\frac{Q_{2\text{-Pol}}}{Q_{1\text{-Pol}}} = \frac{\sqrt{2B\left[n'^2\ 2\Delta f\right]\frac{1}{2}} + \sqrt{2B\left[2sn'\ \Delta f + n'^2\ 2\Delta f\ \frac{1}{2}\right]}}{\sqrt{2B\left[n'^2\ 2\Delta f\right]} + \sqrt{2B\left[2sn'\ \Delta f + n'^2\ 2\Delta f\right]}} \tag{5.9}$$

and simplify we get a ratio of 0.8 for $Q_{2\text{-Pol}}/Q_{1\text{-Pol}}$. This improvement in performance by using a polariser at the output of the transmission link has been previously demonstrated in [151] at 5 Gbit/s and from equation 5.9 above it is evident that the improvement is bit rate independent. It is worth noting however that the spread of receiver sensitivity values across the seven tributary channels remained approximately the same (1.3 dB without demultiplexing stage and 1.5 dB with demultiplexing stage).

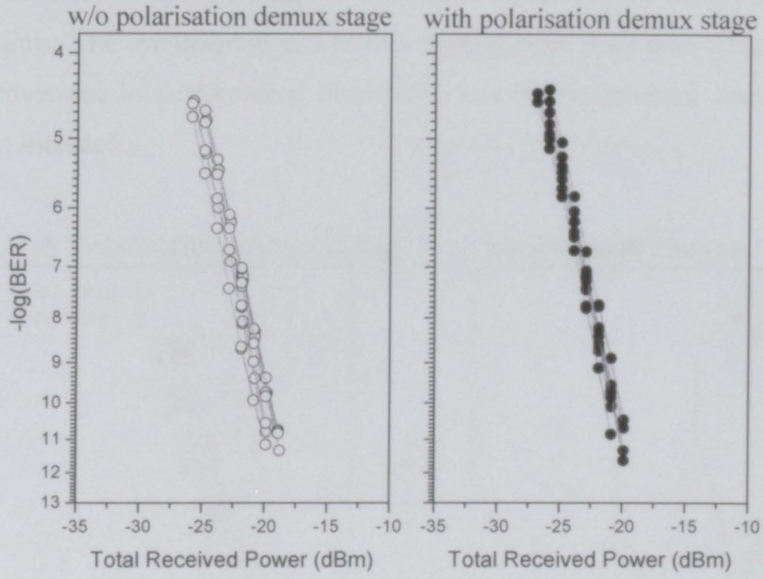
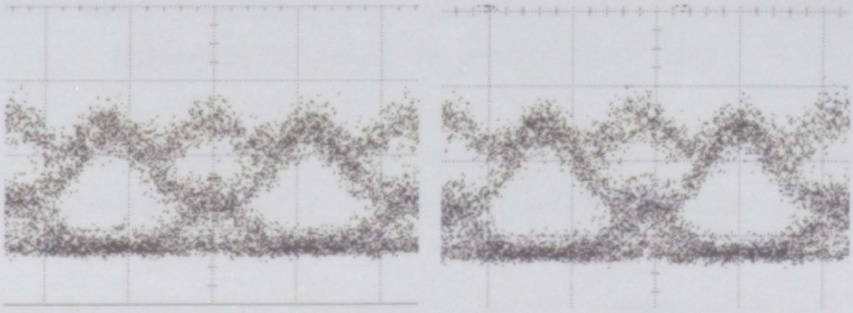



**Figure 5.5. –log(BER) vs total received power for 7 channel single polarisation CoWDM without (left) and with (right) polarisation demultiplexing stage**

Figure 5.6 shows the received 42.6 Gbit/s eye diagrams for tributary # -3 (tributary which exhibited average performance).



(a) (b)

**Figure 5.6. 42.6 Gbit/s single polarisation CoWDM received eye diagrams for tributary #-3 without (a) and with (b) polarisation demultiplexing stage**

The eye diagrams in figure 5.6 show a clear open centre with the noise pushed to the eye crossing. The eye diagram in 5.6(b) is slightly more open than 5.6(a) verifying the improvement in performance observed when the polarisation demultiplexing stage was included.

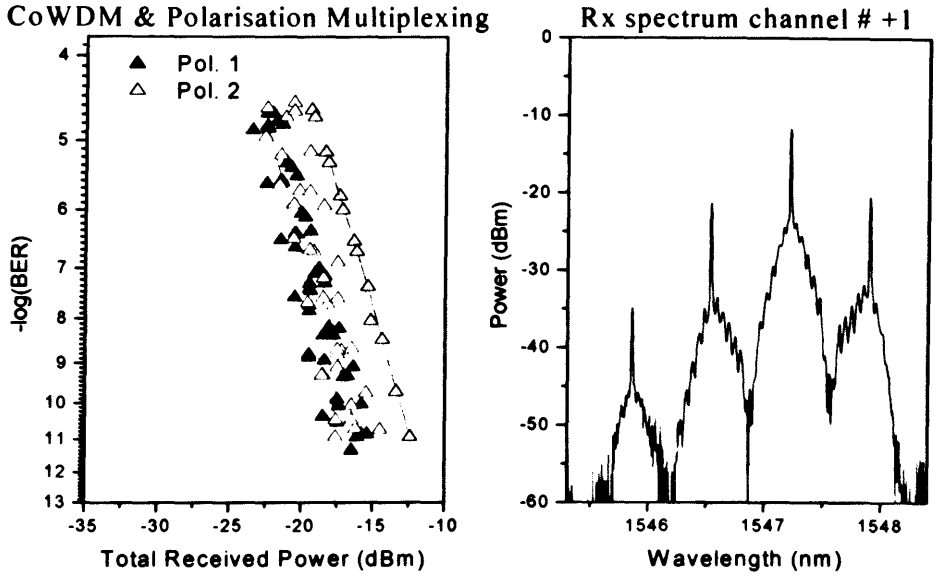



**Figure 5.7. –log(BER) as a function of total received power for all 14 CoWDM tributaries incorporating polarisation multiplexing (left). Received spectrum (.01nm bw) for channel # 1, polarisation 1 (right)**

Figure 5.7 above shows the receiver sensitivity curves for all 14 tributary channels (7 in each polarisation state) from the 2 bit/s/Hz polarisation multiplexed CoWDM signal.

The spread in receiver sensitivities of approximately 5.5 dB can be attributed to a number of features of the experimental implementation described in detail later in this section. For comparison if we consider an EDFA NF of 5.2 dB to determine the theoretical limit of the receiver sensitivity a 596.5 Gbit/s NRZ signal would be expected to have a receiver sensitivity of approximately –20 dBm.

In order to compare these results figure 5.8 shows the receiver sensitivity curves for single 42.6 Gbit/s NRZ signal (squares), single polarisation 1 bit/s/Hz CoWDM (circles) and polarisation multiplexed CoWDM on the same axes. The average total receiver sensitivity was increased by ~7dB between the single channel case and the single polarisation CoWDM result. This is close to the expected increase of 8.4 dB given the sevenfold increase in the number of channels, and the slight variation was attributed to the effect of the tight filtering in the receiver on the single NRZ signal. A further increase of 4.2 dB in the average receiver sensitivity was obtained with CoWDM and PolMUX. 3 dB of this increase can again be explained by the doubling of the channel count from 7 to 14, leaving a penalty of only 1.2 dB arising from PolMUX, taking into account the noise filtering benefits of the PBS, and with small penalty (< 0.5 dB) if such effects are neglected. As we have already seen this penalty could easily be attributed to slight misalignments of the angle of polarisation of the signal at the receiver or PMD in the system. Importantly, in addition to such low overall penalties, there are no signs of an error-floor for any of the 14 tributary channels shown in figure 5.8.

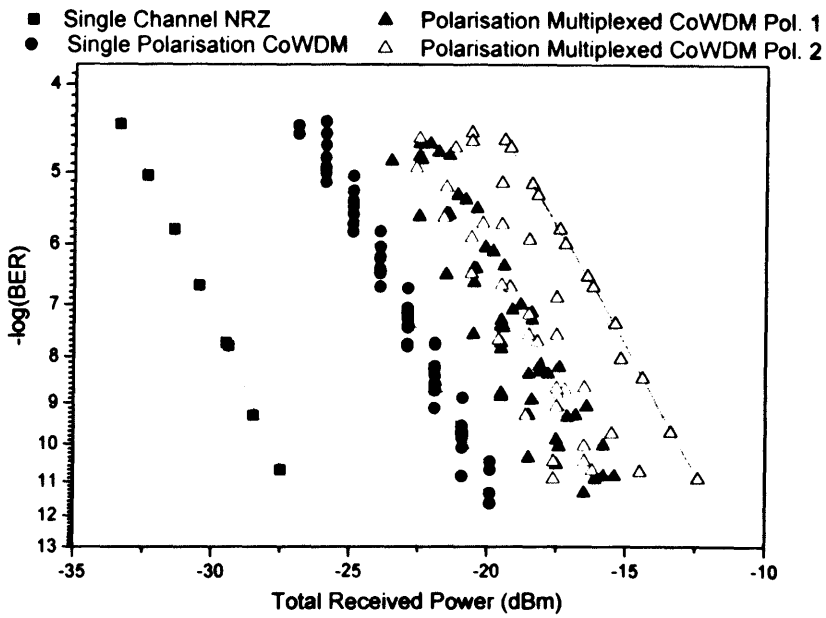



**Figure 5.8. Receiver sensitivity curves for back-to-back single channel (closed squares), single polarisation CoWDM (closed circles) and polarisation multiplexed CoWDM (open and closed triangles)**

This net 1.2 dB penalty is consistent with polarisation multiplexing penalties reported in other experiments [152], and was primarily due to small misalignments of the manual polarisation controllers. Some penalty may also be attributed to residual PMD in the system, predominantly from the fibre amplifiers that were employed in the experiment. This is because PMD causes the output polarisation to vary with frequency which results in crosstalk at the receiver. It was shown in [148] that when the DGD is equal to 20 % of the filtered rise time of the signal a 20 % reduction in the upper rail occurs which corresponds to a 1 dB EOP. The PMD figure of the EDFA used in our receiver was 0.7 ps which amounts to only approximately 6% of the risetime of the pulse so the EOP penalty arising from PMD for a CoWDM signal is approximately 0.2 dB. This is small when compared to that which would affect a 160 Gbit/s OTDM signal, which due to the reduced rise time (~1-2 ps) would suffer from a large 2.75 dB EOP which would make the signal unrecoverable without using FEC [153]. Figure 5.9 below shows the maximum

transmission distance for a 1 dB power penalty as a function of bit rate when PMD is the limiting factor for both single polarisation and PDM signals. The PMD figure of the fibre was taken to be 0.04 $ps/\sqrt{km}$ which is a realistic figure for SMF [154].

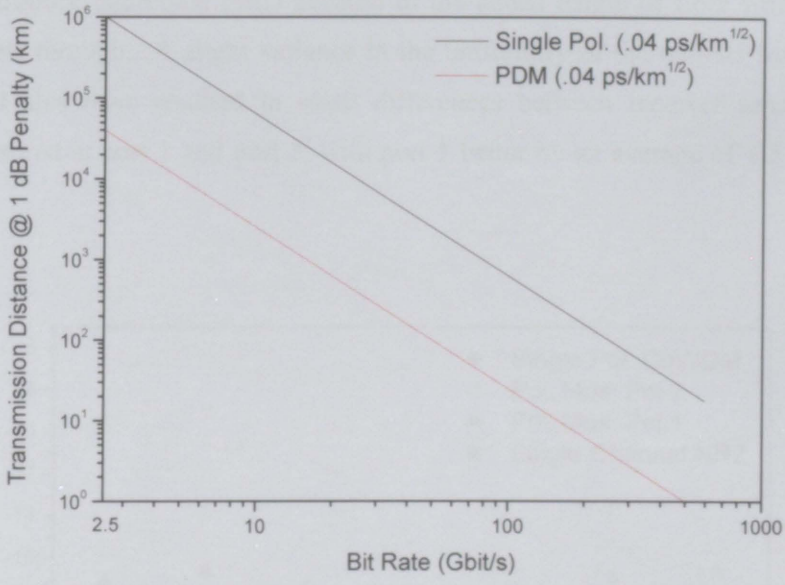



**Figure 5.9. Transmission distance at 1 dB EOP vs Bit rate for single polarisation (black solid line) and polarisation division multiplexed signal (red dashed line)**

A PDM system is 5 times more susceptible to PMD than a non PDM system which has demonstrated PMD statistics that allow for a value of the mean fibre DGD value to be 10% of the bit period of the signal [148]. Therefore a 596 Gbit/s CoWDM PDM signal would be expected to have the same transmission performance as a 40 Gbit/s PDM signal which is approximately 160 km. For comparison a single polarisation 596 Gbit/s NRZ signal would be severely limited by PMD to a transmission distance of 20 km.

In the CoWDM case any penalty arising from PMD could be easily compensated with standard 40 Gbit/s PMD compensators located between the channel selection filter and PBS, as the detected optical bandwidth of each channels

is narrow. Figure 5.10 below shows an overview of the receiver sensitivity results for each system configuration which was investigated. It is clear that the three channels with the highest spread for each polarisation (channels -2, 0 and +2) passed through the path in the transmitter containing the piezo fibre stretcher, which may serve to introduce additional PMD because of the added length of fibre which the signal travels through. A slight variance in the uniformity of the outputs from the PBS would also have resulted in small differences between receiver sensitivity values measured at port 1 and port 2, with port 1 better by an average of 1.5 dB in each case.

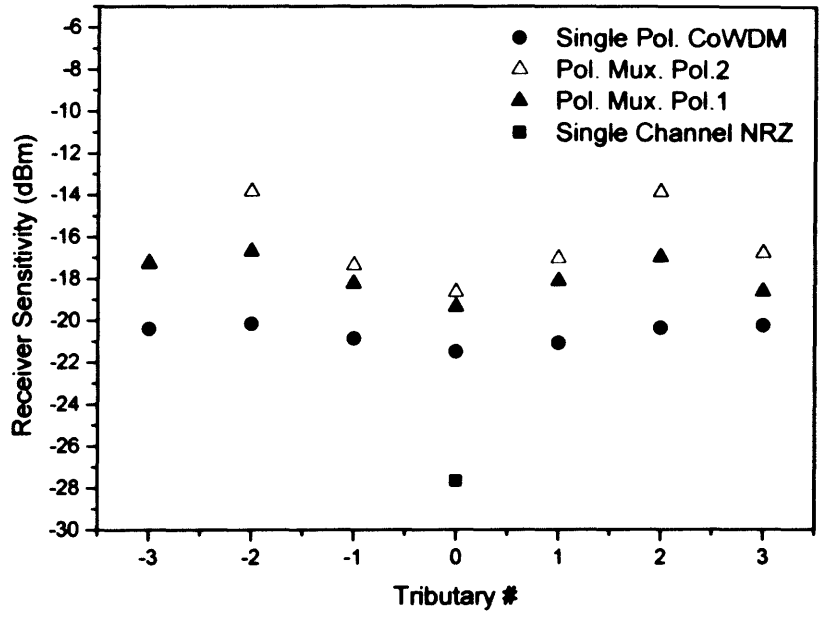



**Figure 5.10. Receiver sensitivities for each tributary**

The introduction of PM amplifiers in the transmitter would improve the tolerance to PMD effects and therefore reduce the spread in the receiver sensitivities. It is reasonable to expect that much of the spread in receiver sensitivities in figure 5.10 could also be significantly reduced to a negligible level by the use of an integrated phase modulator or a fully integrated 7 channel data modulator array.

The received CoWDM eye-diagrams for tributary # -3 for both polarisation states are shown in figure 5.11. Clearly the transition from 298 Gbit/s to 596 Gbit/s did not affect the shape of the eyes, leaving them open at the centre, but introduced somewhat more noise to the eye crossing, suggesting that the high frequency crosstalk terms are slightly distorted by the combined action of slight polarisation misalignment, PMD and the PBS.

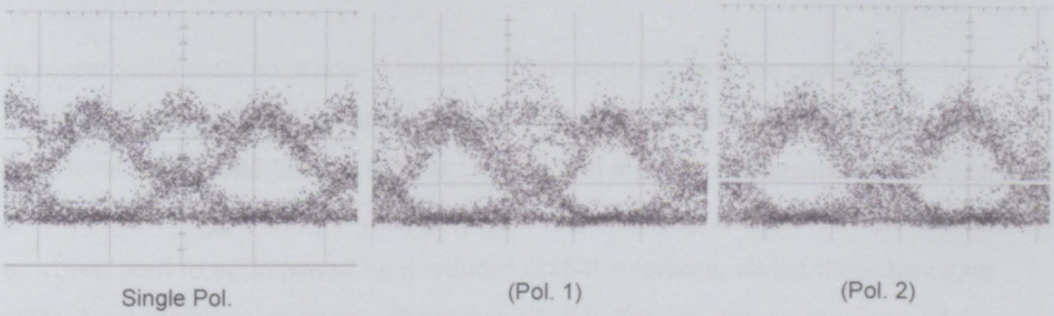



**Figure 5.11. Eye diagrams for tributary -3 for both single polarisation CoWDM and for both polarisation states**

Furthermore, there is no significant difference in the shape of the eye diagrams between each polarisation state.

### 5.2.4 Summary

In this section we have shown that Coherent WDM combined with polarisation multiplexing is an effective method to increase the ISD of a fixed bandwidth system thus enabling high transmission capacities, all the while maintaining a simple transmitter setup based on NRZ coding. 596.4Gbit/s overall capacity was generated at 42.6 Gsymbol/s using a single DFB laser by adding polarisation multiplexing to incoherently combine two CoWDM sources, with 42.6 Gbit/s for each tributary channel. Low penalty, error-free performance was obtained for all 14 tributary channels. An average penalty of only 1.2dB was observed, which we believe was

due to slight polarisation misalignment and PMD from the receiver amplifiers and the piezo fibre stretcher.

## *5.3 Long Haul Transmission Experiment using CoWDM [155]*

### 5.3.1 Overview

In recent years there have been a number of efforts to increase the capacity per laser of long haul optical transmission networks. Proposed solutions include the use of multilevel modulation formats such as DQPSK and high speed transmitters based on OTDM technology [156, 157, 158]. Techniques utilizing multi-level modulation, however, tend to be impaired by a reduced OSNR tolerance, whilst those based on OTDM are polarization mode dispersion (PMD) limited due to the reduced bit period. We have shown in chapters 3 and 4 that the CoWDM transmission format can achieve high ISD values with a simple transmitter and receiver configuration (as high as 1 bit/s/Hz using NRZ modulation and no transmitter pre-filtering) which lowers implementation complexity and cost. CoWDM also operates at a low symbol rate with respect to the overall line rate giving good tolerance to the effects of fibre-induced dispersion and PMD. The results presented in chapter 4 also indicate that CoWDM is compatible with standard dispersion maps designed for long haul systems. Consequently the CoWDM transmission format can be considered as a strong candidate for use in long-haul terrestrial transmission systems. Currently installed LH terrestrial (>600 km) systems are typically composed of ~100 km spans of SSMF which may have high PMD values [159]. The purpose of the simulation and experimental work described in this section is to investigate the transmission performance of a CoWDM signal in such a transmission link. This work simultaneously confirms the potential and verifies the performance features of CoWDM in a long haul link. Both experimental and simulation results are presented which show the measured Q-factor of all seven 40 Gbit/s CoWDM tributary channels resulting in a total signal bandwidth of 280 Gbit/s to be above the FEC

threshold for a transmission distance of 1,200 km, confirming the compatibility of CoWDM with dispersion managed, hybrid amplified, terrestrial fibre spans. Figure 5.12 below shows transmitted distance as a function of the bit rate per laser for a number of transmission experiments reported in the literature.

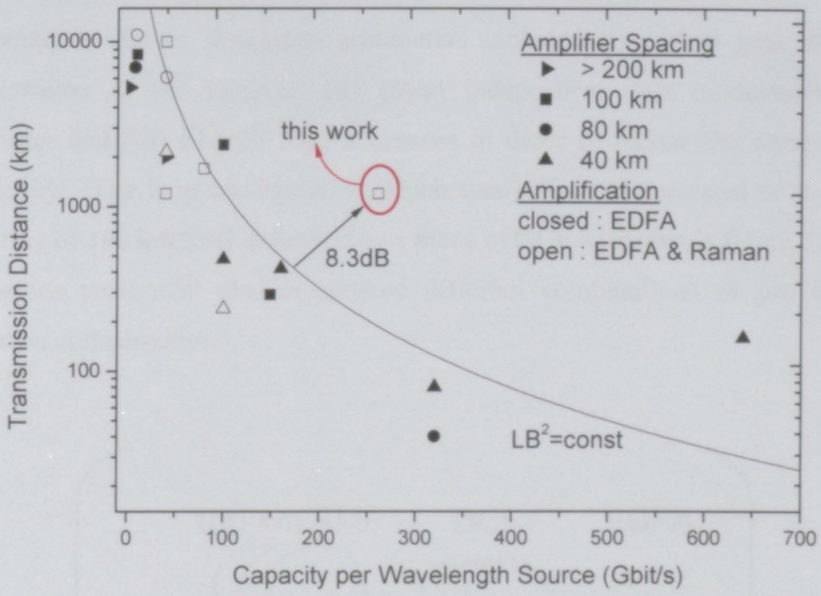



**Figure 5.12. Recent transmission results for varying repeater spacing and amplification schemes with a '$LB^2$ = constant' trendline**

The closed symbols represent systems where a hybrid EDFA/Raman amplification was used and the open symbols are for EDFA amplified systems only. The work presented in this section fits in the long haul (LH) bracket and achieves a significantly higher capacity per wavelength source than other systems transmitting over similar distances.

### 5.3.2 Long Haul Transmission Simulations

Simulations of the CoWDM transmission experiment for a range of transmission distances (800, 1200 and 1600 km) were performed using VPI Transmission Maker version 7.2. In order to investigate the non-linear performance of a 7 x 40 Gbit/s tributary CoWDM signal at high launch powers the effect of PMD in the loop was not included. Other simulation parameters included (i) perfect post dispersion compensation at the receiver, (ii) seven independent data modulators in the transmitter and (iii) 512 bit data sequences in order to reduce the computational complexity. The loop configuration which was simulated consisted of four spans consisting of 100 km SMF followed by a piece of DCF as shown in figure 5.13. The simulations performed also considered different combinations of pre and post dispersion compensation.

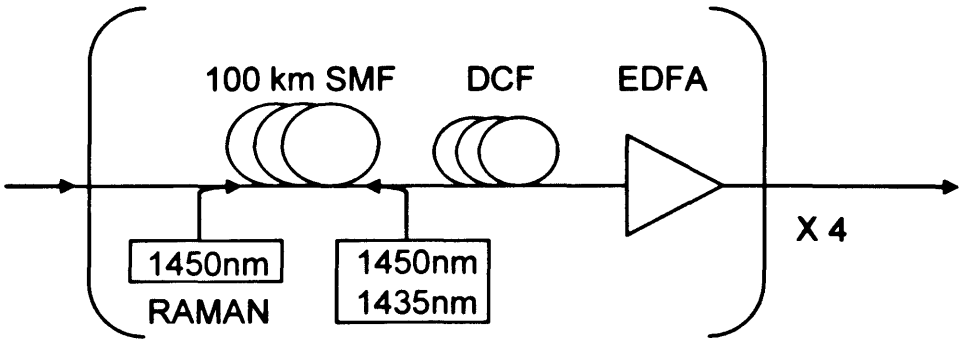



**Figure 5.13. Simulated loop configuration**

Amplification of the signal was simulated by 4 EDFAs each with a noise figure of 5.5 dB and both forward (1450 nm) and backward (1450nm and 1435nm) Raman pumping. The full list of parameters relating to these components is presented in table 5.1 and 5.2. These parameters were chosen to represent the experimental system as accurately as possible. For example the slight variations in

the dispersion of the SMF reflected the actual transmission fibre which was used for the experimental work.

| Table 1 | SMF | DCF |
|---|---|---|
| **Length** | 100 km | - |
| **Dispersion** | 1712 to 1718 ps/nm | -1649 to -1672 ps/nm |
| **Loss** | 20 dB | 7.6 to 8.2 dB |
| **PMD** | 0.04 ps | 0.5 ps |

| Table 2 | Raman Amplifiers |
|---|---|
| **Gain (co)** | 4.5 dB |
| **Gain (contra)** | 11.5 dB |
| **Raman Efficiency** | 0.42 $W^{-1}km^{-1}$ |

| SMF | Length(km) | n2($m^2$/W) | D (ps/nm) |
|---|---|---|---|
| Span 1 | 100 | 2.7 10-20 | 1715 |
| Span 2 | 100 | 2.7 10-20 | 1718 |
| Span 3 | 100 | 2.7 10-20 | 1714 |
| Span 4 | 100 | 2.7 10-20 | 1712 |

**Table 5.1 & 5.2: Simulation parameters**

Simulations were performed for transmission distances of 800 km (triangles), 1,200 km (squares) and 1,600 km (circles) and the Q-factor was evaluated for the worst tributary in each case and is shown as a function of total launch power in figure 5.14. The red dashed line at 9.1 dB represents the FEC threshold for a standard concatenated RS code with 6.7% overhead and the dashed green line at 15.5 dB represents a BER of $10^{-9}$. The values of the simulated pre-compensation for 800 km, 1200 km and 1600 km were -140 ps/nm, -280 ps/nm and -280 ps/nm respectively and the signal was perfectly post compensated before the Q-factor was evaluated. Again these values were chosen to reflect the experimental loop configuration which had a residual dispersion of 140 ps/nm.




**Figure 5.14. Q-factor as a function of the total signal launch power for 800 km (triangles), 1200 km (squares) and 1600km (circles)**

The figure shows system performance above the FEC threshold (red dashed line) for a broad range of launch power levels, 15 dB for 800 km, 11 dB for 1,200 km and 6 dB for 1,600 km. The optimum launch power levels are at 4 dBm, 3 dBm and 2 dBm for 800 km, 1,200 km and 1,600 km respectively. At higher launch powers the Q-factor begins to decrease. This is as expected given the increased impact of nonlinear effects on system performance at higher launch power. The results of the simulations indicated that transmission of CoWDM over long-haul distances (>1000 km) in a transmission link based on 100 km spans of SMF was feasible. Much of the experimental work described in the following sections was carried out at the France Telecom research laboratories in Lannion, France.

### 5.3.3 40 Gbit/s CoWDM

In the experimental work described elsewhere in this thesis a 42.6 GHz sine wave was used to generate the seven channel optical comb which was subsequently modulated with 42.6 Gbit/s data in a phase preserving modulator array to give the CoWDM signal. In this section however due to the unavailability of a 42.6 Gbit/s pattern generator (this work was carried out in France and the shipping of the 42.6 PPG and ED was not feasible) the bit rate of the tributary signals was limited to 40 Gbit/s, and in order to achieve CoWDM a 40 GHz clock signal was used to generate the optical comb. However the interleaver and filter configurations in the transmitter and in the pre-amplified optical receiver remained the same (i.e. optimised for a bit rate of 42.6 Gbit/s). Therefore in order to quantify the effect this change in the bit rate would have on the system a comparison between CoWDM generated at the different bit rates was carried out before travelling to France. The experimental setup used was as described in Chapter 4 and an overview diagram is presented in figure 5.15.

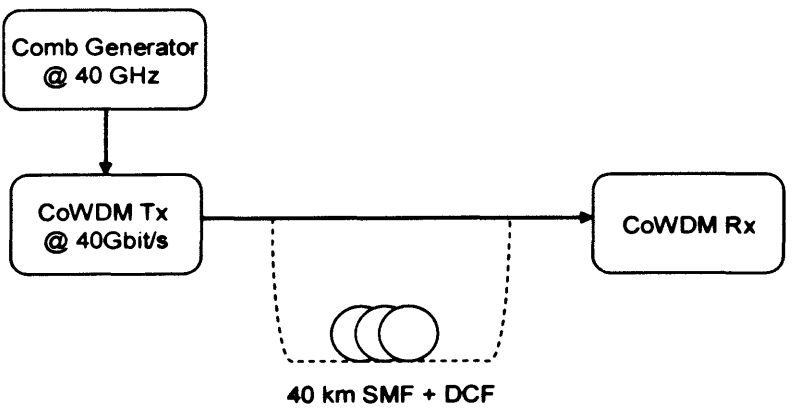



**Figure 5.15. 40 Gbit/s CoWDM experimental setup**

A DFB laser centred at 1547.2 nm was used as input to the comb generator and each of the seven resultant tributaries was encoded with 40 Gbit/s NRZ PRBS ($2^7$-1) data

using the same transmitter configuration as described earlier in the thesis. The receiver sensitivity curves of all seven 40 Gbit/s CoWDM tributaries in the back-to-back configuration are shown below.

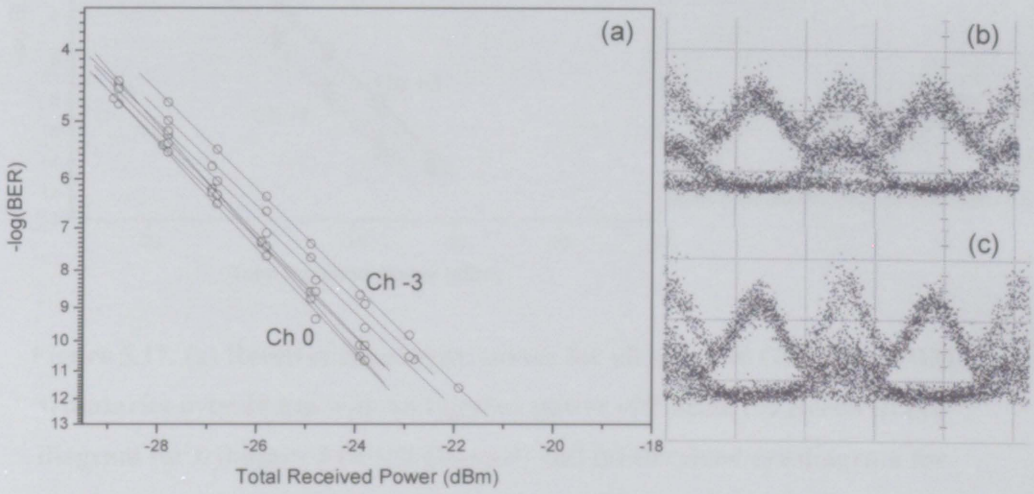



**Figure 5.16. (a) Receiver Sensitivity curves for all seven 40 Gbit/s CoWDM in back-to-back configuration. (b) Received eye diagram for channel -3 (worst channel) and (c) Received eye diagram for channel 0 (best channel)**

The average receiver sensitivity value was -24.3 dBm and there was a spread of 1.3 dB in the results. The worst channels were those at the edge (channel ±3). This was probably due to slightly incorrect filter alignment as there was no reference channel with which to align the asymmetric dis-interleaver in the receiver. The centre channels (channel 0 and channel ±1) showed the best performance.

The 40 Gbit/s CoWDM signal was then transmitted over 40 km of SMF, as shown in figure 5.17 with a total launch power of approximately 7 dBm. This transmission distance was chosen due to the available range of both SMF and DCF at the time of the investigation. This launch power level was chosen as it is in the middle of the range of launch powers investigated in chapter 4 (figure 4.28), i.e. it is high enough so that the system is not noise limited and low enough so that non-linear effects do not affect the transmission of CoWDM in a standard fibre link.

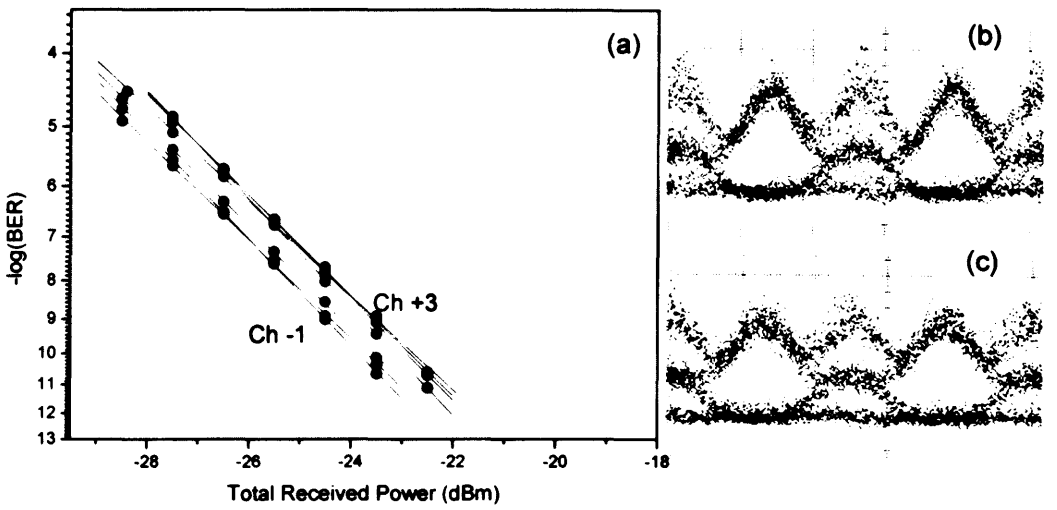



**Figure 5.17. (a) Receiver Sensitivity curves for all seven 40 Gbit/s CoWDM tributaries over 40 km with an injected power of 7 dBm, (b) Received eye diagram for tributary 3 (worst channel) and (c) Received eye diagram for tributary -1 (best channel)**

The average receiver sensitivity for the transmitted CoWDM signal was -23.9 dBm with a spread of only 1 dB across the seven tributaries. The receiver sensitivity penalty at a BER of $10^{-9}$ arising from transmission therefore was only 0.4 dB which can be attributed to the additional components in the transmission system. It is also worth noting that none of the 40 Gbit/s tributaries show any sign of an error floor either in the back-to-back case or for transmission. If we compare the 40 Gbit/s receiver sensitivities to those measured for the 42.6 Gbit/s back-to-back configuration we can see a 2.7 dB average improvement in the average receiver sensitivity at a BER of $10^{-9}$. The expected improvement due to the decrease in bit rate from 42.6 to 40 Gbit/s is approximately 0.3 dB. The remaining 2.4 dB improvement can be attributed to a number of experimental features including improved performance of components such as the DFF, data amplifiers and data modulators in the transmitter at the lower frequency.

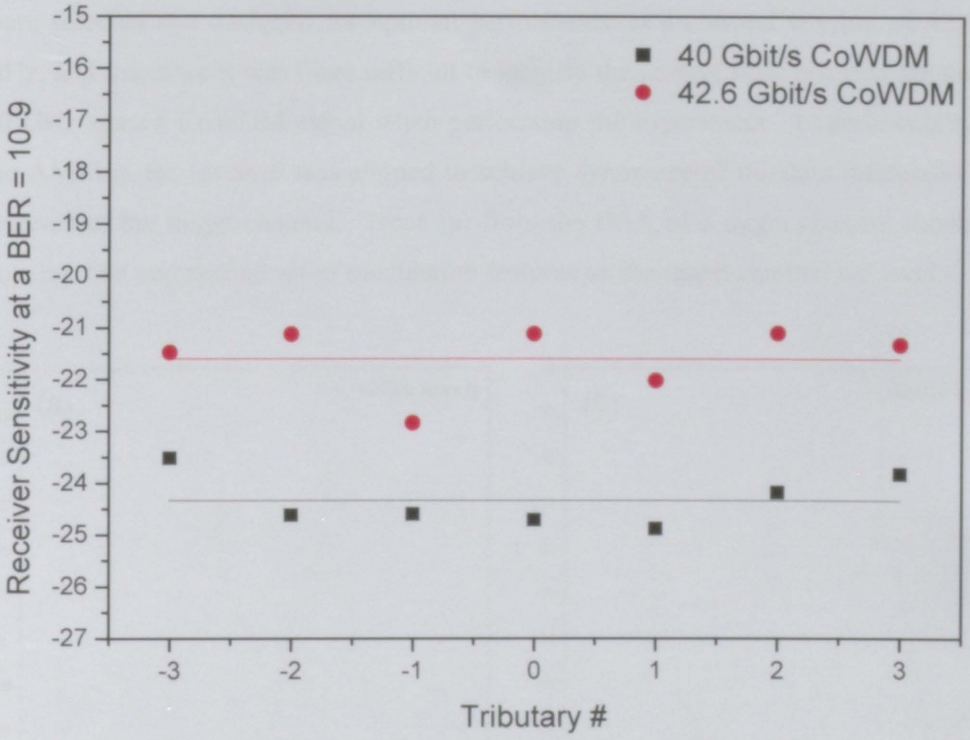



**Figure 5.18. Receiver sensitivities of all 40 Gbit/s (black squares) and 42.6 Gbit/s (red circles) CoWDM tributaries in back-to-back configuration with average lines (dashed traces)**

In figure 5.19 the received spectra for tributary 3 are shown for both 40 Gbit/s and 42.6 Gbit/s CoWDM in the back-to-back configuration. The inferior performance of the tributaries located at the edge of the 40 GHz spaced CoWDM spectrum can be attributed to imperfect filtering of tributaries adjacent to the target tributary by the filters which were optimised for 42.6 GHz channel spacing. This is evident in figure 5.19 (a) where peaks around the target channel have not been completely suppressed in the 40 GHz spectrum. In contrast these peaks are not visible in the 42.6 GHz spectrum

Another reason for the slightly (approximately 1 dB for the transmitted case) decreased performances of the 40 Gbit/s tributaries at the edges of the CoWDM spectrum was most likely the slight misalignment of the asymmetric disinterleaver in the receiver. These mis-alignments arose from the fact that the receiver side filters

were selected and designed for optimal performance at a channel spacing of 42.6 GHz, and therefore it was more difficult to identify the correct filter position for the 40 GHz spaced CoWDM signal when performing the experiment. Experimentally the AMZI at the receiver was aligned to achieve symmetry of the data modulation features of the target channel. Trace (a) from the OSA of a target channel shows how the first and second set of modulation features on the target channel are level.

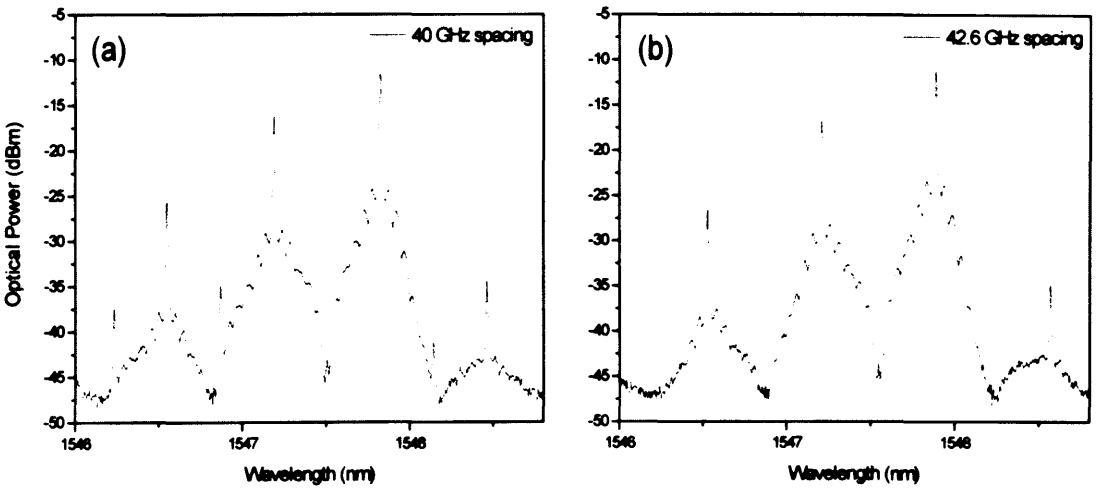



**Figure 5.19. Optical spectra for tributary 3 for both (a) 40 GHz and (b) 42.6 GHz channel spacing**

Therefore despite using a non-optimised filter configuration the 40 GHz spaced CoWDM system was shown to operate error free over both back-to-back and a 40 km SMF link. The transmission experiment using the 40 GHz channel spacing resulted in an almost negligible 0.4 dB penalty from the back-to-back case

### 5.3.4 Experimental Setup

For the experimental work described in this section most of the equipment required to implement the CoWDM transmitter and receiver was relocated from the lab in Cork, Ireland to a lab in France Telecom, Lannion, France and was operated in non-ideal conditions. For example the CoWDM transmitter unit which would normally

be positioned on an air table to prevent vibrations from affecting the data interferometer was positioned on the floor of the lab due to space constraints. The experimental configuration described in this section is presented in figure 5.20. The comb generator module (5.20 (a)) and the phase preserving data encoding section (5.20(b)) were almost identical to those reported in chapter 3.3 and 3.4, but with the use of a 10 Gbit/s 4-channel pattern generator multiplexed to 40 Gbit/s, and the centre wavelength at 1552.2 nm. The odd and even comb frequencies were demultiplexed by a dis-interleaver and independently NRZ data (and data-bar) encoded with a true $2^{31}$-1 PRBS.

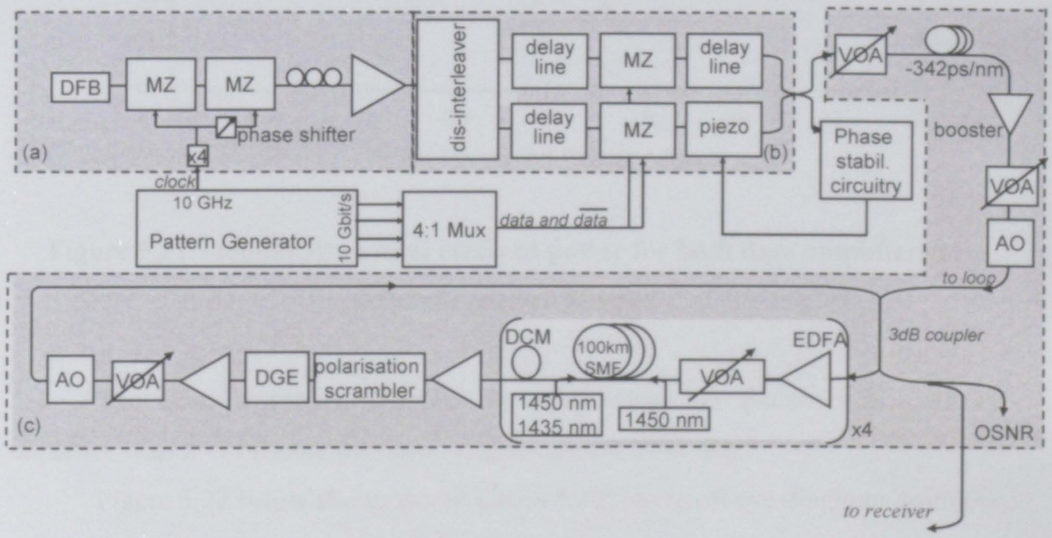



**Figure 5.20. Experimental setup for long-haul transmission with CoWDM**

An average pattern dependent back-to-back receiver sensitivity penalty of about 1 dB between data PRBS of lengths $2^7$-1 and $2^{31}$-1 was observed at a BER of $10^{-9}$, due to the frequency response of the data amplifiers in the transmitter at 40 Gbit/s. This is presented in the figure 5.21 below where the receiver sensitivity curves for a single 40 Gbit/s NRZ channel are plotted.

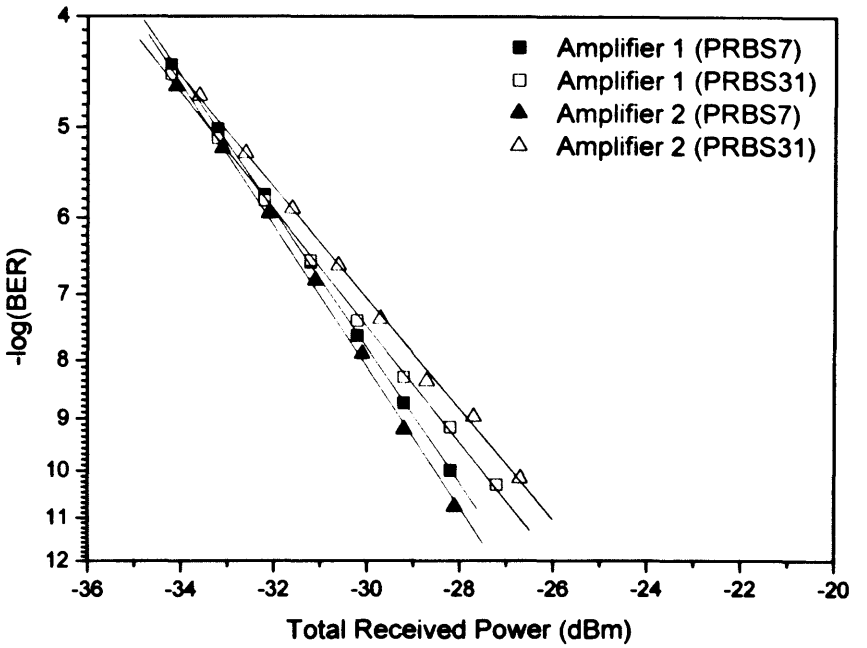



**Figure 5.21. –log(BER) vs total received power for both data amplifiers at different pattern lengths**

The closed symbols represent the setup where the pattern was a PRBS sequence with $2^7$-1 bits and the open symbols are for $2^{31}$-1 bits.

Figure 5.22 below shows the 40 Gbit/s NRZ electrical eye diagrams from the data and data-bar outputs of the DFF in the transmitter. The same DFF as was described in chapter 3 was used for this work. The 40 GHz clock signal which acted as the drive signal for the comb generator is shown in figure 5.23.

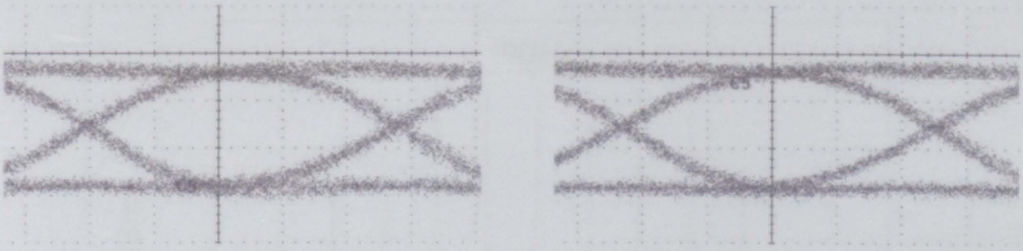



**Figure 5.22. 40 Gbit/s data and data-bar electrical eye diagrams from output of DFF**

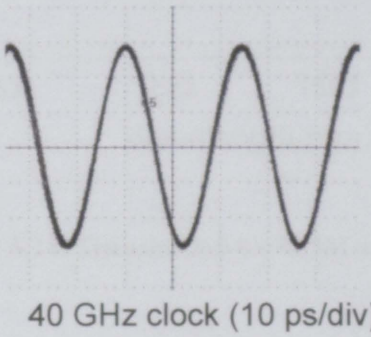



**Figure 5.23. 40 GHz clock signal**

At the output of the data encoding section, the odd and even tributaries were multiplexed together using a passive coupler resulting in a co-polarised 280 Gbit/s signal as shown in figure 5.24. It is worth noting the absence of spectral modulation on the $2^{31}$-1 spectrum when compared to the $2^{7}$-1 versions shown earlier due to the higher pattern length. This feature of the spectrum makes it slightly more difficult to align the AMZI in the receiver as it is no longer possible to balance the modulation features on the spectrum.

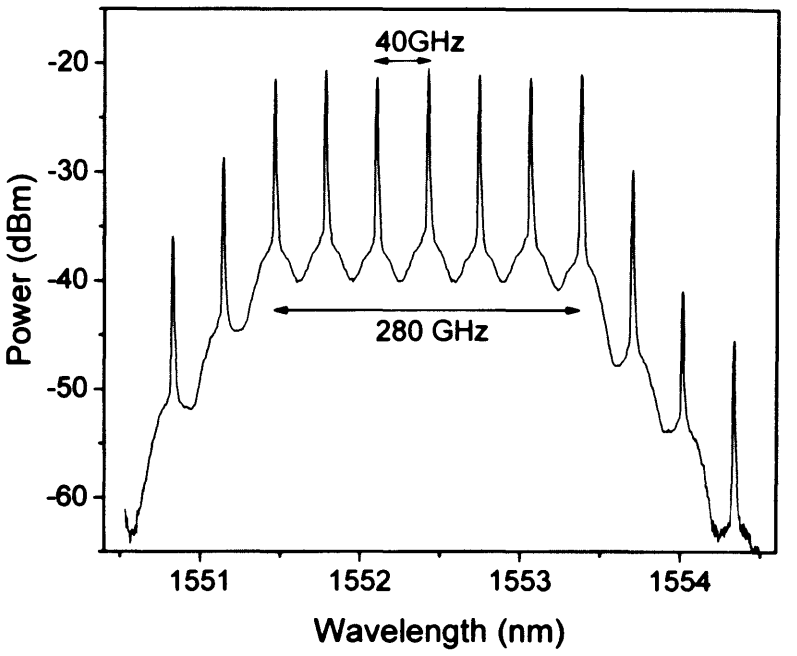



**Figure 5.24. Transmitted CoWDM spectrum**

At this point, a simple phase stabilisation circuit was used to provide feedback to the electrically driven piezo fibre stretcher, allowing for full control and stabilisation of the relative optical phase between the two arms. The 280 Gbit/s signal was then pre-compensated (-342 ps/nm) before entering the recirculating loop, shown in figure 5.20 (c), which comprised 4 spans, each of 100 km of SMF, followed by a slope matched dispersion compensating module (DCM) which compensated for both the dispersion and the slope of the 100 km SMF spans. This loop is the same as described in [160]. An EDFA (NF of 5.5 dB) and a VOA preceded each fibre span in order to control the signal launch power, and the remaining span loss was compensated using forward (1450 nm, gain = 4.5 dB) and backward (1450 nm and 1435 nm, gain = 11.2 dB) Raman amplification (pump power = 5 W) in each span of SMF. After the 4 spans the signal was launched into a polarisation scrambler synchronously modulated with the loop round-trip period, which minimised the loop induced polarization effects [161, 162]. A dynamic gain

equalizer (DGE) suppressed the ASE noise away from the narrow bandwidth (~2.3 nm) CoWDM signal, whilst a pair of EDFAs overcame these loop specific insertion losses. This suppression of the ASE prevents the noise from being amplified as it propagates through the loop which would have a negative impact on the performance of the system. A pair of acousto-optical (AO) switches and a 3 dB coupler were used to switch the transmitted signal out of the loop to the receiver after a preset number of circulations. The residual chromatic dispersion and differential group delay (DGD) of the loop were approximately 140 ps/nm and 1.6 ps per loop respectively.

The preamplified receiver was similar to the one described in chapter 3 and is shown in figure 5.25. It included a concatenated tuneable band-pass filter (0.64 nm bandwidth) and an AMZI with a FSR of 85.2 GHz to select each individual tributary. A fixed amount of post-compensation was added at this stage to compensate for the residual dispersion at each transmission length. This post-compensation was not exact and therefore some residual dispersion existed after transmission. In the case of the 800 km transmission experiment this post dispersion consisted of approximately 3.4 km of SMF giving an overall estimated residual dispersion of -4 ps/nm. In the 1200 km case the post dispersion consisted of 2.57 km of SMF and a DCM with a value of -135 ps/nm. This resulted in an approximate residual dispersion value of -13.3 ps/nm. It must be stressed that these figures are estimates only and the post-dispersion in each case was selected to give the optimum BER performance at the receiver.

Each of the seven 40 Gbit/s tributary WDM channels was detected using two high speed photodiodes (PD), one feeding a phase-locked loop clock recovery unit (CRU) specially optimised for NRZ signals, whilst the other was electrically demultiplexed to 10 Gbit/s. Due to the loop operation, error rate measurements were effectively averaged over all four 10 Gbit/s tributaries at each signal burst sent to the error detector. A typical received back-to-back CoWDM eye diagram is shown in figure5.25, where the crosstalk terms are positioned at the eye crossing and the eye is open at the centre, as expected for a CoWDM signal.

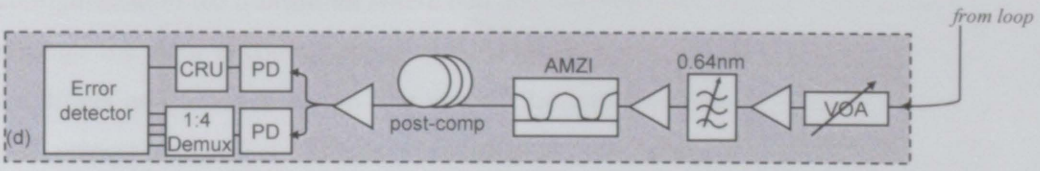



**Figure 5.25. Pre-amplified receiver**

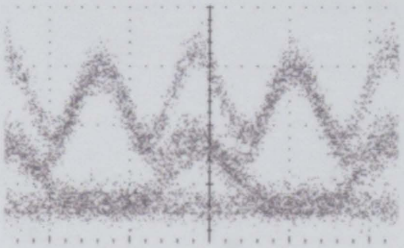


**Figure 5.26. CoWDM back-to-back eye diagram**

### 5.3.5 Experimental Results

The results presented in this section show the experimental transmission performance of a 280 Gbit/s CoWDM signal over 800 km and 1,200 km. Firstly, the experimental Q-factor measurements at the optimum launch power for all seven 40 Gbit/s tributaries are plotted in figure 5.27. This optimum launch power was obtained by measuring the receiver sensitivity of the worst tributary (# -1) across a range of launch powers. In Chapter 4 it was demonstrated that FEC codes can be used with CoWDM with no additional penalty, and therefore the average measured Q-factors for 800 km and 1,200 km of 12.1 dB and 10.7 dB provide a 3.0 dB and 1.6 dB FEC margin (for a concatenated RS 7% overhead code as detailed in G.975 [51]) respectively. Transmission of a 280 Gbit/s signal over 1,200 km represents a bit rate-distance product of approximately 336 Gbit-Mm/s for a single laser. In both the 800 km and 1,200 km cases is appears that the even numbered channels slightly outperform the odd numbered channels. This can be explained by the experimental

configuration of the transmitter where odd and even channels traverse different paths through the data encoding stage and the performance of the components (data amplifiers and modulators) on one arm of the interferometer is slightly improved with respect to the other. The worst tributary in both cases is # -1, yet even at 1,200 km the Q-factor remains over 1 dB away from the FEC limit.

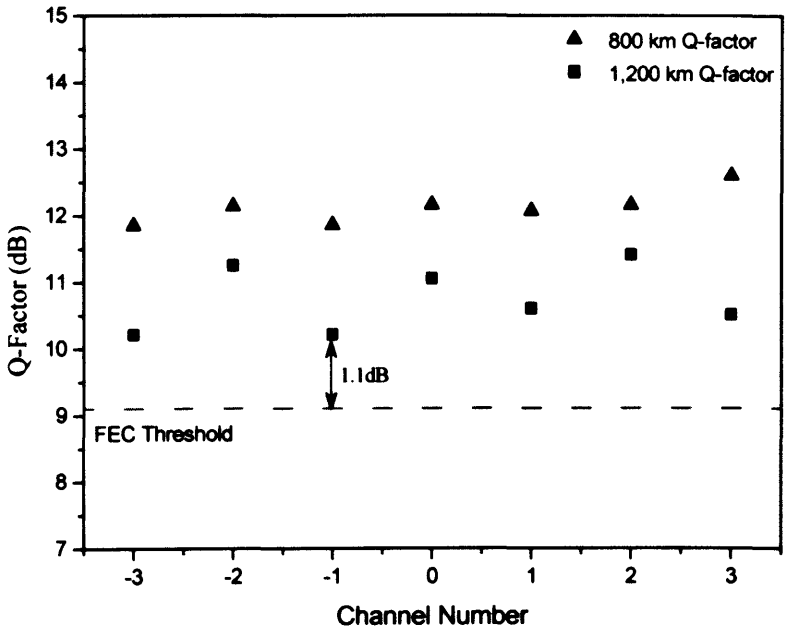



**Figure 5.27. Measured Q-factor for each tributary channel for 800 km and 1,200 km**

Figure 5.28 shows a received eye diagrams for the best and worst channel for both transmission distances. The eyes appear degraded in terms of OSNR relative to the back-to-back eye shown in figure 5.26 but are recoverable to an error rate of less than $10^{-15}$ using FEC. The characteristic shape of the CoWDM eye is still just about visible.

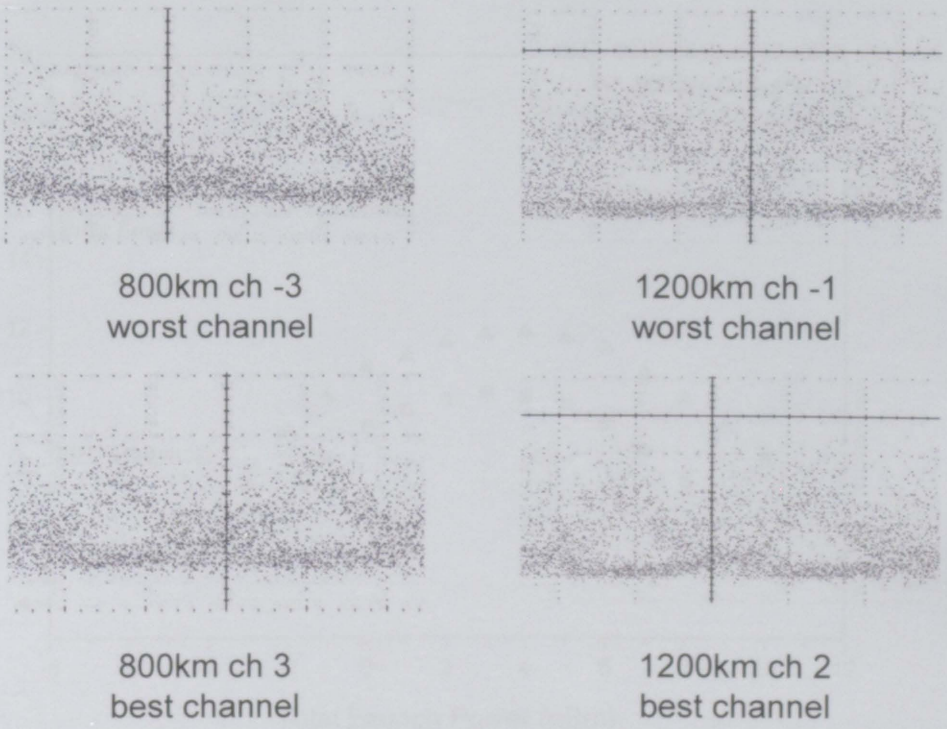



**Figure 5.28 Received 40Gbit/s CoWDM eye diagrams for best and worst tributaries**

In order to evaluate the non-linear tolerance of the system the Q-factor of the worst channel was measured for a range of total input signal power levels and these results are presented in figure 5.29 for both 800 km and 1,200 km transmission distances. The input signal power levels were adjusted by setting the variable optical attenuators after the EDFA appropriately.



University College Cork Library

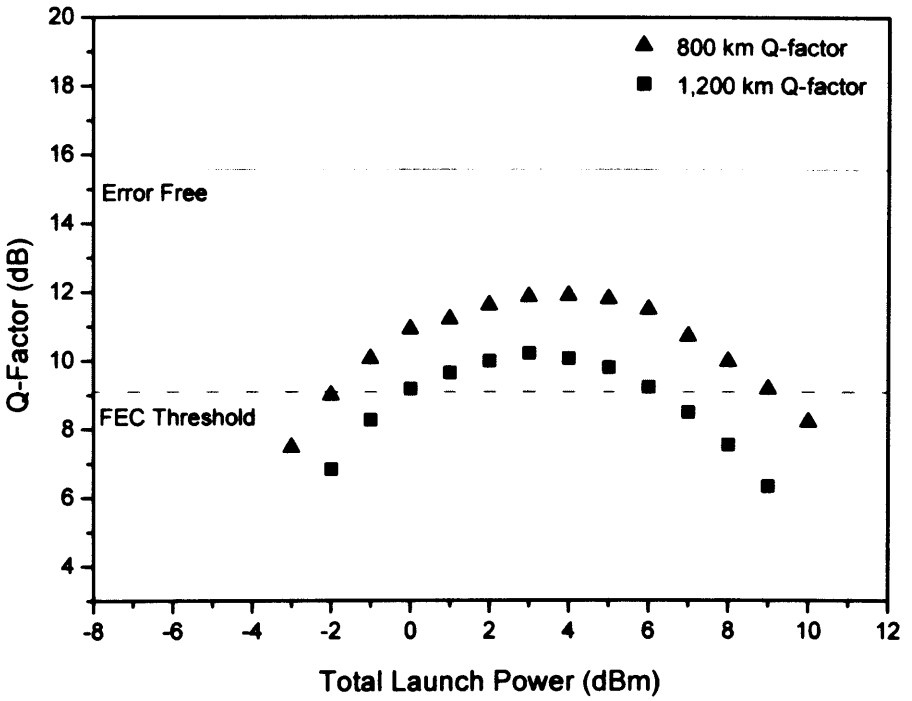



**Figure 5.29. Measured Q-factor as a function of total launch power for 800 km and 1,200 km**

The optimum total signal launch powers for 800 km and 1,200 km are +4 dBm and +3 dBm respectively. It is also clear that for a wide range of launch powers (10 dB for 800 km and 6 dB for 1,200 km), Q-factor measurements are above the FEC threshold of 9.1 dB (represented in figure 5.29 by the dashed line, enabling a post-FEC BER $<10^{-15}$), illustrating robust performance with an aggregate capacity of 261 Gbit/s. For comparison, the simulation results shown in figure 5.14 for these two distances are presented alongside the experimental results in figure 5.30.

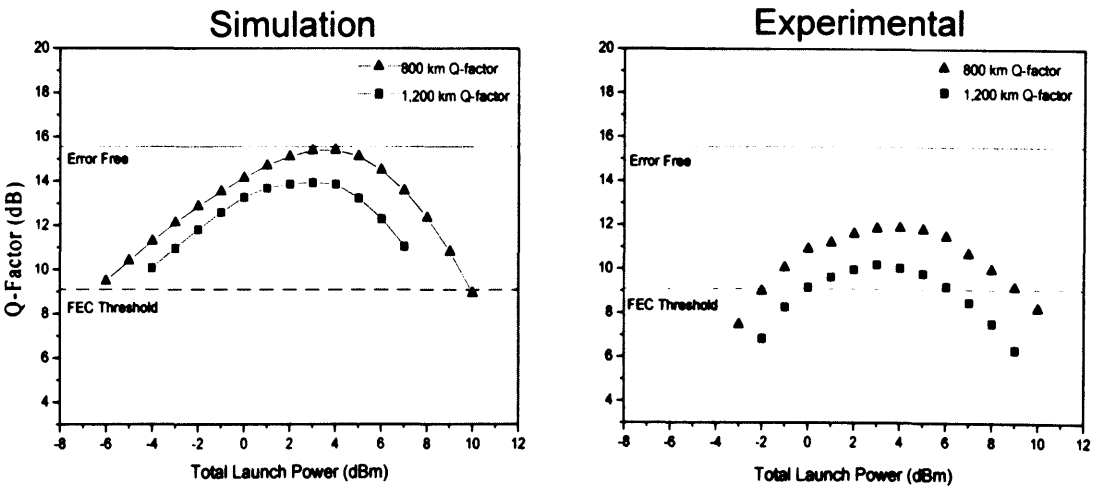



**Figure 5.30. Measured and simulated Q-factor as a function of launch power for 800 km (triangles) and 1,200 km (squares)**

A 3.6 dB difference in the performance at the optimum launch powers between the experimental results and the simulations is evident. Some of this difference can be explained by the 1 dB pattern dependent receiver sensitivity penalty arising from the frequency response of the data amplifiers. The simulations were carried out using a 512 long bit pattern in order to decrease the computational complexity. The remaining 2.6 dB penalty can be attributed to the differences in the phase optimisation, and non-optimal post-dispersion compensation in the experiments. The phase was individually optimised for each of the seven tributaries in the simulations whereas the experimental setup was limited to two modulators with phase control on one of the arms. As demonstrated in chapter 4, figure 4.24, the two modulator case represents a worst case scenario when compared to the seven modulator case. In addition the -4 ps/nm estimate value of the residual dispersion in the 800 km transmission case would account for approximately 1.7 dB penalty in line with figure 4.23 shown in chapter 4.

It was observed that the predicted optimum input power to the SMF closely agrees with the experimentally measured values for both 800 km and 1,200 km. This feature of the results, together with the fact that the 3 dB penalty between the

simulated and measured Q factor values can be well explained by the pattern sensitivity and the non-optimal residual dispersion suggests that the numerical model accounts for all dominant impairments of the system, and that the estimated residual DGD of the loop (2.26 ps and 2.77 ps for 800 km and 1,200 km respectively) did not significantly affect the CoWDM signal. This tolerance to the effect of PMD is in marked contrast to alternative approaches achieving similar capacities per wavelength source which are significantly limited by similar levels of PMD [163].

In figure 5.31 the achieved OSNR (right axis, open symbols), defined as the total signal power divided by the noise power normalised to a 0.1nm bandwidth, is compared to the measured Q-factor (left axis, closed symbols) of tributary # -1 (worst tributary in figure 5.27) as a function of the total launch power into the SMF for both 800 km (triangles) and 1,200 km (squares) distances.

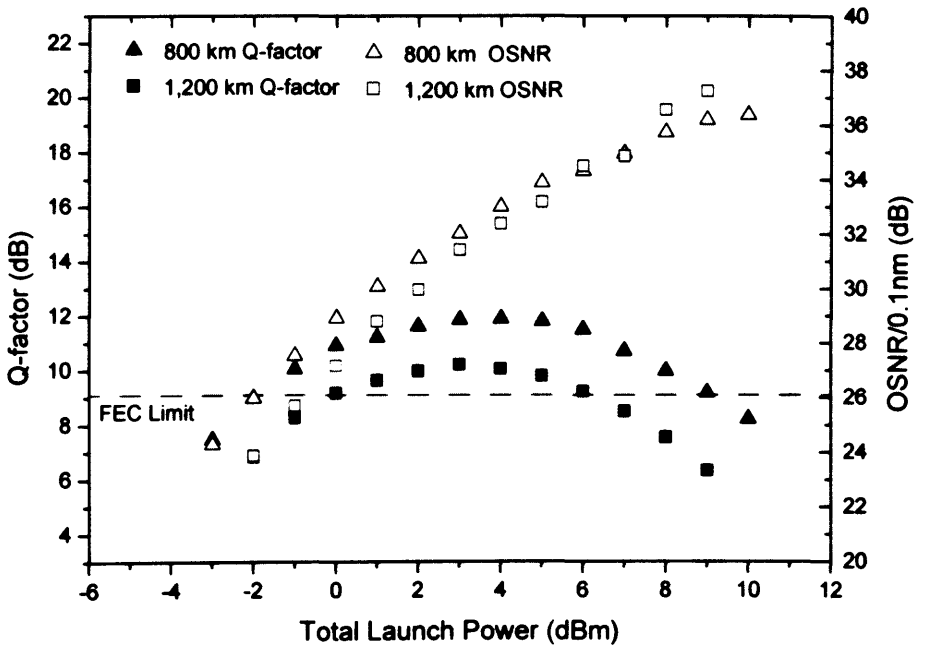



**Figure 5.31. Measured Q-factor and OSNR as a function of launch power for 800 km and 1,200 km**

The optimum launch powers for 800 km (+4 dBm) and for 1200 km (+3 dBm) correspond to OSNR figures of 33 dB and 31.4 dB respectively. At low launch powers it is evident from the overlaying OSNR and Q-factor traces that the system is OSNR limited with a required OSNR ~26 dB (BER=$10^{-4}$), again reflecting the observed ~3 dB penalty when compared to analytical predictions for an OSNR limited 42.6 NRZ system [164]. At higher launch powers, as the OSNR continues to increase with increasing launch power, non-linear effects in the transmission fibre result in the degradation of the measured Q-factor for the 280 Gbit/s signal. We have shown previously in chapter 4 that, for a strongly dispersion managed system, self-phase modulation within the individual tributaries is the primary non-linear effect responsible for this degradation, thus exhibiting similar behaviour to a conventional 100 GHz spaced 40 Gbit/s NRZ WDM system. From the shape of the OSNR and Q-factor curves as the launch power is increased shown in figure 5.31 it is possible to infer that this system is exhibiting similar behaviour to conventional 100 GHz spaced 40 Gbit/s NRZ WDM systems.

### 5.3.6 Summary

In this section the successful transmission of a 280 Gbit/s CoWDM signal over distances of 800 km and 1,200 km has been presented. Transmission was performed in a 100 km span recirculating loop with hybrid Raman/EDFA amplification and long data pattern lengths, yielding a bit rate-distance product of 313 Gbit-Mm/s, for a single wavelength source. Comparison of optimum launch power values between experimental results and the results of simulations performed without taking the effect of PMD into consideration suggest that CoWDM was not significantly affected by the PMD (2.77 ps DGD) in the experimental system. This is a significant advantage of the CoWDM format as a similar amount of PMD would represent a significant difficulty for a 300 Gbit/s OTDM system for example. Many installed fibre links are affected by the effects of PMD which must be taken into account when considering upgrades to the system. The Q-factor for each of the 7 tributaries was measured to be above the FEC limit after transmission, confirming

the compatibility of CoWDM with dispersion managed, hybrid amplified, terrestrial fibre spans.

## *5.4 Multi-banded CoWDM [165]*

### 5.4.1 Introduction

High spectral density point-to-point transmission systems have been developed over the years to meet the growing capacity demands on telecommunication networks. In addition to requiring high point-to-point capacity these networks must also be capable of switching and routing large amounts of data across networks in a cost effective fashion which often contain a large number of routing nodes. In numerous applications, this is achieved by band switching [166, 167, 168, 169, 170] where high capacity bands are required. Such bands can be formed either by a number of channels each at very high bit rates (160+ Gbit/s), or by a larger number of closely-spaced dense WDM channels, each at lower bit rates (~40 Gbit/s). Recent developments in this area are based on OTDM technology, where single-channel bands of 160+ Gbit/s are implemented by OTDM multiplexing, which require polarisation interleaving of adjacent bands to achieve the required high spectral density values [171].

In this section we look at how CoWDM, as has been presented throughout this work can be modified to achieve ultra-high overall capacities while retaining its key advantages such as high ISD and low implementation complexity. The multi-banded approach also allows for the possibility of switching CoWDM on a band by band basis which makes CoWDM an attractive solution for high capacity transparent optical networks of the future.

### 5.4.2 Multi-banded CoWDM

In previous chapters a comb generator based on a single DFB laser was used to generate the 7 channel optical comb with an inter-channel spacing of 42.6 GHz which was subsequently data modulated to form the CoWDM signal. In the multi-banded CoWDM configuration the increase in capacity was achieved by replacing the single wavelength source with a bank of '*n*' lasers spaced by an appropriate frequency (depending on the number of wavelength channels, '*m*' generated by the comb generator in the system, *m*= 7 in this case) thus creating '*n*' bands of '*m*' phase locked channels. These channels would then be individually data encoded using a bank of '*n x m*' independent data modulators. A schematic of this setup is shown in figure 5.32 below.

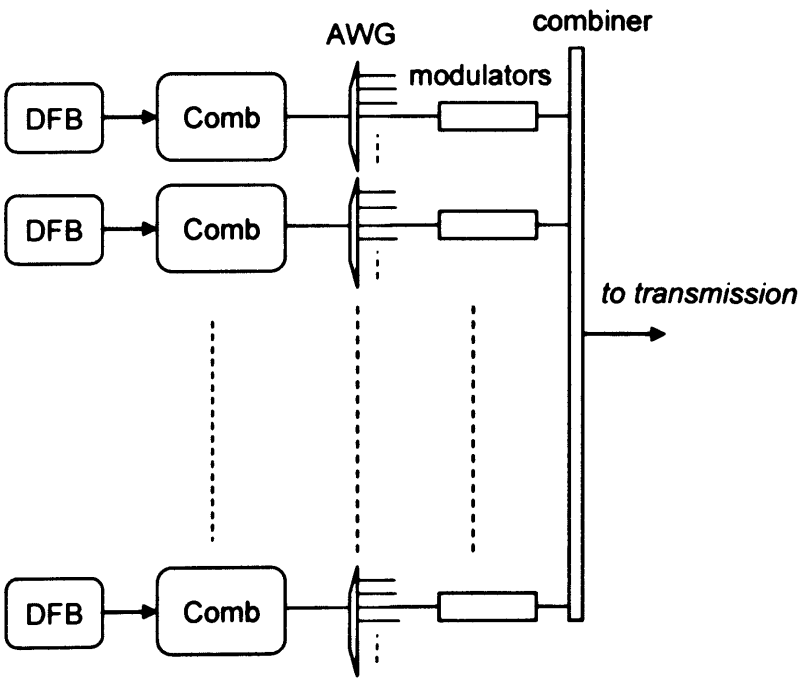



**Figure 5.32. Schematic of a multi-banded CoWDM setup**

The square filter placed after the comb generator allows for the reduction of the size of the unwanted sidebands beyond the comb and thus reduces the size of the guard band necessary between adjacent bands. Figure 5.33 shows a simulated multi-banded CoWDM spectrum containing a total of 49 lines generated using a bank of 7 independent DFB lasers multiplexed together and launched into the comb generator. A guard band of 85.2 GHz separates the bands in this simulation.

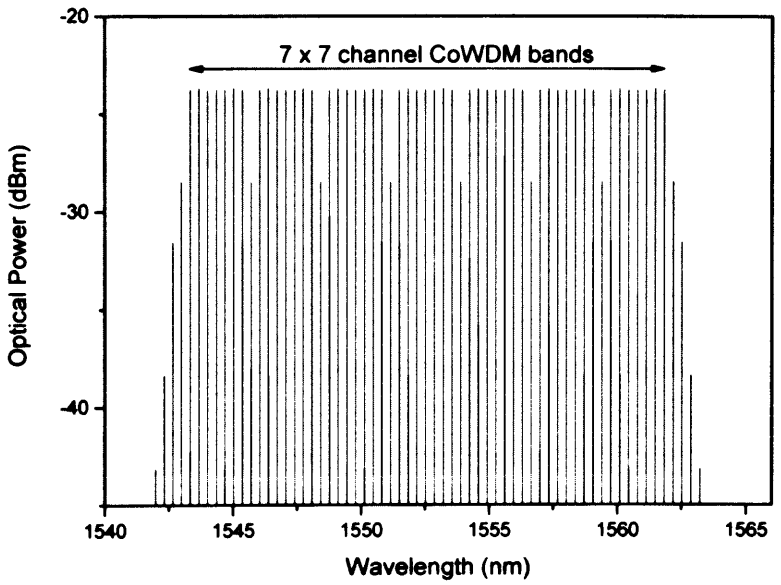



**Figure 5.33. Simulated multi-banded (49 channels) optical comb**

### 5.4.3 Experimental Setup

Figure 5.34 shows a schematic of the experimental set-up for multi-banded CoWDM transmission, where each band is derived from an independent DFB laser. As shown in figure 5.34, five lasers, separated by 340.8 GHz (chosen to allow for optimum tradeoff between ISD and interference arising from overlapping side-modes), were passively multiplexed, and seven phase locked channels per laser were generated by two consecutive Mach-Zehnder modulators (as shown in Chapter 4), each driven

with a 42.6 GHz clock, with amplitude of 2.1 Vπ (comb generator), resulting in a total of 35 channels ranging from 1548.4 to 1562.9 nm as shown in 0.2 nm resolution in figure 5.35. The experiment was restricted to five bands of CoWDM because of the DFB lasers which were available.

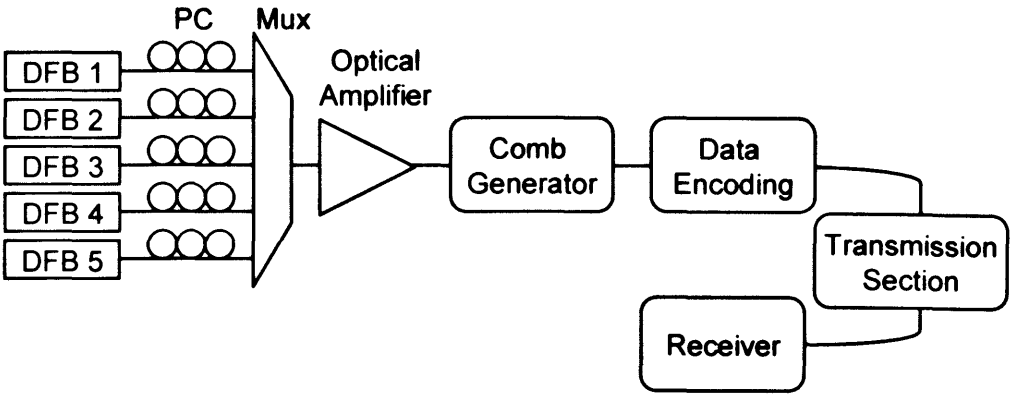



**Figure 5.34. Multi-banded CoWDM experimental setup**

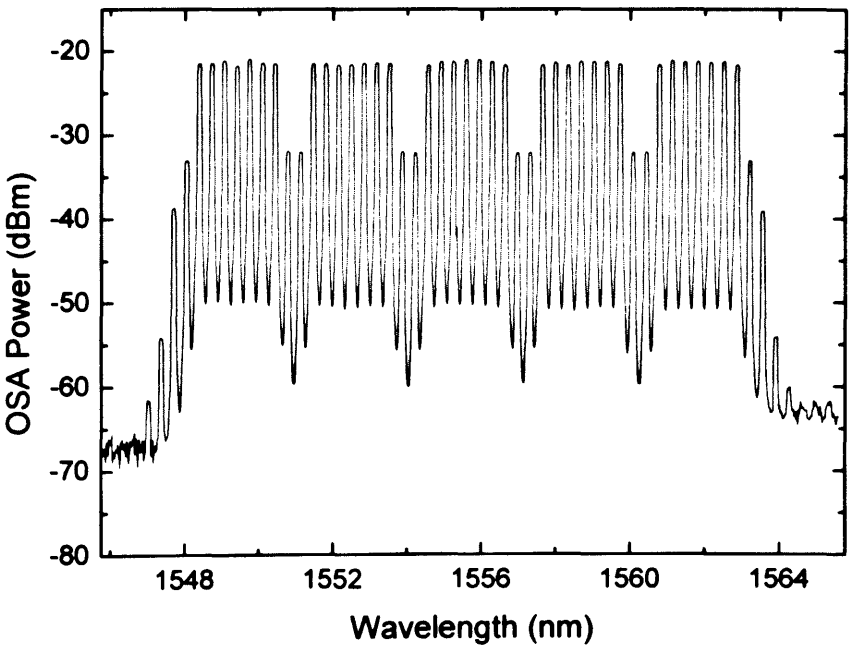



**Figure 5.35. 35 channel comb spectrum (5 independent DFB's)**

A flatness of less than 0.7 dB over the entire comb spectrum was achieved using the same feedback loop as described in chapter 3 over all 35 channels. For the purpose of flattening the comb it was sufficient to monitor a single band so no adjustment was made to the control circuit described earlier in the thesis. A dispersion compensated optical amplifier was introduced to maintain an adequate signal-to-noise ratio. The dispersion compensated amplifier also prevented dispersion from affecting the edge channels of the increased bandwidth CoWDM signal.

A guard-band of 127.8 GHz between bands minimised the inter-band cross-talk arising from the finite side-mode-suppression ratio in the comb generator of 11 dB. This guard band value was selected to be a multiple of the channel spacing as this meant that no tuning of the AMZI at the receiver was necessary when going from band to band. The presence of these guard bands resulted in a marginal decrease in the ISD of the system to 0.83 bit/s/Hz. As mentioned in chapter 1 the ISD of a system where the channel spacing is not constant can be defined as

$$ISD = \frac{Total\ Capacity}{Total\ Bandwidth}\ \text{bit/s/Hz} \tag{5.10}$$

In this case the overall capacity of the system is 35 x 42.6 Gbit/s = 1.49 Tbit/s and the total employed bandwidth is 1.79 THz resulting in the ISD figure quoted above of 0.81 bit/s/Hz. In an ideal system a filter after the comb generator would reduce the impact of unwanted sidebands and the size of these guard bands could be reduced significantly which would result in the ISD approaching the limit value for a single polarisation NRZ CoWDM system of 1 bit/s/Hz.

In a real system, five phase-preserving arrays of seven modulators would be used to individually data encode each of the channels. The relative phase between adjacent channels needs only to be controlled within any given band, and not across the entire multi-banded spectrum. In our experimental setup the phase was stabilised using the circuitry described in Chapter 3. For simplicity within this demonstrator, adjacent channels were separated by a dis-interleaver with FSR of

85.2 GHz, followed by PRBS $2^7$-1 NRZ data encoding at 42.6 Gbit/s using two $LiNbO_3$ Mach-Zehnder modulators (data encoding section in figure 5.34). In this way, the dominant cross-talk from adjacent channels was fairly included. Delay lines and a feedback controlled piezo fibre stretcher were used to maintain optimum performance, while polarisation controllers ensured co-polarised signals at the output of the interferometer, which were passively multiplexed by a simple wavelength independent coupler. The transmitted spectrum, consisting of 35 x 42.6 Gbit/s channels is shown in figure 5.36.

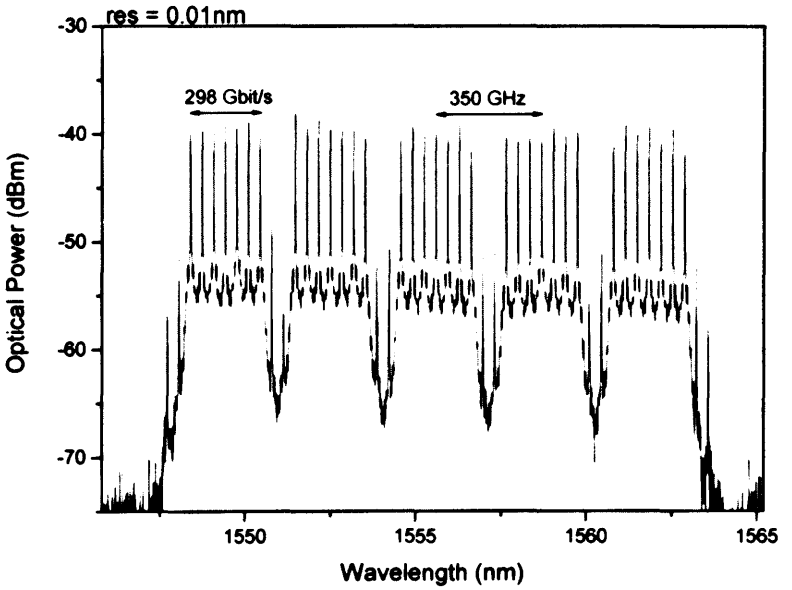



**Figure 5.36. Optical spectrum before transmission**

The transmission section shown in figure 5.37 consisted of a pre-compensated unrepeated link of 80.4 km SMF-28e. Variable optical attenuators and EDFAs were used to control launch powers and to overcome the link losses.

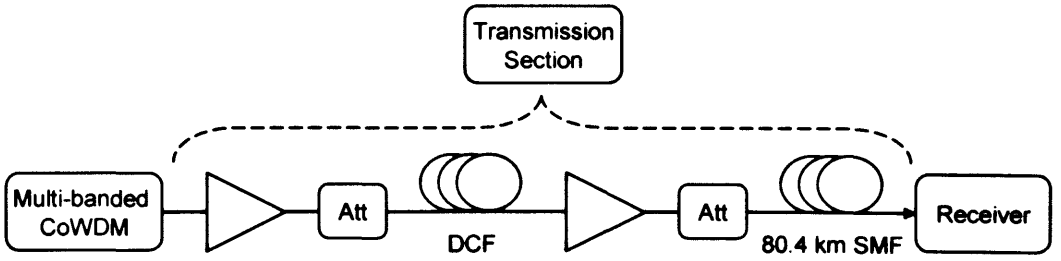



**Figure 5.37. Transmission link**

Finally, as described in Chapter 3 a simple pre-amplified receiver was used, which comprised a Mach-Zehnder dis-interleaver with FSR of 85.2 GHz and a 0.64 nm tunable filter, as described previously, along with a commercially available 42.6 GHz clock recovery module and photodiodes.

### 5.4.4 Multi-banded Results

The spectrum after transmission, prior to filtering, is plotted in figure 5.38, and shows no evidence of non-linear effects, when compared to the spectrum before transmission shown in figure 5.36. Moreover, it shows a compact, square-like encoding shape for each band, without the use of pre-filters to minimise inter-band spectral overlap. The effects of the data modulation can also be seen on the spectrum.

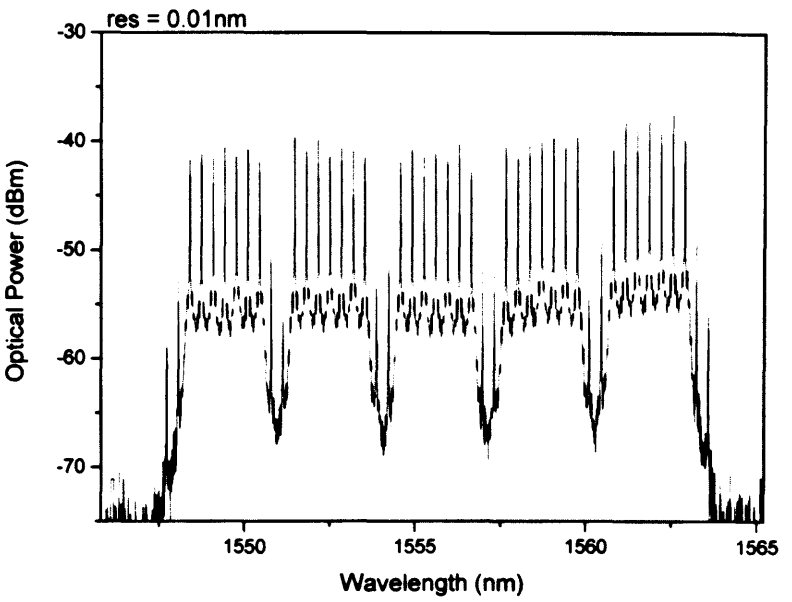



**Figure 5.38. Optical spectrum after transmission over 80.4 km**

The non-uniformity (~5 dB) in the received power levels for both back-to-back and transmission cases is attributed to the wavelength sensitivity within the comb generation module, imbalances between data modulators in the transmitter, and residual gain variation in the transmission amplifiers.

The performance of each individual channel for the five bands before and after transmission was analysed by measuring the receiver sensitivity at a BER of $10^{-9}$ and the corresponding values are presented in figure 5.39 below.

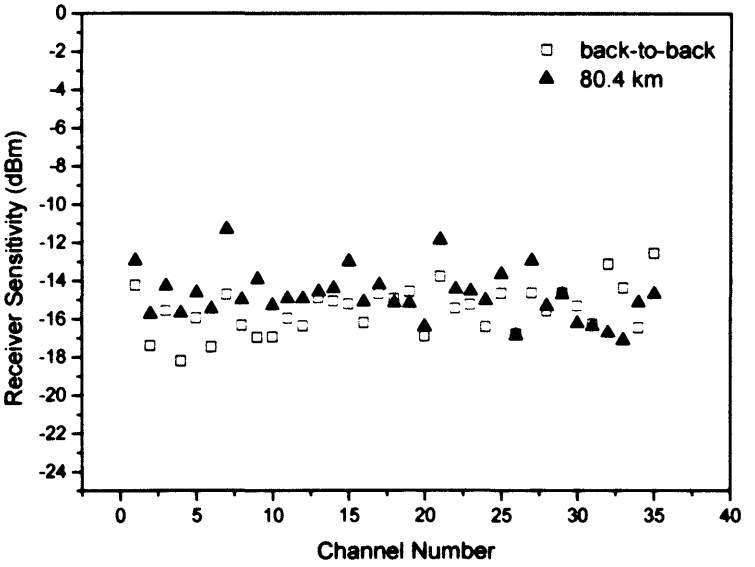



**Figure 5.39. Receiver sensitivity values for all 35 channels in back-to-back configuration (open squares) and after 80.4 km transmission (closed triangles)**

The receiver sensitivity values for each tributary as a function of the peak power in the received OSA spectrum is plotted in figure 5.40. The grey dashed arrow is a guide to the eye and shows the dominant trend of increasing receiver sensitivity with increasing peak power as measured on the OSA.

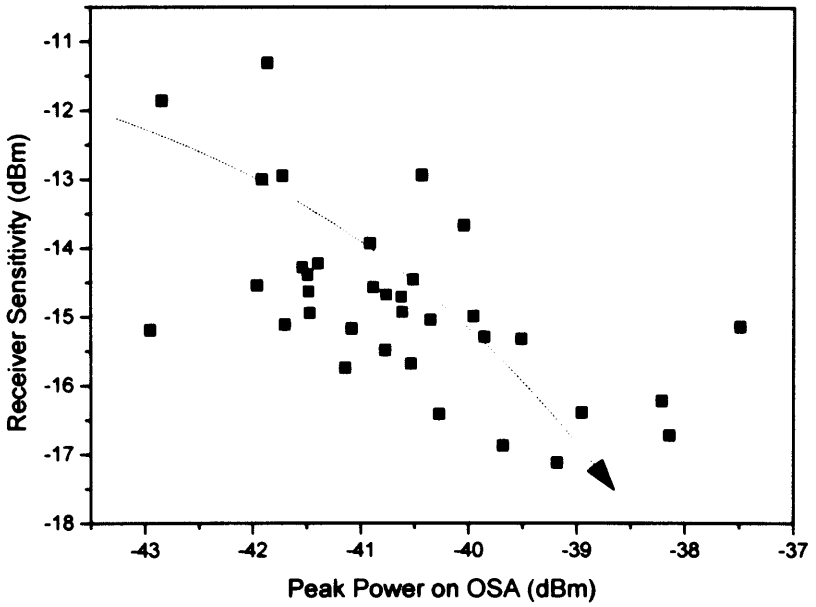



**Figure 5.40: Receiver sensitivity as a function of peak channel power for all 35 tributaries**

The receiver sensitivity curves for all 35 tributaries are plotted in figure 5.41 top panel (back-to-back case) and figure 5.41 bottom panel (after transmission over 80.4 km). It is clear from examining these figures that all of the tributaries run error free and there is no evidence of an error floor. There is a noticeable difference in the performance between the odd and even tributaries, especially after transmission. The difference between the average receiver sensitivity values is approximately 1 dB in the back-to-back case and 1.3 dB after transmission with the even tributaries outperforming the odd.

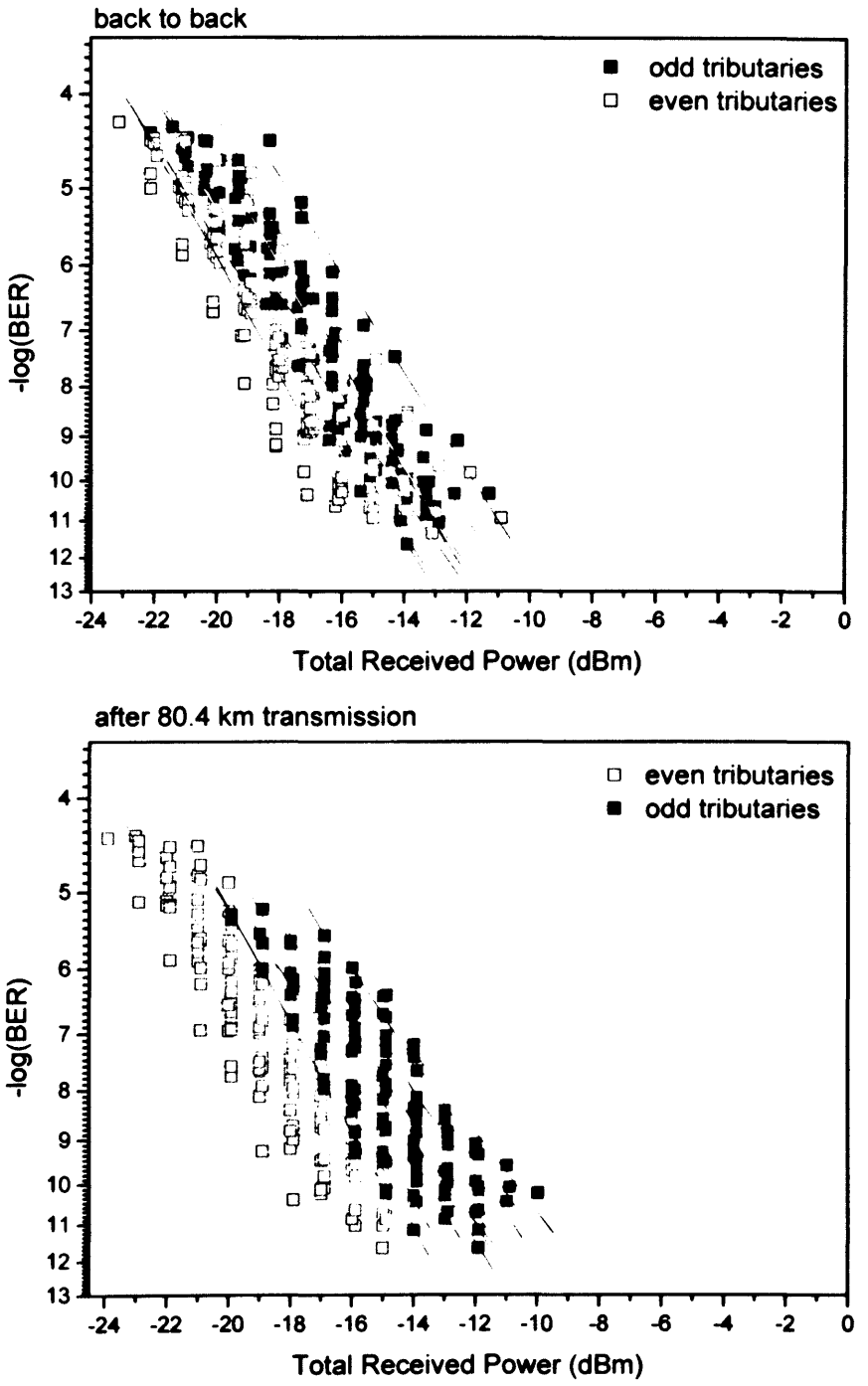



**Figure 5.41. Receiver sensitivity curves for all 35 tributaries in the back to back configuration (top panel) and after transmission (bottom panel)**

Clearly the observed spread in receiver sensitivity of approximately 5.7 dB across the 35 channels is highly correlated to the received power variations described above. The average receiver sensitivity for the back-to-back case was measured to be -15.5 dBm and a relatively small penalty of 0.7 dB was observed for the 80.4 km transmission case (average Rx sensitivity = -14.8 dBm).

In fact certain channels experienced an improved performance after transmission, for example a 1.2 dB improvement in average receiver sensitivity after transmission for the 1562-nm-band was observed. This was primarily due to the wavelength-dependent amplifier gain tilt which favoured higher wavelengths. Note that, despite running at a bit rate of 42.6 Gbit/s which is the standard ITU-T G.975.1 FEC line rate, multi-banded CoWDM did not require FEC to achieve error-free performance, as we have previously demonstrated for the single banded case in Chapter 4.

Further detailed results are shown in figure 5.42, where receiver sensitivity curves and received eye diagrams (5 ps/division grid) for three randomly chosen channels (4, 16 and 30), for back-to-back, are presented.

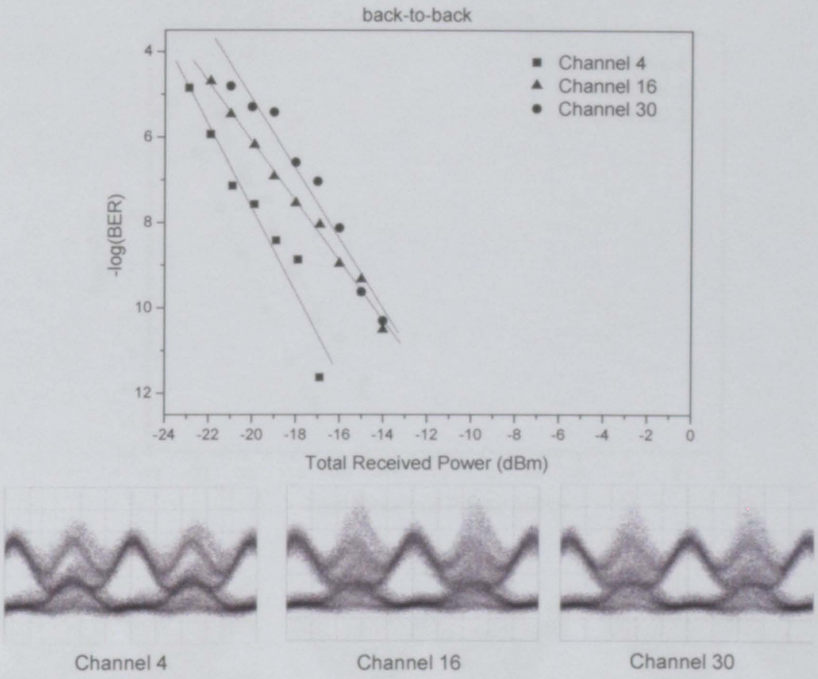



**Figure 5.42. Receiver sensitivity curves and eye diagrams for channels 4, 16 and 30 (back to back)**

Figure 5.43 shows the corresponding measurements for 80.4 km transmission. It is evident from the eye-diagrams that there is slightly more crosstalk evident in the transmitted eyes. However little or no distortion at the centre of the eye was observed between the back-to-back and transmission cases. Channel 4 (1549.4 nm), positioned at the centre of a band, exhibits a slightly different level of distortion than channel 30 (1559.7 nm), which was located at the edge of its band, though this had a minor impact on the recorded receiver sensitivity for the channel.

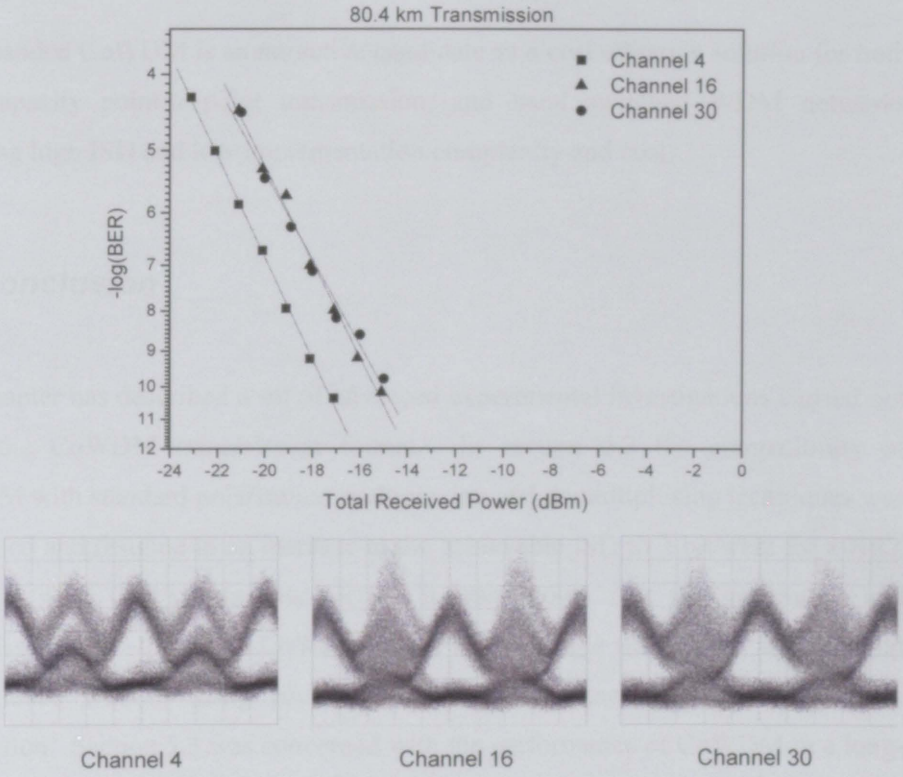



**Figure 5.43. Receiver sensitivity curves and eye diagrams for channels 4, 16 and 30 (80.4 km transmission)**

### 5.4.5 Summary

In this section multi-banded CoWDM operation has been introduced and demonstrated resulting in a system with a capacity of approximately 1.5 Tbit/s from 5 independent lasers. A net information spectral density of 0.83 bit/s/Hz was achieved using five co-polarised CoWDM bands of 298 Gbit/s each, and with no prefilters at the transmitter and employing NRZ modulation. This could be further increased by a reduction in the size of the guard bands by eliminating unwanted side bands from the comb spectrum, or alternatively by using advanced multilevel modulation formats instead of NRZ modulation in the transmitter. The multi-banded CoWDM system achieved error free performance in both the back-to-back configuration and after transmission over 80.4 km of SMF-28e®. We believe that

multi-banded CoWDM is an attractive candidate as a cost effective solution for both high capacity point-to-point transmission, and band switched WDM networks requiring high ISD and low implementation complexity and cost.

## 5.5 Conclusion

This chapter has described a set of advanced experimental investigations carried out using the CoWDM transmission format. In section 5.2 the compatibility of CoWDM with standard polarisation multiplexing and demultiplexing techniques was confirmed and resulted in an increase in the achievable ISD to 2 bit/s/Hz for a NRZ signal at 42.6 Gbit/s. In this section it was shown that the generation and transmission of a ~0.6 Tbit/s CoWDM signal from a single wavelength source could be achieved without using advanced filtering techniques and with NRZ data modulation. Section 5.3 was concerned with the performance of CoWDM in a long-haul transmission link which was implemented using a re-circulating loop with characteristic features typical of currently installed standard long-haul links. The primary result from this work was the transmission of a 280 Gbit/s CoWDM signal over a total distance of 1,200 km of standard SMF. The recirculating loop consisted of 100 km spans and was amplified using a hybrid Raman/EDFA amplification scheme. The measured Q-factors for all seven tributaries were above the FEC threshold and comparison with simulated results showed that CoWDM has a high relative tolerance to the effects of PMD in the loop compared to other high bit-rate solutions.

Finally in section 5.4 multi-Tbit/s CoWDM operation was achieved by combining a multi-banded comb generator with the CoWDM transmission format which gave a total capacity of 1.5 Tbit/s that was transmitted error free over 80.4 km of standard SMF without the need for FEC codes. This work verified the ease of scalability in terms of capacity of CoWDM, as it showed that by simply using additional DFB's in the comb generator extra capacity is easily obtained. The compatibility of CoWDM with techniques such as polarisation multiplexing and

hybrid amplification schemes has strengthened its position as a potential candidate for use in high ISD medium and long-haul optical networks. In addition to this the high capacity achievable by using the multi-banded approach outlined in this chapter coupled with the potential for band switching applications makes CoWDM attractive as a transmission format for modern optical networks where routing of optical signals throughout the network must be taken into account.

# Chapter 6

# Conclusions and Future Work

## 6.1 Introduction

The purpose of this chapter is to review the major findings of the thesis, present the conclusions of the work and suggest possibilities where further work might be carried out to extend the topics covered in this thesis. In section 6.2 the major technical highlights presented in the thesis are reviewed. Section 6.3 contains the conclusions relating to these technical highlights and reviews the position of CoWDM as a candidate transmission format for modern high ISD optical networks. Finally in section 6.4 a number of areas where additional work could be carried out are introduced and briefly discussed.

## 6.2 Technical Findings/Achievements

The demand for higher bandwidth services continues to increase and modern optical communication networks are under increasing pressure to provide a flexible reliable and cost efficient service. This requirement for higher per-fibre capacities at lower per transmitted bit cost has led to the development of high information spectral density systems. There are a number of enabling technologies which allow for increased spectral density in fixed bandwidth WDM systems but many of these such as mutli-level modulation formats and PDM require an increased level of implementation complexity.

This thesis has investigated a novel transmission format, CoWDM for use in high ISD systems, which has a number of distinct advantages over previously reported approaches. This section reviews the main technical findings of this work

The technical highlights presented in this work are reviewed below.

1. It was shown theoretically in chapter 2 that by constraining the channel spacing of a standard WDM system to be equal to the bit rate and by maintaining a fixed phase relationship between adjacent channels in the transmitter the level of crosstalk in the system could be controlled and minimised. This novel transmission technique is called CoWDM and formed the subject of the majority of this work.
2. A CoWDM transmitter and an alignment strategy for optimising the transmitters performance was proposed and experimentally implemented in chapter 3. This lead to the first error free back-to-back demonstration of a 298 Gbit/s CoWDM system.
3. In order to provide an optical comb source for the CoWDM transmitter a technique for optical comb generation (7 x 42.6 Gbit/s channels) based on a pair of cascaded $LiNbO_3$ amplitude modulators was demonstrated in chapter 3. This work was extended to an 11 channel comb (bandwidth = 426 GHz) by using a pair of Versawave electro-optic polarisation modulators.
4. The importance of the optical phase relationship between the channels in the transmitter was experimentally demonstrated and a phase selection and stabilisation circuit was implemented in chapter 3.
5. The first transmission of a 298 Gbit/s CoWDM signal with an ISD of 1 bit/s/Hz over 80 km of SMF was demonstrated in chapter 4. All seven tributary channels were measured to be error free after transmission and no sign of an error floor was detected. Received eye diagrams and spectra were presented.
6. The error free transmission distance was extended to 112 km of dispersion managed fibre later in chapter 4 which confirmed CoWDMs compatibility with standard existing dispersion maps designed for widely spaced 40 Gbit/s NRZ WDM systems. This demonstration also revealed that the nonlinear processes limiting CoWDM at high launch powers are the same as those that

would degrade a single NRZ channel operating at the tributary line rate (~40 Gbit/s).

7. An investigation of the effect of fibre induced dispersion on CoWDM showed that the effects of dispersion on the CoWDM signal also scale with the tributary line rate (42.6 Gbit/s) rather than the overall bit rate (298 Gbit/s).
8. In chapter 4 it was also shown that standard RS FEC codes were compatible with the CoWDM transmission format. Furthermore both single and concatenated FEC code performances were shown to be similar for a single channel NRZ signal and a multi-channel CoWDM signal implying that the error statistics governing a single NRZ channel are the same as those for a CoWDM signal.
9. A CoWDM signal with an ISD of 2 bit/s/Hz and a capacity of 596 Gbit/s was demonstrated in chapter 5 where CoWDM was combined with polarisation division multiplexing. All 14 tributaries were measured to be error free without using FEC. Residual penalties affecting this system were attributed to features of the implementation
10. In chapter 5 CoWDM was successfully transmitted over 1,200 km of SMF with all tributaries above the FEC threshold. This experiment was carried out in France Telecom labs Lannion, France, and used a recirculating loop configuration with hybrid Raman/EDFA amplification. This represented an overall bandwidth distance product of 313 GbitMm/s from a single laser. Comparison of the experimental results with simulations indicated that CoWDM was robust against PMD in the loop.
11. A multi-banded CoWDM signal giving a total capacity of approximately 1.5 Tbit/s was transmitted error free without the use of FEC over 80.4 km in chapter 5. This high capacity was achieved using only 5 DFB lasers arranged in a multi-banded configuration.

## 6.3 Conclusions

The primary conclusion of this thesis is that Coherent Wavelength Division Multiplexing (CoWDM) is a promising transmission format for use in modern optical communication networks. These networks are under increasing demand to deliver high bandwidth services in a cost effective fashion. One way to achieve this is by increasing the ISD of fixed bandwidth systems by either increasing the bit rate per channel or decreasing the channel spacing. We have shown that a CoWDM based solution to this problem can achieve up to 1 bit/s/Hz in a single polarisation without the use of advanced modulation formats, transmitter pre-filtering or other complicated techniques. In terms of capacity we have demonstrated error free transmission of a ~0.3 Tbit/s signal from a single wavelength source, which can be doubled to ~0.6 Tbit/s by using polarisation division multiplexing in the transmitter. In addition to this the tolerance of CoWDM to impairments such as fibre induced nonlinearities, dispersion and PMD have been shown to scale with the tributary line rate (~42 Gbit/s) instead of the overall bit rate (~0.3 Tbit/s) giving it a distinct advantage over other high bit rate solutions such as OTDM which can be severely limited by these impairments at such bit rates. Modern optical communication networks are also transmitting signals over increasingly long distances with the metro and core networks beginning to merge, and transmission distances over thousands of kilometres required in the LH network. Any novel transmission format has to not only be capable of transmission over such distances but must also be compatible with existing installed infrastructure (fibre type, amplification scheme etc.) so that any upgrade of the system remains cost effective. The experimental work performed with France Telecom resulted in the transmission above FEC threshold of a ~0.3 Tbit/s CoWDM signal over 1,200 km of SMF using a hybrid EDFA/Raman amplification scheme. Such a scheme is typical of many installed networks confirming CoWDMs potential for use in these networks. The total capacity of a CoWDM signal is scalable by adding more wavelength sources to the comb generator as was demonstrated in the multi-banded CoWDM experiment

where a total capacity of 1.5 Tbit/s was achieved using a bank of 5 DFB lasers as input for the comb generator.

In summary we believe that as a transmission format CoWDM provides an attractive combination of high ISD, scalable capacity and high tolerance to fibre-induced impairments without using complicated expensive techniques. These features, together with demonstrated compatibility with existing infrastructure and transmission over LH distances makes CoWDM a very promising candidate for optical communication networks of the future.

## *6.4 Future Work*

This section considers some of the areas which future work could be carried out in relation to CoWDM and the other topics covered in this thesis.

### 6.4.1 Information Spectral Density/Capacity Increase

Thus far we have demonstrated up to 2 bit/s/Hz ISD by combining polarisation division multiplexing (PDM) with a 1 bit/s/Hz standard NRZ CoWDM signal. In addition to this there are a number of additional techniques which can be applied to further increase the ISD of the CoWDM signal. The most obvious of these is to implement CoWDM with advanced modulation formats instead of NRZ. By moving to a modulation format such as DQPSK, where two bits are encoded per symbol the ISD can be doubled. By using these advanced modulation formats together with PDM ISDs of up to 4 bit/s/Hz should be achievable in combination with CoWDM. Figure 6.1 below summarises the increase in the ISD achieved using CoWDM with respect to other reported results.

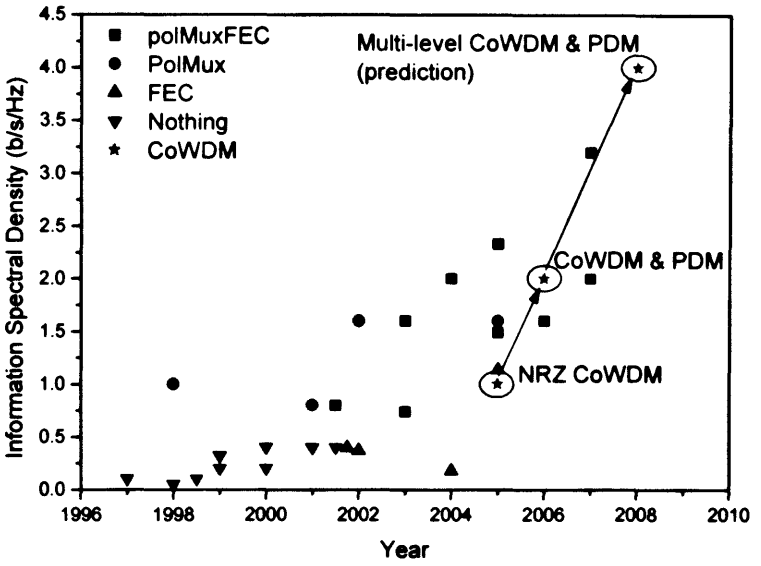



**Figure 6.1. ISD evolution showing potential for up to 4 bit/s/Hz ISD using CoWDM with PDM and multi-level modulation formats**

By increasing the ISD of a fixed bandwidth WDM system the capacity is also inherently increased and because a comb generator is used as a source for CoWDM very high bit rate distance product results can potentially be achieved. By combining all the techniques discussed in this thesis (namely CoWDM, advanced comb generation and PDM) together with a multi-level modulation format such as DQPSK it should be possible to achieve record ISD and bit rate distance product values. For example a system based on the CoWDM transmission format with an 11 channel comb generator, DQPSK modulation format and PDM should be able to achieve almost 2 Tbit/s from a single wavelength source which could then be transmitted over several thousand km of fibre with FEC.

### 6.4.2 Integration

In chapter 1 we saw how large numbers of discrete components integrated together using PIC technology can be used to achieve high ISD values at 40 Gbit/s in a cost effective package. One of the next stages in the development of CoWDM as a candidate transmission format for high ISD optical communication systems is to dramatically reduce the size of the transmitter to a scale where it can be packaged in a similar fashion to a PIC solution. For this to happen it is necessary to use EAMs instead of MZMs in both the comb generation and the data encoding sections as they can be much more easily integrated onto a PIC. There are a number of advantages to reducing the size of the transmitter module. Firstly the amount of fibre in the transmitter would be significantly reduced with all the optical signals routed in waveguides on the PIC. Because of this it may no longer be necessary to actively control the optical phase relationship between the channels once it was set at an optimised value. In addition to this the smaller packaged device would potentially reduce power consumption and be less susceptible to temperature fluctuations. The comb generator module, if packaged might also be of interest as a stand-alone optical source for some DWDM systems given its good flatness and high SMSR values. We have shown that an optical comb generator based on two cascaded amplitude modulators is capable of generating up to 11 flat optical lines which could subsequently be modulated at a reduced bit rate of 10 Gbit/s. Such a solution may have application as an optical source in the 100 Gbit Ethernet application space which has been attracting a lot of research attention in recent years [172, 173, 174, 175].

# Appendix A

## Publications and Conference Papers
## October 2003 – September 2007

T. Healy, F.C. Garcia Gunning, E. Pincemin, B. Cuenot and A.D. Ellis, '1,200 km SMF (100 km spans) 280 Gbit/s Coherent WDM Transmission using Hybrid Raman/EDFA Amplification', accepted for publication at European Conference on Optical Communications (ECOC), Sept. 2007.

T. Healy, F.C. Garcia-Gunning, A.D. Ellis and J.D. Bull, 'Flat 11 Phase-locked Channels Optical Comb Generator using Low-Drive Voltage Modulators', Technical Digest of Conference on Lasers and Electro-Optics (CLEO) Europe, Paper C16-2-THU, Jun 2007.

F.C. Garcia-Gunning, T. Healy, X. Yang and A.D. Ellis, '0.6Tbit/s Capacity and 2bit/s/Hz Spectral Efficiency at 42.6Gsymbol/s Using a Single DFB Laser with NRZ Coherent WDM and Polarisation Multiplexing', Technical Digest of CLEO Europe, Paper CI8-5-FRI, Jun 2007.

B. Cuenot, F.C. Garcia-Gunning, M. McCarthy, T. Healy and A.D. Ellis, 'Transmission Impairments for 298.2Gbit/s Coherent WDM over 600km of Standard Single Mode Fibre' Technical Digest of CLEO Europe, Paper CI8-4-FRI, Jun 2007.

T. Healy, F.C. Garcia-Gunning, A.D. Ellis and J.D. Bull, 'Multi-wavelength source using low drive-voltage amplitude modulators for optical communications', Optics Express, Vol. 16, Issue 6, pp. 2981-2986 (2007).

A.D. Ellis, F.C. Garcia-Gunning and T. Healy, Irish and International Patent Application on alignment of Coherent WDM, Publication No. WO/2007/043032, International Application No. PCT/IE2006/000109.

T. Healy, F.C. Garcia-Gunning and A.D. Ellis, 'Phase Stabilisation of Coherent Modulator Array', Technical Digest of Optical Fiber Communications (OFC), Paper OTuI5, 2006.

T. Healy, A.D. Ellis, F.C. Garcia-Gunning, B. Cuenot and M .Rukosueva '1b/s/Hz Coherent WDM Transmission over 112km of Dispersion Managed Optical Fibre', , Technical Digest of OFC, OThR4, 2006.

A.D. Ellis, F.C. Garcia-Gunning and T. Healy, 'Coherent WDM: The Achievement of High Information Spectral Density through Phase Control within the Transmitter', Technical Digest of OFC, Invited Paper JThB10 OFC 2006.

F.C. Garcia-Gunning, T. Healy and A.D. Ellis, 'Dispersion Tolerance of Coherent WDM', Photonic Technology Letters, Vol. 18, No. 12, June 15, 2006.

T. Healy, F.C. Garcia-Gunning and A.D. Ellis, 'Performance Evaluation of FEC Codes in a 42.6 Gbit/s CoWDM Optical Transmission System', Paper Tu 3.2.5, ECOC, September 2005.

F.C. Garcia-Gunning, T. Healy, R.J. Manning and A.D. Ellis, 'Multi-banded Coherent WDM Transmission', Proceedings of ECOC, Paper Th4.2.6, Sept. 2005.

F.C. Garcia-Gunning, T. Healy and A.D. Ellis, '298 Gbit/s Coherent WDM Transmission over 80km of SMF at 1bit/s/Hz Spectral Efficiency', Proceedings of ECOC, Paper We3.2.6, Sept. 2005.

A.D. Ellis, F.C. Garcia-Gunning and T. Healy 'Optical Multiplexing for High Speed Systems', ICTON, July 2005.

T. Healy, F.C. Garcia-Gunning, A.D. Ellis, 'Performance Evaluation of FEC Codes in a 42.6 Gbit/s CoWDM Optical Transmission System', P2:67, EGAS37 Dublin, 2005.

# References

[1] T.H. Maiman, "Stimulated Optical Radiation in Ruby," Nature, Vol. 187, No. 4736 pp. 493-494, Aug. 1960.

[2] N. Lindgren, "Optical Communication – A Decade of Preparation", Proceedings of the IEEE, Vol. 58, No. 10, pp. 1410-1418, Oct. 1970.

[3] K.C.Kao and G.A.Hockham, "Dielectric-Fibre Surface Waveguides for Optical Frequencies," Proceedings of IEE, Vol.133, pp.1151-1158, Jul. 1966.

[4] F.P. Kapron and D.B. Keck, ","Applied Physics Letters, Vol. 17, pp. 423-425, 1970.

[5] D.G. Foursa, C.R. Davidson, M. Nissov, M.A. Mills, L. Xu, J.X. Cai, A.N. Pilipetskii, Y. Cai, C. Breverman, R.R. Cordell, T.J. Carvelli, P.C. Corbett, H.D. Kidorf and N.S. Bergano, "2.56 Tb/s (256x10Gb/s) transmission over 11,000 km using hybrid Raman/EDFAs with 80 nm of continuous bandwidth", Technical Digest of Optical Fiber Communications, Paper FC3-1, 2002.

[6] J.-X. Cai, D. G. Foursa, C. R. Davidson, Y. Cai, G. Domagala, H. Li, L. Liu, W. W. Patterson, A. N. Pilipetskii, M. Nissov, and N.S. Bergano, "A DWDM Demonstration of 3.73 Tb/s over 11,000 km using 373 RZ-DPSK Channels at 10 Gb/s", Technical Digest of Optical Fiber Communications, Paper PD22-1, 2003.

[7] G. Charlet, E. Corbel, J. Lazaro, A. Klekamp, R. Dischler, P. Tran, W. Idler, H. Mardoyan, A. Konczykowska, F. Jorge, and S. Bigo, "WDM Transmission at 6-Tbit/s Capacity Over Transatlantic Distance, Using 42.7-Gb/s Differential Phase-Shift Keying Without Pulse Carver," Journal of Lightwave Technology, Vol. 23, No. 1, pp. 104–107, Jan. 2005.

[8] R.J.Mears, L.Reekie, I.M.Jauncey, and D.N.Payne, "Low-noise Erbium-Doped Fibre Amplifier at 1.54pm", Electronics Letters, Vol. 23 (19), pp.1026-1028, 1987.

[9] M. J. O'Mahony, C. Politi, D. Klonidis, R. Nejabati, and D. Simeonidou, "Future Optical Networks", Journal. of Lightwave Technology, Vol. 24, No. 12, pp.4684–4696, Dec. 2006.

[10] S.J. Park, C.H. Lee, K.T. Jeong, H-.J. Park, J.G. Ahn, and K.H. Song, "Fiber-to-the-Home Services Based on Wavelength-Division-Multiplexing Passive Optical Network", Journal. of Lightwave Technology, Vol. 22, No. 11, pp.2582–2591, Nov. 2004.

[11] B. Bakhshi, M. Manna, G. Mohs, D.I. Kovsh, R.L. Lynch, M. Vaa, E.A. Golovchenko, W.W. Patterson, W.T. Anderson, P. Corbett, S. Jiang, M.M. Sanders,

H. Li, G.T. Harvey, A. Lucero, and S.M. Abbott, "First Dispersion-Flattened Transpacific Undersea System: From Design to Terabit/s Field Trial", Journal. of Lightwave Technology , Vol. 22, No. 1, pp.233–241, Jan. 2004.

[12] S.S. Lee, H. Cho, S-K. Lim, K-M. Yoon, Y-G. Lee, and J. Ko, "Field trial of 1.6 b/s (40 channels x 40 Gb/s) NRZ signals over 511 km standard single mode fiber using conventional optical amplifiers", Proceedings of IEEE International Conference on Communications, Vol. 3, pp. 1598-1602, May 2005.

[13] T. Otani, M. Hayashi, M. Daikoku, K. Ogaki, Y. Nagao, K. Nishijima and M. Suzuki, "Field trial of 63 channels 40Gbit/s dispersion-managed soliton WDM signal transmission over 320km NZ-DSFs," Technical Digest of Optical Fiber Communications, Paper FC9, 2002.

[14] D. Chen et al., "3.2Tb/s field trial (80x40Gb/s) over 3 x 82 km SSMF using FEC, Raman and tunable dispersion compensation," Technical Digest of Optical Fiber Communications, Paper PD36, 2001.

[15] H. Masuda, H. Kawakami, S. Kuwahara, A. Hirano, K. Sato and Y. Miyamoto , "1.28 Tbit/s (32x43 Gbit/s) field trial over 528km (6x88 km) DSF using L-band remotely-pumped EDF/distributed Raman hybrid inline amplifiers", Electronics Letters, Vol. 39 No. 23, pp. Nov. 2003.

[16] S. Ten, M. Sauer, E. Kolltveit, 1. Hurley, D. Dalgoune, J. Femer, S. Colby and D. Witzel, "1.6 Tb/s (40x40 Gb/s) transmission over 1200 km of field-deployed dispersion-managed fiber", Technical Digest of Optical Fiber Communications, Paper TuS3, 2003.

[17] K. Iwatsuki, J. Kani, H. Suzuki, and M. Fujiwara, "Access and Metro Networks Based on WDM Technologies", Journal of Lightwave Technology, Vol. 22, No. 11, pp.2623–2630, Nov. 2004.

[18] J.H. Lee, C.H. Kim, Y-G. Han, and S.B. Lee, "WDM-Based Passive Optical Network Upstream Transmission at 1.25 Gb/s Using Fabry–Pérot Laser Diodes Injected With Spectrum-Sliced, Depolarized, Continuous-Wave Supercontinuum Source", IEEE Photonics Tech. Letters, Vol. 18, No. 20, pp. 2108-2110 Oct., 2006.

[19] G. Talli and P.D. Townsend, "Hybrid DWDM-TDM long-reach PON for next-generation optical access", Journal of Lightwave Technology, Vol. 24, No. 7, pp. 2827 – 2834, Jul., 2006.

[20] H. Suzuki, J. Kani, T. Nakamura, M. Teshima and K. Iwatsuki, "High-spectral-efficiency DWDM access network supporting 10-Gbps access services" Technical Digest of Optical Fiber Communications, Paper ThQ5, 2003.

[21] O.E. DeLange, "Wide-Band Optical Communication Systems: Part II-Frequency-Division Multiplexing, Proceedings of the IEEE, Vol. 58, No. 10, pp. 1683-1690, Oct. 1970.

[22] B. Zhu, L. Leng, A. H. Gnauck, M. O. Pedersen, D. Peckham, L. E. Nelson, S. Stulz, S. Kado, L. Gruner-Nielsen, R. L. Lingle, Jr., S. Knudsen, J. Leuthold, C. Doerr, S. Chandrasekhar, G. Baynham , P. Gaarde, Y. Emori, and S. Namiki, "Transmission of 3.2 Tb/s (80 x 42.7 Gb/s) over 5200 km of UltraWave$^{TM}$ fiber with 100-km dispersion-managed spans using RZ-DPSK format", Proceeding of European Conference on Optical Communications, Paper PD4.2, Sept. 2002.

[23] A. R. Chraplyvy, A. H. Gnauck, R. W. Tkach, R. M. Derosier, C. R. Giles, B. M. Nyman, G. A. Ferguson, J. W. Sulhoff, and J. L. Zyskind, "One-third Terabit/s transmission through 150 km of dispersion-managed fiber," IEEE Photonics Technology Letters, Vol. 7, pp. 98-100, 1995.

[24] M.J. O'Mahony, "Optical multiplexing in fiber networks: progress in WDM and OTDM", IEEE Communications Magazine, Vol. 33, No. 12, pp. 82-88, Dec. 1995.

[25] J .Chesnoy, V. Lemaire and S. R. Barnes, "Submarine Communications The New Age of WDM Connectivity", Proceedings of European Conference on Optical Communications, Paper WeC.1.2, 1996.

[26] E. Lowe, "Current European WDM deployment trends", IEEE Communications Magazine, Vol. 36, No. 2, pp. 46-50, Feb. 1998.

[27] T.C. Wright, "The Digital Synchronous Hierarchy Standard", Proceedings of 2nd IEE National Conference on Telecommunications, pp. 297-302, Apr. 1989.

[28] T. Imai, Y. Hayashi, N. Ohikawa, T. Sugie, Y. Ichihashi and T. Ito, "Field Demonstration Of 2.5 Gbit/s Coherent Optical Transmission Through Installed Submarine Fibre Cables", Electronics Letters, vol 26, no 17, pp. 1407-1409 Aug. 1990.

[29] T. Welsh, R. Smith, H. Azami and R. Chrisner, "The FLAG Cable System", IEEE Communications Magazine, Vol. 34, Issue 2, pp. 30-35, Feb. 1996.

[30] P.Mamyshev, C. Rasmussen and B. Mikkelsen, "Technical and Commercial Perspective of 40Gbs Transmission", Proceedings of IEEE Lasers and Electro-optics Society, Vol.2, pp. 685-686, Paper WZ3, Nov. 2004.

[31] M. Birk, L. Raddatz, D. Fishman, S. Woodward, and P. Magill, "Field trial of end-to-end OC-768 transmission using 9 WDM channels over 1000km of installed fiber," Technical Digest of Optical Fiber Communications, Paper TuS4, 2003.

[32] D. Caccioli, A. Paoletti, A. Schiffini, A. Galtarossa, P. Griggio, G. Lorenzetto, P. Minzioni, S. Cascelli, M. Guglielmucci, L. Lattanzi, F. Matera, G. M. Tosi Beleffi, V. Quiring, W. Sohler, H. Suche, S. Vehovc, and M. Vidmar, "Field Demonstration of In-Line All-Optical Wavelength Conversion in a WDM Dispersion Managed 40-Gbit/s Link", IEEE Journal of Selected Topics on Quantum Electronics, Vol. 10, No. 2, Mar./Apr. 2004.

[33] D.Z. Chen, T.J. Xia, G. Wellbrock, P. Mamyshev, J.J. Zik, S. Penticost, G. Grosso, A. Dismukes, P. Perrier and H. Fevrier, "New Field Trial Distance Record of 3040 km on Wide Reach WDM with 10 and 40 Gbps Transmission Including OC-768 Traffic Without Regeneration", Journal of Lightwave Technology, Vol. 25, No. 1, pp. 28-37, Jan. 2007.

[34] A.H. Gnauck, G. Charlet, P. Tran, P.J. Winzer, C.R. Doerr, J.C. "25.6-Tb/s C+L-Band Transmission of Polarization Multiplexed RZ-DQPSK Signals" Technical Digest of Optical Fiber Communications, Paper PDP19, 2007.

[35] T. Otani, M. Hayashi, M. Daikoku, K. Ogaki, Y. Nagao, K. Nishijima, and M. Suzuki, "Investigation of System Upgradability Over Installed Fiber-Optic Cable Using 40-Gb/s WDM Signals Toward Multiterabit Optical Networks", Journal of Lightwave Technology, Vol. 21, No. 4, pp. 947-952, Apr. 2003.

[36] B. Clesca, S. Gauchard, C. Coeurjolly, J.-P. Thiery, L. Pierre, and L. Berthelon, "The WDM answer to line-rate increase within the terrestrial fiber-based networks", Proceedings of Global Telecommunications Conference, pp 1925-1929, Nov. 1996.

[37] M. Brodsky, N.J. Frigo, M. Boroditsky and M. Tur, "Polarization Mode Dispersion of Installed Fibers", Journal of Lightwave Technology, Vol. 24, No. 12, pp.4584–4599, Dec. 2006.

[38] W. Weiershausen, R. Leppla, F. Rumpf, R. Herber, A. Mattheus, A. Gladisch, A. Hirano, Y. Kisaka, Y. Miyamoto, S. Kuwahara, M. Yoneyama, and M. Tomizawa, "PMD outage measurements in a joint field trial of a 43-Gb/s NTT WDM transmission system within DT's installed fiber environment," Technical Digest of Optical Fiber Communications, Paper WP3, 2004.

[39] G. P. Agrawal, Nonlinear Fiber Optics, Academic Press, 1989.

[40] L. Paradiso, P. Boffil, L. Marazzil, N.D.Vecchia, M. Arfiglia and M. Martinelli, "Experimental XPM, SPM, FWM Penalty Evaluation in Very Dense WDM Optical Systems", Technical Digest of Conference on Lasers and Electro Optics, Paper CWG2, 2005.

[41] S. Betti, G. De Marchis and E. Iannone, "Polarization Modulated Direct Detection Optical Transmission Systems", Journal of Lightwave Technology, Vol. 10, No. 12, pp.1985–1997, Nov. 1992.

[42] Y. Frignac, S. Bigo and J.-P. Hamaide, "NRZ versus RZ format in Nx40 Gbit/s ~WDM terrestrial transmission systems with high spectral efficiency of 0.4 bit/(s.Hz)", Proceedings of European Conference on Optical Communications, Paper ThB.1.1, 2001.

[43] G. Bosco, A. Carena, V. Curri, R. Gaudino, P.Poggiolini, "On the Use of NRZ, RZ and CSRZ Modulation Formats for Ultra-dense WDM Systems at 40 Gbit/s", Proceedings of European Conference on Optical Communications, Paper P3.7, Sept. 2002.

[44] P.J. Winzer and R.J. Essiambre, "Advanced Optical Modulation Formats", Proceedings of the IEEE, Vol. 94, No. 5, pp.952-984, May 2006.

[45] A. H. Gnauck and P. J. Winzer, "Optical Phase-Shift-Keyed Transmission", Journal of Lightwave Technology, Vol. 23, No. 1, Jan. 2005.

[46] Y. Zhu, K. Cordina, N. Jolley, R Feced, A. Kee, R Rickard and A. Hadjifotiou, "1.6 bit/s/Hz orthogonally polarized CSRZ–DQPSK transmission of 8x40 Gbit/s over 320 km NDSF", Technical Digest of Optical Fiber Communications, Paper TuF1, 2004.

[47] B. Milivojevic; A.F. Abas; A. Hidayat; S. Bhandare; D. Sandel; R. Noe; M. Guy and M. Lapointe "1.6-b/s/Hz 160-Gb/s 230-km RZ-DQPSK polarization multiplex transmission with tunable dispersion compensation", Photonics Technology Letters, Vol. 17, no 2, pp. 495-497, Feb. 2005.

[48] H.D. Kidorf, A. Lucero, J.-X. Cai, G. Lenner F.W. Kerfoot, C.R. Davidson, Y. Cai, J. Li, J. Chen, M. Nissov and A.N. Pilipetskii, "Forward Error Correction Techniques in Long-Haul Optical Transmission Systems", Proceedings of Lasers and Electro-optics Society, Paper WK1, Nov. 2001.

[49] C.E. Shannon, "A Mathematical Theory of Communication", The Bell System Technical Journal, Vol. 27, pp. 379–423, 623–656, Jul., Oct. 1948.

[50] R.W Hamming, "Error detecting and correcting codes" Bell Systems Technology Journal. Vol. 29, pp. 147-160, 1950.

[51] ITU-T Study Group 15 (1997-2000), "Forward Error Correction for Submarine Systems", ITU-T Recommendation G.975, Oct. 2000.

[52] I. Reed and G. Solomon, "Polynomial Codes Over Certain Finite Fields", Journal of the Society of Industrial and Applied Mathematics", Vol. 8, pp 300-304, 1960.

[53] A. Agata, K. Tanaka, and N.Edagawa, "Study on the Optimum Reed–Solomon-Based FEC Codes for 40-Gb/s-Based Ultralong-Distance WDM Transmission", Journal of Lightwave Technology, Vol. 20, No. 12, pp.2189-2195, Dec. 2002.

[54] C. Berrou, A. Glavieux and P Thitimajshima, "Near Shannon Limit Error-Correcting Coding and Decoding: Turbo-Codes", IEEE International Conference on Communications, pp 1064-1071, May 1993.

[55] I.B. Djordjevic and B. Vasic, "Projective Geometry LDPC Codes for Ultralong-Haul WDM High-Speed Transmission", IEEE Photonics Technology Letters, Vol. 15, No. 5, pp 784-786, May 2003.

[56] N. Yoshikane and I. Morita, "1.14 b/s/Hz spectrally-efficient 50 x 85.4 Gb/s transmission over 300 km using copolarized CS-RZ DQPSK signals", Technical Digest of Optical Fiber Communications, Paper PDP38, 2004.

[57] K. Tanaka, I. Morita and N. Edagawa, "Study on Optimum Pre-Filtering Condition for 42.7 Gbith CS-RZ DPSK Signal", Technical Digest of Optical Fiber Communications, Paper TuF2, 2003.

[58] D. van den Borne, S.L. Jansen, E. Gottwald, P.M. Krummrich, G.D. Kohe and H. de Waardt, "1.6-b/s/Hz Spectral Efficiency 40 x 85.6-Gb/s Transmission Over 1,700 km of SSMF using POLMUX-RZ-DQPSK." Technical Digest of Optical Fiber Communications, Paper PDP34, 2006.

[59] D-S. Ly-Gagnon, S. Tsukamoto, K. Katoh and K. Kikuchi, "Coherent Detection of Optical Quadrature Phase-Shift Keying Signals With Carrier Phase Estimation", Journal of Lightwave.Technology, Vol. 24, No. 1, pp. 12-21, Jan. 2006.

[60] M.K. Smit: "New focusing and dispersive planar component based on an optical phased array", Electronics Letters, Vol. 24, pp. 385-386,1988.

[61] M.K. Smit, "InP photonic integrated circuits", Proceedings of IEEE Lasers and Electro-Optics Society, Vol. 2, pp:843 – 844, Nov. 2002.

[62] C.G.M. Vreeburg, T. Uitterdijk, Y.S. Oei, M.K. Smit, F.H. Groen, E.G. Metaal, P. Demeester and H.J. Frankena, "First InP-based reconfigurable integrated add-drop multiplexer", Photonics Technology Letters, Vol. 9, No. 2, pp. 188-190, Feb. 1997.

[63] C.G.P. Herben, "InP-based Optical Cross-Connects for WDM Networks", Proceedings of IEEE Lasers and Electro-Optics Society Vol. 2, pp. 407 – 408, Nov. 1999.

[64] E.J. Skogen, C.S. Wang, J.W. Raring, G.B. Morrison, and L.A. Coldren, "Small-Footprint, High-Efficiency, Integrated Transmitters for High-Speed Optical

Interconnect Applications," Proceedings of Integrated Photonics Research, Paper IThD2, Jun. 2004.

[65] J.-M. Verdiell, T. L. Koch, B. I. Miller, M. G. Young, U. Koren, F. Storz, and K. F. Brown-Goebeler "A WDM Receiver Photonic Integrated Circuit With Net On-Chip Gain", IEEE Photonics Technology Letters, Vol. 6, No. 8, pp. 960-962 Aug. 1994.

[66] G. Raybon, U. Koren, M.G. Young, M.A. Newkirk, P.B. Hansen, B.I. Miller, M. Chien, M. Zirngibl, C. Dragone, B. Tell, H.M. Presby, and C.A. Burrus, "1.7 Gbit/s transmission over 217 km using a 16×1 photonic integrated circuit transmitter", Electronics Letters, Vol. 29, No.14, pp. 1295-1296, Jul. 1993.

[67] R. Nagarajan, M. Kato, J. Pleumeekers, P. Evans, D. Lambert, A. Chen, V. Dominic, A. Mathur, P. Chavarkar, M. Missey, A. Dentai, S. Hurtt, J. Ba¨ck, R. Muthiah, S. Murthy, R. Salvatore, S. Grubb, C. Joyner, J. Rossi, R. Schneider, M. Ziari, F. Kish and D. Welch, "Single-chip 40-channel InP transmitter photonic integrated circuit capable of aggregate data rate of 1.6 Tbit/s", Electronics Letters, Vol. 42, No. 13, pp. 771-773, Jun. 2006.

[68] R. Nagarajan, M. Kato, V.G. Dominic, C.H. Joyner, R.P. Schneider, Jr., A.G. Dentai, T. Desikan, P.W. Evans ,M. Kauffman, D.J.H. Lambert, S.K. Mathis, A. Mathur, M.L. Mitchell, M.J. Missey, S. Murthy, A.C. Nilsson, F.H. Peters, J.L. Pleumeekers, R.A. Salvatore, R.B. Taylor, M.F. Van Leeuwen, J. Webjorn, M. Ziari, S.G. Grubb, D. Perkins, M. Reffle, D.G. Mehuys, F.A. Kish and D.F. Welch, "400 Gbit/s (10 channel x 40 Gbit/s) DWDM photonic integrated circuits", Electronics Letters, Vol. 41, No. 6, pp. 347-349, Mar. 2005.

[69] A.D. Ellis and F.C.Garcia-Gunning, "Achievement of 1 bit/s/Hz information spectral density using coherent WDM", Technical Digest of Optical Fiber Communications, Page 3, Vol. 4, Mar. 2005.

[70] E. Yamazaki, F. Inuzuka, A. Takada, K. Yonenaga and T. Morioka, "Inter-channel crosstalk cancellation by encoding with adjacent channels in coherent WDM", Technical Digest of Optical Fiber Communications, Paper JThB6, Mar. 2006.

[71] S. K. Shin, C. H. Kim, and Y. C. Chung, "Directly Modulated 2.5 Gb/s 16-Channel WDM Transmission Over 640 km of Single-Mode Fiber Using Dispersion Compensating Fiber", IEEE Photonics Technology Letters, Vol. 11, No. 6, pp 742-744, Jun. 1999.

[72] N. Chand, K. Kojima, F. Bosch, P. Kiely, H. Ransijn, G. Salvador, W. Xiucheng, T. Olson, G. Salamanca and B. Kasper, "10.7 Gbit/s transmission over 75 km SSMF using 1.3 um directly modulated uncooled transmitters at 85° C," in

Proceedings of European Conference on Optical Communications, Paper 5.3.2, 2002.

[73] U. Fischer, "10 Gbit/s transmission over 69 km of non-dispersion-shifted singlemode fibre with CPFSK direct modulation of 1.55 μm BH DFB laser", Electronics Letters, Vol. 28, No.14, pp1306-1306, Jul. 1992.

[74] B. Wedding, W. Pohlmann, H. Gross, and O. Thalau, "43 Gb/s transmission over 210 km SMF with a directly modulated laser diode," in Technical Digest of European Conference on Optical Communications, Paper Mo 4.3.7, 2003.

[75] K. Sato, S. Kuwahara, S.; Y. Miyamoto, and N. Shimizu, "40 Gbit/s direct modulation of distributed feedback laser for very-short-reach optical links", Electronics Letters, Vol. 38, No. 15, pp. 816-817, Jul. 2002.

[76] K. Nakahara, "40-Gb/s Directly Modulated Lasers", Proceedings of IEEE Lasers & Electro-Optics Society, PaperTuBB2, pp.402-403, Oct. 2006.

[77] E.L. Wooten,K.M. Kissa,Alfredo Yi-Yan, Edmond J. Murphy, Donald A. Lafaw, Peter F. Hallemeier, D. Maack, D.V. Attanasio, D.J. Fritz, G.J. McBrien and D.E. Bossi, "A Review of Lithium Niobate Modulators for Fiber-Optic Communications Systems", IEEE Journal of Selected Topics in Quantum Electronics, Vol 6, No. 1, pp 69-82, Jan/Feb 2000.

[78] W. Pieper, R. Ludwig, C. M. Weinert, B. Kuhlow, G. Przyrembel, M. Ferstl, E. Pawlowski, and H. G. Weber, "4-Channel 40-Gb/s Unrepeatered OTDM Transmission Over 100-km Standard Fiber", Vol. 10, No. 3, pp 451-453 Mar. 1998.

[79] Y. Miyamoto, A. Hirano, K. Yonenaga, A. Sano, H. Toba, K. Murata and O.Mitomi, "320Gbit/s (8 x 40 Gbit/s) WDM transmission over 367 km with 120 km repeater spacing using carrier-suppressed return-to-zero format", Electronics Letters, Vol. 35 No. 23, pp. 2041-2042, Nov. 1999.

[80] T. Otani, M Hayashi, M. Daikoku, K. Ogaki, Y. Nagao, K. Nishijima and M. Suzuki, "Field trial of 63 channels 40 Gbit/s dispersion-managed soliton WDM signal transmission over 320 km NZ-DSFs", Technical Digest of Optical Fiber Communications, Paper FC9-2, 2002.

[81] M. Nakazawa; K. Suzuki, H. Kubota, Y. Kimura, Y. Yamada, K. Tamura, T. Komukai, and T. Imai, "40 Gbit/s WDM (10 Gbit/s×4 unequally spaced channels) soliton transmission over 10000 km using synchronous modulation and narrow band optical filtering" Electronics Letters, Vol. 32, No. 9, pp. 828-830, Apr. 1996.

[82] N. Banno, H. Akahori, K. Hara and N. Koyanagi, "Yokogawa Technical Report English Edition", No. 34, 2002.

[83] G.P. Agrawal, "Fiber Optic Communication Systems", Wiley, 2002.

[84] T. Healy, F.C. Garcia-Gunning, A.D. Ellis and J.D. Bull, "Multi-wavelength source using low drive-voltage amplitude modulators for optical communications", Optics Express, Vol. 16, Issue 6, pp. 2981-2986, 2007.

[85] S. C. Zeller, G. J. Spuhler, L. Krainer, R. Paschotta and U. Keller, K P. Hansen, "Frequency comb generation with 50-GHz channel spacing in the telecom C-band", Technical Digest of Conference on Lasers and Electro-Optics Europe, pp. 221, 2005.

[86] J. Capmany, D. Pastor and B. Ortega, "Microwave signal processing using optics", Technical Digest of Optical Fiber Communications, Paper OThB1, 2005.

[87] J. Azaña, N.K. Berger, B. Levit, and B. Fischer, "Broadband Arbitrary Waveform Generation Based on Microwave Frequency Upshifting in Optical Fibers", Journal of Lightwave Technology, Vol. 24, No. 7, pp 2663-2675 Jul. 2006.

[88] S. Yamashita and G.J. Cowle, "Bidirectional 10-GHz Optical Comb Genereation with an Intracavity Fiber DFB Pumped Brillouin/Erbium Fiber Laser", IEEE Photonics Technology Letters, Vol. 10, No. 6, pp. 796-798, Jun. 1998.

[89] H. Sanjoh, H. Yasaka, , Y. Sakai, K. Sato, H. Ishii, and Y. Yoshikuni, "Multiwavelength Light Source with Precise Frequency Spacing Using a Mode-Locked Semiconductor Laser and an Arrayed Waveguide Grating Filter", IEEE Photonics Technology Letters, Vol. 9, No. 6, pp 818-820, Jun. 1997.

[90] T. Sakamoto, T. Kawanishi and M Izutsu, "Optoelectronic oscillator using a LiNbO3 phase modulator for self-oscillating frequency comb generation" Optics Letters, Vol. 31, No. 6, pp. 811-813, Mar. 2006.

[91] H. Takara, T. Ohara, K. Mori, K. Sato, E. Yamada, Y Inoue, T. Shibata, M. Abe, T Morioka and K-I. Sato, "More than 1000 channel optical frequency chain generation from single supercontinuum source with 12.5GHz channel spacing" Electronics Letters, Vol. 36, No. 35, pp. 2089-2090, Dec. 2000.

[92] T. Ohara, H. Takara, T. Yamamoto, H. Masuda, T. Morioka, M. Abe, and H.Takahashi "Over-1000-Channel Ultradense WDM Transmission With Supercontinuum Multicarrier Source", Journal of Lightwave Technology, Vol. 24, No. 6, pp. 2311-2317, Jun. 2006.

[93] M. Fujiwara, M. Teshima, J. Kani, H. Suzuki, N. Takachio and K. Iwatsuki, "Optical carrier supply module using flattened multicarrier generation based on sinusoidal amplitude and phase hybrid modulation", IEEE Journal of Lightwave Technology, Vol. 21 No. 11, pp. 2705-2714, Nov. 2003.

[94] J.J. O'Reilly, P.M. Lane, R. Heidemann and R. Hofstetter, "Optical generation of very narrow linewidth millimetre wave signals", Electronics Letters, Vol. 28, No.25, pp. 2309-2311, Dec. 1992.

[95] Q. Chen and X. Guan, "Spectrum analysis of phase amplitude modulation", IEEE Transactions on Broadcasting, Vol. 36, No. 1, pp. 34-36, Mar. 1990.

[96] T. Healy, F.C. Garcia-Gunning, A.D. Ellis and J.D. Bull "Flat 11 Phase-locked Channels Optical Comb Generator using Low-Drive Voltage Modulators", Technical Digest of Conference on Lasers and Electro-Optics Europe, Paper C16-2-THU, Jun 2007.

[97] J.D. Bull, N.A.F. Jaeger, H. Kato, M. Fairburn, A. Reid and P. Ghanipour, "40 GHz electro-optic polarization modulator for fiber optic communications systems," Proceedings SPIE, 5577, pp. 133-143, 2005.

[98] A. H. Meitzler, H. F. Tiersten, A. W. Warner, D. Berlincourt, G. A. Coquin and F. S. Welsh III, "IEEE Standard on Piezoelectricity", ANSI/IEEE Standard, Mar. 1987.

[99] T. Healy, F.C. Garcia-Gunning and A.D. Ellis, "Phase Stabilisation of Coherent Modulator Array", Technical Digest of Optical Fiber Communications, Paper OTul5, 2006.

[100] Y. Hibino, "An array of photonic filtering advantages: arrayed-waveguide-grating multi/demultiplexers for photonic networks", IEEE Magazine on Circuits and Devices, Vol. 16, No. 6, pp. 21-27, Nov. 2000

[101] M.K. Smit, "Progress in AWG Design and Technology", Proceedings of IEEE/LEOS Workshop on Fibres and Optical Passive Components, pp.26 – 31, Jun., 2005.

[102] A.D. Ellis and F.C. Garcia Gunning, "Spectral Density Enhancement Using Coherent WDM", IEEE Photonics Technology Letters, Vol. 12, No. 2, pp. 504-506 Feb. 2005.

[103] P.S. Cho, G. Harston, C.J. Kerr, A.S. Greenblatt, A. Kaplan, Y. Achiam, G. Levy-Yurista, M. Margalit, Y. Gross, and J.B. Khurgin, "Investigation of 2-b/s/Hz 40-Gb/s DWDM Transmission Over 4 100 km SMF-28 Fiber Using RZ-DQPSK and Polarization Multiplexing", IEEE Photonics Technology Letters, Vol. 16, No.. 2, pp. 656-658, Feb 2004.

[104] K. Tanaka, I. Morita, and N. Edagawa, "Study on Optimum Pre-Filtering Condition for 42.7 Gbit/s CS-RZ DPSK Signal", Technical Digest of Optical Fiber Communications, Paper TuF2, 2004.

[105] T. Tsuritani, I. Morita, A. Agata, N. Edagawa, "Study on optimum optical pre-filtering condition for highly spectral-efficient ultralong-haul transmission using 40Gbit/s CS-RZ signal and all-Raman repeaters", Technical Digest of Optical Fiber Communications, Paper FE4, 2003.

[106] C. Wree, N. Hecker-Denschlag, E. Gottwald, P. Krummrich, J. Leibrich, E.-D. Schmidt, B. Lankl, and W. Rosenkranz, "High spectral efficiency 1.6-b/s/Hz transmission (8 x 40 Gb/s with a 25-GHz grid) over 200-km SSMF using RZ-DQPSK and polarization multiplexing," IEEE Photonic Technology Letters, Vol. 15, No. 9, pp. 1303–1305, Sept. 2003.

[107] I. Morita, T. Tsuritani, N. Yoshikane, A. Agata, K. Imal and N. Edagawa, "100 % Spectral-Efficient 25 X 42.7 GBit/s Transmission Using Asymmetrically Filtered CS-RZ Signal and a Novel Crosstalk Suppressor", Proceedings of European Conference on Optical Communications, Paper PD4.7, 2002.

[108] R.J. Manning, X. Yang, R.P. Webb, R. Giller, F.C. Garcia Gunning, A.D. Ellis, "The 'Turbo-Switch' - a Novel Technique to Increase the High-speed Response of SOAs for Wavelength Conversion", Technical Digest of Optical Fiber Communications, Paper OWS8, 2006.

[109] F.C. Garcia-Gunning, T. Healy and A.D. Ellis, "298 Gbit/s Coherent WDM Transmission over 80km of SMF at 1bit/s/Hz Spectral Efficiency", Proceedings of European Conference on Optical Communications, Paper We3.2.6, Sept. 2005.

[110] Y. Shen, K. Lu, and W. Gu, "Coherent and Incoherent Crosstalk in WDM Optical Networks", Journal of Lightwave Technology, Vol. 17, No. 5, pp. 759-764, May 1999

[111] P.J. Winzer, M. Pfennigbauer and R.-J. Essiambre, "Coherent Crosstalk in Ultradense WDM Systems", Journal of Lightwave Technology, Vol. 23, No. 4, pp. 1734-1744, Apr. 2005.

[112] Y. Cai, "Performance Limits of FEC and Modulation Formats in Optical Fiber Communications", Proceedings of IEEE Lasers and Electro-optics Society, pp. 488-489, Paper WH1, Oct. 2006.

[113] A. Agata, K. Tanaka, and N. Edagawa, "Study on the Optimum Reed–Solomon-Based FEC Codes for 40-Gb/s-Based Ultralong-Distance WDM Transmission", Journal of Lightwave Technology, Vol. 20, No. 12, pp. 2189-2195, Dec. 2002.

[114] G. C Clark Jr. and J. Bibb Cain: "Error Correction Coding for Digital Communications", Plenum Press, New Yolk, Third Printing, March 1988.

[115] S. Lin and D.J. Costello Jnr., "Error Control Coding", Pearson Prentice Hall, 2004.

[116] O. Sab, "FEC techniques in submarine transmission systems", Technical Digest of Optical Fiber Communications, Paper TuF1-1, 2001.

[117] G. D. Forney, Jr., "Concatenated Codes", MIT Press, 1966.

[118] G. D. Forney, Jr ., "Burst-Correcting Codes for the Classic Bursty Channel", IEEE Transactions on Communications Technology, Vol. com-19, No. 5, pp. 772-780, Oct. 1971.

[119176] E.R Berlekamp and P. Tong, "Improved Interleavers for Algebraic Block Codes," U. S. Patent 4559625, Dec., 1985

[120] www.mathworks.com

[121] T. Healy, F.C. Garcia-Gunning and A.D. Ellis, "Performance Evaluation of FEC Codes in a 42.6 Gbit/s CoWDM Optical Transmission System", Proceedings of European Conference on Optical Communications, Paper Tu3.2.5, Sept. 2005.

[122] http://www.eccpage.com/ (Simon Rockliffe)

[123] F.C. Garcia-Gunning, T. Healy and A.D. Ellis, "Dispersion Tolerance of CoWDM", IEEE Photonics Technology Letters, Vol. 18, No. 12, pp. 1338-1340, Jun. 2006.

[124] C. D. Poole, R. W. Tkach, A. R. Chraplyvy, and D. A. Fishman, "Fading in Lightwave Systems Due to Polarization-Mode Dispersion", IEEE Photonics Technology Letters, Vol. 3, No. 1, pp. 68-70, Jan. 1991.

[125] J. Song, and C. Fan, "A Simplified Dispersion Limit Formula for IMDD Systems and its Comparison with Experimental Results", Journal of Lightwave Technology, Vol. 12, No. 3, pp. 546-550, Mar 1995.

[126] G. Charlet, S. Lanne, L. Pierre, C. Simonneau, P. Tran, H Mardoyan, P. Brindel, M. Gorlier, J.-C. Antona, M. Molina, P. Sillard, J. Godin, W. Idler and S. Bigo, "Cost-optimized 6.3 Tbit/s-capacity terrestrial link over 17 /spl times/ 100 km using phase-shaped binary transmission in a conventional all-EDFA SMF-based system", Technical Digest of Optical Fiber Communications, Paper PD25-1, 2003.

[127] D. Simeonidou, N.H. Taylor, M.S. Chaudhry, K.P. Jones, P.R. Morkel, "Straight-line 4×2.5 Gbit/s WDM transmission over 2600 km on a manufactured optically-amplified submarine cable system with 95 km repeater spacing" IEE Colloquium Towards Terabit Transmission, pp. 17/1-17/5, May 1995.

[128] S. Song, J. Livas, "Four-wave mixing induced Q-factor variations in WDM systems", Proceedings of Conference on Lasers and Electro-Optics, 2000. Paper CWK69, May 2000.

[129] M.J. Ablowitz, R.L. Horne, E. Spiller, G. Biondini, S. Chakravarty , "Four-wave mixing in strong dispersion-managed WDM soliton systems", Technical Digest of Nonlinear Optics: Materials, Fundamentals, and Applications, Paper ThB6-1 , Aug. 2000.

[130] S. Ten, K.M. Ennser, J.M. Grochocinski, S.P. Burtsev, V.L. da Silva, "Comparison of four-wave mixing and cross phase modulation penalties in dense WDM systems", Technical Digest of Optical Fiber Communication, Paper ThC4-1, 1999.

[131] G. R. Walker, D. M. Spirit, P. J. Chidgey, E. G. Bryant and C. R. Batchellor, "Effect of Fibre Dispersion on Coherent Optical Transmission System", Electronics Letters, Vol. 28, No. 11, pp. 989-991, May 1992.

[132] K. Inoue, K. Nakanishi, K. Oda and H. Toba, "Crosstalk and Power Penalty Due to Fiber Four-Wave Mixing in Multichannel Transmissions", Journal of Lightwave Technology, Vol. 12, No. 8, pp 1423-1439 Aug 1994.

[133] M. Suzuki, N. Edagawa, "Dispersion-Managed High-Capacity Ultra-Long-Haul Transmission", Journal of Lightwave Technology, Vol. 21, No.4, pp. 916-928, Apr. 2003.

[134] K. Sekine, N. Kikuchi, S. Sasaki and Y. Uchida, "Dispersion compensated 80Gbit/s WDM transmission over 1171 km standard singlemode fibre", Electronics Letters, Vol. 31 , No. 13 pp.1080-1082, Jun. 1995.

[135] J. Fatome, S. Pitois, P. Tchofo-Dinda, D. Erasme and G. Millot , "Experimental comparison of classical and dense dispersion managements for 160-Gb/s transmission systems", Proceedings of Conference of Lasers and Electro-Optics Europe, pp. 488, 2005.

[136] T. Healy, A.D. Ellis, F.C. Garcia-Gunning, B. Cuenot and M. Rukosueva, "1b/s/Hz Coherent WDM Transmission over 112km of Dispersion Managed Optical Fibre", Technical Digest of Optical Fiber Communications, Poster OThR4, 2006.

[137] W.D. Cornwell, H.O. Edwards, N.H. Taylor, D.S. Lotay, S.A. Smith, and S. Hamidi, "Comparison of 64 x 10 Gb/s NRZ and RZ transmission over 6,000 km using a dispersion-managed fiber solution", Technical Digest of Optical Fiber Communications, Paper WP4, 2002.

[138] B. Bakhshi, M. Vaa, E.A. Golovchenko, W.W. Patterson, R.L. Maybach, and N.S. Bergano, "Comparison of CRZ, RZ and NRZ modulation formats in a 64 x

12.3 Gb/s WDM transmission experiment over 9000 km", Technical Digest of Optical Fiber Communications, Paper WF4-1, 2001.

[139] J-X. Cai, C.R. Davidson, M. Nissov, H.Li, W.T. Anderson, Y. Cai, L. Liu, A.N. Pilipetskii, D.G. Foursa, W.W. Patterson, P.C. Corbett, A.J. Lucero, and N.S. Bergano, "Transmission of 40-Gb/s WDM Signals Over Transoceanic Distance Using Conventional NZ-DSF With Receiver Dispersion Slope Compensation", Journal of Lightwave Technology, Vol. 24, No. 1, pp. 191-200 Jan. 2006.

[140] C. Rasmussen, T. Fjelde, J. Bennike, F. Liu, S. Dey, B. Mikkelsen, P.Mamyshev, P. Serbe, P. van der Wagt, Y. Akasaka, D. Harris, D. Gapontsev, V. Ivshin, and P. Reeves-Hall, "DWDM 40G Transmission Over Trans-Pacific Distance (10 000 km) Using CSRZ-DPSK, Enhanced FEC, and All-Raman-Amplified 100-km UltraWave Fiber Spans", Journal of Lightwave Technology, Vol. 22, No. 1, pp. 203-207 Jan. 2004.

[141] T. Tsuritani, K. Ishida, A. Agata, K. Shimomura, I. Morita, T. Tokura, H. Taga, T. Mizuochi, N. Edagawa, and S. Akiba, "70-GHz-Spaced 40 42.7 Gb/s Transpacific Transmission Over 9400 km Using Prefiltered CSRZ-DPSK Signals, All-Raman Repeaters, and Symmetrically Dispersion-Managed Fiber Spans", Journal of Lightwave Technology, Vol. 22, No. 1, pp. 215-223 Jan. 2004.

[142] F.C. Garcia-Gunning, T. Healy, X. Yang and A.D. Ellis, "0.6Tbit/s Capacity and 2bit/s/Hz Spectral Efficiency at 42.6Gsymbol/s Using a Single DFB Laser with NRZ Coherent WDM and Polarisation Multiplexing", Proceedings of Conference of Lasers and Electro-Optics Europe, Paper C-18-FRI, Jun. 2007.

[143] C. Herard and A. Lacourt, "New multiplexing technique using polarization of light", Applied Optics, Vol. 30, No. 2, pp. 222-231, Jan. 1991.

[144] P.M. Hill, R. Olshansky, and W. K. Burns, "Optical Polarization Division Multiplexing at 4 Gb/s", IEEE Photonics Technology Letters, Vol. 4, No. 5, pp. 500-502, May 1992.

[145] L.E. Nelson, "Challenges of 40 Gb/s WDM Transmission", Technical Digest of Optical Fiber Communications, Paper ThF1-1, 2000.

[146] H. Masuda, A. Sano, T. Kobayashi, E. Yoshida, Y. Miyamoto, Y. Hibino, K. Hagimoto, T. Yamada, T. Furuta and H. Fukuyama, "20.4-Tb/s (204 x 111 Gb/s) Transmission over 240 km using Bandwidth-Maximized Hybrid Raman/EDFAs", Technical Digest of Optical Fiber Communications, Paper PDP20, 2007.

[147] C. Fludger, T. Duthel, D. van den Borne, C. Schulien, E.-D. Schmidt, T. Wuth, E. de Man, G.D. Kohe, H. De Waardt, "10 x 111 Gbit/s, 50 GHz spaced, POLMUX-TZ-DQPSK transmission over 2375 km employing coherent

equalisation", Technical Digest of Optical Fiber Communications, Paper PDP22, 2007.

[148] D. Sandel, F. Wüst, V. Mirvoda, and R. Noé , "Standard (NRZ 1 40 Gb/s, 210 km) and Polarization Multiplex (CS-RZ, 2 40 Gb/s, 212 km) Transmissions With PMD Compensation", IEEE Photonics Technology Letters, Vol. 14, No 8, pp. 1181-1183, Aug. 2002.

[149] L.E. Nelson and H. Kogelnik, "Coherent crosstalk impairments in polarization multiplexed transmission due to polarization mode dispersion", Optics Express, Vol. 7, No. 10, pp. 350-361, Nov. 2000.

[150] T. Widdowson, "Ultra-long haul optical fibre transmission systems", PHD Thesis

[151] A. Sano, H. Masuda, Y. Kisaka, S. Aisawa, E. Yoshida, Y. Miyamoto, M. Koga, K. Hagimoto, T. Yamada, T. Furuta and H. Fukuyama, "14-Tb/s (140x111-Gb/s PDM/WDM) CSRZ-DQPSK transmission over 160 km using 7-THz bandwidth extended L-band EDFAs." Proceedings of European Conference on Optical Communications, Paper Th4.1.1, 2006.

[152] M. Karlsson, P. A. Andrekson, and H. Sunnerud, "High-speed OTDM and Impact of PMD", Proceedings of Lasers and Electro-optics Society, Paper Tuz2, Nov. 1999.

[153] http://www.corning.com/docs/opticalfiber/CO9562.pdf

[154] T. Healy, F.C. Garcia Gunning, E. Pincemin, B. Cuenot and A.D. Ellis, "1,200 km SMF (100 km spans) 280 Gbit/s Coherent WDM Transmission using Hybrid Raman/EDFA Amplification", accepted for publication at European Conference on Optical Communications, Sept. 2007.

[155] H. Takara, K. Uchiyama, I. Shake and T. Morioka, "Ultra-high speed OTDM transmission systems and sub-systems" Technical Digest of Conference on Lasers and Electro-Optics, Paper CThU3, May 2001.

[156] I. Morita, and N. Edagawa, "Study on optimum OTDM signals for long-distance 40 Gbit/s transmission", Technical Digest of Optical Fiber Communications, Paper TuA4, 2002.

[157] A.N. Pilipetskii, "High-Capacity Undersea Long-Haul Systems", IEEE Journal of Selected Topics in Quantum Electronics, Vol. 12, No. 4, pp. 484-496, Jul./Aug. 2006.

[158] N.S. Bergano, "Wavelength Division Multiplexing in Long-Haul Transoceanic Transmission Systems" Journal of Lightwave Technology, Vol. 23, No. 12, pp. 4125-4139 , Dec. 2005.

[159] A. Tan, E. Pincemin, Y. Jaouen, A. Tonello, S. Wabnitz, J.D. Ania-Castañón, V. Mezentsev, S.K.Turitsyn , L. Grüner-Nielsen, "Can SSMF handle ULH 40-Gb/s WDM transmission, to be published in Proceedings of European Conference on Optical Communications, 2007"

[160] I.T. Lima, Jr., L.-S. Yan, B.S. Marks, C.R. Menyuk and A.E. Willner, "Experimental verification of the penalty produced by polarization effects in fiber recirculating loops", Technical Digest of Optical Fiber Communications, Paper CThD2, 2003.

[161] I.P. Kaminow, "Polarization in Optical Fibers", IEEE Journal of Quantum Electronics, Vol. QE-17, No. 1, Jan. 1981.

[162] H.-G. Weber, R. Ludwig, S. Ferber, C. Schmidt-Langhorst, M. Kroh, V. Marembert, C. Boerner, and C. Schubert, "Ultrahigh-Speed OTDM-Transmission Technology", Journal of Lightwave Technology, Vol. 24, No.12, pp. 4616-4627, 2006.

[163] M. Pfennigbauer and P.J. Winzer, "Choice of MUX/DEMUX Filter Characteristics for NRZ, RZ, and CSRZ DWDM Systems", Journal of Lightwave Technology, Vol. 24, No. 4, pp. 1689-1696, 2006.

[164] F.C. Garcia-Gunning, T. Healy, R.J. Manning and A.D. Ellis "Multi-banded Coherent WDM Transmission", Proceedings of European Conference on Optical Communications, Paper Th4.2.6, Sept. 2005.

[165] L. Noirie, M. Vigoureux, E. Dotaro, "Impact of intermediate traffic grouping on the dimensioning of multi-granularity optical networks", Technical Digest of Optical Fiber Communications, Paper TuG3- 1, 2000.

[166] L. Noirie, "The Road Towards All-Optical Networks", Technical Digest of Optical Fiber Communications, Paper FA1, 2003.

[167] E. Ciaramella, "Introducing Wavelength Granularity to Reduce the Complexity of Optical Cross Connects" IEEE Photonics Technology Letters, Vol. 12, No. 6, pp. 699-701, Jun. 2000.

[168] L.-W. Chen, P. Saengudomlert and E. Modiano, "Uniform vs. Non-uniform Band Switching in WDM Networks", Proceedings of International Conference on Broadband Networks, pp. 219-228, Oct. 2005.

[169] A.A.M. Saleh and J.M. Simmons, "Architectural Principles of Optical Regional and Metropolitan Access Networks", Journal of Lightwave Technology, Vol. 17, No. 12, Dec. 1992.

[170] A Suzuki, X. Wang, Y. Ogawa and S. Nakamura "10 x 320Gb/s (3.2Tb/s) DWDM/OTDM transmission in C-band by semiconductor-based devices", Paper Th4.1.7, Proceedings of European Conference on Optical Communications, 2004.

[171] C. Schubert, R.H. Derksen, M. Möller, R. Ludwig, C.-J. Weiske, J. Lutz, S. Ferber, A. Kirstädter, G. Lehmann, and C. Schmidt-Langhorst, "Integrated 100-Gb/s ETDM Receiver", Journal of Lightwave Technology, Vol. 25, No. 1, pp. 122-129, Jan. 2007.

[172] A. Zapata, M. Düser, J. Spencer, P. Bayvel, I. de Miguel, D. Breuer, N. Hanik, and A Gladisch, "Next-Generation 100-Gigabit Metro Ethernet (100 GbME) Using Multiwavelength Optical Rings", Journal of Lightwave Technology, Vol. 22, No. 11, pp. 2420-2434, Nov. 2004.

[173] H. Toyoda, S. Nishimura, M. Okuno, T. Yamaoka and H. Nishi, "A 100-Gb-Ethernet subsystem for next-generation metro-area network", IEEE International Conference on Communications, Vol. 2, pp. 1036 – 1042, May 2005.

[174] M. Daikoku, I. Morita, H. Taga, H. Tanaka, T. Kawanishi, T. Sakamoto, T. Miyazaki, and T. Fujita, "100-Gb/s DQPSK Transmission Experiment Without OTDM for 100G Ethernet Transport", Journal of Lightwave Technology, Vol. 25, No. 1, pp. 139-145,Jan. 2007.

[175] T. Ono and Y. Yano, "Key Technologies for Terabit/Second WDM Systems with High Spectral Efficiency of Over 1 bit/s/Hz", IEEE Journal Of Quantum Electronics, Vol. 34, No. 11, Nov. 1998.

[176] S.Tsukamoto, D-S. Ly-Gagnon, K. Katoh and K. Kikuchi, "Coherent Demodulation of 40-Gbitls Polarization-Multiplexed QPSK Signals with 16-GHz Spacing after 200-km Transmission", Technical Digest of Optical Fiber Communications, Paper PDP29, 2005.